Automatic Detection and Analysis of High Frequency Oscillations in the Human Electroencephalogram

Rina Zelmann

Department of Biomedical Engineering

McGill University, Montréal, Canada

September 2012

A thesis submitted to McGill University in partial fulfillment

of the requirements of the degree of Ph.D.

In memory of Sabina Katz de Zelmann

(Pomorzany, 08 July 1928 – Buenos Aires, 30 August 2012)

Abstract

High Frequency Oscillations (HFOs; 80-500Hz) are spontaneous short-duration small-amplitude EEG patterns that are emerging as a biomarker of tissue capable of generating epileptic seizures. In order to propel the clinical utilization and systematic study of HFOs, it is important to develop robust automatic detectors and to provide a framework to ensure stability in their identification; this is the first goal of this thesis. Although HFOs have mostly been studied with intracranial electrodes, they have also been recorded on the scalp. A fundamental question is to understand how is it possible to see these small events on the scalp given the powerful skull attenuation; this is the second goal of this thesis.

The first goal is addressed by designing a procedure to systematize the study of HFOs and by developing an automatic detector. A procedure that allows to control for consistency among readers and to evaluate if a selected interval provides stable information, for automatic and visual identification of HFOs, is first presented. This procedure is now routinely used when identifying interictal HFOs. This study is the first to evaluate the minimum duration needed to obtain consistent information when marking the EEG and showed that analyzing 5min of interictal EEG provided the same information as longer intervals. The approach is applicable to any type of EEG event.

An automatic detector of HFOs is then described, which takes an original approach in first detecting baseline segments free of oscillatory activity and then using a statistical threshold obtained from these local baselines to detect HFOs. The detector performs better than other detectors, in particular in active channels and in channels without clear baseline. A comparison of existing detectors on the same dataset is presented to analyze their performance, to show that optimizing on a particular type of data improves performance in any detector, and to emphasize the issues involved in validation.

The second goal of this thesis is the study of the spatial distribution of cortical activity at the time of scalp HFOs. As HFOs are produced by small brain regions, and since the EEG is greatly attenuated before reaching the scalp, HFOs are mostly recorded with intracranial electrodes. Surprisingly, HFOs have been recently observed also on the scalp EEG. Using simultaneous scalp and intracranial recordings, we showed that even though the generators of HFOs have small spatial extent, they can be observed on the scalp with small amplitude and focal extent. We showed that these small extent events are undersampled on the scalp with the density of standard electrode systems, and on cortical grids with the standard inter-electrode spacing of 1cm. A dense distribution of scalp electrodes seems necessary to fully spatially sample HFOs on the scalp. This opens the possibility of systematically studying HFOs non-invasively.

By developing methods for the detection and analysis of HFOs, we expect to improve the systematic study of intracranial and scalp HFOs, moving towards their clinical application as a biomarker of epileptogenic tissue.

Résumé

Les oscillations de haute fréquence (OHF; 80-500 Hz) constituent des évènements EEG spontanés de courte durée et de faible amplitude qui émergent en tant que biomarqueur du tissu pouvant générer les crises épileptiques. Afin de promouvoir l'utilisation clinique et l'étude systématique des OHF, il est important de développer des détecteurs automatiques fiables et de fournir un cadre visant à garantir la stabilité de leurs résultats. Il s'agit là du premier objectif de la présente thèse. Les OHF ont principalement été étudiées à partir d'électrodes intracrâniennes, mais elles ont également été enregistrées à l'aide d'électrodes placées sur le cuir chevelu. Il convient alors de comprendre comment l'on peut observer ces évènements de faible envergure du fait de l'atténuation importante du crâne, ce qui constitue le second objectif de cette thèse.

Pour répondre au premier objectif, nous avons conçu une procédure visant à systématiser l'étude des OHF et avons élaboré un détecteur automatique. Ainsi, nous présentons d'abord une procédure permettant d'assurer l'uniformité entre les lecteurs et d'évaluer si un intervalle choisi offre des renseignements stables pour un repérage visuel et automatique des OHF. À l'heure actuelle, cette procédure est communément utilisée quand les OHF intericталes sont repérées. Cette étude est la première à évaluer la durée minimale nécessaire à l'obtention de renseignements cohérents pour le marquage des EEG et elle a démontré que l'analyse de 5 minutes d'EEG interictal offre la même information que des intervalles de plus longue durée. Cette approche est applicable à tout type d'évènements EEG.

Nous avons ensuite décrit un détecteur automatique d'OHF, qui suit une approche originale en détectant d'abord des segments de base dénués d'activités oscillatoires avant d'utiliser un seuil statistique obtenu à partir de ces valeurs de base locales pour déterminer les OHF. Ce détecteur est plus efficace que d'autres détecteurs, notamment pour les canaux actifs et les canaux sans valeur de base claire. Une comparaison entre les détecteurs existants pour le même ensemble de

données est présentée afin d'analyser leur performance respective, de démontrer que l'optimisation d'un certain type de données améliore l'efficacité de tous les détecteurs et de mettre en évidence les problèmes en jeu dans la validation.

Le second objectif de la présente thèse est d'étudier la distribution spatiale de l'activité corticale au moment des OHF enregistrées sur le cuir chevelu. Dans la mesure où les OHF sont produites par de petites régions cérébrales et que l'EEG est fortement atténué avant d'arriver au cuir chevelu, les OHF sont surtout enregistrées à l'aide d'électrodes intracrâniennes. Il est étonnant que dernièrement, des OHF aient également été observées sur des EEG enregistrés sur le cuir chevelu. En se basant sur les enregistrements simultanés sur le cuir chevelu et intracrâniens, nous avons démontré que, même si les régions génératrices d'OHF sont faiblement étendues sur le plan spatial, les OHF peuvent être observées à l'aide d'électrodes placées sur le cuir chevelu avec une faible amplitude et une étendue focale. Nous avons établi que ces évènements de faible étendue sont sous-échantillonnés sur le cuir chevelu avec la densité des systèmes standards d'électrodes et sur les grilles corticales avec l'espacement standard de 1 cm entre les électrodes. Il semble nécessaire d'avoir une répartition dense des électrodes sur le cuir chevelu afin de représenter spatialement de façon exhaustive les OHF enregistrées sur le cuir chevelu. Cela ouvrirait la voie à une étude systématique non invasive des OHF.

Avec l'élaboration de méthodes de détection et d'analyse des OHF, nous souhaitons améliorer l'étude systématique des OHF intracrâniennes et du cuir chevelu, dans l'optique d'une application clinique en tant que biomarqueur du tissu épileptogène.

Acknowledgements

This project was supported by the National Science and Engineering Research Council (NSERC) Postgraduate Scholarship (PGSD), by the DAAD short-term scholarship, by the Savoy Foundation, and by the Canadian Institutes of Health Research (CIHR) Grants MOP-10189 and MOP-102710.

I am most grateful to Dr. Jean Gotman for the impeccable supervision of this thesis. I lack words to express the extent of my gratitude for his advice and guidance not only in professional issues, but also in all other fundamental aspects.

Many thanks to my PhD Committee: Dr. Robert Funnell, Dr. Jean-Marc Lina, and Dr. Benoit Champagne for their helpful comments and suggestions. I am grateful to Dr. François Dubeau for his advice and expertise in clinical matters.

Special thanks to my collaborators in the different projects: Dr. Maeike Zijlmans, Dr. Julia Jacobs, Dr. Claude E. Châtillon, Dr. Francesco Mari, and Dr. Federico Melani for the visual marking of events. Thanks go to Rahul Chander for the concept of baseline detection. I am grateful to all of them for their hard work, their passion for research, and their friendship.

I am grateful to Prof. Dr. Andreas Schulze-Bonhage from the University of Freiburg for making the simultaneous scalp and intracranial data available for my research. Many thanks to Dr. Matthias Dümpelmann for his help in obtaining the data and to Francois Tadel and Dr. Sylvain Baillet for their suggestions on using Brainstorm for the simulations. I am grateful to Dr. Jean-Marc Lina for his help in the methodological aspects of this project. Special thanks to Dr. Julia Jacobs for her supervision and for being instrumental in different aspects of this collaborative project.

Special thanks to Anne-Claire Pizzera for translating the abstract to French. Many thanks to Nicole Drouin, Lorraine Allard, and all the technicians and staff

of the EEG department for the acquisition of the EEG data, for their professionalism, and their readiness to help. Special thanks to Pina Sorrini, Toula Papadopoulos, Maria G. Di Nezza, and Nancy Abate for their help in administrative matters. Many thanks to Natasha Zazubovits for her help in data management.

Many thanks to the students and fellows in the LAB for making every day at work such an enjoyable journey. Especially to Dr. Pierre LeVan for the fruitful discussions over the years, to Dr. Eliane Kobayashi for the clinical advice, to Dr. Christophe Grova for the interesting discussions, to Dr. Louise Tyvaert for her optimism, to Dr. Friederike Möller for the profound talks, and to Dr. Francesca Pittau for teaching me the role of the amygdala.

I am profoundly in debt to Pablo JP Cingolani for his patience, his encouragement, and for everything else. All my gratitude goes to my family for their unconditional support, for their understanding, and their love.

Contributions of Authors

Manuscript #1: Improving the identification of High Frequency Oscillations

Authors: Rina Zelmann, Maeike Zijlmans, Julia Jacobs, Claude-E. Châtillon, and Jean Gotman.

Rina Zelmann had the idea of using information theory and alignment techniques to evaluate stability in the marking of High Frequency Oscillation events (HFOs), designed the methods, implemented the procedure, interpreted the results, and wrote the manuscript.
Maeike Zijlmans had the idea of using kappa coefficient within the procedure to evaluate inter reviewer concordance, visually identified the HFOs, and helped interpreting the results.
Julia Jacobs and Claude-E. Châtillon visually identified the HFOs, and helped interpreting the results.
Jean Gotman supervised the project and revised the manuscript.

Manuscript #2: Automatic detector of High Frequency Oscillations for human recordings with macroelectrodes

Authors: Rina Zelmann, Francesco Mari, Julia Jacobs, Maeike Zijlmans, Rahul Chander, and Jean Gotman.

Rina Zelmann developed and implemented the HFOs detector, designed the parameter optimization methods, interpreted the results, and wrote the manuscript.
Francesco Mari, Julia Jacobs, Maeike Zijlmans visually identified the gold standard events (HFOs and baselines).
Rahul Chander had the idea of detecting baseline segments as the first step in HFO detection, design, and implemented a detector (Chander 2007).
Jean Gotman supervised the project and revised the manuscript.

Manuscript #3: A comparison between detectors of High Frequency Oscillations

Authors: Rina Zelmann, Francesco Mari, Julia Jacobs, Maeike Zijlmans, François Dubeau and Jean Gotman.

Rina Zelmann designed a block of the detector to consider channels with high frequency continuous background activity, implemented the complete version of the MNI detector, implemented the other detectors with their default and optimized configurations, had the idea of using different gold standards to evaluate their performance, interpreted the results, and wrote the manuscript.
Francesco Mari, Julia Jacobs, and Maeike Zijlmans visually identified the gold standard events (HFOs and baselines).
François Dubeau supervised the clinical aspects of the project.
Jean Gotman supervised the project and revised the manuscript.

Manuscript #4: The scalp EEG can see very small cortical generators of epileptic activity

Authors: Rina Zelmann, Jean-Marc Lina, Andreas Schulze-Bonhage, Jean Gotman, and Julia Jacobs.

Rina Zelmann designed and implemented the methods to analyze simultaneous scalp and intracranial EEG, had the idea to study spatial patterns of similar scalp events, had the idea of using a linear model between subdural and scalp contacts, implemented the simulations, interpreted the results, and wrote the manuscript.
Jean-Marc Lina collaborated in the implementation of the simulation to estimate the spatial extent on the scalp of the sources.
Andreas Schulze-Bonhage supervised the acquisition of the data.
Jean Gotman supervised the methodology of the study, had the idea of simulating small sources to estimate their extent on the scalp, and revised the manuscript.
Julia Jacobs had the idea of studying simultaneous scalp and intracranial recordings, supervised the project, and revised the manuscript.

Statement of originality

To the best of our knowledge:

- The procedure presented in chapter 5 was the first procedure developed to evaluate if a selected interval provides stable information for automatic and visual identification of HFOs. This study was the first to assess the duration of EEG that must be interpreted in order to obtain reliable estimates. The presented approach is original and applicable to any event marking in the EEG, and possibly to other fields.

- The automatic detector presented in Chapter 6 provides an original approach in first detecting baseline segments without rhythmic activity and then incorporating this local information for the detection of HFOs using a statistical threshold obtained from the detected baseline. It is the first detector to explicitly consider channels with continuous HF activity background. This study was the first comparison among detectors of HFOs and was the first to show the importance of optimizing any detector for a particular type of data.

- The study presented in Chapter 7 is the first one to study simultaneous scalp and intracranial EEG recordings in the high frequency range. This study is the first to describe the spatial patterns of subdural activity at the time of the peak of scalp HFOs. It is the first to show that even though small cortical regions seem to generate HFOs, they can be recorded on the scalp EEG with low amplitude and in a very focal region. It is the first study to show that there is probably undersampling of HFOs on the grids and on the scalp.

Table of Contents

Chapter 1. *Introduction*

Epilepsy is the second most common neurological disorder (after stroke), affecting about 1 in 200 Canadians (Tellez-Zenteno *et al.,* 2004). Epileptic syndromes are characterized by recurrent seizures that could originate from a variety of underlying causes. EEG is the principal diagnostic tool of epilepsy. By measuring the electrical signal generated in the brain, the EEG is a direct measure of the neuronal activity with high temporal resolution. EEG plays a major role for the identification of the epileptic syndrome and in the localization of the epileptic focus.

About 30% of patients with epilepsy do not respond to medication aimed at stopping seizures. Some of these patients, with a suspected circumscribed region causing the seizures, are candidates for surgery. When successful, removal of this region leads to a cessation of seizures. The definition of the region capable of generating seizures and the delineation of the resection area are based on the combined analysis of clinical seizure semiology, scalp video-EEG, neuroimaging, and neuropsychology. When the epileptogenic focus is not clear from these non-invasive techniques, intracranial EEG recordings can be considered. The objective of intracranial EEG is to obtain a precise localization of the seizure onset zone to be able to tailor the surgical resection to include all the regions suspected to produce seizures, while sparing eloquent regions.

The traditional EEG frequency bands considered clinically relevant (up to 40 or 70 Hz) have been recently challenged by the discovery of High Frequency Oscillations (HFOs; 80-500Hz). HFOs are short-duration small-amplitude spontaneous events that are mostly recorded with intracranial electrodes. HFOs are emerging as a reliable biomarker of tissue capable of generating epileptic seizures. The HFO rate is higher within the area of the brain where seizures originate (Bragin *et al.,* 1999b, Urrestarazu *et al.,* 2007), regardless of the lesions (Jacobs *et al.,* 2009a). HFOs are related with epileptogenesis, since they appear in

experimental animals that later develop spontaneous seizures (Bragin *et al.,* 2004). HFOs behave like seizure with respect to medication, increasing with withdrawal of medication (Zijlmans *et al.,* 2009b). Post-surgical studies indicate that removal of regions with high rate of HFOs is associated with seizure freedom, while poor outcome is obtained if these regions are not removed (Jacobs *et al.,* 2010b, Wu *et al.,* 2010).

The identification of these spontaneous events is challenging. Visual marking of HFOs can be performed but it is highly time consuming and subjective. Consistency and stability of the markings must be evaluated. Automatic detection would greatly facilitate the investigation of HFOs as biomarkers of epileptogenic tissue, and is likely necessary to propel future clinical applications. Fully automatic detection is desirable, but given the lack of a formal definition of HFOs high specificity and high sensitivity are difficult to achieve. A possible solution is semi-automatic detection in which HFOs are first automatically detected with high sensitivity but low specificity and then visually validated by expert reviewers.

Since HFOs are thought to be generated by regions of about 1 cubic millimetre (Bragin *et al.,* 2002), it should only be possible to record them with grids and strip placed over the surface of the brain or with depth electrodes inserted in the brain. Surprisingly, HFOs have been recently identified on the scalp (Andrade-Valença *et al.,* 2011, Kobayashi *et al.,* 2010b). The detection of HFOs non-invasively, on the scalp EEG, could be useful to evaluate the development of epilepsy in large patient populations, for predicting surgical outcome, and for planning electrode implantation. Understanding the cortical correlates of scalp HFOs is a paramount step towards their utilization clinically.

The objective of this thesis is the development of methods to improve the systematic study of HFOs, with the goal of moving towards the clinical application of HFOs as a biomarker of epileptogenic tissue.

This thesis is organized in the following way. Chapters 2, 3, and 4 provide the necessary background. Chapter 2 presents fundamental aspects of EEG and chapter 3 of epilepsy. Chapter 4 introduces HFOs and their relation to epilepsy. Chapters 5, 6, and 7 present the manuscripts that are the core of this thesis. Chapter 5 describes a procedure to control for consistency between human readers of HFOs, to evaluate if a selected interval provides stable information for automatic and visual identification of HFOs, and to assess the duration of EEG that must be interpreted in order to obtain reliable estimates. Chapter 6 presents an automatic detector of HFOs, which first detects baseline segments without rhythmic activity and then incorporates this information to detect HFOs. A comparison with other detectors is also presented. Chapter 7 presents a study on the spatial distribution of underlying cortical activity at the time of scalp HFOs. It is shown that although the generators of HFOs are small, they can be recorded on the scalp with low amplitude and in a very focal region. Finally, the conclusions and possible future developments are presented in chapter 8.

Chapter 2. *Electroencephalography*

Electroencephalography (EEG) records the electrical signals generated by the brain. EEG is the principal tool for the diagnostic of epilepsy. It is used for the identification of the epileptic syndrome and in the location of the epileptic focus. Its application extends beyond epilepsy to the assessment of the state of the brain in the intensive care unit; anaesthesia monitoring; the evaluation of neonates; and in cognitive neurosciences. The EEG is acquired from electrodes placed on the scalp or with intracranial electrodes over the dura, over the cortex, or deep in the brain.

Electrophysiology was born at the end of the 18th century in Bologna. The famous experiment of Luigi Galvani, in which the contraction of a frog's leg was generated, laid down the basic concept of electrical conductivity in living animals (what he called "animal electricity"; Galvani 1791). More than a century later, in the late 1920s, the first human EEG was recorded by Hans Berger. He was the first one to report on the alpha rhythm and described the EEG as a "window into the brain" (Berger 1929). He even conceived the EEG as a rhythmic sequence of activity of large groups of cortical neurons (Gloor 1969).

In this chapter the underlying mechanisms of EEG generation are presented; scalp and intracranial recordings of EEG are described; the concept of volume conduction applied to the EEG is explained; the physical characteristics of the skull are presented; the forward and inverse problems to localize the focus of activity are introduced; normal EEG activity is illustrated; and artefacts that may affect the EEG are described. Pathological EEG activity will be dealt with in the next chapter on epilepsy.

2.1 *Underlying mechanisms of EEG generation*[1]

The brain consists of about 10^{10} neurons that exchange information and about 10^{10} glial cells that support the neurons' function. Communication between neurons takes place at the synapse terminals. Synaptic terminals are located at the neuron's highly branched dendrites and at the soma (Figure 2.1.A). Large neurons can have up to 10^5 synapses. The neuron integrates the information in the soma and if the amplitude is larger than a threshold, an action potential is produced. The action potential is propagated through the axon, endings in a presynaptic terminal, which in turn produces a new synapse closing the communication loop. Myelin surrounding the axon speeds up communication between distant neurons and effector cells.

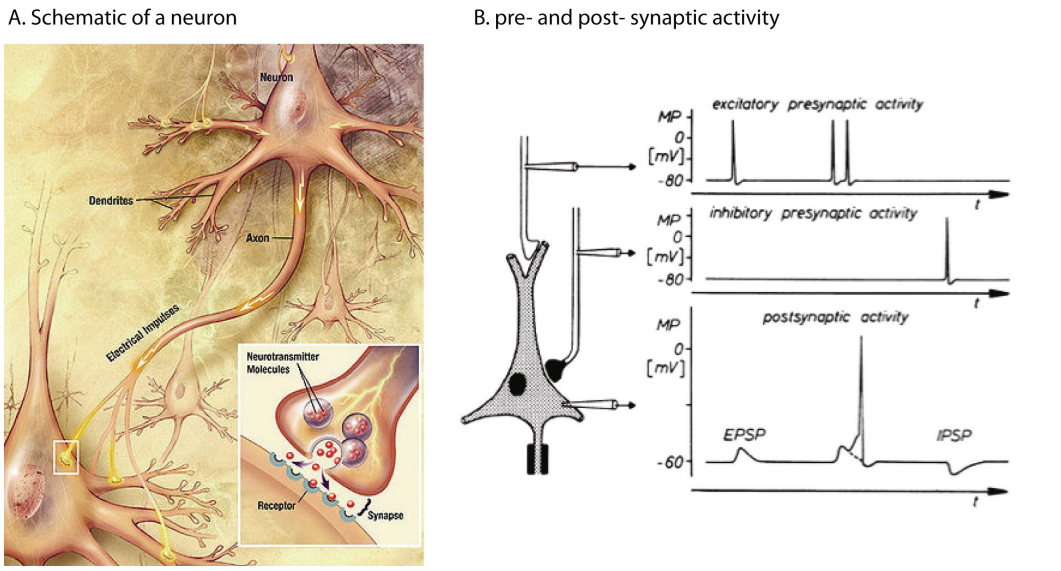

Figure 2.1. Schematic representation of a neuron and generation of postsynaptic potentials. A) A neuron is composed of dendrites, soma, and axon. Inset: synapsis. From: wikipedia.org. B) Postsynaptic potentials can be excitatory (EPSP) or inhibitory (IPSP). From (Speckmann and Elger 2005).

This section lays down the basic principles of EEG generation. Details on non-synaptic mechanisms of EEG generation, such as gap junctions and ephaptic coupling, will be discussed in Chapter 4 – High Frequency Oscillations (HFOs), where the possible mechanisms of HFO's generation are presented.

[1] Parts of this section, in particular "electrical activity at the cellular level", were originally written in my Master's Thesis (Zelmann 2007).

2.1.1 *Electrical activity at the cellular level*

The membrane potential depends upon the difference in membrane permeability to different ions and the intra- and extra-cellular concentration of the specific ions, mainly potassium (K^+), sodium (Na^+), calcium (Ca^{2+}), and chloride (Cl^-). During rest, the concentration gradient and the electrical gradient for each individual ion type are in equilibrium. Na^+/ K^+ pumps maintain the intracellular concentrations low for Na^+ and high for K^+. This results in the inside of the cell being negative with respect to the outside. The resting membrane potential is about -70mV, similar to the K^+ equilibrium potential (Widmaier *et al.,* 2006). When a neuron receives neural impulses at a synapse, this state of equilibrium is no longer maintained. If the synapse is excitatory, the neurotransmitters bind to specific ion channels and allow Na^+ to enter the cell, stimulating in turn voltage-gated Na^+ channels and increasing the membrane potential, which becomes depolarized (more positive). Apart from the inward flow of Na+, Ca^{2+} spikes produce an inward current in the dendrites of large amplitude (20-50mV) (Buzsáki *et al.,* 2003). Since the cell is depolarized, the generated synaptic potential is called an excitatory postsynaptic potential (EPSP). On the contrary, if the synapse is inhibitory, the resulting postsynaptic potential (IPSP) hyperpolarizes the cell, making the membrane potential more negative. If the temporal and spatial summation of hundreds of postsynaptic potentials produce a depolarization that reaches a critical threshold potential (around -50mV) at the triggering zone, an action potential (AP) is generated (Figure 2.1.B). Since the AP is produced by the opening of many voltage-gated Na^+ channels in a positive feedback loop, the membrane potential increases, reaching about 30mV, which is close to the Na^+ equilibrium potential. As the Na^+ channels get quickly inactive and the potassium channels open, the AP ends rapidly and the resting equilibrium is restored after the refractory period. The AP is thus a brief, impulse-like electrical signal that propagates without attenuation along the axon towards its target cells. The axon terminals are in turn presynaptic terminals that release neurotransmitters with the arrival of the AP. The neurotransmitters diffuse across the synaptic cleft and bind to the receptors in the postsynaptic neuron (Figure

2.1.A; inset). In this way, information is propagated from one neuron to the following one by converting an electrical signal (the AP) into a chemical signal (the neurotransmitters) and back into an electrical signal (EPSP & IPSP) in the postsynaptic neuron.

2.1.2 *EEG generation*

EEG recorded on the scalp is mainly due to synchronously occurring postsynaptic potentials of cortical pyramidal cells in layers III, IV, and V (Ebersole and Pedley 2003). Pyramidal cells are arranged parallel to each other and perpendicular to the surface of the cortex with their apical dendrites near the cortical (pial) surface and their axonal poles facing towards the subcortical white matter (Figure 2.2). Moreover, thalamocortical afferents into the cortex have extensive ramifications reaching thousands of cortical neurons. Thus, an action potential originating from a single thalamic neuron could simultaneously induce EPSPs and IPSPs in a large number of pyramidal neurons. Given their structural organization, these synchronously excited neurons create virtually identical, similarly oriented electric fields of finite and macroscopic extent that can be represented as a dipolar layer (Gloor 1985).

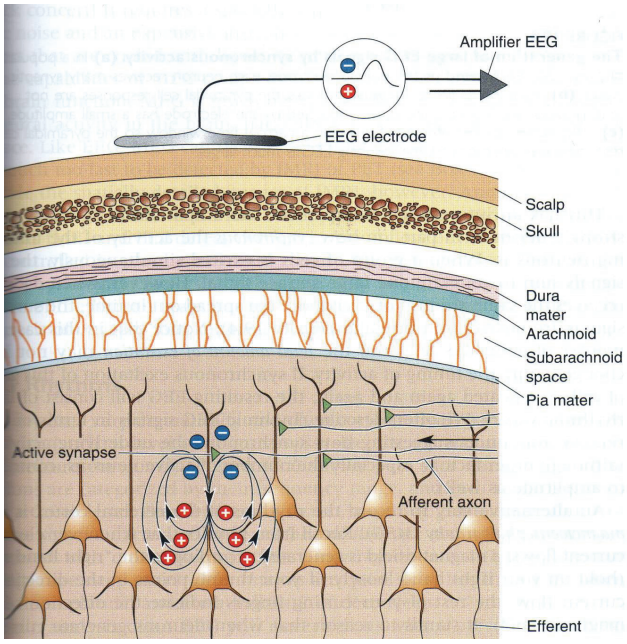

Figure 2.2. EEG on the scalp represents primarily the summation of postsynaptic potentials of a large number of synchronous pyramidal cells. From: (Bear *et al.,* 2007).

Because EPSPs and IPSPs have a duration of 10-250ms, there is no need for perfect synchrony for these potentials to overlap, allowing the effective temporal-spatial summation of their individual contributions. On the contrary, APs only last 1-2ms and therefore tend not to coexist in time. In addition, the propagation of action potentials can be thought as equivalent to a quadrupole, which attenuates more rapidly with distance (Nunez and Srinivasan 2006). Hence, even though APs have a much larger amplitude than EPSPs and IPSPs, the latter long lasting potentials account for most of the cerebral activity recorded on the scalp.

The same concept of spatio-temporal overlap could be used to understand why low frequency potentials are measured on the scalp with larger amplitudes than higher frequency signals. Lower frequency signals have a longer duration, allowing for a larger time span during which cortical potentials could overlap. This implies that a larger area of relatively simultaneously activated neurons could contribute to the recorded scalp EEG, even if the degree of synchrony is not so stringent (Gloor 1985).

Intracranial electrodes can record small extent sources because they are close to the generators. When a microelectrode is located close to the cell body layer of cortical structures, the recording EEG potentials contain action potentials and postsynaptic potentials. Moreover, during epileptic activity, a large number of neighboring neurons fire within a short interval. Thus, not only microelectrodes but also clinical intracranial macroelectrodes are likely to record a combination of synaptic activity and AP during an epileptic discharge (Buzsáki *et al.,* 2003).

2.1.3 *Volume conduction and EEG*

Even though the EPSPs have an amplitude in the order of millivolts, only microvolts are normally recorded on the scalp. On the one hand, the signal is attenuated with the square of the distance and due to the high resistivity of the skull (discussed in detail in section 2.3.2). On the other hand, since the cerebral cortex is a highly convoluted structure, the spatial location, size, and orientation

of the dipolar layers also determine whether a source would be visible on the scalp and its topography (Buzsáki *et al.,* 2003).

The relation between orientation and recorded activity is best understood by the concept of solid angle: "The potential generated by a dipole layer in a volume conductor measured at any point within (or at the surface of) this conductor is proportional to the solid angle subtended by the dipole layer at the point of measurement" (Gloor 1985). Thus, the potential measured is independent of the detailed structure of the dipolar layer, but depends only on the "apparent size" seen by the electrode. When a neuron is depolarized, it creates a potential proportional to a small solid angle observed by the electrode, corresponding to the cross-sectional area at the boundary of the active and the inactive parts of the neuron. When thousands of cortical pyramidal neurons are excited simultaneously as explained above, their individual solid angles sum up, producing a potential that is proportional to a large solid angle, and can therefore be measured by the EEG (Figure 2.3.A) (Gloor 1985). Thus, the potentials generated in a small region and measured on the scalp have a bell shape, with the maximum close to the generating region, falling slowly across the scalp (Figure 2.3.A). The closer the source is to the surface, the larger the angle, resulting in larger amplitude.

Electrical current always flows following the path of lowest resistivity. In a homogenous medium, it is also the shortest path. However, in an inhomogeneous medium the path of lowest conductivity might not be the shortest (Nunez and Srinivasan 2006). Since the current is confined inside the head volume, current lines are compressed when they approach the surface, producing a larger potential than in an infinite homogeneous medium. Given the low conductivity of the skull, the potential falls off more rapidly in the skull than in the brain and the scalp, resulting in smaller maximum amplitude (Figure 2.3.B *top*). The bell shape of the potential distribution (explained above) on the scalp is further flattened since the potential falls more slowly as the angle increases (Figure 2.3.B *bottom*). Thus, the potential measured on the scalp is more smeared than if conductivities across layers were the same (Nunez and Srinivasan 2006). This effect is stronger the

closer the source is to the surface. Moreover, the skull anisotropy (see section 2.3.2) enhances this smearing effect (Wolters *et al.,* 2006). This is independent of temporal frequency, since the skull is purely resistive in the frequencies of interest. Thus, electrical signals from the brain can be instantaneously measured on the scalp, but the smearing effect must be considered.

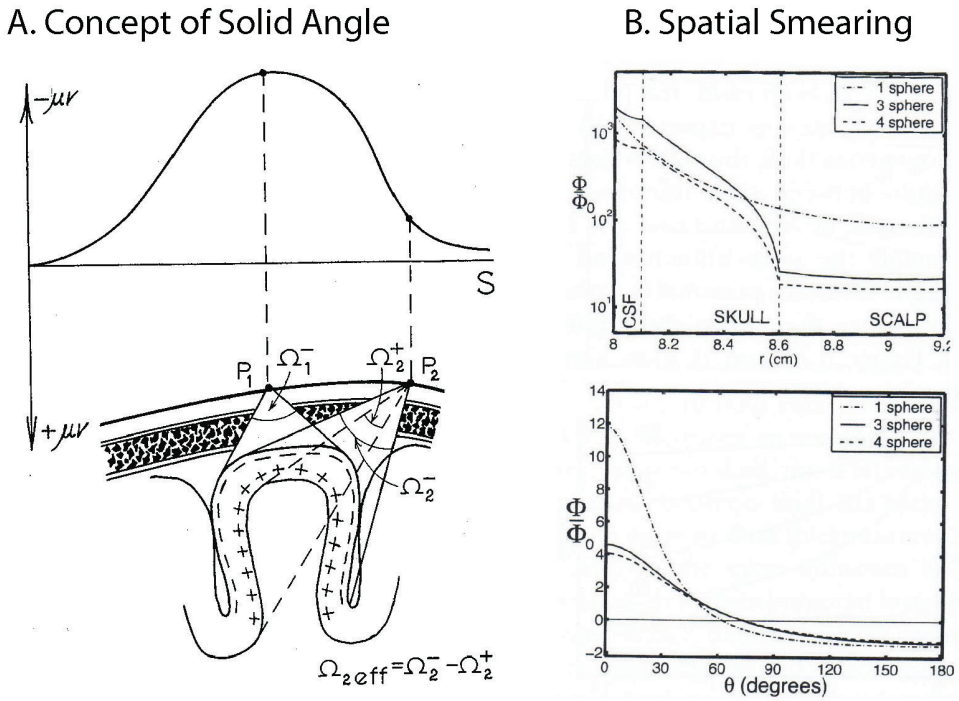

Figure 2.3. Volume conduction in inhomogeneous media. A) EEG recordings can be understood based on the solid angle concept, since the difference in potential between electrodes P1 and P2 depends on the difference between the solid angle seen by each electrode. From: (Gloor 1985). B) Spatial smearing on the scalp. The potential ratio (Φ/Φ_0) with respect to an infinite homogenous medium depends on the conductivity ratio and thickness of each layer. *Top*: The amplitude would gradually decrease with distance if all conductivities were the same (1-sphere model). Since the conductivities are different (3-sphere model), the electric field falls off more rapidly in the skull, resulting on reduced amplitude on the scalp. Source located at r=7cm. *Bottom*: The potential distribution on the scalp falls more slowly with angular distance for the 3-sphere than for the 1-sphere model, illustrating the smearing effect. Source located at r=5cm. In both plots, adding CSF (4 sphere model) produces a small decrease in scalp potential. From: (Nunez and Srinivasan 2006).

During an epileptic spike, thousands of excitatory synapses can occur simultaneously in the apical dendrites (situated in the most superficial layer). The generated EPSPs produce the inflow of positive ions into the cells, resulting in extracellular currents flowing from the soma and the basal dendrites to the apical dendrites (Gloor 1985). These currents correspond to a negative potential recorded on the scalp. In clinical interpretation of EEG recordings the source is

sometimes assumed to be where there is a maximum negativity on the EEG (Ebersole 2009). However, this assumption that the source lies underneath the electrode, is valid only if the source has radial orientation; in other words if it is located in the cortical gyrus underlying the point of measurement on the scalp. Examples of radial sources that produce a large solid angle in the overlying electrode are illustrated by the schematic in Figure 2.3.A (position P1) and by the voltage map of dipole 2 in Figure 2.4. On the contrary, sources that are tangential to the surface of the brain produce a topography without a maximum on top of them, but rather with positive-negative in both sides of the brain, as illustrated by dipole 1 in Figure 2.4. Tangential sources originate from one side of a sulcus; the basal part of the brain, such as orbitofrontal and basal temporal regions; or the midline (Ebersole 2009). Sources in opposite sulci cancel each other, since they have opposite orientations, while sources at the bottom and crown of gyri sum up. The equivalent orientation of a source that comprises several gyri and sulci depends on the overall solid angle seen by the electrode (Figure 2.3.A). Since the EEG measures the potential between two electrodes the resulting amplitude depends on the difference of solid angles (Ω_{2eff}) between electrodes (P1 & P2).

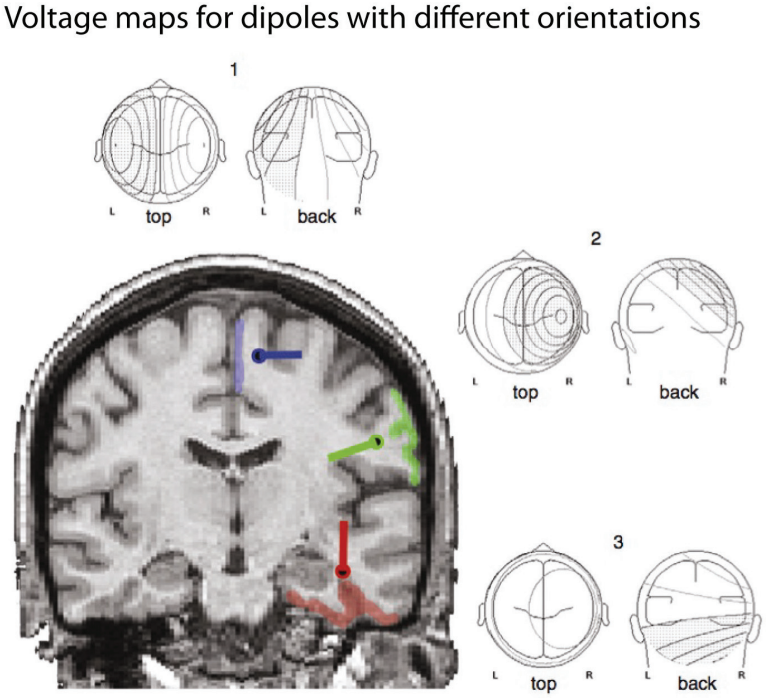

Figure 2.4. Examples of voltage maps obtained on the scalp for different dipolar orientations. From: (Ebersole 2009).

2.2 *Recording the EEG*

The EEG is a direct measure of the neuronal activity with high temporal resolution since the electric potential is conducted almost instantaneously from its point of generation to the point of measurement. In the following sections scalp and intracranial EEG recordings are presented.

2.2.1 *Scalp EEG recording*

Scalp EEG measures the potential difference between two electrodes located at the surface of the scalp. In clinical settings, the International 10–20 system for electrode placement (Jasper 1958) is used as the standard. The 10–20 system can be interpreted as a "*coordinate system*" where letters indicate general brain location and numbers represent the hemisphere (Figure 2.5).

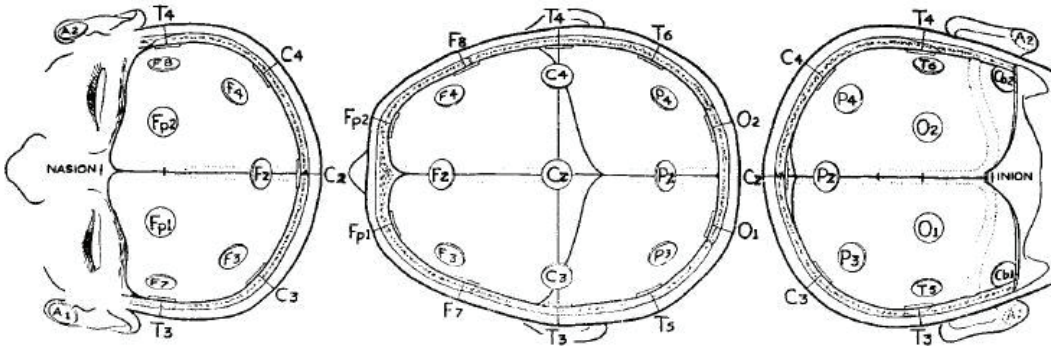

Figure 2.5. The International 10-20 system. The cerebral regions are represented by one or two letters: Fp– frontopolar; F– frontal; C– central; P– parietal; T– temporal; O– occipital. Odd numbers represent the left hemisphere, even numbers the right hemisphere, while the letter z is used to indicate the midline. From: (Jasper 1958).

Anatomical landmarks determine the standard placement of the electrodes. Starting by measuring the distance between the nasion and the inion and between pre-auricular points, the 21 electrodes are spaced by 10% or 20% of the measured distances. This positioning method can be replicated consistently over time and across laboratories, since it is relative to the subject's head size. Additional electrodes can be placed with predictable location, such as in the 10-10 system, in which 10% is used as the inter-electrode interval resulting in 64 electrodes. In addition, several centers use caps with 64, 128, or 256 electrodes uniformly distributed. When assessing the number of electrodes needed to obtain accurate

source localization, there was increased accuracy up to 64 electrodes, but little gain in using more (Lantz *et al.,* 2003). At realistic noise levels, using 64 or more electrodes does not change spatial resolution (Ryynanen *et al.,* 2004). Thus, more contacts are not necessarily better, at least for traditional EEG recordings. In low noise environments (as is the case of HF band), a large number of electrodes would allow the accurate reconstruction of more small sources (Ryynanen *et al.,* 2004). In chapter 7 we show that a large number of electrodes, with small inter-electrode distance may be important to accurately record High Frequency Oscillations on the scalp.

Since the scalp EEG measures the relative potential between two points, the selection of the reference recording electrode is important. Although ideally a far reference should be chosen, it has to be within the body since the scalp-air interface is a perfect insulator. A good practice is to place the recording reference in the midline. This reduces environmental noise since the recording is performed between two electrodes placed on the scalp (i.e. both contacts record similarly the environmental activity). In addition, this reference minimizes EMG artefacts since there is almost no muscle contraction in the center of the scalp. The visualization montage can then be chosen. In a referential montage, the potential in each electrode is compared to that of a single electrode, the common reference. In common averaged reference, all the potentials of all the electrodes are averaged and used as a reference. In the bipolar montage, the potential is obtained from the difference between adjacent electrode pairs. This allows for an easier localization of focal abnormalities, and is therefore commonly used for epileptic spike identification.

2.2.2 *Intracranial EEG recording*

During the pre-surgical evaluation of some patients with intractable epilepsy, intracranial EEG is recorded using surgically implanted electrodes. The main objective of intracranial EEG is to obtain a precise localization of the seizure onset zone and to tailor surgical resection to include all the regions suspected to produce seizures, while sparing eloquent regions.

There are three types of invasive electrodes: epidural, subdural, and depth electrodes (Figure 2.6). Epidural electrodes are pegs in direct contact with the dura. Subdural electrodes are grids or strips placed under the dura, over the surface of the brain. There are sometimes referred as electrocorticography (ECoG), even though the term was originally coined to refer only to intraoperative cortical recordings. Intracerebral depth electrodes are needle like electrodes inserted inside the brain. Since the electrodes are implanted stereotactically into deep regions of the brain, StereoElectroEncephaloGraphy (SEEG) is a common term for depth recordings.

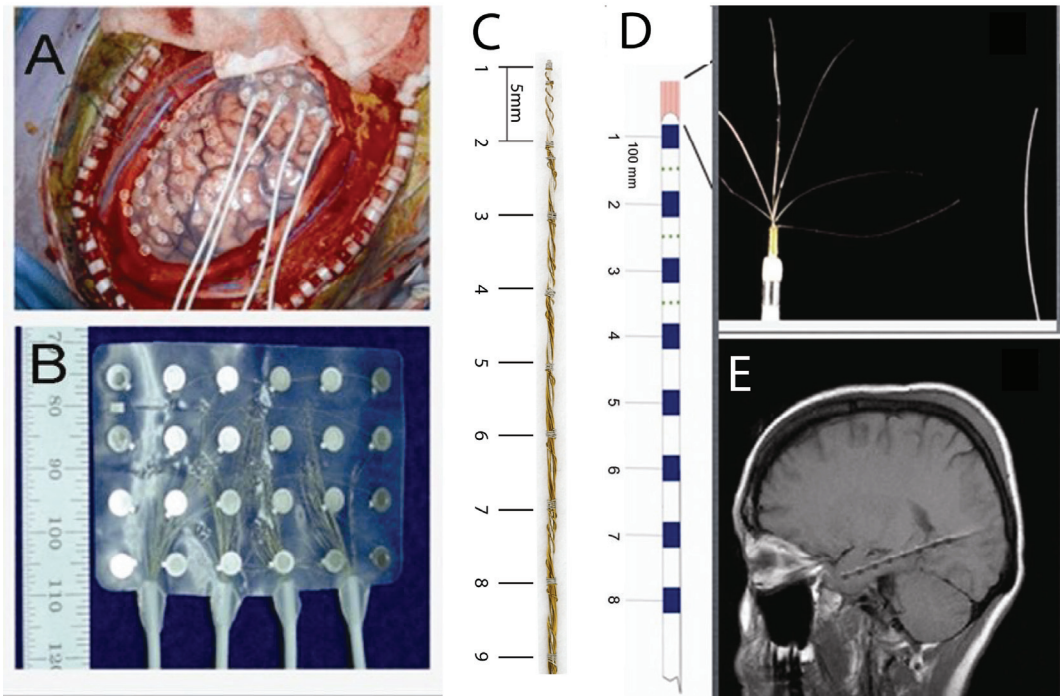

Figure 2.6. Different types of intracranial electrodes. A) Implantation of subdural grid. B) Dimensions of subdural silastic grid. C) Depth macroelectrodes fabricated on site at the Montreal Neurological Hospital. D) Depth electrode with bundle of microelectrodes at the tip of a macroelectrode. E) Post-implantation MRI shows the trace of a depth electrode. Modified from (Worrell *et al.,* 2012).

A critical advantage of intracranial over non-invasive recordings is the possibility to reach deep regions (such as amygdala and hippocampus), which cannot be recorded on the scalp since the generators are small or are not arranged perpendicular to the surface (Wennberg *et al.,* 2011). Invasive recordings have also several advantages in terms of quality of recording over scalp EEG. The

amplitude is larger than for scalp, because there is no attenuation due to the skull; there is no spatial smearing, since the signal is recorded within the closed head volume; and the spatial resolution is better than on scalp recordings. Invasive approaches are not as vulnerable as the scalp EEG to most of the physiological artefacts, such as ocular and muscular. However, blinking affects frontal subdural recordings (Ball *et al.,* 2009) and muscular artefacts during seizures also appear in intracranial recordings (Otsubo *et al.,* 2008). For more details on artefacts see section "2.5.Artefacts in the EEG".

Intracranial EEG has also limitations. As the amount of recording sites is limited, several brain regions remain unexplored. This restricted spatial sampling could result in missing the epileptic focus. In particular, depth electrodes only record from sources near the electrodes. Grids only cover parts of the cortex and could suffer from spatial aliasing (Nunez and Srinivasan 2006). When analyzing intracranial EEG recordings it is important to remember that one is only looking where the electrodes are, but there might be activity coming from other regions. Thus, appropriately planning the location of the electrodes is critical for the success of the investigation.

Electrode size and implantation technique vary from centre to centre. Depth electrodes consist of metallic contacts distributed along a flexible or rigid wire. In commercial depth electrodes, the area of the contacts is 3-10mm^2. At the Montreal Neurological Hospital (MNH) some of the electrodes used are fabricated on-site and consist of nine contacts 5mm apart from each other, with an effective surface area of 0.85mm^2 for the tip and 0.8mm^2 for the other contacts (Figure 2.6.C). The data presented in chapters 5 and 6 was recorded with MNH macroelectrodes. Clinical depth electrodes with a bundle of micro contacts (40μm) exiting the tip (Figure 2.6.D) are used by the UCLA group to record HFOs in the hippocampus (e.g. Bragin *et al.,* 1999b, Staba *et al.,* 2002). Clinical subdural grids and strips are composed by a silastic grid and disc shape electrodes of 4-5mm^2 (Figure 2.6.B). Data in chapter 7 were recorded with grids and strips.

The implantation of grids requires a craniotomy, while strips and depth electrodes can be inserted through burr holes. Epidural pegs are minimally invasively placed. Complications related with the surgery, although rare, may occur during implantation and removal of the electrodes.

The decision on placing one or another type of electrode depends on the question that the intracranial investigation is trying to answer and the expertise of each centre (Kahane and Dubeau in press). For instance, depth electrodes allow for good sampling of deep areas such the hippocampus, the amygdala, and the insula. Subdural electrodes have a larger coverage and are especially suitable when a focus in the cortical convexity is suspected or when a large area needs to be investigated. Different types of intracranial electrodes are sometimes combined.

2.2.3 *Intracranial correlates of scalp EEG recordings*

As explained above, not only attenuation but also location, orientation, relative synchrony, and cortical extent of the source determine whether intracranial activity is visible on the scalp. From simultaneous scalp and intracranial EEG recordings the intracranial correlates of scalp EEG can be studied. A cortical area of at least 6cm^2 was originally suggested to be necessary for an epileptic spike to be seen on scalp (Cooper *et al.,* 1965). Recently, this value was further increased to a cortical area of at least 10cm^2 (Tao *et al.,* 2007). Even though the most prominent scalp spikes were associated with about 20cm^2 of temporally overlapping cortical activation, cortical spikes of smaller extent can be recorded on the scalp (Tao *et al.,* 2007). A computational model of EEG generation also suggests that a large cortical region must be active to observe activity on the scalp (Cosandier-Rimele *et al.,* 2008). Moreover, only when at least 8-15 subdural electrodes (8-15cm^2) are active in the lateral cortex, a seizure could be observed on the scalp (Hashiguchi *et al.,* 2007). Not only the spatial extent, but also a good degree of phase synchronization was important.

This commonly accepted spatial extent of several square centimetres needed to observe an event non-invasively was obtained in all cases from unfiltered recordings. However, it has not been evaluated for higher frequency ranges in which the noise characteristics may be different. In chapter 7, we present a study on the cortical correlates of scalp HFOs.

When performing simultaneous recordings, there is an additional risk of infection involved in having electrodes attached to the scalp at the same time as intracranial electrodes. Technical limitations of simultaneous recordings include the breach effect associated with the skull defect created after implantation (see also section "2.3.2.Conductivity of scalp, skull, and brain") and the attenuation effect of the silastic membrane holding the electrodes when using subdural grids (Tao *et al.,* 2007). The former, however, does not seem to avoid the propagation of spikes and is probably small compared to skull impedance. If attenuation takes place it should have a similar effect on the background, thus maintaining the signal to noise ratio.

Only activity from the neocortex relatively close to the skull can be recorded on the scalp. Alarcon estimated the intensity of a source in deep hippocampal structures of about 2nA.m and showed that such a source could not be visible on subdural or scalp contacts given the distance and attenuation (Alarcon *et al.,* 1994). In line with this, it has been recently demonstrated that scalp visible spikes in mesial temporal lobe epilepsy arise from the lateral temporal neocortex without involvement or propagation from the hippocampus (Wennberg *et al.,* 2011). In addition, when ictal activity was confined to deep structures, it was not visible on the scalp regardless of the signal amplitude (Hashiguchi *et al.,* 2007). From a volume conduction perspective, given the geometry of the hippocampus, it can approximate a closed field, limiting the spread of potential outside its boundaries (Nunez and Srinivasan 2006).

Projecting the location of scalp electrodes over the surface of the brain can help understanding from which areas we are recording or stimulating. This

analysis enables a better understanding of the underlying cortical generators and the variability in the recordings from different areas. Methods for the 10-20 system (Okamoto *et al.,* 2004, Towle *et al.,* 1993) and 10-10 system exist (Koessler *et al.,* 2009). This is important not only to better understand the correlates of scalp recordings, but also to better target non-invasive brain stimulation, such as transcranial magnetic stimulation.

In addition to simultaneous scalp and intracranial recordings, recently subdermal electrodes (Ives 2005), which are placed under the skin, have been inserted during intracranial investigations. Due to the low invasiveness and low risk of infection, they can be safely placed at the end of the surgical implantation of intracranial electrodes. At the MNH implantation of subdermal electrodes in patients started in 2010. Subdermal electrodes provide an excellent sleep staging method during the full two weeks recording (Jacobs *et al.,* 2010a). The most important advantage of subdermal over scalp simultaneous recordings is probably in terms of stability. Subdermal electrodes allow high quality recording for the extent of the implantation, while quality of simultaneously scalp recording deteriorates after the first day (since impedance highly depends on good contact, but re-gluing the scalp electrodes implies an extra risk of infection). Subdermal electrodes can provide an advantage in terms of artefacts, likely because the impedance is stable and similar in all contacts during all the recording period (Young *et al.,* 2006).

2.3 *Finding the generator of scalp EEG activity*

Finding the underlying cortical sources that generate a scalp EEG pattern is an underdetermined problem (Helmholtz 1853). The EEG obtained at tenths or at most hundreds of sensors located on the scalp can originate from different combinations of amplitude, size, orientation, and location within the 3D volume of the brain. In order to provide realistic constrains to obtain a likely estimate of the source in this ill posed problem, it is important to understand the physical

characteristics of the brain, skull, and scalp. Moreover, it is important to understand the limitations and assumptions of the inverse solutions.

2.3.1 *The skull is purely resistive*

An important characteristic of the skull that for some reason is sometimes wrongly considered (e.g. Burgess 2003) is the fact that the skull is purely resistive at the frequencies of interest (Oostendorp *et al.,* 2000, Tang *et al.,* 2008).

Gabriel and colleagues (2009) reviewed the literature and conducted a well-controlled experiment in small pigs measuring the conductivity from 10Hz to 1MHz. They showed that the skull conductivity is practically constant up to at least 10kHz (Gabriel *et al.,* 2009). The skull is mainly composed of three layers: inner compact bone, diploe, and outer compact bone. Due mainly to variations in diploe, different skull locations result in different conductivities. In an impressive study, Tang and colleagues computed the conductivity of 388 skull samples obtained from 48 patients (Tang *et al.,* 2008). Because skull flaps were obtained directly from surgery, they maintained their normal fluid filling. Temperature was controlled to approach an *in vivo* setting. The conductivity varied considerably for different skull structures, and remained constant for each from 1Hz to 10kHz (Figure 2.7). For higher frequencies, the resistivity increased dramatically. Using stimulation in humans, the skull was also found to be purely resistive, since the stimulated squared pulse maintained its shape between of 10Hz to at least 1kHz (Oostendorp *et al.,* 2000).

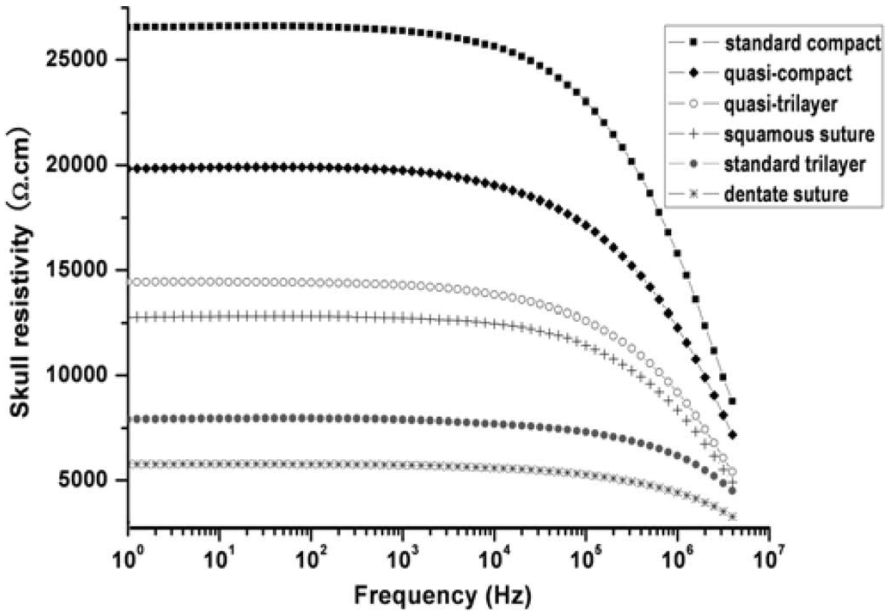

Figure 2.7. Resistivity of the skull from 1Hz to 4MHz. Skull samples with different structures have different resistivities, but each one is stable from 1Hz to 10kHz. Skull samples are divided based on the percentage of diploe to compact bone. For instance, standard compact refers to pure compact bone without any diploe while standard trilayer corresponds to a large percentage of diploe thickness. Squamous and dentate sutures are samples of skull where bone joints are found (from: Tang *et al.,* 2008).

The conductivity of every type of tissue is modified when exposed to high frequencies (Gabriel *et al.,* 2009). In the case of skull, conductivity starts to change at about 100kHz. This change also occurs for brain tissue and is even more dramatic for skin's conductivity, which changes linearly above 100kHz (Gabriel *et al.,* 2009). This is of concern for the exposure to RF frequency but not for the analysis of EEG activity since the skull is purely resistive at the frequencies of interest for clinical or cognitive research.

2.3.2 *Conductivity of scalp, skull, and brain*

Obtaining a reliable measure of the conductivity of the scalp, skull, and brain is fundamental to obtain an accurate forward model. A common and reasonable assumption is that the scalp and the brain are highly conductive, since they are soft tissue, and have similar conductivity values (about 0.3 S/m). Since the conductivity ratio between layers is sufficient to compute the forward model, the conductivity ratio between skull and brain is usually reported and will be the focus of this section.

The first study measured the conductivity of a human half-skull in an electrolytic tank (Rush and Driscoll 1968). They found a skull to brain conductivity ratio of 1/80. Importantly, they indicated that the variability in skull thickness affects the local conductivity and their results were independent of frequency in the range 50Hz-5kHz. Since then, the ratio of 1/80 has been widely adopted. Indeed, even though at this point it is known that this value is too high, 1:1/80:1 is the default in most software packages that compute the EEG forward and inverse problems (e.g. *OpenMEEG* (Gramfort *et al.,* 2010, Kybic *et al.,* 2005); *NFT* (Acar and Makeig 2010)).

In an elegant study, Oostendorp and colleagues challenged this value. They measured the conductivity of a fresh skull placed in a saline bath. In addition, the potential distribution on the scalp on two subjects was measured after stimulating with a small current between two scalp contacts. Both the *in vitro* and the *in vivo* experiments revealed a skull conductivity of 0.015S/m. They estimated the conductivity ratio as 1:1/15:1 (resistivity ratio range in vivo for all measurements: 13:21)(Oostendorp *et al.,* 2000). If considering 0.3S/m as the brain conductivity, the ratio is increased to 1/20.

Following this experiment that challenged the traditional value, a number of studies continued to investigate this question using different techniques. For instance, Lai and colleagues (2005) stimulated subdural contacts and recorded on the scalp in five pediatric patients with epilepsy implanted during their pre-surgical evaluation. They found that the resistivity ratio was 25 +/- 7 (range: 18-34) (Lai *et al.,* 2005). The adult's skull has a harder consistency than the child's skull, resulting in a lower conductivity (Peyman *et al.,* 2007) and this relation varies linearly with age (Hoekema *et al.,* 2003). In agreement with this, a ratio of 20-50 in six adult subjects was reported using electric impedance tomography (Goncalves *et al.,* 2003). Moreover, a simulation study showed that using a brain-to-skull conductivity ratio of 15-25 produced better localization accuracy than a ratio of 80 (Wang *et al.,* 2009). Based on these studies, we decided to use a conductivity ratio of 1:1/25:1 in our simulations (Chapter 7).

Even though the different tissues are usually considered homogenous, different regions and directions have distinct conductivity. An important aspect to generate accurate models of the head is to consider the anisotropy of the skull and the brain. In the case of the brain, the average conductivity is about 0.3S/m (0.33S/m in (Goncalves *et al.,* 2003); 0.29S/m for white matter and 0.26S/m for grey matter in (Latikka *et al.,* 2001)). Grey matter can be considered homogeneous, but the anisotropy of white matter gives a conductivity difference of ~10 between the longitudinal and cross sectional directions (Nicholson 1965). In the case of the skull, the local conductivity is highly related to the bone's local structure. The 3 layers of the skull have different properties, with the middle layer having much smaller conductivity than the external layers (Akhtari *et al.,* 2002). The conductivity linearly decreases with bone thickness (Law 1993), and this in turn is related to the proportion of diploe component (Tang *et al.,* 2008), which is the middle layer composed of spongy bone. The presence of suture lines results in an increase of local conductivity, since they are filled with cartilages and fluids (Law 1993, Tang *et al.,* 2008). The cerebrospinal fluid (CSF), which has a conductivity of about 1.5 S/m (Gabriel *et al.,* 2009), is stable across subjects and can also be included in the head model.

Skull holes alter the electrical signal recorded on the scalp (Heasman *et al.,* 2002). Burr holes created during surgery produce a large localization error, particularly for radial dipoles below the hole and tangential dipoles at the edges of the hole (Bénar and Gotman 2002, Li *et al.,* 2007). When filling the burr holes with methacrylate, which is commonly done after implantation, the localization error is reduced (Bénar and Gotman 2002).

Given the variability across subjects and within an individual's head, a non-invasive method to obtain the conductivity ratios should be ideally used prior to the calculation of the forward model. Electric impedance tomography is an interesting possibility (Goncalves *et al.,* 2003), but requires an independent session and equipment. Recently, Lew and colleagues (Lew *et al.,* 2009) proposed

a method to estimate the scalp to skull conductivity ratio based on the MRI of the subject and evoked potential data with high signal to noise ratio.

2.3.3 *Forward model*

The goal of a forward model in the context of the localization of neuronal sources is to determine the potential field on the scalp that result from the primary current sources in the brain (Mosher *et al.,* 1999). The quasi-static approximation of Maxwell equations holds in the frequencies of interest (Plonsey and Heppner 1967) allowing to consider the electric field independent of the magnetic field and therefore to neglect all the time derivatives. The scalp-air interface acts as a perfect insulator, making the head a closed volume of electric propagation. Thus, using this boundary condition for the quasi-static electric field, results in a simplified expression that relates the potential to the primary current source, the conductivity of the tissue, and the distance to the electrodes.

The forward model represents a linear relation between the sources and the recording electrodes. The forward problem is well posed, since for a given dipolar source of known intensity, location, and orientation, the resulting potential on the scalp is unique. There are three types of forward models depending on the complexity of the method chosen to represent the head.

In geometrical models, the head is represented as spheres of different conductivities. In particular, 3-layer models represent the scalp, skull, and brain as concentric spheres each with constant conductivity (Figure 2.8.A; (Rush and Driscoll 1968). As the skull is purely resistive, the potential on the scalp depends solely on the amplitude and location of the sources and on the thickness and conductivity of the layers. Under these assumptions, analytical methods can be derived, making this approach computationally appealing. These simple models usually work well in the central and parietal regions, since they are well represented by spheres, but fail to represent occipital or temporal areas.

Boundary element methods (BEM) compute the surface potentials at the boundaries between isotropic regions. A head mesh is obtained by tessellating the scalp, the inner and outer layers of the skull, and the brain surfaces (Figure 2.8.B). When the surfaces are obtained based on the MRI of each subject, they can provide an accurate representation of each compartment's shape. The accuracy depends on the size of the triangles used to generate the surfaces. The surfaces are considered as piecewise constant conductivity fields and the potential at the surface is obtained. A constraint is that each surface is considered homogenous and isotropic. Another constraint is that the sources are perpendicular to the surface. In particular, *OpenMEEG* (Gramfort *et al.,* 2010, Kybic *et al.,* 2005); used in the simulations in chapter 7) implements a symmetric BEM which has the advantage of reducing the error for sources close to the boundaries (Kybic *et al.,* 2005) and has better accuracy than other BEM solvers (Gramfort *et al.,* 2010).

Finite element methods (FEM; (Wolters *et al.,* 2006) and finite difference methods (FDM; (Kauppinen *et al.,* 1999) can represent the full complexity of the volume. Thus, a potential at any point of the volume can be obtained. The anisotropy of the skull and white matter can be therefore considered. For instance, diffusion tensor imaging could be used to incorporate white matter anisotropy into the model (Figure 2.8.C; (Wolters *et al.,* 2006). However, FEM and FDM are computationally very expensive. Figure 2.8 presents an example of each type of model.

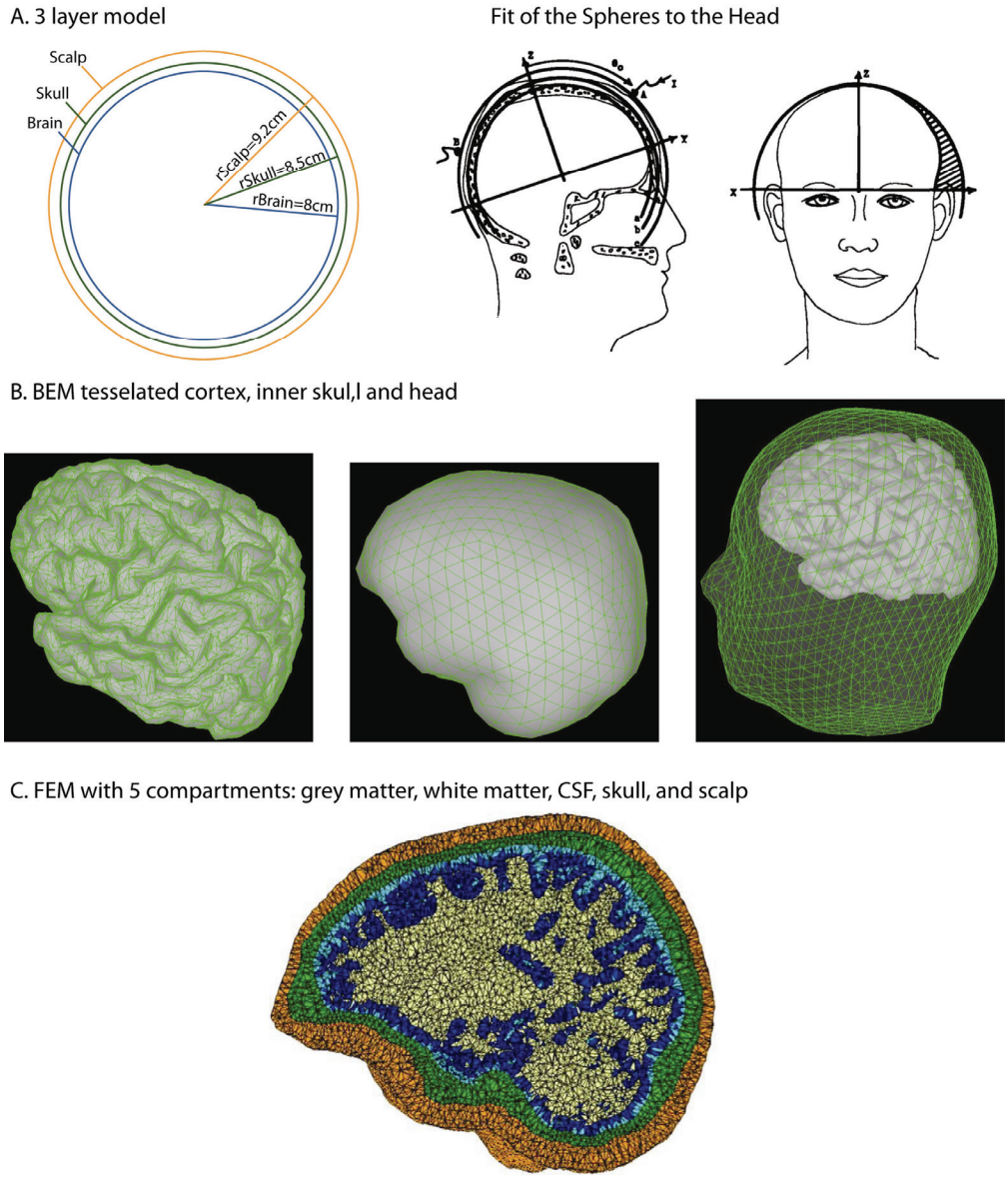

Figure 2.8. Head Models. A) 3-Layer concentric spherical model and fit of the model to the head (from: Rush and Driscoll 1968). B) Boundary element model (created using Brainstorm). C) Finite element model with white matter anisotropy. From: (Wolters *et al.,* 2006).

The intensity of a source in the cortex is estimated in the 2nA.m (Alarcon *et al.,* 1994) to 10nA.m range (Baillet *et al.,* 2001, Hämäläinen *et al.,* 1993). Thus, 5nA.m was chosen in our simulations as the intensity of the distributed sources (Chapter 7). The forward model is useful to create simulations to analyze potential profiles (as presented in Chapter 7) and is a necessary tool for the computation of the inverse problem.

2.3.4 *Inverse problem*

The inverse problem can be summarized as follows: Given measurements on the scalp, localize the region that most likely generates these potentials and estimate its extent and the corresponding current intensities. The inverse problem does not have a unique solution since an infinite number of different generators in the volume conductor could give rise to the potential distribution observed on the scalp (Helmholtz 1853).

Thus, to find a unique suitable solution in this underdetermined problem, constrains must be applied. A priori assumptions can be physical, physiological, functional, or mathematical. Algorithms to solve the inverse problem assume one or several of these constrains. They can be broadly divided in whether the sources are considered as few equivalent dipoles, or a large number of dipoles distributed on the cortical surface (Baillet *et al.,* 2001). The concept of the sources represented as dipolar layers arise from the macrocolumns of pyramidal cells simultaneously active, as explained above. In dipolar models, the mathematical simplification is to consider a single point dipole representing the overall activity generated in a region.

Since dipolar models assume that a small number of dipoles (fewer than the number of measurements) can represent the underlying brain activity, the problem becomes overdetermined. In general the idea is to place a few dipoles in the brain, apply the forward model to obtain the resulting scalp potential based on them, and compute the difference with the real scalp potential. Iterating this procedure provides the solution with minimum difference from reality, the best fitting dipolar configuration (usually in least square sense). Optimization techniques could result in incorrect local minima solutions (de Peralta Menendez and Gonzalez Andino 1994). This could be overcome by considering the dipolar sources as having fix location with varying time and estimating their locations from the whole interval (Scherg *et al.,* 1999) or with scanning techniques. Beamforming approaches (Van Veen *et al.,* 1997) act as a spatial filter to find regions of interest (i.e. where the signal might have originated). Thus, the sources

are found by evaluating the contribution of a particular brain location to the recordings, while ignoring all other brain regions. Multiple signal classification (MUSIC; Mosher *et al.,* 1992) is based on scanning with a single dipole the whole head and projecting into a signal subspace (obtained from eigenvalue decomposition of the data). The locations with the best projections are selected (Mosher *et al.,* 1992). Dipolar methods have been widely used, although careful interpretation of the results is needed since they may produce misleading localization, especially for spatially large extended sources (Kobayashi *et al.,* 2005). Interestingly, a software for dipole source localization recently obtained FDA approval (Elekta-Neuromag, Oy, Helsinki, Finland).

Distributed algorithms assume a large number of sources situated along the cortical surface, which implies an anatomical constraint. These distributed sources are considered to represent activity from pyramidal neurons oriented parallel to each other and perpendicular to the surface (Dale and Sereno 1993). Within this group, the minimum norm (MN) method finds the source distribution with minimum energy (Hämäläinen and Ilmoniemi 1994) while low-resolution brain electromagnetic tomography (LORETA) obtains the smoothest sources distribution with a generalized minimum-norm estimate (Pascual-Marqui *et al.,* 1994). Bayesian approaches introduce anatomical and temporal smoothness constraints a priori to obtain the a posteriori estimate of the sources (Baillet and Garnero 1997).

Hybrid combinations of dipolar and distributed algorithms have been proposed (Baillet *et al.,* 2001). In addition, other functional constraints, such as defining the number of dipoles based on PET (Michel *et al.,* 2004) or weighting the sources based on EEG/fMRI activations (Liu *et al.,* 1998), can be incorporated. Moreover, comparing different sources localization models and allowing the data to decide which one is the most appropriate has been developed within a Bayesian framework (Daunizeau *et al.,* 2006). This idea of model selection has also been applied to assess from the data the relevance of several forward models (Henson *et al.,* 2009). Not only finding the central point of a

source is important, but also accurately estimating the extent of the source. In this regard, a comparison between different inverse models showed that distributed models could estimate extended sources (Grova *et al.,* 2006). Moreover, the authors proposed that a combination of models could result in improved accuracy (Grova *et al.,* 2006).

The inverse problem in epilepsy has been traditionally performed on averaged spike activity to obtain a good SNR. However, independent spikes may arise from slightly different locations and orientations. Recently a method to apply the inverse problem to individual events has been proposed (Poolman *et al.,* 2008). In addition, seizure initiation (when not heavily contaminated by muscle artefact) could be localized (Merlet and Gotman 2001). Recently a method has been developed to apply the inverse problem to oscillatory activity (Lina *et al.,* 2012). This could be useful for the application of the inverse problem to scalp HFO recordings.

Source localization can be clinically useful. For instance, it can help to focus the analysis of anatomical images leading to the identification of regions with subtle cortical abnormalities such as dysplasias (Ebersole 2009). A large prospective study (152 patients) showed the possible value of source localization as part of the pre-surgical evaluation for epilepsy surgery (Brodbeck *et al.,* 2011). The sensitivity to locate the focus within the removed area was 84% with a specificity of 88% (Brodbeck *et al.,* 2011).

2.4 *Normal physiological EEG patterns*

The normal EEG can be defined as simply the absence of identifiable abnormalities, since there is no single feature that characterizes the normal EEG (Chang *et al.,* 2011). Importantly, normal EEG activity reacts to different situations and stimuli presenting characteristic patterns of oscillations or rhythms.

The first rhythm to be identified in humans was the alpha rhythm (8-13Hz; Berger 1929). The alpha rhythm has maximum amplitude in the occipital lobe and

it is best seen during wakefulness with the eyes closed; eye opening suppresses the alpha rhythm (Figure 2.9.A).

Central mu rhythm (8-12Hz) and beta activity (13-25Hz) over the sensorimotor area contralateral to the side of movement are reduced during movement execution (Jasper and Penfield 1949). Even though mu and alpha rhythms occur in the same frequency band, there are considered distinct rhythms since they react differently (Figure 2.9.B). After the movement finishes, there is a fast short lasting beta band increase over the side contra-lateral to the movement. A voluntary motor response elicits also a slow time-locked and phase-locked event-related response (MRP; <4Hz).

Theta band activity (4-7Hz) is largely observed in the hippocampus. It has been linked to temporal encoding and retrieval; episodic and working memory; and long-term plasticity (Buzsáki 2002, Hasselmo 2005).

Gamma activity (30-80Hz) seems related to information binding. Details on cognitive activity in gamma and ripple (80-200Hz) bands will be given in chapter 4, section "4.2.Physiological HFOs".

Different sleep stages are characterized by particular EEG activity (Chang *et al.,* 2011). The transition between stages varies with age. In adults, the onset of drowsiness (stage 1) is characterized by the replacement of alpha with low-voltage slow activity. As drowsiness gets deeper vertex sharp waves appear over the midline. During stage 2, the background slows; sleep spindles and K-complexes appear, with maximum over the vertex (Figure 2.9.C). K-complexes are evoked by external stimuli and are therefore considered as micro-arousal states. As sleep deepens, slow activity, particularly delta (1-3Hz), increases in amplitude and becomes more frontal. Indeed, increase in delta power is a common measure of slow wave sleep (stages 3 & 4), especially in the absence of EOG and EMG information. Finally, REM sleep consists of low voltage polyrhythmic activity with periods of alpha waves. During REM ocular artefacts are observed.

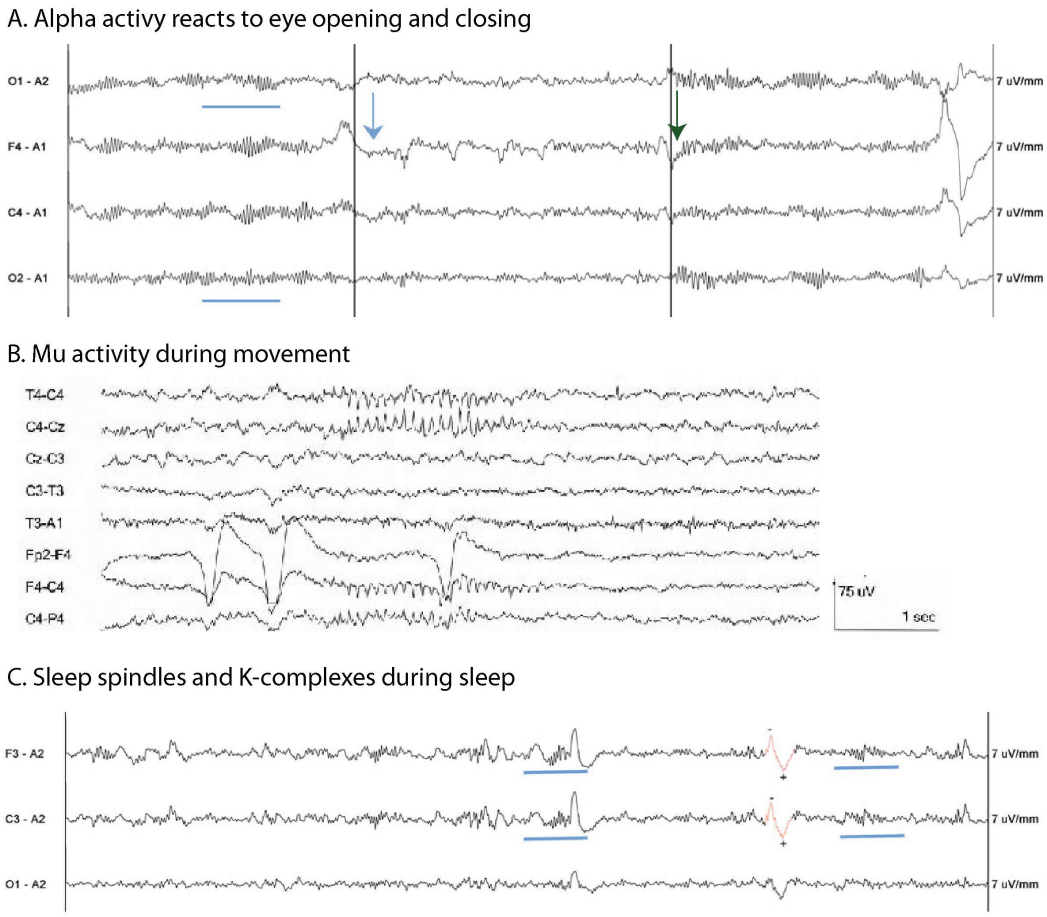

Figure 2.9. Examples of normal EEG recorded on the scalp. A) Alpha rhythm during eye opening and closing. Alpha rhythm is indicated by blue line; blue arrow indicates eyes opening; green arrow indicates eyes closing. B) Mu activity in central region (from: Stern and Engel 2004). C) Sleep spindles and K-complex. Spindles are indicated by blue lines; K-complexes are shown in red. A and C modified from (Attarian and Undevia 2012).

The ability to record normal brain activity with intracranial electrodes is limited by the location of the electrodes. All normal brain rhythms observed on the scalp can be recorded with intracranial electrodes (Kahane and Dubeau in press). Compared to scalp rhythms, the amplitude of intracranial rhythms is larger; the morphology is usually sharper, in part because there is no smearing but also because it is modified depending on the proximity to the source. Figure 2.10 illustrates an example of alpha activity recorded by depth electrodes located in the occipital lobe. Almost each patient implanted with intracranial EEG electrodes is a unique case. Thus, to robustly identify epileptiform discharges it is important to first get familiar with the normal background activity of the recordings.

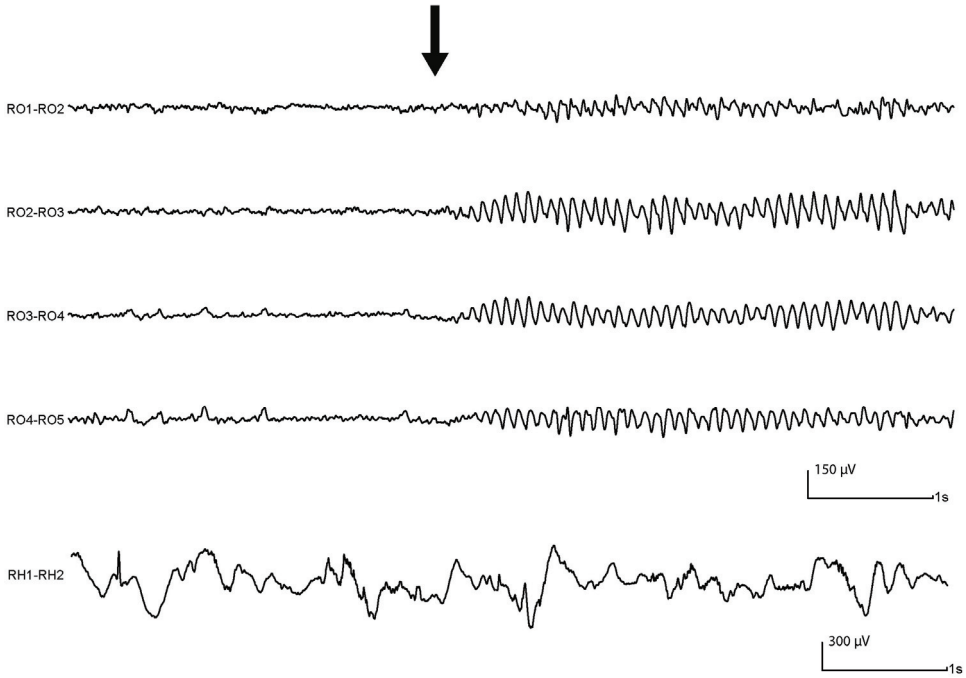

Figure 2.10. Normal Alpha activity recorded with depth electrodes. Reactivity to eye opening and closing (indicated by black arrow) is evident in the occipital electrodes (RO). No changes in background activity are observed in the hippocampus at the same time (RH). From (Melani *et al.,* in press).

Even though intracranial electrodes are solely implanted to obtain clinical information, cognitive research can take advantage of the fact that patients remain in the hospital for days waiting for their seizures to occur. In recent years, a large body of knowledge on gamma activity has been obtained from intracranial recordings. This will be described in chapter 4, section "4.2.Physiological HFOs".

2.5 *Artefacts in the EEG*

Since the signal of interest is the electrical activity of the brain, any other signal, regardless of whether it is physiological or environmental, is considered noise and as a consequence must be dealt with. Artefacts can therefore be of external origin or originate in the person's body.

Non-physiological noise can arise from the instrumentation or from the environment (Dworetzky *et al.,* 2011). The electrodes, the amplifier, or the wires can produce instrumentation noise. For instance, movement of the head or body can induce artefacts due to the movement of the electrode wire; changes in the

contact between an electrode and the scalp, results in low impedance. Environmental noise includes 50/60Hz contamination; electromagnetic artefacts from hospital equipment; and glitches from electric stimulators, such as pacemakers (Dworetzky *et al.,* 2011).

Several types of physiological artefacts affect the scalp EEG (Figure 2.11), mainly cardiac, respiratory, muscular (EMG), and ocular (EOG). Cardiac artefacts produce rhythmic activity synchronized with heartbeat. Respiratory movements produce slow fluctuations. EMG activity has a wide frequency range, maximal at frequencies higher than 30Hz and usually larger amplitude than the EEG signal. Chewing, swallowing, and contracting the jaws produce muscular artefacts mostly on temporal contacts. Contraction of facial muscles induces activity that contaminates the temporal and frontal electrodes. Seizures that involve movements produce large EMG activity that obscures the concomitant EEG. Blinking is characterized by high–amplitude signals maximally recorded at frontopolar electrodes. Eye movements introduces low-frequency (<4Hz) high-amplitude signal recorded mostly in frontopolar electrodes. Lateral eye movement is observed in the lateral frontal regions. Eye movements in particular are important in cognitive science, since they can be locked to the activity under investigation (Figure 2.11.D) and can be mistakenly considered as cognitive activity (Yuval-Greenberg *et al.,* 2008). In the frequency of interest for the detection of HFOs (above 80Hz), there is still contamination from EMG and EOG activity. Studies on scalp HFOs have been recorded during sleep to minimize the presence of these artefacts (as in Chapter 7, Zelmann *et al.,* submitted).

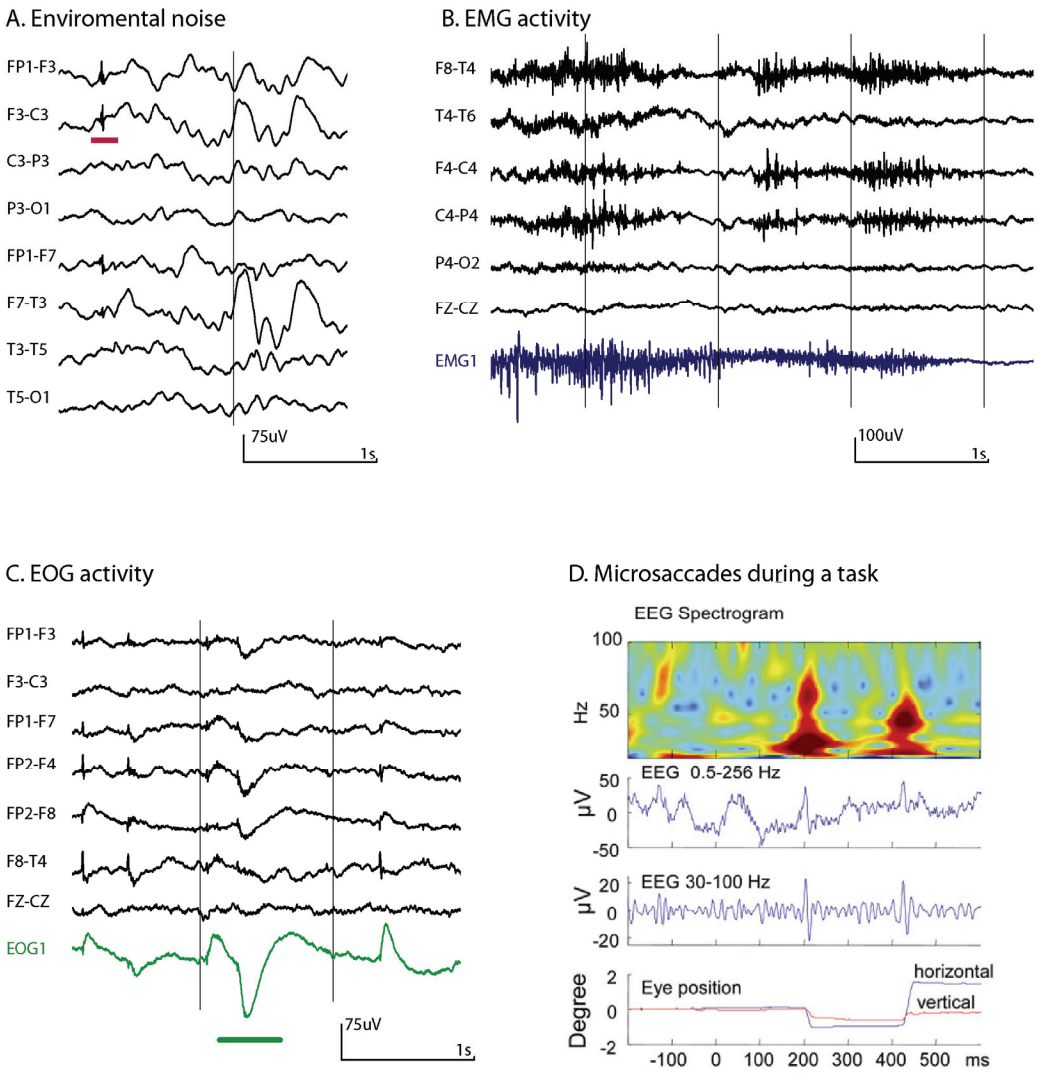

Figure 2.11. Physiological artefacts on the scalp EEG. A) Environmental noise (indicated by red line). B) EMG activity. C) EOG activity mainly recorded in Fp channels. A, B and C are recordings from the same patient as in Figure 7.1. D) Gamma activity induced by microsaccades should not be confused with cognitive activity (from: Yuval-Greenberg *et al.,* 2008).

Intracranial EEG is affected to a lesser extent by these artefacts, but nevertheless the effects of artefacts must be considered. The same way that electrical activity from the brain travels outwards and reaches the scalp, EMG and EOG activity can travel inwards from the muscles and the eyes to the brain. EMG can therefore be recorded with intracranial EEG, particularly during seizures (Otsubo *et al.,* 2008). Blinking as well can be recorded, prominently over the anterior part of the brain (Ball *et al.,* 2009). Eye movement also produces activity on structures near the extraocular muscles that can be recorded with depth

electrodes (Jerbi *et al.,* 2009) and with grids (Kovach *et al.,* 2011). Even though they do not obscure the intracranial EEG signal, artefacts can be confused with brain activity.

Chapter 3. *Epilepsy*

Epilepsy affects 5.2-5.6/1000 Canadians (Tellez-Zenteno et al., 2004), being the second most common neurological disease, after stroke. Epilepsy incidence is highest in children below 5 years old and in the elderly, but it can manifest itself at any point in life. Epilepsy is as old as humankind. There are reports of focal epilepsy from more than 3000 years ago. The high prevalence of epileptic conditions and the lifetime characteristic of the disorder make its economic burden very large. Moreover, intractable seizures, which accounts for 30% of the patients, are particularly costly compared to other chronic diseases (Theodore *et al.,* 2006).

In this chapter, possible underlying causes of epilepsy are presented; different types of epileptic seizures are described; EEG epileptic patterns are illustrated; the diagnosis and treatment options are depicted with emphasis on the pre-surgical evaluation of patients with intractable epilepsy. In addition, animal models of epilepsy are described.

3.1 *Epileptic syndromes and their classification*

A large number of brain disorders can cause epileptic seizures (Niedermeyer 2005c). Brain damage during early life is one of the most important causes. Infections of the central nervous system may be the cause of epilepsy that starts only years after. Craniocerebral trauma can cause epilepsy as a sequel of the injury, but it is important to distinguish chronic epilepsy from cases in which convulsions occur in the acute stage of the trauma. Intracranial tumours and other space occupying lesions can manifest themselves as epileptic seizures. In most of these cases focal attacks occur. Cerebrovascular accidents could be the cause of seizures not only during the event, but also at the time preceding the stroke or after the stroke due to scar formation. Genetic predisposition could facilitate the appearance of seizures, particularly in primary generalized epilepsy.

The characteristics of a seizure depend on whether parts of the brain or the entire brain get involved during the event, on the underlying basic epileptic condition, and on the age of the patient (Niedermeyer 2005c). Epileptic seizures can be broadly classified as *generalized* or *partial* seizures.

Generalized seizures include *absence* seizures, *myoclonic* seizures, *atonic* seizures, *tonic* seizures, *clonic* seizures, and *tonic-clonic* seizures (Niedermeyer 2005c). Typical *absence* seizures (traditionally called "petit mal") consist in loss or reduction of consciousness and maybe accompanied by mild clonic, tonic, or atonic components. The onset and cessation of absences is generally abrupt. Hyperventilation and photic stimulation can induce absence seizures and are useful diagnostic tools. *Myoclonic* seizures are characterized by a rapid involuntary muscle contraction (jerk). *Atonic* seizures are characterized by a sudden loss of tone and possible subsequent drop. *Tonic-clonic* seizures (also referred as "grand mal") start with a massive generalized tonic spasm, with immediate loss of consciousness; this is followed (after 10-20 seconds) by the clonic phase; then, a succession of brief and violent flexor spasms of the entire body lasting about 1minute can be observed.

Partial (focal) seizures comprise *simple partial* seizures, *complex partial* seizures, and partial seizures evolving to *secondarily generalized* seizures (Niedermeyer 2005c). *Simple partial* seizures, in which consciousness is preserved, can consist of motor, somatosensory, autonomic, or psychic signs. During *complex partial* seizures, consciousness is impaired and automatisms are usually present. Partial seizures can evolve into a secondary generalization.

The location of the focus in partial epilepsy determines the associated clinical manifestations and its related electrographic signature. Mesial temporal epilepsy is typically characterized by complex partial seizures. They usually start with an epigastric aura, followed by automatisms, and loss of consciousness. The mesial temporal lobe is particularly susceptible to seizures, but seizures can originate from anywhere in the brain. The frontal lobe accounts for about 30% of the

seizures and is prone to epilepsy developed after brain injury (Van Gompel *et al.,* 2008). Seizures originated from the central regions are usually associated with involuntary movement of the extremities and focal twitching, sometimes involving orderly propagation to adjacent parts of the body. Seizures coming from somatosensory regions are associated with paresthesia in the contralateral side, such as tingling on the face. Seizures coming from the supplementary motor area are characterized by an asymmetric change of posture of the upper extremities ("fencing" posture). Frontal lobe hypermotor seizures are associated with complex usually agitated movements. In addition, seizures generated in the occipital lobe account for 5-10% of the patients and are usually associated with primary visual phenomena or with visual hallucinations. Seizures generated in the posterior temporal neocortex are associated with auditory hallucinations or with vertigo. Insular epilepsy sometimes starts with a sensation of strangulation, followed by paresthesia around the mouth, and a complex partial seizure (Isnard *et al.,* 2004). Thalamic involvement is associated with lost of consciousness and is involved in absences.

3.2 *Epileptic EEG patterns*

In the EEG of an epileptic patient, abnormal electrical patterns can be distinguished from background. These patterns can be interictal or ictal, depending on whether clinical symptoms or signs accompany the EEG discharges. Their morphology, spatial distribution, frequency, and duration depend on the type of epilepsy, age of the patient, and level of awareness (Niedermeyer 2005a).

Interictal epileptiform discharges (IEDs), detected with scalp or intracranial recordings, can be divided in spikes, sharp waves, spike and slow wave, and polyspikes. In particular, spikes are transient sharp events that can be clearly distinguished from background activity with pointed peak and duration of 20 to 70ms. They are hypersynchronous events due to excessive simultaneous neuronal discharge (Niedermeyer 2005a). Some types of epilepsy have stereotypical IEDs and seizure patterns. However, similar etiology can result in different IEDs. For

instance, in patients with focal cortical dysplasia (FCD) spike and waves, runs of polyspikes, or sharp waves can be observed (Figure 3.1). Although great inter-subject variability exists, the IEDs are usually consistent within each patient.

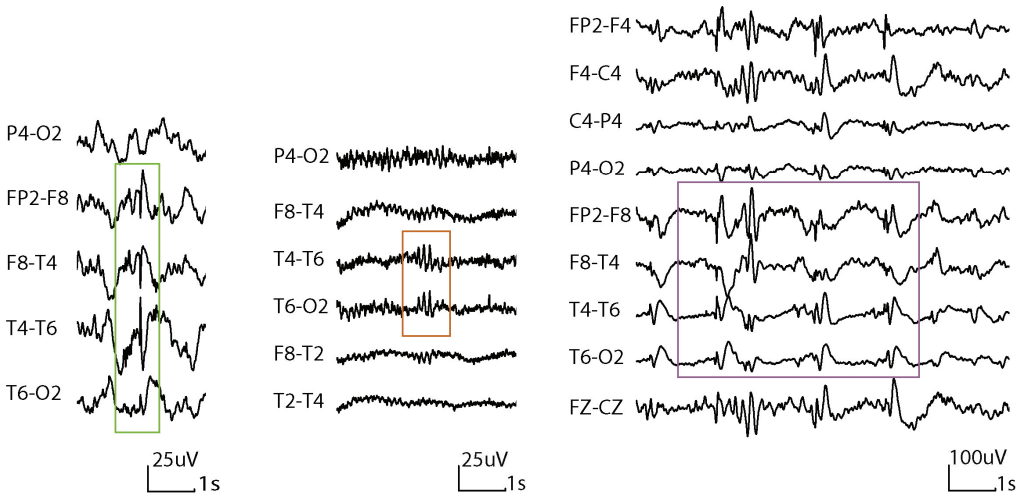

Figure 3.1. Examples of scalp interictal epileptiform discharges in 3 FCD patients.

Spikes recorded with intracerebral electrodes can have a similar morphology as in the scalp, but have usually a complex spatial distribution. There is considerable inter- and intra-subject variability in the morphology and amplitude of these discharges. When analyzing intracranial recordings, it is important to keep in mind that the absolute amplitude is not related with the severity of the underlying condition, but with the location and orientation of the generators. Figure 3.2 illustrates examples of interictal spikes recorded with depth electrodes.

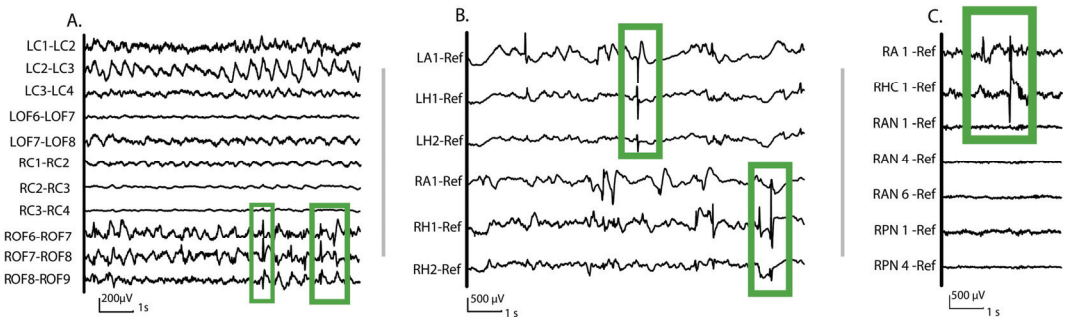

Figure 3.2. Examples of spikes recorded with intracranial depth electrodes. A) Patient with FCD displayed in bipolar montage. Note different scale than others, but same scale as Figure 3.3. B) Patient with Right Hippocampus malrotation and atrophy (referential montage). C) Patient with nodular heterotopia (referential montage). From: (Jacobs *et al.,* 2008a, Jacobs *et al.,* 2009a).

Ictal EEG patterns may be a prolongation of the habitual interictal pattern of a patient or a completely different pattern (Niedermeyer 2005a). For instance, absence epilepsy is characterized by a spike and slow wave complex at 3Hz. Short bursts are associated with interictal activity while prolong spike-wave bursts are considered an ictal event, usually accompanied by clinical manifestation such as staring. The difference between interictal and ictal events seems however arbitrary, since it may not be feasible to assess level of consciousness during events lasting a few seconds. In the case of partial seizures, the ictal pattern is most often different from the isolated interictal spikes. For instance, in mesial temporal epilepsy the interictal scalp discharges are usually anterior temporal spikes or sharp waves, but there might be a completely different ictal pattern. As explained in chapter 2, section "2.2.3.Intracranial correlates of scalp EEG recordings", spikes and seizures observed in the scalp anterior temporal channels are probably due to activity propagated to the lateral neocortex rather than generated in the mesial temporal structures. Figure 3.3 illustrates a seizure recorded with depth electrodes in humans.

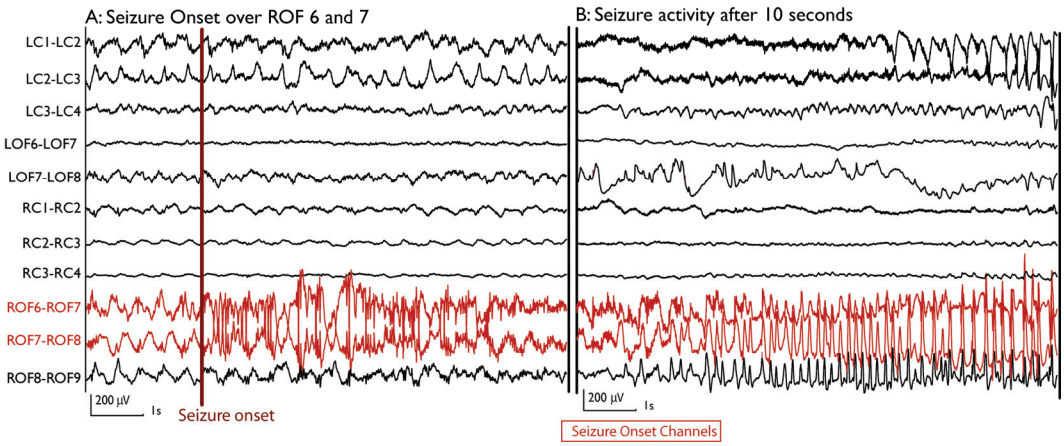

Figure 3.3. Examples of a seizure recorded with intracranial depth electrodes. A) Example of a seizure in a patient with FCD (same as in Figure 3.2.A) recorded with intracranial electrodes and visualized in bipolar montage. The channels that correspond to the seizure onset are in red. Dark red line: the time of seizure onset. B) After 10sec the seizure spreads to other contacts (LCA1-LCA2). From: (Jacobs *et al.,* 2009a).

It is important to distinguish between the *seizure onset zone* (SOZ), the *irritative zone*, the *lesional zone*, and the *epileptogenic zone*. The diagram in Figure 3.4 illustrates their possible differences and overlap. The SOZ is the region

of the brain where seizures initiate. The epileptogenic zone is a theoretical concept defined as the minimum amount of brain that must be resected to make the patient seizure free (Luders *et al.,* 2006). The epileptogenic zone cannot be identified in practice. At most when surgery is successful it is possible to affirm that the resection included the epileptogenic zone. Not only the SOZ, but also regions of early propagation or a surrounding lesion may be part of the epileptogenic zone. The irritative zone is the area of the brain that produces spikes and usually contains the SOZ, but it can have a much larger extent and may include areas where no seizures are originated. A similar situation arises from the relation between epileptogenic zone and lesions. In some cases the lesion (e.g. a tumour) is the clear cause of the patient's seizures, but not all lesions are epileptogenic and some inactive lesions could become epileptogenic (are potential foci). For instance in FCD only the tip of the lesion is visible on MRI, but the epileptogenic zone may be more extensive, while in nodular heterotopia only a few nodules (if any) are epileptogenic. Invasive recordings are usually performed to understand which of the nodules must be removed. Even though the SOZ does not always precisely localize the epileptogenic zone, which can be more extensive, localizing the SOZ is usually the goal of every investigation (Rosenow and Luders 2001). However, during the 7-15 days that a patient remains hospitalized, recording typical seizures is not always feasible, while if interictal abnormalities exist, they are more likely to be recorded (assuming correct location of electrodes).

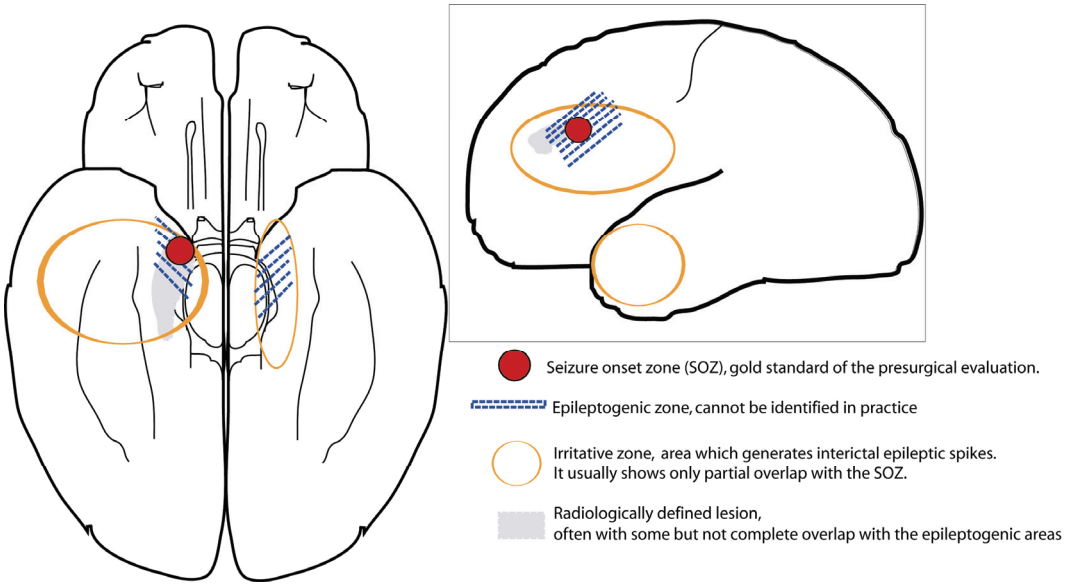

Figure 3.4. Schematic illustrating the differences and overlap between the epileptogenic zone (in blue), the seizure onset zone (in red), the lesional zone (in grey), and the irritative zone (in orange). Modified from (Jacobs *et al.,* 2012).

Recently a new EEG biomarker of epileptogenicity has been discovered. As presented in the next chapter, pathological HFOs are spontaneous events that can be observed interictally and seem to be linked directly to the epileptogenic zone.

3.3 *Diagnosis and treatment of epilepsy*

The diagnosis of epilepsy is not trivial, since a seizure is only the final manifestation of a variety of underlying causes within this heterogeneous group of syndromes. There are three basic categories of diagnosis: etiologic, seizure, and syndrome diagnosis (Chadwick *et al.,* 2008). Each of these levels must be identified for each patient. The etiologic diagnostic identifies the cause of epilepsy, which as explained above can be very different and in many cases unknown. Brain imaging is particularly useful to find an underlying lesion; genetic tests allow the identification of predisposition and familial variants; patient's clinical and pre-natal history is important to find a possible cause. Proper seizure diagnostic is achieved with EEG and video monitoring. The patient's and family description is not always accurate, particularly for nocturnal seizures. In addition, some patients have more than one type of seizures. Routine EEG and prolonged video EEG monitoring are necessary to obtain a complete idea of the

interictal and ictal activity. The syndrome is diagnosed based on seizure semiology, clinical history, EEG, and anatomical MRI. Diagnosing the syndrome allows categorization and therefore provides a framework for therapeutic options, prognosis, and duration of therapy.

Based on a careful diagnosis a correct treatment can be followed. Treatment should be focused in the improvement of the health-related quality of life of the patient rather than only in stopping the seizures (Chadwick *et al.,* 2008). Usually achieving seizure control, improves patient's quality of life, but the ideal "no seizures, no side-effects" is not feasible to achieve. In some cases, side effects from antiepileptic drugs (AEDs) could result in a worse burden than the seizures and permanent cognitive damage after surgical resection could have seriously disabling effects. Thus, physical, mental, and social health, rather than only treating seizures should be considered.

More than two thirds of the patients (~70%) with epileptic seizures can be successfully treated with medication. AEDs act on different mechanisms. AEDs could work on voltage-dependent ion channels, mainly Na^+, but also Ca^{2+} channels or on the enhancement of synaptic inhibition through GABAergic systems. Some AEDs increase inhibition of excitatory synapses, particularly glutamate receptors, while others act on the modulation of neurotransmitter release (Macdonald and Rogawski 2008). Some AEDs act on several of these mechanisms. The AED of choice depends on the epileptic syndrome, but also on gender, age, and comorbidities. For instance, in absence epilepsy a common medication is valproic acid, which is believed to act on GABA systems, and is effective in about 75% of the patients. However, valproic acid has been associated with malformations in children of treated mothers, and it should be avoided during pregnancy. Moreover, useful drugs in adults may have important adverse effects in children. For example, drugs that can successfully treat focal epilepsy in adults (e.g. carbamazepine) can make seizures, such as myoclonus or spasms, worse in children (Pellock *et al.,* 2008).

The relative efficacy is rapidly reduced with the addition of more AEDs. About half of the patients (47%) responded to the first AED, 13% more to the second AED, and only an additional 3% to three or more AEDs (Kwan and Brodie 2000). Thus, failure to two AEDs is a strong indicator of possible intractability.

3.3.1 *Intractable epilepsy*

Thirty percent of the epileptic patients are refractory to medication, meaning that these patients did not respond to two or three appropriately selected and administered AEDs. This number gives an overall estimate but the resistance to drugs is more common in certain types of epilepsy than in others.

Mesial temporal epilepsy with hippocampal sclerosis (MTS) is the most frequent type of intractable epilepsy. The onset appears in adolescence or adulthood, but it is often associated with febrile seizures during childhood. Only 11 to 25% of patients with MTS can obtain seizure freedom with AEDs (Blume 2008). MTS patients are candidates for surgery with very good prognosis (see next section).

Malformations of cortical development are other common causes of intractable epilepsy. This groups a variety of disorders that arise from disruption during the formation of the human cortex: during cell proliferation, neuronal migration, or cortex organization (Guerrini and Barba 2010). In particular, FCD originates from abnormal migration, maturation, and cell death during brain development. This results in abnormal laminar structure of the cortex, the appearance of balloon cells, and dysmorphic neurons (Guerrini and Barba 2010). Since the lesion is not usually completely visible with MRI, invasive EEG recordings are often necessary to delineate the SOZ. Seizure semiology depends on the location of the lesion. Since lesions are situated in the neocortex, FCD patients were selected to study the cortical correlates of scalp HFOs (Chapter 7). Periventricular nodular heterotopias are characterized by neurons that never migrated, remaining proximal to the lateral ventricles (Guerrini and Barba 2010).

Seizures can arise from only some of the nodules and/or from the surrounding cortex. Therefore, depth electrodes are usually implanted to define the SOZ. Polymicrogyria consists of an abnormally large number of small gyri, resulting in an irregular cortical surface (Guerrini and Barba 2010). Patients usually have intellectual disabilities and usually present a variety of clinical problems apart from seizures. Curative surgery is not usually an option for this group. FCD and nodular heterotopia patients with focal abnormalities, have usually normal cognitive capacities. Surgical prognosis in these patients is related with complete resection of the epileptogenic area and is discussed in the next section.

Cavernous malformations are vascular malformations that result in clusters of mulberry-like appearance in the brain. Seizures are present in 26-50% of the patients and originate from the surrounding tissue (Batra *et al.,* 2009). Surgical prognosis is good if enough surrounding tissue is resected (see also next section).

Patients with multifocal epilepsy or diffuse abnormalities are usually refractory to medication, but limited options currently exist for this group of patients.

3.4 *Surgical treatment of epilepsy*

For some patients with pharmaco-resistant epilepsy and a suspected focal generator, the surgical resection of the affected area can be considered. When epilepsy surgery is successful, the patient becomes seizure-free.

Surgical resection early in the course of the disorder is desirable, because in some cases the disease can progress into status epilepticus and even cause sudden unexpected death, since some seizures are related to cardiac or respiratory anomalies that can cause a cardiac arrest, and simply because of the disability caused by the seizures. Early intervention is particularly important in children for whom epilepsy can be detrimental to mental development and plasticity can minimize permanent deficits (Engel and Shewmon 1993).

Between 60 and 70% of surgical candidates are mesial temporal patients. The first temporal resection was performed by Penfield and Cole in 1928 in a patient with post-traumatic epilepsy, in which the temporal lobe showed an atrophic lesion when exposed (Feindel 1993). Surgical patients with MTS are operated with a selective amygdalo-hippocampectomy or a resection of the anterior temporal lobe. About 66% of the patients are seizure-free at five years follow-up, regardless of the procedure (Tellez-Zenteno et al., 2005). On the one hand, memory decline is reported, as expected after hippocampal resection. On the other hand, a relative improvement in general intelligence has also been reported (Chabardes *et al.,* 2011), probably due to cessation of the seizures.

A precise delineation of the epileptogenic tissue, beyond the information obtained from MRI, is important to achieve good surgical outcome in patients with malformations of cortical development. While these patients are potential candidates for surgical treatment, only 60% of suspected lesional patients achieve seizure freedom after surgery. In particular, for nodular heterotopias a focal EEG generator predicts a good outcome, regardless of the lesions (Aghakhani *et al.,* 2005). Thus, defining the area to remove within or outside the lesion is important. In FCD the prognosis is associated with the completeness of the resection (Chern *et al.,* 2010), but the complete lesion is not always visible with standard MR imaging. Moreover, for cavernous malformations the question is how much of the surroundings of the cavernoma to remove, since outcome improves with extensive resection (Kim *et al.,* 2011). For these patients, it is important to ensure the resection of areas beyond the lesion visible on MRI without extending it outside the epileptogenic zone, to preserve eloquent areas.

With the advent of new technology and knowledge in neuroscience many patients that would not have been considered candidates ten years ago, can now be considered for surgical intervention. Anatomical and functional imaging techniques can find subtle lesions and help target the implantation. Advances in neuronavigation allow the implantation in places such as the insula that were

rarely considered before. Increasing understanding of brain functions allows identifying possible sequel and avoiding eloquent areas.

3.4.1 *Pre-surgical evaluation of epilepsy*

Intracranial EEG recordings can be considered when the area to remove cannot be delineated from non-invasive recordings. In some cases, non-invasive techniques give only a rough estimate of the epileptogenic region but cannot ensure the precise location of the focus. In other cases, there is disagreement across modalities (e.g. EEG pointing to the right temporal lobe, but lesion on the left hippocampus). In others, there could be more than one possible epileptogenic region (e.g. either hippocampi or several lesions).

Before undergoing surgery, these patients are recorded with implanted electrodes (described in Chapter 2), to obtain a more accurate location of the onset of seizures and to more precisely establish the boundaries of the resection. Although the use of implanted electrodes implies a certain risk for the patient, it is small compared to the benefits that could be gained (Ebersole and Pedley 2003). The sites of implantation are determined according to the clinical history, semiology of the seizures, neuroimaging, neuropsychology, and prolonged scalp EEG information. Other factors are the avoidance of critical areas and vicinity of major arteries (Niedermeyer 2005b). Patients remain in the hospital generally during 1 or 2 weeks and are constantly being monitored to detect seizures and interictal paroxysms with the goal of identifying the SOZ. An obvious successful result of an invasive investigation is the delineation of a unique focus. A less obvious but nevertheless extremely valuable conclusion is the suggestion of a poor prognosis, such as a focus in eloquent areas, a diffuse focus or more than one SOZ, for instance in bitemporal lobe seizures. Although these patients are not candidates for curative surgery, palliative surgery can be sometimes suggested. In addition, new therapeutic options such as deep brain stimulation can be considered. Even with depth EEG recordings, there are patients for whom the delineation of the epileptogenic region remains impossible.

Neuropsychological tests can help in the lateralization and localization of the epileptic focus and are routinely used during the evaluation. For instance, the dominant hippocampus is tested with verbal memory test, the non-dominant hippocampus with non-verbal tests, and frontal-lobe functions can be tested with sorting and word fluency tests. These tests are also useful to evaluate cognitive function before and after surgery. Language representation must be assessed before surgery in patients with suspected non-typical speech representation. During the etomidate speech and memory test (eSAM) one hemisphere is temporarily inactive and a series of memory and language tests are administered (Jones-Gotman *et al.,* 2005). In this way, language can be lateralized and the ability of a patient to retain memory capabilities after a mesial temporal resection can be evaluated.

During the invasive investigation, electrical stimulation is usually performed to reproduce the patient's typical seizure or aura and to map eloquent areas (Kahane and Dubeau in press). An electrical current is applied between contiguous intracranial contacts. To evoke a clinical response or an after discharge, the intensity is progressively increased until a response is obtained or the safe maximum is reached. Intensity of the high frequency pulses (50/60Hz) varies from 0.2 to 3.6mA for the temporal lobe and up to 8mA for other regions. For functional mapping low frequency pulses (1Hz) are used to map the motor areas to avoid unpleasant involuntary movements, and high frequency for mapping visual, sensory, auditory, or language areas. Care is taking not to evoke unpleasant sensations or after discharge. By stimulating with a bipolar montage, focal currents are produced. The information obtained from the stimulation complements the analysis of spontaneous seizures during the pre-surgical evaluation (Kahane and Dubeau in press). Thus, a better delineation of the epileptogenic area is achieved.

3.5 *Animal models of epilepsy*

Experimental models of epilepsy are important to understand the mechanism of the epileptic syndromes and study the effect of therapy. *In vitro* preparations are useful to understand the basic mechanism underlying seizures. *In vivo* models allows to study seizures and epileptic syndromes. In relation to new AEDs, animal models are useful to identify new compounds, study their specificity, compare new vs. established AEDs, analyze their chronic efficacy, and study the adverse effects of the drugs (Loscher 2011). In the same way that many epileptic syndromes exist, specific animal models have been developed to mimic a variety of them. In this section, animal models of epilepsy are described, with emphasis in those models studied to understand the mechanisms of HFOs (in Chapter 5).

Brain slices allows studying basic mechanisms of epileptiform discharges and oscillations. Due to their mechanical stability, intracellular recording can be precisely obtained. Seizures are triggered by changing the milieu or by applying electric stimuli. In particular, hippocampus-entorhinal cortex slices have been extensively studied to understand mesial temporal epilepsy (Avoli *et al.,* 2002).

A topical convulsant (e.g. penicillin) can be applied to brain slices or animals' cortex to acutely generate focal seizures. Electrical stimulation induces after discharges, which in turn could evolve into seizures. These models are useful to study propagation and mechanisms of partial seizures (Fisher 1989).

Kainic acid is used to induce complex partial seizures during hours to days (Fisher 1989). After injection of kainic acid, rats present spontaneous periodic arrest of activity, autonomic behaviour (e.g. chewing), complex movements, and even secondary generalization. Spikes can be observed in the hippocampus.

Tetanus toxin injected into the rat's hippocampus results in a chronic model of complex partial seizures. Typical seizures consist of arrest of activity, followed by myoclonic jerks, and, sometimes, secondary generalization. About 100 seizures a day occur spontaneously during a month after injection (Fisher 1989).

Kindling models are produced by repetitively electrically stimulating the limbic system, usually the amygdala. Afterwards, the animal is more susceptible to generate seizures, presumably because the brain became more excitable. Different type of seizures, from simple to generalize can be obtained by applying a small stimulus (that would not normally induce a seizure) in kindled animals (McNamara 1984). In particular, in the amygdala-kindled Wistar rat with exposure to AEDs during the kindling, the animals become drug resistant not only to exposed AED, but also to a large number of AEDs, mimicking intractable epilepsy (Loscher 2011).

The pilocarpine model resembles all the stages of mesial temporal epilepsy (Curia *et al.,* 2008). The rats first go into status epilepticus following systemic injection of pilocarpine, which resembles an initial precipitating injury, commonly found in MTS. After a latent period, the rats start to have spontaneous seizures, which are poorly controlled with AEDs, as is usually the case in MTS. Widespread lesions appear in the model, particularly in the hippocampal and parahippocampal regions, which could resemble the hippocampal atrophy of MTS.

Genetic models have been developed to study generalized epilepsy. For instance, the genetic absence epilepsy rat from Strasbourg (GAERS), have spontaneous spike-wave discharges concomitant with behavioural arrest. With this model of absence seizures, thalamic involvement has been shown. In addition, GAERS animals respond to AEDs normally administered for absences (Marescaux *et al.,* 1992).

Models of malformation of cortical development also exist. When rats are exposed to an antimitotic agent *in utero* and later induced a seizure (e.g. with kainate), they do not respond to any of the established AEDs. This model is an example of a two-hit model of intractable epilepsy (Loscher 2011).

Thus, a variety of animal models exist with characteristics similar to diverse epileptic syndromes. Some of these models have been used to study the mechanism of HFOs, described in the next chapter.

Chapter 4. *High Frequency Oscillations*

Traditionally only frequencies up to 40 or 70 Hz have been considered clinically relevant. Even though about 75 years ago the first mention of high frequency (HF) activity (up to 300Hz) was published (Adrian and Matthews 1934) and the term gamma (>35Hz) was coined (Jasper and Andrews 1938), only in the last two decades the clinical and cognitive relevance of HF activity has been recognized.

Pathological High Frequency Oscillations (HFOs) are spontaneous small-amplitude short-duration EEG oscillatory patterns in the 80-500Hz range related to epileptogenesis. HFOs were first recorded with microelectrodes in animals and humans in mesial temporal structures (Bragin *et al.,* 1999b). These EEG patterns occurring in the absence of specific stimuli have been recorded during interictal (Staba *et al.,* 2002, Urrestarazu *et al.,* 2007), pre-ictal (Jacobs *et al.,* 2009b), and ictal (Jirsch *et al.,* 2006) periods. Physiological HF evoked activity is ubiquitous in the human brain and seem related with most of the information processing functions with high task specificity (Lachaux *et al.,* 2012). In cognitive studies the evoked response to particular stimulus can be averaged to increase SNR, instead of analyzing individual spontaneous events, as is the case of spontaneous pathological HFOs.

In this chapter the possible underlying mechanisms of HFO generation will be addressed; then, physiological HF activity will be presented; this will be followed by a description of pathological HFOs and their relation to epileptic tissue; finally the state of the art of automatic detection and analysis of spontaneous HFOs will be discussed.

4.1 *Mechanism of HFO generation*

Individual neurons can sustain narrowband oscillations at a wide range of frequencies, which could represent information coding (Buzsáki and Draguhn 2004). For instance, thalamic reticular pacemaking neurons are accountable for the formation of sleep spindles (Steriade 2003). Neurons have to be coupled together to generate oscillations visible on the EEG. Neurons can be linked by chemical synapses, electrical synapses (gap junctions), electric fields (ephaptic), or fluctuations in ions' extracellular concentration (Jefferys *et al.,* 2012). Slow oscillations recruit a large number of neurons over a large spatial extent, while HFOs are confined to a small spatial extent ((Buzsáki and Draguhn 2004); see also chapter 2, section "2.1.3.Volume conduction and EEG"). Slow oscillations are mediated mainly by chemical synapses (as presented in chapter 2, section "2.1.2.EEG generation"). Several mechanisms could generate HFOs and are discussed below.

Physiological ripples (80-200Hz) occur in the mesial temporal lobe and in the neocortex and the underlying mechanisms are likely similar to each other (Staba and Bragin 2011). In the hippocampus, the local interaction between interneurons and pyramidal cells triggers a ripple oscillation of short duration (Ylinen *et al.,* 1995). Although gap junctions and ephaptic fields could contribute to the generation of hippocampal ripples, the main activity arises from inhibitory synapses and synchronous discharges of pyramidal cells. Hippocampal physiological ripples represent the most synchronous patterns in the mammalian brain (Buzsáki and Lopes da Silva 2012). Contrary to what is expected (see chapter 2, section "2.1.3.Volume conduction and EEG"), the amplitude is larger for ripples than for gamma oscillations. A possible explanation is that at higher frequencies there is not only temporal overlap of synaptic potentials but also of action potentials (Buzsáki and Lopes da Silva 2012). In line with this, task-evoked broadband power changes (up to 150Hz) were correlated with multi-unit activity in humans (Manning *et al.,* 2009). In addition, pyramidal neurons and interneurons modified their firing rate during physiological ripples in humans

(recorded in the hippocampus contralateral to the SOZ), with interneurons starting to discharge earlier in the oscillation (Le Van Quyen *et al.,* 2008).

Slow cortical oscillations allow for the binding of other faster rhythms (beta, gamma, and ripples), through corticocortical and corticothalamic connections (Steriade 2006). For instance, physiological ripples in the hippocampus are associated with large amplitude sharp waves and the association is called SPW-R. SPW-Rs emerge as a property of the network, with 50-100 thousand neurons activated simultaneously during an event. SPW-Rs in the hippocampus are associated with spindles in the neocortex, which could be responsible for the transmission of memories to the neocortex during sleep ((Siapas and Wilson 1998); see also next section). In the neocortex, spontaneous ripples occur during the depolarizing phase of slow-wave oscillations during sleep (Grenier *et al.,* 2001). In the occipital cortex, spontaneous physiological HFOs were phase-locked to slow-waves during sleep (Nagasawa *et al.,* 2012). Beta, gamma, and probably ripple oscillations are voltage-dependant, since they are selectively sustained during the depolarization phase of slow-waves during sleep and during the steady depolarization of cortical neurons during waking state (Steriade 2006).

Pathological HFOs have been observed in *in vitro* brain slices and in *in vivo* models of spontaneous seizures. Fast ripples (FR; 250-500Hz) were first described in the kainic acid model of chronic epilepsy (Bragin *et al.,* 1999b). Since then, HFOs have been recorded in several other *in vivo* models. The same regions that generate spontaneous seizures also generate HFOs in the pilocarpine model (Levesque *et al.,* 2011), in the intrahippocampal tetanus toxin model (Jiruska *et al.,* 2010), and HF activity changes in a model of infantile spasms (Frost *et al.,* 2011). Some differences between models exist. For instance, in the kainic acid model all rats that developed epilepsy had FR in the latent period (Bragin *et al.,* 2004), but FRs were not observed in all animals with seizures in the pilocarpine model (Levesque *et al.,* 2011). HFOs in these *in vivo* models have roughly similar morphology and comprise the same frequency range, but this does not mean that the underlying mechanisms are the same. *In vitro* studies showed

that HFOs appear when neuronal networks are hyperexcitable which can be obtained from a variety of underlying mechanisms, such as convulsant drugs, synchronization by gap junctions, or increase of extracellular K^+ (Jefferys *et al.,* 2012). Thus, oscillations in the same frequency band are not necessarily the same phenomenon.

It has been suggested that pathological HFOs might be related to neuronal loss, since FRs were originally observed only in regions with neuronal loss in an animal model of status epilepticus (Bragin *et al.,* 1999c) and since the rate of FRs is correlated with hippocampus atrophy (Ogren *et al.,* 2009). However, HFOs were also observed in non-lesional models (e.g. tetanus toxin; (Jiruska *et al.,* 2010)), in non-lesional patients (Andrade-Valença *et al.,* 2012), and are higher in the SOZ regardless of the lesion (Jacobs *et al.,* 2009a). Thus, HFOs seem related to the underlying epileptogenicity of the tissue rather than only to the pathology.

While gamma and ripple oscillations could be explained mainly by synaptic (chemical) activity and neuronal firing, FRs encompass a higher frequency range than the maximal firing rate of individual neurons (Figure 4.1). Bursts of action potentials are aligned to individual FR cycles, but the frequency of individual cells is poorly correlated with the frequency of FRs (Ibarz *et al.,* 2010). Thus, FRs are likely an emergent property of the network. An interesting hypothesis is the out-of-phase cluster (Foffani *et al.,* 2007, Ibarz *et al.,* 2010, Jiruska *et al.,* 2010). The main idea is that independent groups of neurons fire simultaneously but slightly out-of-phase from each other, resulting in an oscillation of higher frequency than individual cells. Different underlying mechanisms, appearing from the combination of normal and pathological neurons, may be sufficient to generate this behaviour (Jefferys *et al.,* 2012). Functional clustering could emerge from a simultaneously active region, since within a large number of neurons activated by a common afferent, the closer the neurons the smaller the phase differences (Ibarz *et al.,* 2010). Electrical (GAP junctions or ephaptic) mechanisms could synchronize neurons, but introducing some jitter that can be recorded as FR oscillations in the EEG (Jiruska *et al.,* 2010). Network

heterogeneities could appear in epileptogenic tissue (e.g. due to axonal sprouting). This could generate topological clusters with some neurons acting as hubs of activity and therefore introducing delays between groups of neurons (Ibarz *et al.,* 2010). Finally, neuronal loss could result in anatomical clusters loosely connected to each other that fire slightly out-of-phase (Jefferys *et al.,* 2012). The frequency variability observed in HFOs within the same region (Blanco *et al.,* 2010, Engel *et al.,* 2009) argues in favour of this hypothesis. Thus, this concept of out-of-phase clustering provides a general framework to explain the emergence of FRs by diverse mechanisms in epileptogenic areas (Jefferys *et al.,* 2012). Figure 4.1 summarizes the mechanisms of generation of pathological HFOs.

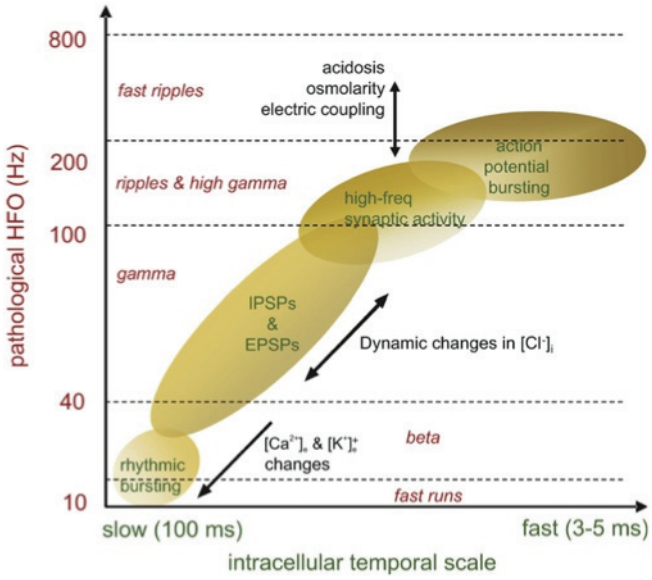

Figure 4.1. Underlying mechanisms of pathological HFOs. Gamma and lower frequency rhythms are obtained from the summation of postsynaptic potentials. Ripples are produced by a combination of postsynaptic potentials and action potentials. FR are faster than the firing rate of individual neurons, and are likely generated by out-of-phase firing. From (Jefferys *et al.,* 2012).

4.2 *Physiological HFOs*

HF activity has been suggested to represent a general electrophysiological index of cortical processing (Gotman and Crone 2011). HF activity seems capable of bonding not only local neurons firing together, but also distant cells. Given that there is large variability in what the literature refers to as *gamma*, and since there is not clear frequency cut to differentiate between gamma and higher bands, in this section we will refer to neuronal activity above 40Hz as HF activity. When referring to specific studies the reported frequency range will be indicated.

When studies are based on the analysis of activity phase-locked to the stimulus, variability between trials is cancelled out by averaging. A narrowband average is obtained if the task-related evoked response consists of rhythmic coherent firing of neurons, resulting in sinusoidal oscillations. When averaging multiple trials in the frequency domain, not only phase-locked (evoked) but also non-phase-locked time-locked (induced) activity is considered and broadband HF activity is usually obtained. The broadband characteristic of the induced response may be due, in part, to a slight difference in neuronal population involved during each trial and the latency in response to each individual stimulus (Crone *et al.,* 2011). Since more variability is associated with larger time lags after stimulus, narrowband evoked activity tends to have shorter time lags than broadband induced activity.

In scalp EEG recordings, narrowband evoked 40Hz oscillations have been first associated with self paced movements (Pfurtscheller *et al.,* 1993) and visual perception (Tallon-Baudry *et al.,* 1996). Time averaging thousands of trials allows recording very HF somatosensory evoked potentials on the scalp (600Hz -(Curio 2000)). Not only evoked, but also induced responses can be recorded on the scalp, which seem related to information binding (Tallon-Baudry *et al.,* 1996).

With intracranial recordings, broadband physiological HF activity was identified during movement execution (60-200Hz - Crone *et al.,* 2006, Leuthardt *et al.,* 2004), language (~100Hz – Crone *et al.,* 2001b), speech discrimination (80-

150Hz – Crone *et al.,* 2001a), visual processing (40-200Hz – Lachaux *et al.,* 2005), and attention (80-150Hz –Ray *et al.,* 2008). Individual HFOs in the hippocampus were related to memory consolidation (~200Hz – (Draguhn *et al.,* 2000); 80-140Hz – (Axmacher *et al.,* 2008)) and in the visual cortex to visual stimuli (80-300Hz – Nagasawa *et al.,* 2012). Interestingly, physiological HFOs had similar characteristics to pathological HFOs recorded in other regions in the same patients (Nagasawa *et al.,* 2012).

Cross-coupling between HFOs and low frequency oscillations seems related to the transmission of information within and across regions. For instance, temporal correlations were found between hippocampal ripples and neocortical spindles (Siapas and Wilson 1998). Within the neocortex, theta oscillations modulate ripples' power during behavioural tasks (Canolty *et al.,* 2006). Within the hippocampus, gamma and ripple oscillations correlated with a different phase of theta oscillations and had differential coupling at different locations (Colgin and Moser 2009). These examples of cross-frequency coupling are suggestive of means of communication within a region and between mesial temporal and frontal areas. Cross-frequency coupling may be associated with the transfer from hippocampal short-term memory to long-term memory neocortical storage (Siapas and Wilson 1998) and with memory encoding (Colgin and Moser 2009).

Given the high anatomical, functional, and temporal specificity of evoked HF activity (Lachaux *et al.,* 2012), it could be useful for cortical mapping. In particular, at the beginning and at the end of a movement, HF activity changes are somatotopically more specific than the concomitant mu and beta band changes. HF activity occurred only during brief intervals and corresponded to the areas mapped with electrical stimulation (Miller *et al.,* 2007a). Since HF activity is also specific to language processing (e.g. Crone *et al.,* 2001b), it could be used also to map language cortex. However, the sensitivity of maps of language based on gamma responses was lower than with electrical stimulation, suggesting that it could be useful to construct a preliminary map, but without replacing cortical stimulation (Sinai *et al.,* 2005).

4.3 *Pathological HFOs*

Although no formal definition exist, pathological HFOs (80-500Hz) can be characterized by spontaneous oscillations of at least four cycles that can be distinguish from background activity, with a typical duration of 30-100ms and an inter-event interval of at least 25ms.

In animal models of epilepsy, HFOs were associated with the SOZ (Bragin *et al.,* 1999b); correlated with high seizure rate (Bragin *et al.,* 2003); and were recorded shortly after induced status epilepticus in rats that subsequently developed spontaneous seizures, but were not seen in rats that did not (Bragin *et al.,* 2004), suggesting a predictive value in the development of epilepsy. In humans, HFOs were first recorded with microelectrodes implanted in temporal regions (Bragin *et al.,* 1999b), and more recently with clinical macroelectrodes in temporal and neocortical regions (Urrestarazu *et al.,* 2007). Interictally, they can be identified more frequently during slow wave sleep than during wakefulness (Bagshaw *et al.,* 2009, Staba *et al.,* 2004).

During ictal activity, increase in HF rhythmic activity was first observed in grids by Fisher (1992) and in depth electrodes by Allen (1992). HFOs during epileptic seizures were restricted to regions of seizure initiation and only infrequently observed in areas of propagation (Jirsch *et al.,* 2006). HFOs were present in the SOZ during spasms (60-150Hz - Akiyama *et al.,* 2005), but the clinical motor manifestation was related with HFOs in the rolandic region and not in the SOZ (Nariai *et al.,* 2011). HFOs remained confined to the same region during interictal and ictal periods, while spikes presented a wider spread during seizures than interictally (Zijlmans *et al.,* 2011). Very high frequency HFOs (up to 800Hz) have been recently observed at the beginning of a seizure (Kobayashi *et al.,* 2010a). In the analysis of ictal HFOs, care must be taken to differentiate HFOs from EMG artefacts provoked by movement during the seizure, particularly in the most superficial channels (Otsubo *et al.,* 2008).

The occurrence of HFOs during the pre-ictal period is controversial. In animal models, HFOs do not seem to be the trigger of seizure generation (Bragin *et al.,* 2005). The rate of spikes without HFOs in the enthorhinal cortex was related with susceptibility to seizure on subsequent days (Levesque *et al.,* 2011). In humans, HFOs increased immediately before seizures in the temporal lobe (Khosravani *et al.,* 2005) while no consistent findings within 15 min before seizures across different etiologies were found (Jacobs *et al.,* 2009b). Pre-ictal periods (22-min before seizures) could be discriminated from interictal periods using wavelet entropy and energy measures in HF range (Gadhoumi *et al.,* 2012). The relation between HFOs and the pre-ictal state is actively being investigated.

During interictal periods, higher rates of HFOs were observed in the SOZ (Bragin *et al.,* 1999b, Urrestarazu *et al.,* 2007) than in other areas; HFO rates correlate with the SOZ better than spikes (Jacobs *et al.,* 2008a), are particularly linked to epileptogenic lesions (Jacobs *et al.,* 2009a) and the ratio between FRs and ripples was higher in atrophic than normal hippocampus (Staba *et al.,* 2007). Even though a large proportion of HFOs co-occur with spikes, HFOs can occur also in non-spiking channels or independently from spikes in spiking channels (Jacobs *et al.,* 2008a). HFO rates (unlike spike rates) increase after a reduction in medication and do not change after seizures, thus mimicking disease "activity" (Zijlmans *et al.,* 2009b). The number of microcontacts that recorded interictal FRs was correlated with seizure frequency in an animal model (Bragin *et al.,* 2003), but this was not confirmed in a human study with macroelectrodes (Zijlmans *et al.,* 2009a). As described in Chapter 3, section "3.4.1.Pre-surgical evaluation of epilepsy", electrical stimulation can be used to help delineating the epileptogenic zone. HFOs were recorded in the areas that responded to stimulation and the rates of HFOs were negatively correlated with the threshold required to elicit a stimulation response (Jacobs *et al.,* 2010c). Using single pulse stimulation, it is possible to evoke pathological HFOs, about 100ms after stimulation. These evoked HFOs were more specific than evoked spikes to delineate the SOZ (van 't Klooster *et al.,* 2011).

Pathological HFOs are characterized as oscillations that stand out from the background. In a recent study the characteristics of this background in mesial temporal structures has been analyzed (Mari *et al.,* 2012). This study showed that the background is sometimes composed of continuous oscillatory activity in HF range, particularly in the hippocampus. When studying the presence of this continuous HF activity background in different brain regions, it was found not only in the hippocampus, but also in the occipital lobe (Melani *et al.,* in press). Figure 4.2 shows examples of spontaneous interictal HFOs in relation to the surrounding background recorded at the MNH.

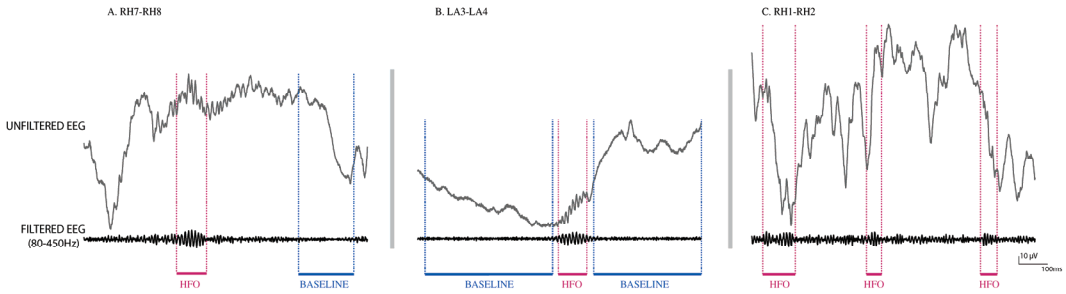

Figure 4.2. Examples of interictal HFOs within different backgrounds recorded with depth macroelectrodes in humans. A) & B) Channels where clear baselines can be found. C) Even though almost no baselines were found in this channel, HFOs were marked. Magenta: visually marked HFOs; blue: visually marked baselines.

An important validation of HFOs as biomarkers of epileptogenic tissue is the relation between removal of HFO-generating tissue and the post-surgical outcome. All post-surgical studies to date were retrospective. A correlation between good surgical outcome and removal of areas with ictal ripples in children was first shown (Ochi *et al.,* 2007). Removal of regions with earliest ictal HFOs during infantile spasms also correlated with good surgical outcome (Nariai *et al.,* 2011). A clear correlation between surgical outcome and removal of tissue generating high interictal HFO rate was also found (Akiyama *et al.,* 2011b, Jacobs *et al.,* 2010b, Wu *et al.,* 2010). In adult patients in whom the areas corresponding to channels containing high rates of HFOs were not removed, the outcome was poor; while in all patients with good surgical outcome, all channels with high rate of HFOs were removed (Jacobs *et al.,* 2010b). The accuracy was better than for spikes or the SOZ (Jacobs *et al.,* 2010b). A similar conclusion was obtained from

intraoperative subdural recordings in children considering only interictal FRs (Wu *et al.,* 2010). Interestingly in cases where HFO regions remained and bad outcome was obtained, a second operation removing the remaining regions with HFOs resulted in seizure freedom (Wu *et al.,* 2010). These retrospective studies suggest a close link between a high rate of HFOs and epileptogenicity. A prospective surgical study involving large number of patients in multiple centers is necessary to further relate the ability of HFOs to help delineating the epileptogenic zone.

It is important to point out that the conclusions in relation to HFO rates are based on the relative number of HFOs within a patient. Moreover, mesial temporal structures have inherently more HFOs than neocortical regions. Thus, there is no absolute threshold to indicate whether a channel has high content of HFOs and should be considered as part of the epileptogenic zone (Jacobs *et al.,* 2012). Other ways to quantify HFOs might provide a better threshold than the rates (see below section "4.4.2.Uncertainties about the detection of HFOs").

HFOs recorded interictally seem to provide a robust measure of epileptogenicity and only some minutes of interictal EEG provide the same information as longer periods (as studied in Chapter 5, Zelmann *et al.,* 2009b). If more studies confirm the clinical relevance of interictal HFOs it would be possible to obtain reliable conclusions from shorter implantation (without the need to wait days for seizures to happen) or with intraoperative recordings.

In summary, pathological HFOs are emerging as a reliable biomarker of tissue capable of producing spontaneous seizures. HFOs can robustly indicate the SOZ, independently of the underlying pathology; HFOs are more specific interictal markers than spikes; HFOs mimic the disease with respect to response to medication; and HFOs are a good indicator of the epileptogenic zone and have even been suggested to be even better than seizures (Jacobs *et al.,* 2010b).

Figure 4.3 presents the same schematic of clinically relevant regions shown in Chapter 3, Figure 3.4. The relation of HFOs to the other clinically relevant zones has been added. In the pre-surgical decision, the HFO zone might soon replace the

irritative zone, especially in cases when the irritative zone is often widespread, as in frontal lobe epilepsy (Zijlmans *et al.,* 2012).

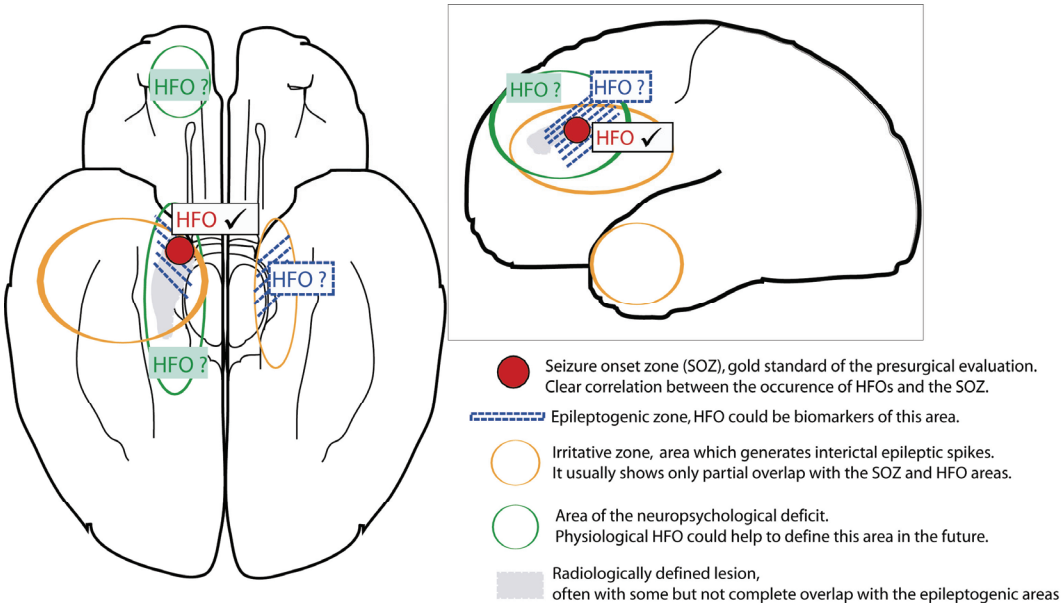

Figure 4.3. Schematic showing the relation between HFO zone, seizure onset zone, lesional zone, irritative zone, and epileptogenic zone. HFOs can identify the SOZ, seem related to the epileptogenic zone, and HFOs may be also a marker of physiological damage in the future. From (Jacobs *et al.,* 2012).

4.3.1 *Is it possible to distinguish pathological from physiological HFOs?*

The distinction between pathological and physiological HFOs remains to be defined (Engel *et al.,* 2009). It has been originally associated (in recordings with microelectrodes) with a difference in frequency, with ripples regarded as normal oscillations, while FRs were considered pathological. However, recent studies suggested that frequency distinction alone is not sufficient to discriminate between pathological and physiological HFOs, at least when recorded with macroelectrodes. The rates of ripples and FRs were higher in the SOZ than outside (Jacobs *et al.,* 2008a, Urrestarazu *et al.,* 2007, Worrell *et al.,* 2008), ripples behaved similarly to FR with respect to surgical outcome (Jacobs *et al.,* 2010b) and medication withdrawal (Zijlmans *et al.,* 2009b). In rats that developed epilepsy, ripples were observed in the dentate gyrus where normal ripple oscillations never occur (Bragin *et al.,* 2004). Thus, ripples and FRs seem to be

associated with tissue that generates seizures. Moreover, when clustering HFOs there was no natural division between ripples and FRs according to frequency, but rather a continuum (Zelmann *et al.,* 2009a) or there was an intermediate cluster that contained a mix of ripples and FR (Blanco *et al.,* 2011). Thus, since the frequency division seems arbitrary at least for recordings with macroelectrodes, no distinction between ripples and FR is implemented during the automatic detection of HFOs (see Chapter 6; Zelmann *et al.,* 2010, Zelmann *et al.,* 2012).

The only distinction to date may come from the underlying mechanisms studied in animal models. Pathological HFOs appear to represent abnormal bursts of action potentials, therefore reflecting the underlying epileptogenicity (Engel *et al.,* 2009). However, when recorded with macroelectrodes in humans pathological and physiological HFOs looked the same (Nagasawa *et al.,* 2012). New characteristics to distinguish between them should be investigated.

4.3.2 *Non Invasive identification of HFOs*

In cognitive neuroscience, HF activity can be seen on the scalp after averaging thousands of trials, since averaging time-locked to a stimulus during a controlled experiment considerably increases the SNR. For instance, averaged scalp activity of somatosensory evoked-potentials up to 600Hz has been identified (Curio 2000) and scalp and subdural recordings showed the same pattern of HF activity during movement (Ball *et al.,* 2008). On the contrary, pathological HFOs are spontaneous events, and as such must be identified individually. Thus, HFOs have been mainly recorded with intracranial electrodes.

Surprisingly, recent studies showed that spontaneous HFOs can be also recorded from the scalp. Ictal gamma activity (50-100Hz) was observed during infantile spasms (Kobayashi *et al.,* 2004) and at the onset of tonic-clonic seizures (Kobayashi *et al.,* 2009). Interictally, paroxysmal gamma activity (above 30Hz), although infrequent, co-localized with the SOZ (Wu *et al.,* 2008). HFOs were first observed on the scalp during continuous spike-waves during slow-wave sleep (Kobayashi *et al.,* 2010b). Furthermore, careful observation of scalp EEG allowed

the identification of interictal HFOs in some patients with focal epilepsy (Andrade-Valença *et al.,* 2011). In all cases the rate of scalp HFOs was much smaller than the usual rate of intracranial HFOs. Figure 4.4 presents an example of HFOs visible on the scalp.

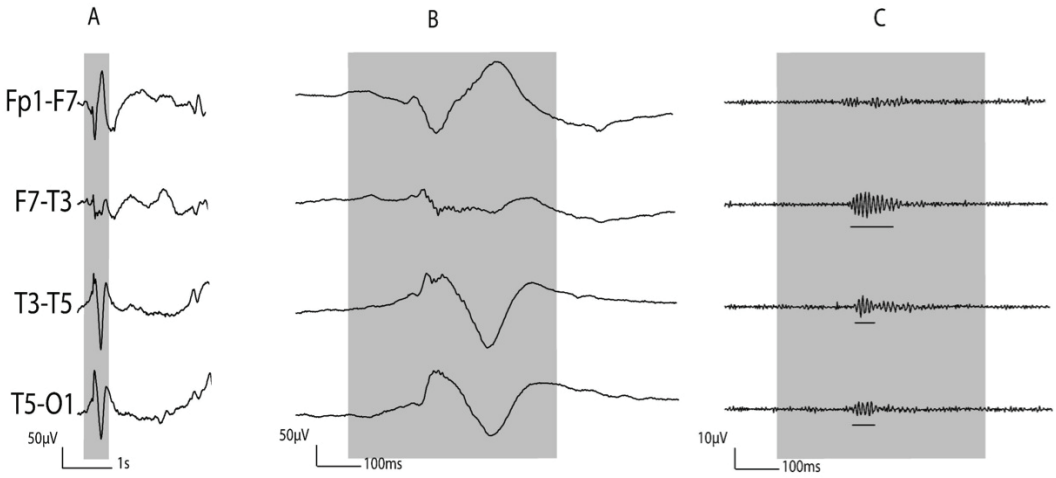

Figure 4.4. Example of HFOs visualized on the scalp. From (Andrade-Valença *et al.,* 2011).

If HFOs could be robustly recorded on the scalp, they might be useful to evaluate AED efficacy, to plan electrodes implantation, and to predict the development of seizures after brain trauma. Since HFOs on the scalp could be recorded during routine EEG investigation, they could be useful to evaluate large patient populations in longitudinal studies. A better understanding of the spatial sampling needed to observe HF brain activity on the scalp is important for the clinical use of scalp HFOs as biomarkers of epilepsy as well as in cognitive research and it is addressed in Chapter 7 (Zelmann *et al.,* submitted).

4.4 *Automatic detection of HFOs*[2]

Automatic detection is crucial for the investigation of HFOs as biomarkers of epileptogenic tissue, and is likely necessary to propel future clinical applications. The automated detection and analysis of large-scale data sets and HFO detectors are areas of active research.

The detection and labeling of interictal and ictal epileptiform activity in EEG records can be broadly categorized into: i) *Expert Manual Review* - considered the gold standard, but could be associated with poor inter-reviewer reliability and not feasible for large data sets. ii) *Supervised Detection* - usually implemented using a high sensitivity automated detection algorithm that may have poor specificity, but is combined with expert review. iii) *Unsupervised Detection* - achieves fully automated detection and data labeling, but requires high specificity and sensitivity detectors to be useful.

As a running definition for the detection of HFOs, the following has been suggested: at least four oscillations of sinusoidal like morphology in the filtered EEG (above 80 Hz) with energy larger than the 95 percentile of the surrounding background (Worrell *et al.,* 2012). In addition, constrains in the time-frequency plane have been empirically proposed by some authors.

4.4.1 *Detection of HFOs*

At the Montreal Neurological Institute the visual labeling of HFOs is usually performed by splitting the screen vertically in two and using an 80Hz high-pass filter on the left and a 250Hz high-pass filter on the right screen. A high order high-pass finite impulse response (FIR) filter is used to obtain a sharp cut-off while avoiding phase distortion. The time resolution is increased to 0.6 sec across the monitor and only up to 10 channels are visualized simultaneously. A ripple is

[2] This section was modified from the originally published section "Automatic Detection of HFOs", written by R. Zelmann, in review following the workshop "High Frequency Oscillations in Cognition and Epilepsy" (Montreal June 2-4, 2011; Worrell et al., 2012).

marked if there is a clear oscillation on the left that is not visible or has a different morphology on the right. A FR is marked if it appears in the right screen.

Visual labeling has provided a good understanding of the relation between HFOs and epilepsy (most clinical papers described in the section "4.3.Pathological HFOs" used visual labeling), but it is very time consuming and subjective. It can be estimated that takes around 10 hours to mark HFOs in a 10-minute 10-channels recording. To achieve consistency across reviewers and to ensure stable labeling, a procedure described in Chapter 5 (Zelmann *et al.,* 2009b) was developed.

Given the massive amounts of EEG data that are collected from patients undergoing evaluation for epilepsy surgery it is likely untenable to only rely on visual review of HFOs. Objective, consistent, accurate labeling of epileptiform activity in large-scale recordings requires automated detectors. Since the objective is the detection of spontaneous HFO events that can be distinguished from ongoing background activity, a logical approach is to compare the energy of the signal with an energy threshold derived from the background. The first step is band-pass filtering the data, to restrict the range of frequencies under consideration. When the energy of the filtered EEG is statistically larger than the threshold during a certain interval, the segment is considered as a possible HFO (Figure 4.5) (Crepon *et al.,* 2010, Gardner *et al.,* 2007, Staba *et al.,* 2002, Zelmann *et al.,* 2010, Zelmann *et al.,* 2012).

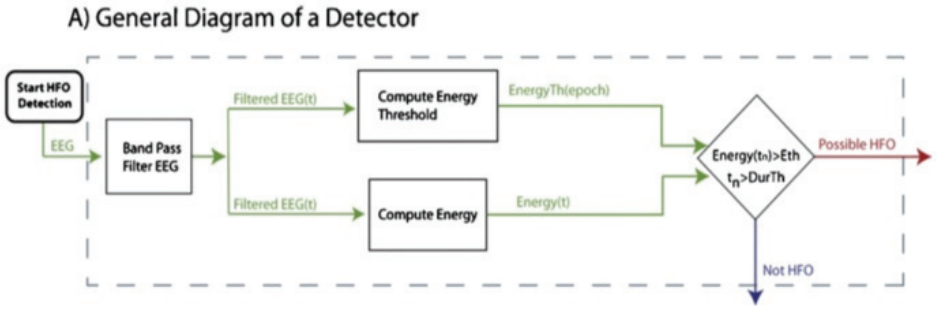

Figure 4.5. Schematic of the automatic detection of HFOs based on energy. From (Worrell *et al.,* 2012).

Under the assumption that HFOs are rare events, some detectors compute the energy threshold based on the entire EEG signal, including the HFO events (Crepon *et al.,* 2010, Gardner *et al.,* 2007, Staba *et al.,* 2002). The main difference among them is the type of energy function that is computed on the filtered signal, either the root mean square amplitude (Staba *et al.,* 2002), the short-time line length (Gardner *et al.,* 2007), or the Hilbert envelope (Crepon *et al.,* 2010). The assumption that HFOs are rare events seems correct in the majority of the EEG channels, but in very active channels or in channels with continuous rhythmic background (Mari *et al.,* 2012) it does not hold. In those cases, performance can be improved by first detecting baseline sections (EEG segments without oscillatory components) and computing the energy threshold based on the energy in the detected baseline as described in Chapter 6 (Zelmann *et al.,* 2010, Zelmann *et al.,* 2012). All these detectors aim at the detection of intracranial HFOs. An automatic detector of scalp HFOs has also been developed based on filter banks and relative power features to separate HFOs from artefacts (von Ellenrieder *et al.,* 2012).

4.4.2 *Uncertainties about the detection of HFOs*

Existing methods for automated intracranial HFO detection implicitly model the events as short-duration, high frequency transients added to background EEG, but there are different implicit specific goals on what to detect as an HFO. Indeed, the definition of HFO differs across research groups.

The cross sectional area of an electrode determines the scale of spatial sampling (Worrell *et al.,* 2012). Thus, small extent activity such as the one generating HFOs was originally recorded with microelectrodes (40μm diameter; 0.001mm^2). However, clinical macroelectrodes also allow for the recording of these small events, although with a lower rate (Worrell *et al.,* 2008). However, since HFOs recording with macrocontacts are related to the epileptogenic region, it has been argued that somehow macroelectrodes might allow recording the most clinically relevant HFOs. When comparing contacts of different sizes within the same range (0.02-0.09mm^2) no significant difference in the rate or characteristics

of the recorded HFOs was found (Châtillon *et al.,* 2011). The range of HFO amplitude (10 to 1000 μV) and duration (30-100 ms) reported spans a wide range, depending on electrode type (macroelectrode vs. microelectrodes, penetrating vs. subdural), proximity to the HFO generators, and the tissue sampled.

Since the analysis is focused in a particular frequency band, the filter characteristics must be taken into account to avoid the detection of false oscillations (Bénar *et al.,* 2010), i.e. sharp transients with spectral content in HFO bands but without actual HFOs in the raw EEG. Such false oscillations are not artefacts (defined as activity originated outside the brain, see Chapter 2), since the sharp spikes originate in the brain. They rather originate from the Fourier transform of a transient that always exhibits a wide range of frequencies. The transient being the result of the additive superposition of all those harmonics, a narrowband filter will generate spurious oscillations in the vicinity of the transient (Gibb's effect). In practice, these false oscillations could be separated from the HFOs of interest, since they have only a few oscillations when an appropriate filter is used. This can be validated by random selection of detected events to verify the presence of discrete HFOs in the unfiltered EEG. Moreover, the issue of whether there is a difference between sharp spikes that contain spectral energy in the HFO range versus spikes that do not has not been thoroughly addressed. This should be further studied, since spikes originating in the seizure onset zone have more high frequency activity than those outside (Jacobs *et al.,* 2011b).

A question that often arises is whether HFOs should be a band-limited event (as in Crepon *et al.,* 2010) or it can be a broadband event (e.g. (Staba *et al.,* 2002); Chapter 6, (Zelmann *et al.,* 2012)). If band-limited, should there be specific spectral boundaries? In other words, should an HFO be defined as an isolated event in the time-frequency map, or could it contain a variety of frequencies within a range? A separate, but related question is whether only those HFOs that occur alone versus those occurring in association with epileptiform EEG spikes are relevant. To date, there is no clear answer to these questions.

To avoid false negatives, the most common approach is to implement the detectors with high sensitivity but low specificity. In this way, most of the HFOs should be detected, at the cost of producing a large number of false positives that then need to be discarded. Visual validation of these possible events is usually performed. Even though human reviewers are not the perfect solution, it is a reasonable approach given that they are the clinical users and that they are considered as the gold standard when identifying other electrophysiological signals, such as spikes, seizures, or the alpha rhythm. To overcome variability among reviewers, a possibility is to consider more than 1 reviewer (as in (Gardner *et al.,* 2007); Chapter 6, (Zelmann *et al.,* 2010)).

The rate of HFOs in a channel seems a reliable marker of underlying epileptogenic tissue and it has been the most commonly used measure. However, other measures (such as: ranking of channel, durations, amplitudes, peak frequency, temporal distributions, and entropy) might turn out to be the most appropriate to characterize HFO activity.

Chapter 5. *Manuscript #1: Improving the identification of High Frequency Oscillations*

5.1 *Context*

Visual marking of HFOs provided a good understanding of the relation of HFOs with epilepsy and was the methodology used in most studies of pathological HFOs in humans (see Chapter 4). Since visual marking is highly time consuming and subjectivity is inevitable, a procedure was required to systematize the visual marking and to obtain a measure of stability in the markings. High rates of interictal HFOs seem related to epileptogenic tissue. Thus, it is important to assess the shortest duration that needs to be marked to obtain a reliable rate of HFOs, which would contain the same information as longer intervals. Since the measure of high rate of HFOs is relative to each patient, not only the rate of HFOs should be evaluated, but also the ranking of the channels (i.e. the relative order of channels with respect to HFO rates within each patient). Evaluating stability in the identification of HFOs is important not only for visual, but also for automatic marking of HFOs.

The following manuscript presents a procedure developed to assess the duration of EEG that must be interpreted in order to obtain reliable estimates in terms of rate of HFOs and ranking of channels with respect to rates, to ensure stability of marked recordings (visual or automatic), and to assess concordance between reviewers. This manuscript was published as (Zelmann R, Zijlmans M, Jacobs J, Chatillon CE, Gotman J. 2009. *Improving the identification of High Frequency Oscillations*. Clin Neurophysiol 120:1457-64).

5.2 *Abstract*

Objective. High Frequency Oscillations (HFOs), including Ripples (80-250Hz) and Fast Ripples (250-500Hz), can be recorded from intracranial macroelectrodes in patients with intractable epilepsy. We implemented a procedure to establish the duration for which a stable measurement of rate of HFOs is achieved. **Methods.** To determine concordance, Kappa coefficient was computed. The information gained when increasing the duration was analyzed in terms of HFO rates and ranking of channels with respect to HFO and spike rates. **Results.** In a group of 30 patients, Kappa was 0.7 for ripples, 0.7 for fast ripples and 0.67 for spikes. Five minutes provided the same information as 10 min in terms of rates in 9/10 patients and with respect to ranking of channels in 8/10 patients; 5/30 patients did not achieve stable measurements of HFOs or spikes and needed marking for 10 min. **Conclusion.** We propose that 5 min provides in most cases the same information as a longer interval when identifying HFOs and spikes in slow wave sleep, and present methods to identify when this is not the case. **Significance.** This procedure is useful to control for consistency between readers and to evaluate if the selected interval provides stable information, for automatic and visual identification of events.

5.3 *Introduction*

High Frequency Oscillations (HFOs), referred to as Ripples (80-250Hz) and Fast Ripples (250-500Hz), are EEG signals recorded from intracranial electrodes in patients with intractable epilepsy. It had been traditionally thought that only signals with frequency components up to the gamma band (40-80Hz) have a clinical meaning. However, recent findings in rodents and humans showed a possible relation of HFOs with epileptogenesis (Bragin *et al.,* 1999a, Bragin *et al.,* 1999b, Jacobs *et al.,* 2008a, Jirsch *et al.,* 2006, Khalilov *et al.,* 2005, Staba *et al.,* 2002, Urrestarazu *et al.,* 2007).

Even though no formal definition exists, HFOs recorded with macroelectrodes can be characterized by oscillations of at least four cycles, with a

typical duration of 80-100ms for ripples and 30-50ms for fast ripples, which can be clearly distinguished from the background activity (Jacobs *et al.,* 2008a), and with an inter-event interval of around 25ms. These EEG patterns occur spontaneously and can be identified more frequently during slow wave sleep (SWS; (Bagshaw *et al.,* 2009, Staba *et al.,* 2004).

Based on these features, HFOs are visually identified by experienced readers or automatically marked by ripple detectors (Khalilov *et al.,* 2005, Staba *et al.,* 2002, Worrell *et al.,* 2008) and sometimes visually validated (Worrell *et al.,* 2008). However, given the lack of a complete definition, subjectivity is inevitable, sometimes resulting in poor agreement among reviewers. Visual marking is also highly time consuming, taking around 10 hours to visually mark HFOs in a 10-channel 10-min recording. The current practice of marking 10-min episodes (Bagshaw *et al.,* 2009, Jacobs *et al.,* 2008a, Staba *et al.,* 2002, Urrestarazu *et al.,* 2007) is an appropriate duration in the sense that stable SWS sections of this duration can be found in most patients with implanted electrodes. When using automatic detection 10- to 30-min intervals are selected (Staba *et al.,* 2007, Staba *et al.,* 2002, Worrell *et al.,* 2008). It is possible, however, that the same amount of information could be obtained with shorter intervals.

The rates of HFOs are the most commonly used measure of HFO occurrence and are believed to be associated with the seizure onset zone (SOZ), not only during seizure generation but also interictally. Indeed, in interictal periods, higher rates of HFOs were observed in the SOZ (Bragin *et al.,* 1999b, Urrestarazu *et al.,* 2007) than in other areas, in particularly linked to epileptogenic lesions (Jacobs *et al.,* 2009a), and showed to be higher in atrophic hippocampus (Staba *et al.,* 2007). The ranking of channels according to rate indicates the relative importance of a channel with respect to the others for each patient, providing an assessment independent of absolute rates.

A procedure is proposed to minimize the EEG duration that needs marking in order to obtain reliable estimates in terms of rates of HFOs and ranking of

channels with respect to rates, and to assess concordance between readers. This procedure is useful for visually marked EEG as well as to ensure that a stable measurement is achieved with automatic detectors.

5.4 *Methods*

5.4.1 *Patient selection and visual marking*

Forty patients with medically intractable epilepsy underwent depth electrode implantation at the Montreal Neurological Hospital between September 2004 and December 2007 because their epileptogenic region could not be localized with non-invasive means. The mean age was 41.7 years (range 20-59). Twenty five were lesional and 15 non-lesional patients. Eighteen patients had seizures originating from mesio-temporal lobe structures and 22 had seizures originated from extra temporal structures (11 neocortical temporal areas, 6 frontal, 3 occipital and 2 centroparietal). All patients had complex partial seizures during the investigation, and 4 patients additionally had generalized tonic-clonic seizures during the investigation. The position of the electrodes was selected exclusively for clinical reasons. During some nights, the depth EEG (SEEG), recorded with the Harmonie system (Stellate, Montreal, Canada), was low-pass filtered at 500Hz and sampled at 2000Hz, allowing for the identification of HFOs. All patients gave informed consent in agreement with the Research Ethics Board of the Montreal Neurological Institute and Hospital.

Two experienced readers visually identified and marked HFOs and spikes in all patients. The marking of ripples and fast ripples was performed by vertically splitting the screen in two, and using an 80Hz high-pass filter on the left half and a 250Hz high-pass filter on the right. A ripple was marked if an event was clearly visible on the side of the 80 Hz filter and did not occur or show the same shape on the side of the 250 Hz filter, as it is defined as a distinct event between 80 and 250 Hz. An event was identified as a fast ripple if it was visible in the 250 Hz filter. Ripples and fast ripples were only regarded as such if their amplitude was clearly

higher than the baseline of the investigated channel and they consisted of at least four consecutive oscillations (Jacobs *et al.,* 2008a). Spikes were marked independently of HFOs on a standard EEG display. All SEEG channels functioning properly were marked using a bipolar montage, resulting in 7-58 channels per patient. The first 10 patients were selected for the development and evaluation of the methods. To this end, their SEEG was visually marked during 10 min of SWS. For the remaining 30 patients, 5 min were marked. In the patients for whom the analysis showed that 5 min was not sufficient to reach a stable measurement, 10 min were marked and re-evaluated.

5.4.2 *Sufficient interval and concordance evaluation*

In order to improve the identification of HFOs and spikes in SEEG, we developed a procedure to ensure a minimum degree of concordance across reviewers and to determine whether the obtained information was representative of the EEG of each patient. We define a stable measurement as a measurement that does not change over time (i.e. the measured rate and ranking of channels remain the same for the different interval lengths). Thus, the marked EEG was considered to be stable at a particular interval if the amount of information obtained in that interval was equivalent to the information of the whole marked EEG in terms of rate of HFOs and spikes and also in terms of ranking of channels according to the rates of HFOs and spikes.

The procedure can be divided in two steps (Figure 5.1), evaluating the agreement between reviewers, then assessing when a stable measurement of the rates and ranking of channels according to the rates is achieved for the marked interval.

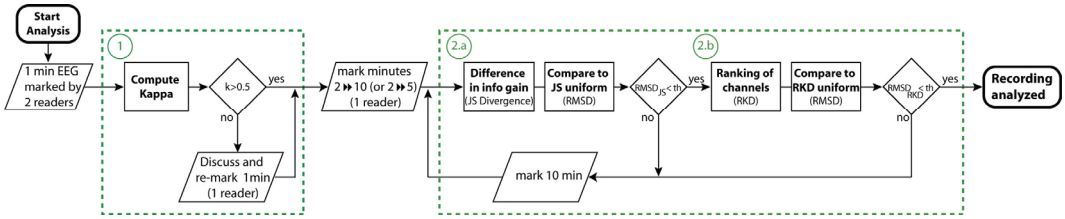

Figure 5.1. Diagram of the complete process. *First step*: Assessing concordance between readers based on Kappa coefficient (1). *Second step*: Evaluating if an interval is representative of the whole marked EEG, in terms of rates (2.a) and ranking of channels (2.b).

5.4.2.1 *Inter-observer agreement*

To determine concordance, the first minute of each EEG was marked by two reviewers. Cohen's Kappa coefficient (Cohen 1960) was computed for this first minute in each channel. This coefficient measures the degree of agreement between two reviewers, taking into account the agreements made by chance. Kappa <0 reflects that the agreement is due to chance and $\kappa = 1$ indicates complete agreement. Kappa =0.5 reflects moderate agreement, and was chosen as the threshold of concordance (Landis and Koch 1977). Thus, channels with $\kappa < 0.5$ were reviewed and discussed jointly by the two reviewers to reach similar marking criteria. They were then remarked by the reviewer that also marked the remaining EEG.

5.4.2.2 *Stable measurement assessment*

An interval was considered representative of the whole EEG if marking this interval resulted in the same amount of information as marking the whole reference interval. This was assessed by two independent methods, Jensen–Shannon (JS) Divergence and Ranking Distance (RKD). The JS Divergence measures the relative information gained when comparing the rate of identified events found in different intervals and in the complete interval (the "true distribution"). The RKD allowed us to identify the changes in the ranking of the identified events for the same intervals.

To determine at which interval length a stable measurement was achieved in most patients, different durations, ranging from 6 sec to 9.5 min, were compared against the 10 min "gold standard". In addition, in order to ensure that there was

no bias towards the beginning or end of the 10-min interval, 10 random start points were used for each interval length. For the second group of patients (marked during 5 min) the different intervals ranged between 6 sec and 4.5 min and were compared against the 5-min interval.

For this second group of patients, the marked 5-min interval was considered stable if an interval of half the length (2.5 min) provided the same information as the 5-min interval (i.e. if at 2.5min the $RMSD_{JS}$ and the $RMSD_{RKD}$, as defined in section 5.4.2.3, were smaller than the threshold). Thus, if this condition was not met, we cannot determine if the 5-min interval is stable and therefore 10 min were marked for that patient.

5.4.2.2.1 JS Divergence

For evaluating the interval length providing stable measurement of rates, the information gained when increasing the interval duration was analyzed in terms of difference in the rate of events. If the rates are time invariant, the law of diminishing returns applies: increasing interval length results in decreasing gain in information. One well known way to measure the information gain is the Kullback–Leibler (KL) Divergence or relative entropy. The KL Divergence quantifies the difference in information gained when using a given distribution (Q) instead of the "true" distribution (P). In our case, P represents the percentage of epochs that contain a given event in the 10-min interval, while Q represents the percentage of epochs that contain a given event for the different time intervals (t). The epoch length was chosen as 50ms for all types of events. Thus, for each of the possible events ripple, fast ripple, spikes and no event:

$$D_{KL}(P||Q_t)_t = \sum_{ev} P(ev)\log\frac{P(ev)}{Q_t(ev)} \qquad \textbf{Equation 5.1}$$

where ev = ripple, fast ripple, spikes or no event

$$P = \begin{bmatrix} R_{10min} \\ FR_{10min} \\ Sp_{10min} \\ noEv_{10min} \end{bmatrix} Q_t = \begin{bmatrix} R_{tmin} \\ FR_{tmin} \\ Sp_{tmin} \\ noEv_{tmin} \end{bmatrix}$$

where interval t= 0.1,0.5,1,1.5,….,9,9.5,10min

Because we are trying to obtain the distance in terms of information gain between the 10-min interval (our "gold standard") and the different interval, a true metric or distance function was needed. A true metric has the following properties: it is non-negative ($d(x,y)\geq 0$); it is zero if and only if the two inputs are equal ($d(x,y)=0$ iif $x=y$); it is symmetric ($d(x,y)=d(y,x)$); and satisfies the triangle inequality ($d(x,z)\leq d(x,y)+d(y,z)$). The KL divergence satisfies the first two properties but it is a non-symmetric measure and does not satisfy the triangle inequality (Cover and Thomas 1991). Moreover, it is possible that for certain epochs there would be no event of a particular type, which would make Q_t equal zero, and the KL Divergence infinite. Thus, the JS Divergence was used instead (Lin 1991). The JS Divergence is a symmetric and smoothed version of the KL Divergence, defined as

$$D_{JS}(t) = \frac{1}{2}D_{KL}(P||M_t) + \frac{1}{2}D_{KL}(Q_t||M_t) \qquad \textbf{Equation 5.2}$$

where $M_t = \frac{1}{2}(P + Q_t)$. Another advantage of the JS Divergence is that its square root ($ND_{JS}(t) = \sqrt[2]{D_{JS}(t)}$) is bounded (not infinite) and satisfies the triangle inequality (Endres and Schindelin 2003). Therefore, we used this true metric for calculation. The ND_{JS} was computed for each patient and each channel.

5.4.2.2.2 Ranking Distance

Not only are the rates per minute important, but so are the ranking of channels according to rates of HFOs (from highest to lowest HFO rate). To determine how the different durations affected the ranking of channels, we implemented an algorithm to measure the distance between two sequences, in our case rankings. The Ranking Distance (RKD) measures the difference between two rankings as the sum of the cost associated with each channel that is not in the "correct" position (with respect to the ranking of the whole interval, our "gold standard").

$$RKD(t) = \sum_{i=1}^{\#Channs} \sum_{j=Pos_t} C_{ij}$$ **Equation 5.3**

where interval t= 0.1,0.5,1,1.5,….,9,9.5,10min

where Pos_t are the new position in the ranking, #Channs the number of channels for that patient. The matrix cost (*C*) measures the cost of being in a different position in the ranking, and was computed as the difference in rates of those channels in the "true" ranking. Thus, C_{ij} is the cost associated with being in position j in the ranking instead of in position *i*.

$$C = \begin{bmatrix} 0 & \dots & C_{1j} & C_{1N} \\ C_{i1} & 0 & C_{ij} & C_{iN} \\ \vdots & \vdots & \ddots & \vdots \\ C_{N1} & \dots & C_{Nj} & 0 \end{bmatrix}$$ **Equation 5.4**

where i=1,2,…, #Channs and j=1,2,…, #Channs

where $C_{ij} = \frac{|\#Ev_i - \#Ev_j|}{K}$

where $\#Ev_i$ is the rate of events in channel *i* for the whole EEG, K is a normalizing constant and C_{ij} equals C_{ji}. By using this cost function, the change in position is taken into consideration as well as the importance of the change as represented by the difference in rate between channels. The RKD score was normalized by dividing by a constant (*K*) such that a RKD score equals 0 only when the rankings are the same, while a RKD score of 1 represents total discrepancy. The RKD is computed for each type of event (ripple, fast ripple and spike) for each patient.

5.4.2.3 *Root Mean Square Difference*

In order to decide when a stable measurement is achieved for each patient, we needed a thresholding approach that was consistent for both methods. Given that the ND_{JS} was calculated for each channel and that the RKD score was calculated for each type of event, we implemented for each of them the root mean square difference (RMSD), which provided a single value for each patient and for each interval.

As a reference distribution and to compute the threshold, we choose a uniform distribution of events with the same number of events as the real data. A uniform distribution of events is the ideal distribution in this case since it has the same rate at any interval length (i.e. we obtain a stable measurement of the rate) and, therefore, the difference in information gained and the difference in ranking would be minimal across the different intervals. For each channel, 10 uniform distributions were produced by distributing randomly but uniformly the same number of total events as the real data over a 10-min interval. On the other hand, a beta distribution of the events with parameters $\alpha=3$ and $\beta=1$ was used to represent the case when most of the events occur at the end of the interval, and therefore the selected interval will not provide a stable measurement of the rates. In this way, one good and one bad possible distribution of events were taken into consideration.

Thus, to assess when a stable measurement is obtained in terms of the information gained in each patient, the ND_{JS} obtained from the data was compared with the ND_{JS} obtained from a uniform distribution with the same rate of events in the 10-min interval (same R_{10min}, FR_{10min}, and Sp_{10min}). The ND_{JS} was computed for the real and corresponding uniform distributions, for each channel and for each starting point. The RMSD between ND_{JS} of each channel and the mean ND_{JS} of the 10 uniform distributions corresponding to the same channel and starting point (see above), was computed for each patient.

$$\mathrm{RMSD_{JS}(t)} = \sqrt[2]{\sum_{c,st} \frac{\left(ND^{real}_{JS_{c,st}}(t) - ND^{unif}_{JS_{c,st}}(t)\right)^2}{N_c + N_{st}}} \qquad \textbf{Equation 5.5}$$

for interval t= 0.1,0.5,1,…,9.5,10 min

where *c* are all possible channels of a patient and *st* are all the possible starting points. Thus, the analysis of stability was done independently for each patient based on the comparison of the ND_{JS} obtained for the patient and the ND_{JS} that corresponds to a uniform distribution with the same total number of events.

For selecting the threshold, the $RMSD_{JS}$ between the ND_{JS} of each uniform distribution and the mean ND_{JS} of all the uniform distributions (across the patients marked for 10 min) was computed, resulting in only one reference $RMSD_{JS}(t)$ value for each interval. It represents the variability of uniform distributions among patients. Because around 40% of the channels had a rate smaller than 1/min considering the complete marked interval (93/240 channels with ripples, 49/100 channels with fast ripples, and 122/304 channels with spikes for the first group of patients), and in order to have at least 1 event representative of the uniform distribution, we chose a 2-min interval as the interval in which to compute the threshold. The threshold ($thRMSD_{JS}$) was then empirically chosen as two times the reference $RMSD_{JS}(t)$, for t= 2min. For example, if for a patient the $RMSD_{JS}(t \geq 3min) < thRMSD_{JS}$, intervals longer than 3 min were considered equivalent to the uniform distribution in terms of information gain, and therefore a 3-min interval was representative of the whole segment of EEG, with no information gained by marking more than 3 min.

An equivalent approach was followed to assess when a stable measurement was reached in terms of ranking of channels. For each patient, the RMSD of the obtained RKD score with respect to the mean RKD score obtained by 10 uniform distributions was performed, similar to the approach followed for the JS Divergence.

$$RMSD_{RKD}(t) = \sqrt[2]{\sum_{ev,st} \frac{\left(RKD^{real}_{ev,st}(t) - RKD^{unif}_{ev,st}(t)\right)^2}{N_{ev}+N_{st}}} \quad \textbf{Equation 5.6}$$

for interval t= 0.1,0.5,1,…,9.5,10 min.

where *ev* are all possible events (ripples, fast ripples and spikes) and *st* are all the possible starting points. A stable measurement was considered to be achieved for a patient at a certain interval, in terms of ranking of channels, when the $RMSD_{RKD}$ was smaller than the threshold. Following the same thresholding approach used for JS Divergence, the threshold ($thRMSD_{RKD}$) was set as two times the reference $RMSD_{RKD}(t)$, for t= 2 min. As before, the reference $RMSD_{RKD}(t)$ was obtained from the RKD scores based on all the uniform

distributions for all patients with respect to the averaged RKD score of the uniforms.

5.5 *Results*

5.5.1 *Inter-reviewer agreement*

This was assessed by two reviewers marking the first minute of each recording. In the first 10 patients, the average κ was 0.6 for ripples, 0.56 for fast ripples and 0.49 for spikes. In order to improve concordance across readers, all channels with $\kappa < 0.5$ were discussed and new criteria were developed. For instance, the gain selected to mark spikes was redefined, whether to consider polyspikes as individual spikes or as one group was decided, and agreement regarding spiky baselines was achieved. The new criteria were considered for the remarking of the channels with low kappa, by one of the readers, and for the second group of patients (30 patients). For the second group, κ was higher: 0.7 for ripples, 0.7 for fast ripples and 0.67 for spikes, showing a clear improvement particularly for spikes.

When analyzing the common features of the jointly marked events, we observed that those HFOs that were identified by both reviewers were those that clearly stand out from the baseline. Moreover, when analyzing those channels with κ around 0.5, we found that the markings were consistent between reviewers and that the overall rates remained similar. In the case of channels with spiky (or bumpy) baselines, it was important to agree on the display gain to have good agreement. There was also sometimes disagreement in the duration of the marked HFOs. In the case of spikes, the use of a common gain to mark was the main factor of improvement. In addition, special attention was paid to avoid the erroneous marking of sleep spindles as events.

5.5.2 *Sufficient Interval*

5.5.2.1 *Initial assessment of the methods*

Once concordance was evaluated for the first minute, the same 10 patients were marked for the remaining 9 min by one reviewer, and the different intervals were compared against the 10-min interval to assess the interval length at which representative information of the whole EEG was reached. Because the JS Divergence and the RK Distance measure different aspect of the obtained information, they can be considered complementary; thus, patient's markings had to provide a stable measurement in both methods at a particular interval length.

In 9 of the 10 patients, an interval of less than 5 min provided the same information as an interval of 10 min, as measured by the JS Divergence (example in Figure 5.2.A). For patient P4 (Figure 5.2.B), for whom this was not the case, only at an interval of 7.5 min was the $RMSD_{JS}$ smaller than the threshold (Figure 5.2.D). Furthermore, if we compare the averaged JS Divergence, across channels for each patient, with the averaged JS Divergence, across channels and across patients, for a uniform and a beta (α=3, β=1) distributions, it can be observed that for all subjects but P4 the mean JS Divergence is similar to the mean JS Divergence for the uniform distributions (Figure 5.2.C). On the contrary, the mean JS Divergence for P4 resembles more the mean JS Divergence for the beta distribution.

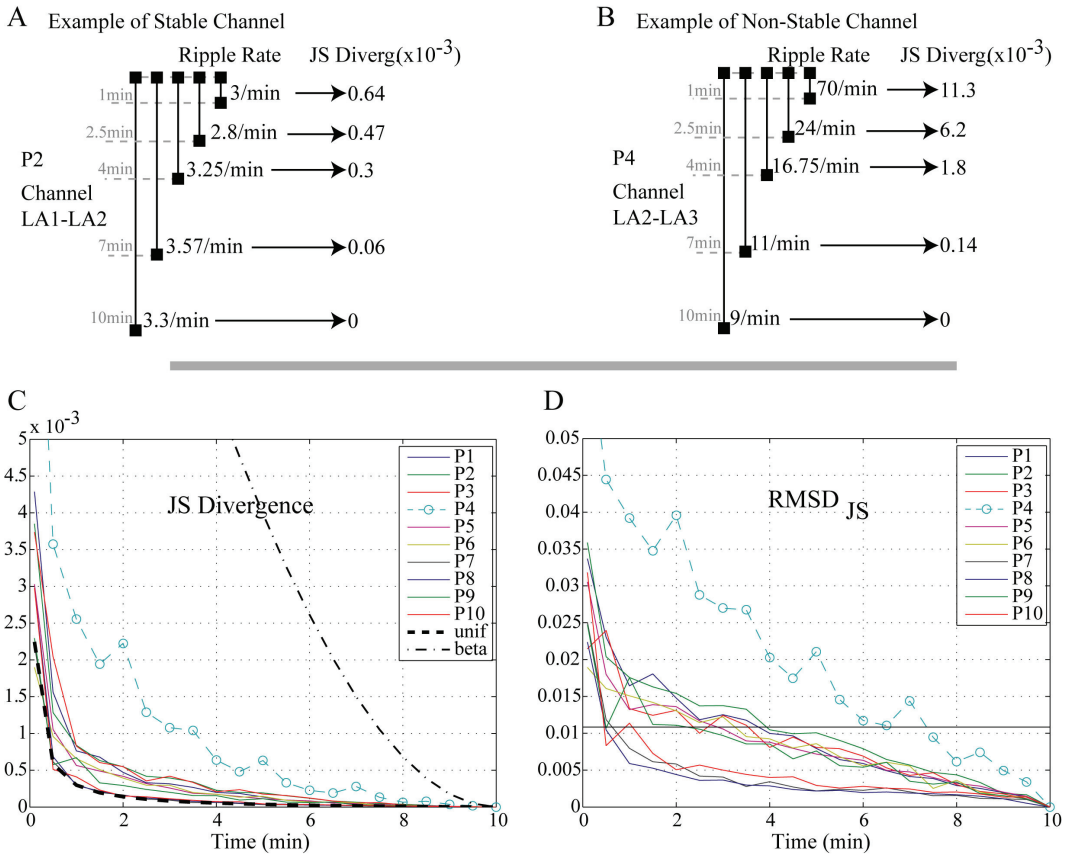

Figure 5.2. The JS Divergence establishes the information gained when increasing the interval length. *Top:* Example of ripple rate for different intervals in one channel and the obtained JS Divergence (which is obtained by pooling ripple, fast ripple and spike rates). A) Example of a stable channel. B) Example of a non stable channel. *Bottom:* C) Comparison of the mean JS Divergence across channels, for the real markings, for a uniform distribution and for a beta distribution (α=3, β=1). D) Root mean square difference ($RMSD_{JS}$) between ND_{JS} (root square of JS Divergence) obtained from the real marking of events and ND_{JS} that would be obtained if a uniform distribution of the events was used instead. Patient with a dashed line and a symbol (o) have a $RMSD_{JS}(t \geq 5min) > thRMSD_{JS}$. The $thRMSD_{JS}$ equals twice the $RMSD_{JS}$ for all uniform distributions at 2-min interval. A 10-min interval is considered as the "gold" standard.

When assessing when a stable measure is obtained regarding the ranking of channels, 8 of 10 patients achieved a stable measurement before 5 min as measured by the RKD (examples in Figure 5.3.A and 5.3.B). The $RMSD_{RKD}$ measures the difference between the obtained RKD and the RKD of a uniform distribution and was smaller than threshold for intervals smaller than 2 min for 8 of the 10 patients. One patient (P7) only obtained an $RMSD_{RKD}$ value smaller than threshold at 5-min intervals, while another (P1) only at 5.5 min (Figure 5.3.D). Furthermore, when analyzing the median value of the RKD (across different event

types and different starting points) all but patient P1 showed a distribution similar to the uniform distribution for intervals of 4 min or longer (Figure 5.3.C).

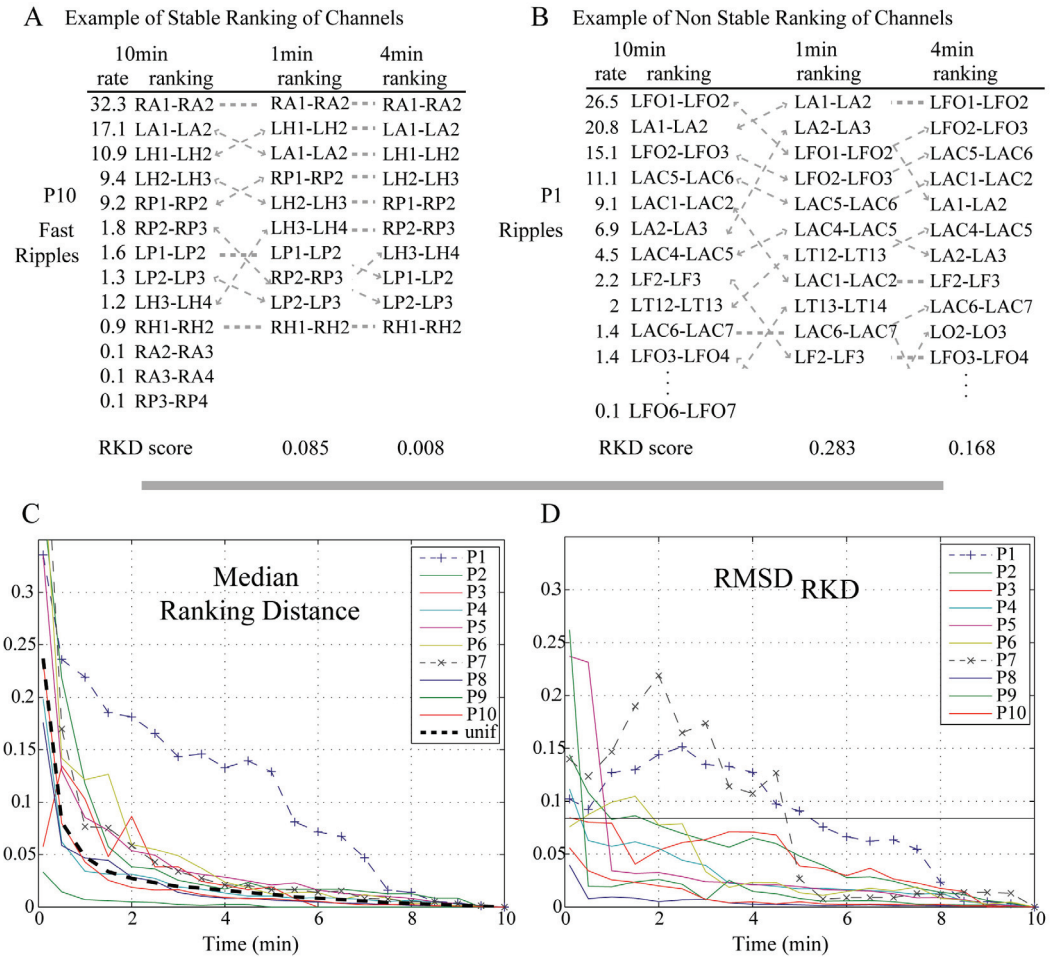

Figure 5.3. The Ranking Distance (RKD) measures the difference in ranking for different intervals. *Top:* Example of difference in ranking and corresponding RKD scores, for 1min and 4min intervals. A) Example of a stable ranking (patient P10 and fast ripples). B) Example of non stable ranking (patient P1 and ripples). *Bottom:* C) Median RKD (across starting points and type of event) for each patient when comparing with the ranking of channels for the 10-min interval. D) $RMSD_{RKD}$ of the RKD score when comparing the obtained score for each interval with the corresponding RKD score for a uniform distribution. Patients with a dashed line and a symbol (+ or x) have a $RMSD_{RKD}(t \geq 5min) > thRMSD_{RKD}$. The $thRMSD_{RKD}$ equals twice the $RMSD_{RKD}$ for all uniform distributions at 2-min interval. A 10-min interval is considered as the "gold" standard.

Thus, a stable measurement of the rates and ranking of channels is achieved for intervals smaller than 5 min for most patients, showing that an interval smaller than 5 min would provide the same relevant information as a 10-min interval for most patients. In particular, in terms of the relative information gained ($RMSD_{JS}$), a stable measurement is achieved for intervals smaller than 5 min for all patients

but one. Moreover, in three patients no information was gained if analyzing intervals longer than 2 min. On the other hand, the ranking of channels ($RMSD_{RKD}$) remained stable for durations longer than 3 min in most patients. Thus, to ensure that the marked interval is representative of the whole EEG for most patients with respect to rates and ranking of channels, 5 min was selected as the interval length to be marked from now on.

5.5.2.2 *Evaluation of the same patients for a 5-min interval*

Since we showed that 5 min is a sufficient interval for most patients, we repeated the same analysis in this group of 10 patients considering the first 5 min as the "gold" standard, resulting in similar conclusions. This further validates the hypothesis that 5 min of marking was sufficient and shows consistency of the methods. Indeed, when these 10 patients were considered to be marked for 5 min and analyzed, the conclusion according to the JS Divergence was that for patient P1 and P4 the $RMSD_{JS}$ was smaller than the threshold only at 4-min intervals (Figure 5.4.A). Moreover, the $RMSD_{RKD}$ indicated that for 2 patients (P1 and P7), marking only 5 min was not enough (Figure 5.4.B). Thus, for the 3 patients for whom the previous analysis concluded that more than 5 min were necessary, the same conclusion was reached. Therefore, these methods seem appropriate to evaluate the length that is sufficient to mark to ensure that all relevant information is captured.

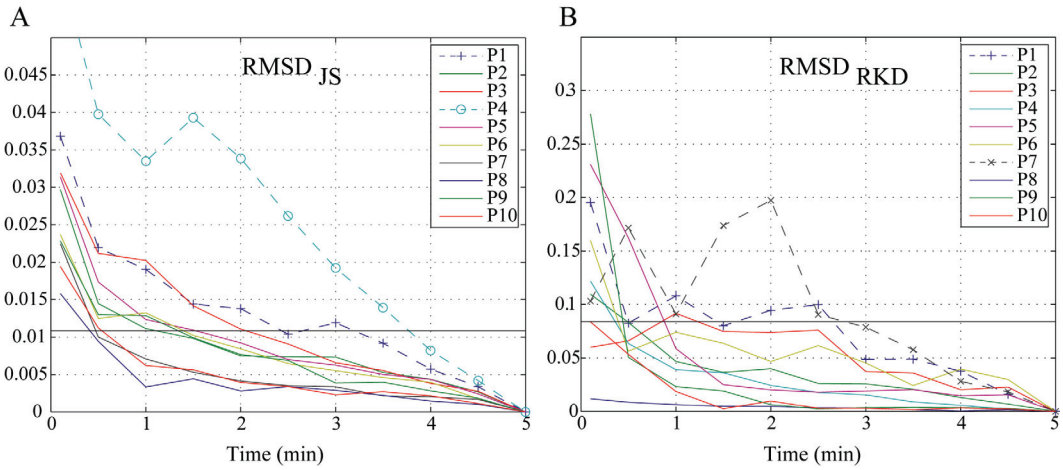

Figure 5.4. When using the procedure to assess if 5 min provide stable measurements for the first group of patients, three patients (P1, P4, and P7) do not present stable measurements as indicated by either A) $RMSD_{JS}$ or B) $RMSD_{RKD}$ (did not have a RMSD smaller than threshold at $t \leq 2.5$min). These are the same three that only reached a stable measurement after 5-min intervals comparing with 10 min.

5.5.2.3 *Evaluation of additional patients marked during 5 min*

The second group, consisting of 30 patients, was visually marked during 5 min and their stability evaluated. For five of these patients, a 5-min interval was not sufficient to provide consistent information in terms of information gained or stability in the ranking of rates of HFOs and spikes (Figure 5.5). Because we are comparing with 5 min as the "gold standard" a stable measurement must be reached well before the 5-min interval for an interval to be considered representative of the whole EEG. Thus, if there is not stable measurement at 2.5-min intervals, we cannot determine whether 5 min are stable or not. According to the $RMSD_{RKD}$, four patients (P2, P5, P13 and P26) did not obtain an $RMSD_{RKD}$ smaller than threshold before 3-min intervals. In addition, for one patient (P29), the $RMSD_{JS}$ remained within the vicinity of the threshold at 2.5 min. As before, an interval was considered representative of the whole marked EEG (in this case 5 min), only when this was indicated by the $RMSD_{JS}$ and the $RMSD_{RKD}$. Therefore, these five patients were marked for 10 min. The analysis of the 10-min interval for these five patients indicates that three of them were actually only stable after 5-min intervals. Indeed, in terms of information gain, the patient (P29) that did not clearly achieved stability before only achieved a $RMSD_{JS}$ smaller than threshold at 5.5-min interval when marked for 10 min. Moreover, the stability

with respect to the ranking of channels was achieved after 5 min by two of the remarked patients (P2 and P13) and at 2-min interval for the other three.

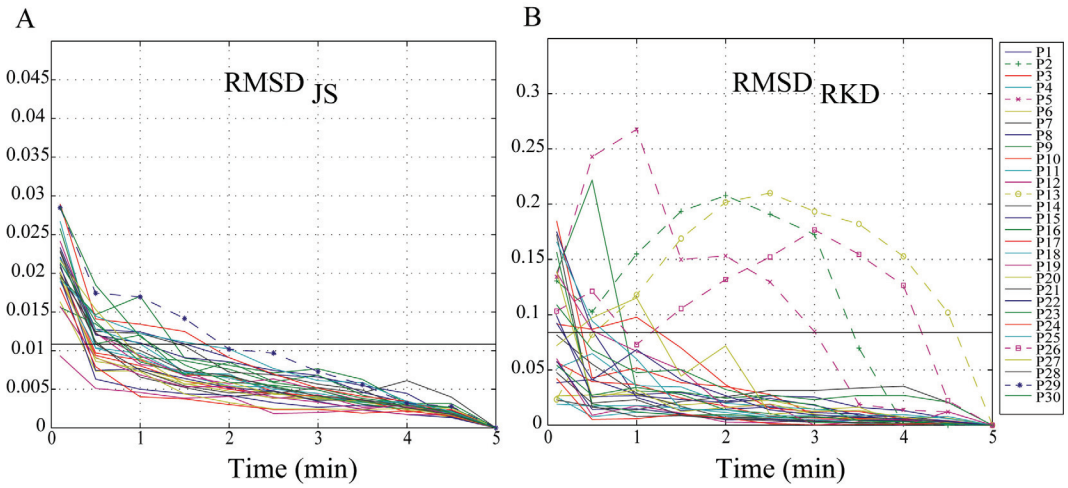

Figure 5.5. Evaluation of the second group of patients (30 patients) marked for 5 min. A) $RMSD_{JS}$. All patients reached stable measurements at 2.5 min according to the JS Divergence, but 1 patient (P29) remained too close to the threshold, and was decided to be marked for 10 min. B) $RMSD_{RKD}$. Four patients did not achieve stability in the ranking of channels and were thus marked for 10 min.

5.6 *Discussion*

We propose a new procedure to assess whether a stable measurement is achieved when identifying HFOs and spikes from intracranial recordings with macroelectrodes. The procedure is suitable to improve the visual identification of the events as well as to ensure stable measurements when using automatic detectors. The methods were first evaluated for 10 patients whose EEG was visually marked, considering a 10-min interval as the "gold standard". It was possible to establish that intervals smaller than 5 min were representative of the whole EEG in most patients. From then on, this procedure is routinely used to evaluate the stability of the rates in all the patients when marked for 5 min. The incorporation of a measure of agreement among reviewers for the first minute improves consistency in the markings and allowed us to become less dependent of the reviewer that marks the complete file.

Until now, our group (Bagshaw *et al.,* 2009, Jacobs *et al.,* 2008a, Urrestarazu *et al.,* 2007) and others (Staba *et al.,* 2002) have chosen 10 min as the interval to

select. Ten minutes seem a reasonable interval given that, from a practical perspective, a longer interval would not be feasible to mark and that SWS is not usually stable for longer periods in patients with implanted electrodes. When using automatic detectors, 20 to 30-min intervals are also selected (Staba *et al.,* 2007). However, no attempt had been made to assess if those intervals were necessary, or if shorter intervals might be sufficient. Moreover, no systematic approach was used to assess whether stable measurements are obtained during the selected intervals. We reported on a method to establish for how long it is reasonable to mark events, to ensure that the relevant information is obtained.

A secondary aim of this study was to help in the formal characterization of HFOs. At present, a few automatic HFOs detectors exist (Khalilov *et al.,* 2005, Staba *et al.,* 2002), but given the lack of a formal definition of HFOs, assessing the performance of an automatic detector is difficult. Thus, by helping to provide a more complete definition of HFOs we hope to help in a better characterization of HFOs, which could lead to the future development of robust automatic detection of these events. For example, the new criteria agreed upon after reviewing the channels with low kappa and the subsequent improvement of the results suggests that the proposed procedure could help towards a standard definition of HFOs. For instance, the recognition of channels with spiky baselines (particularly the deepest hippocampus channels), will allow for the proper recognition and particular analysis of these channels. If not considered apart from the rest, these channels could influence the training of automatic detectors. In addition, in some cases with disagreement, we observed that different subjective thresholds were used by the two reviewers for marking each patient. This is a good indicator that the signal to noise ratio of the HFOs was not consistent across patients and that it has to be taken into account when designing an automatic detector. Furthermore, discrepancies with respect to the duration of the HFOs were observed in some cases, when one reviewer marked one event while the other marked two. It would be important to define not only a minimum duration, but also an end point of an HFO. Therefore, by incorporating a measure of

information stability together with a better characterization of HFOs, we aim to improve the reliability of automatic detectors.

Given that different start points can be used for the analysis, the procedure could also tell us which interval/s within the complete marked interval are those that are not stable. This aspect was not explored in detail in this paper, but could be particularly useful to determine which intervals provide stable measurements when using automatic detectors. There are many reasons for an interval of any length not to be stable. For instance, a patient can change sleep stage, there could be a change in the baseline, and there could be even changes in rates or ranking of channels due to a change in the epileptic activity. In those cases, it would be possible to use these methods to analyze different intervals, to separate between intervals and utilize only the selected ones for the subsequent processing. Previous studies showed correlation with the SOZ, suggesting that the ranking of channels and HFO rates may be able to distinguish between SOZ and non-SOZ areas (Jacobs *et al.,* 2008a). The RK Distance could also be used to assess a difference in ranking of channels in terms of rates between different types of events (e.g. ranking of ripples vs. ranking of spikes), or channel location. Further investigation in this direction could provide a better understanding of the characteristics of HFOs.

A valid measurement of HFO events is essential for clinical use such as the identification of epileptic or potentially epileptic regions during intracranial investigations. This could help the delineation of the surgical extent and in the prediction of surgical outcome if post-surgical outcomes are evaluated. This would be possible, according to our results, after evaluating only 5 min of EEG.

Finally, this study was limited to events marked during SWS using a bipolar montage. Given that the largest amount of HFOs occur during SWS (Bagshaw *et al.,* 2009, Staba *et al.,* 2004), we decided to develop and test our methods in events marked during this stage. Even though the procedure can be used for other stages and montages, the conclusions cannot be generalized without further

validation. Moreover, we assumed that 10 min provide a stable measurement and used only one 10-min interval per patient as the "gold standard". The methodology we propose can be applied to any interval length and future studies using an automatic detector for different intervals could provide further validation.

In conclusion, the procedure presented in this study provides an approach to assess the duration of EEG that must be interpreted to obtain a representative measurement of HFO and spike rates from intracranial recordings with macroelectrodes in patients with epilepsy, and to optimize the time needed to mark these events. We propose that 5 min provides, in most cases, the same information as a longer interval, in terms of a stable measurement of rates and ranking of channels. We present a method to identify when this is not the case and thus more data needs to be marked. The following procedure is suggested for each patient: 1 min is marked by two readers (which could be human readers or an automatic approach) and concordance is evaluated. Once there is good agreement in the first minute, the remaining 4 min are marked by one of the reviewers and the 5-min interval is then evaluated for stability. When a stable measurement of the rates is not obtained within the 5-min interval, the following 5 min are also marked, and so on. These methods are useful to control for consistency between reviewers and to evaluate if the selected interval provides consistent information, or if a longer one is needed. Moreover, this procedure ensures a stable measurement in terms of rates and ranking of channels, when automatically detecting HFOs and spikes.

5.7 *Acknowledgements*

This study was supported by Grant MOP-10189 from the Canadian Institutes of Health Research. R.Z. was supported by National Science and Engineering Research Council (NSERC) Postgraduate Scholarship (PGSD). M.Z. was supported by the Netherlands Organization for Scientific Research (NWO)

AGIKO-Grant No.92003481, the University Medical Center Utrecht (internationalization grant) and the “Stichting de drie lichten”.

5.8 *Significance*

This manuscript presented a procedure useful to control for consistency between readers and to evaluate if the selected interval provides stable information, for automatic and visual identification of events. It was shown that a 5-min interval provided the same information, in terms of HFO rates and ranking of channels with respect to the rate, as longer periods. EEG studies of event rates usually select a fixed duration arbitrarily. This study was the first to define a minimum duration necessary to obtain consistent marking in terms of event rate. This original approach is applicable to any event marking in the EEG, and could be easily extended to other fields. Since published, this procedure has been used to ensure consistency and evaluate stability in the marking of HFOs in all patients implanted with macroelectrodes at the MNI (15-20 patients per year).

Chapter 6. *Automatic detection of High Frequency Oscillations*

6.1 *Context*

Visual analysis of HFOs is highly time-consuming and subjectivity is inevitable. Consistency in the markings can be achieved with the procedure developed in the manuscript presented in the previous chapter. For the systematic study of HFOs and to propel the clinical application of HFOs as biomarkers of epileptogenic tissue, automatic detection of HFOs is necessary.

Since the idea is to create a clinical and research tool, the definition of HFOs originating from expert reviewers ("four-oscillations that clearly stand out from background") should be followed as closely as possible. With this in mind, baseline segments (i.e. segments without HFOs) can be first detected, and then this information incorporated to detect HFOs. Only a handful of detectors were developed before and they were based on the comparison of the energy at a particular time point with the energy of the whole EEG segment (including the HFOs of interest), under the assumptions that HFOs are rare events. However, this assumption does not hold in all channels, and the incorporation of local baseline information could improve performance. Since each detector was developed with a different implicit definition of what to detect as HFOs, a comparison in the same dataset is important. In order to compare with a gold standard, visual marking obtained using the procedure described in the previous chapter can be used.

This chapter is composed of two manuscripts. The first one presents the first version of the automatic detector of HFOs. This manuscript was published as (Zelmann R, Mari F, Jacobs J, Zijlmans M, Chander R, Gotman J. 2010. *Automatic detector of high frequency oscillations for human recordings with macroelectrodes*. Conf Proc IEEE Eng Med Biol Soc 2010:2329-33). The second

manuscript presents the complete version of the automatic detector and a comparison with other detectors. Emphasis is placed in the importance of training a detector for a particular dataset and not using a detector "out of the box". Issues involved in validating the detections are highlighted. This manuscript was published as (Zelmann R, Mari F, Jacobs J, Zijlmans M, Dubeau F, Gotman J. 2012. *A comparison between detectors of high frequency oscillations*. Clin Neurophysiol 123:106-16).

Manuscript #2: Automatic detector of High Frequency Oscillations for human recordings with macroelectrodes

6.2 *Abstract*

High Frequency Oscillations (HFOs) in the EEG are a promising biomarker of epileptogenic tissue. Given that the visual marking of HFOs is highly time-consuming and subjective, automatic detectors are necessary. In this study, we present a novel automatic detector that detects HFOs by incorporating information of previously detected baselines. The detector was trained on 72 channels and tested on 278, achieving a mean sensitivity of 96.8% with a mean false positive rate of 4.86%. This low rate is reasonable since only visually marked baseline segments were considered as the true negatives. This detector could be useful for the systematic study of HFOs and for their eventual clinical application.

6.3 *Introduction*

Epileptic conditions affect approximately 0.5% of the population (Niedermeyer 2005c). About 20% of the patients are refractory to medication, so in some cases with presumed focal epilepsy the resection of the epileptic focus can be considered. When non-invasive techniques (scalp EEG and imaging) give only a rough estimate of the epileptogenic region but cannot ensure the precise location of the focus, invasive recording are sometimes required.

Traditionally, only frequencies up to 70Hz were considered of clinical relevance. Recent findings in rodents and humans showed the presence of higher frequency activity (up to 500Hz) and a possible relation of High Frequency Oscillations (HFOs) with epileptogenesis (Bragin *et al.,* 1999a, Bragin *et al.,*

1999b, Jacobs *et al.,* 2008a, Jirsch *et al.,* 2006, Staba *et al.,* 2002, Urrestarazu *et al.,* 2007).

HFOs are spontaneous EEG patterns in the range 80-500Hz, consisting of at least 4 oscillations that can be distinguished from background. The lack of a quantitative definition makes the detection of HFOs difficult and subjective. Visual marking of HFOs can be performed (e.g. (Jacobs *et al.,* 2008a, Urrestarazu *et al.,* 2007)), but it is highly time consuming (it takes about 10 hours to visually mark HFOs in a 10-channel 10-minute recording) and subjectivity is inevitable. Thus, the development of automatic HFO detectors is crucial for the systematic study of HFOs and for their eventual utilization in clinical settings.

Only a handful automatic detectors based on different energy functions exist (Crepon *et al.,* 2010, Gardner *et al.,* 2007, Staba *et al.,* 2002). In all these detectors the energy of the signal is compared with a threshold that is computed based on the segment of EEG under consideration (including the events), under the assumption that HFOs are rare events.

In this study, we propose a different approach in which we first detect baseline segments and then compute the energy threshold with respect to those baselines. By considering the detected baselines locally, the characteristic of the background surrounding the events is considered for detection. This is particularly important in channels where the background is not perfectly flat and in channels where a large number of interictal epileptiform discharges (spikes) are present.

6.4 *Methods*

6.4.1 *Patient information*

Between September 2004 and April 2008, 45 patients with medically intractable epilepsy underwent depth macro-electrode (surface area 0.8mm^2) implantation at the Montreal Neurological Hospital. The depth EEG (SEEG), recorded with the Harmonie system (Stellate, Montreal, Canada), was low-pass

filtered at 500Hz and sampled at 2000Hz, allowing for the identification of HFOs. Twenty patients were randomly selected, but one had to be excluded due to continuous artefacts. All patients gave informed consent in agreement with the Research Ethics Board of the Montreal Neurological Institute and Hospital (MNI).

6.4.2 *Channels and events selection*

HFO events were identified independently by two experienced reviewers in all functioning channels during one minute of slow wave sleep with the method described in (Jacobs *et al.,* 2008a). We considered as our gold standard those events jointly marked by the two reviewers. The duration of the gold standard (visual) HFO events was the intersection between their markings. In addition, baseline segments (where it was clear that no oscillation was present) were visually marked.

Channels with nearly continuous high frequency activity or less than one visually identified HFO or baseline were excluded from this study. The database therefore consisted of 19 one-minute sections, each with 6 to 36 channels. Given that the variability within channels of a patient is as large as the variability across patients, all channels were considered independently. Twenty percent of the channels were randomly selected and used for training the detector, resulting in 278 channels for testing the performance of the detector. Of these channels, 97 were temporal and 181 were neocortical (NC); 73 were in the seizure onset zone SOZ of the patient. These channels included 5238 visually identified HFO events and 51076 visually identified baselines that were used as the gold standard events. The mean length of the baselines was 237ms (range: 70 to 398ms).

6.4.3 *Automatic detection of HFOs*

Given that HFO are short oscillatory events that "stand out" from background activity, a logical approach to identify these events is an energy based detector. Existing automatic HFO detectors are based on the comparison of the energy of the signal with the EEG epoch that includes the events. The main difference among published detectors is the type of energy function that is computed on the

filtered signal, either the root mean square (RMS) amplitude (Staba *et al.,* 2002), the short-time line length (Gardner *et al.,* 2007), or the Hilbert envelope (Crepon *et al.,* 2010). In contrast, this detector tries to look at the problem from a perspective more similar to the way that human reviewers mark: by comparing the EEG with the surrounding previously identified baseline.

6.4.4 *The MNI detector*

The proposed detector (referred to as *MNI detector*) consists of a baseline detector block and an energy based event detector block (that incorporates the baseline information). The MNI detector aims to detect as many events as possible, even if a large number of false detections take place.

The first step is the detection of baselines. We define as baselines, segments of EEG where there is no oscillatory activity of any kind. The baseline detector (Chander 2007) is based on the wavelet entropy (WE) which measures the degree of randomness (vs. oscillatory behaviour) in the signal (Rosso *et al.,* 2001). To enhance the oscillatory characteristics of the signal, the WE was applied to the autocorrelation of the filtered (80-450Hz) signal (Chander 2007). Thus, the wavelet power is computed as

$$W_n(a,b) = \left|\frac{1}{\sqrt{a}}\int_{t=0}^{L} r_n(t)\psi^*\left(\frac{t-b}{a}\right) dt\right|^2 \qquad \textbf{Equation 6.1}$$

where $\psi(a,b)$ is chosen as the complex Morlet wavelet and $r_n(t)$ is the autocorrelation of the n^{th} EEG segment of length L=75ms. The normalized wavelet power is

$$P_n(a,b) = \frac{W_n(a,b)}{\sum_a W_n(a,b)} \qquad \textbf{Equation 6.2}$$

and the WE_n is obtained as

$$WE_n(b) = -\sum_a P_n(a,b)\log_{10}[P_n(a,b)] \qquad \textbf{Equation 6.3}$$

For a white noise signal, there will be similar contributions at all scales and the maximum WE is obtained as $WE_{max} = \log_{10}(1/\#a)$ where #a is the number of possible scales. Thus, a segment is considered as baseline (ie: without oscillatory behaviour) when the minimum WE_n for segment n is larger than the threshold obtained from training (0.56 WE_{max}).

The next block detects possible HFOs based on the energy defined as the moving average of the root mean square amplitude of the filtered signal. Each channel is band-pass filtered (80-450Hz) and segments with energy above threshold during more than 15ms were considered HFOs. The energy threshold is obtained by computing the empirical cumulative distribution function (CDF) of each 2-sec baseline segment and returning the value at the 95 percentile as the threshold. Thus, as indicated in (Gardner *et al.,* 2007), no assumption regarding the normality of the energy distribution is necessary. This block of the detector is similar to (Staba *et al.,* 2002) in the energy function and to (Gardner *et al.,* 2007) in the threshold computation, but unlike all the other detectors, the MNI detector considers the threshold with respect to the detected baselines. A band-pass FIR equirriple filter was used (f_{Stop1}=70Hz; f_{Pass1}= 80Hz; f_{Pass2}=450Hz; f_{Stop2}=460Hz; stopband attenuation = -60dB). The signal was filtered forward and backwards to obtain zero-phase. All processing was implemented based on MATLAB. All values were obtained from the optimization described below.

Therefore, instead of considering the energy with respect to the complete EEG (as in Crepon *et al.,* 2010, Gardner *et al.,* 2007, Staba *et al.,* 2002), the EEG is divided in segments where 2 seconds of baseline are found (e.g. if in the first 12 seconds of data, there are 2 seconds of detected baselines, this 12 seconds are considered as an epoch and the energy threshold of the epoch is unique). In this way, the local characteristics of the baseline around the point of interest are considered in a similar way than it is considered when visually marking HFOs.

6.4.5 *Performance metrics*

Receiver Operating Characteristic (ROC) curves measure the performance of the detector when varying the energy threshold, representing different levels of sensitivity/ specificity. The visually marked HFOs were considered as the true positive (P) events and the visually marked baselines as the true negative (N) events. Segments of EEG where nothing was visually marked by the reviewers were not taken into account, under the assumption that there might be HFOs in those segments, which were not visible to the human reviewer. The average ROC was computed by computing the ROC curve for each channel and averaging each threshold value across channels (Fawcett 2006).

Thus, a TP was an HFO identified by the automatic detector that was visually marked; a FP was an automatically detected event that actually corresponded to a visually marked baseline; a FN was a visually marked HFO that was missed by the automatic detector; and a TN was a visually marked baseline where no HFOs were identified.

In addition, Cohen's Kappa coefficient (Cohen 1960) was computed to compare the automatic detector with the gold standard in each channel. This coefficient measures the degree of agreement between two reviewers (in this case one human and one automatic), taking into account the agreements made by chance. Kappa < 0 reflects an agreement due purely to chance and Kappa = 1 indicates complete agreement.

Not only are the percentages of detected HFOs important, but also whether the order of the channels with respect to the relative number of events is preserved, since channels with a high rate of HFOs have been associated with the SOZ (Jacobs *et al.,* 2008a) and their removal with good surgical outcome (Jacobs *et al.,* 2010b). The Ranking Distance (RKD; Zelmann *et al.,* 2009b) measures the cost of obtaining a different order of channels (ordered from more to fewer events) when detecting events automatically compared to the order obtained when visually identified events. For instance, if channel A has 3 visually detected

events, channel B 25 and channel C 5, we expect the automatic detector to detect more events in channel B than in the other two. RKD score ranges from 0 to 1, with 0 representing exactly the same ranking, and 1 corresponding to a ranking completely upside down. An RKD score smaller than 0.2 is usually considered as a measure of good agreement. Thus, even though we accept a large number of false positives under the assumption that there might be events not seen by the reviewer, the relative number of false positives to true positives must be equivalent in all the channels. For this measure, the automatically detected events identified in the whole EEG are considered.

6.4.6 *Parameter optimization*

The parameters of the baseline detector were optimized on 36 channels with the following criteria: maximize the duration of detected baseline that overlaps with the reference, constrained by global (median across channels) FPR ≤ 0.05 (FPR=1-Specificity). Each channel "voted" their best parameters (i.e. the parameters to obtain the largest baseline overlap), and the set of parameters with most votes was selected.

For optimizing the parameters of the second block, the events detector, a similar approach was taken with another 36 channels. In this case, each channel "votes" with its best parameters to obtain maximum Kappa, constrained by: global FPR ≤ 0.1; FPR per channel ≤ 0.2; Sensitivity per channel ≥ 0.8. In both cases, each channel could vote for more than one parameter set (i.e. more than one set of parameters could yield the maximum sensitivity).

6.5 *Results*

The optimized parameters of the MNI detector were: duration of each baseline segment = 75ms; wavelet entropy threshold = 0.56 of WE_{max}; minimum duration of HFO event = 15ms; energy threshold = 95 percentile of CDF of baseline; short RMS window = 10ms; baseline length = 2s. Twenty of the 36 channels voted for the selected baseline parameters, while 15 of the 36 channels

voted for the selected parameters of the HFOs detector block (and 11 channels voted for a very similar set). This set of parameters is used for the following results, unless specified.

HFO events were detected when their energy was larger than a threshold computed from automatically detected baselines. To illustrate this concept, Figure 6.1 shows an example of a correctly detected baseline and HFO.

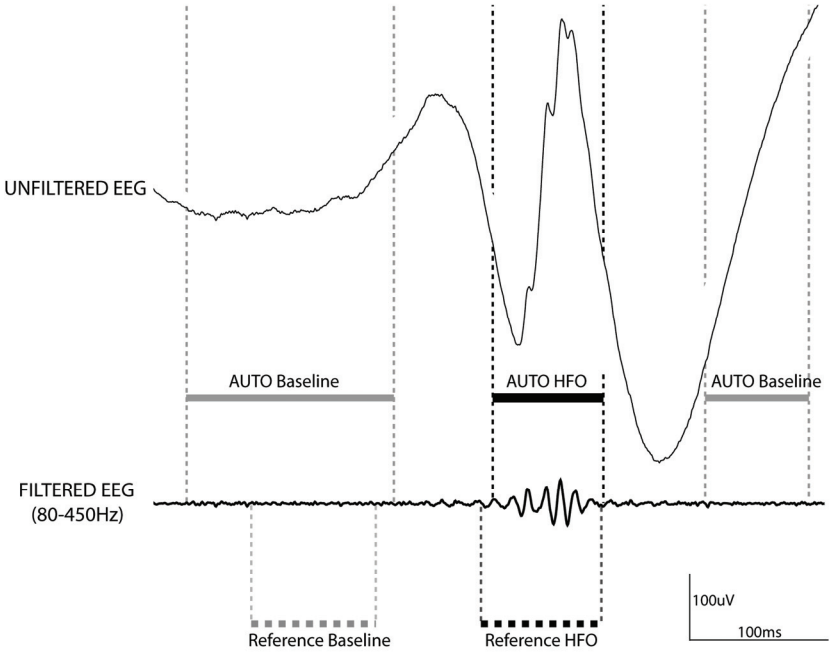

Figure 6.1. Example of detected HFO event surrounded by detected baselines. Top: unfiltered EEG segment; bottom: filtered (80-450Hz) EEG. The concordance between automatically detected (AUTO) HFOs and visually identified (reference) HFOs is excellent.

The performance of the detector (with a threshold of 95%) was: Sensitivity 96.8 +/- 11.41% (median: 100%) and FPR: 4.86 +/- 8.91% (median: 2.19%), averaged across channels (Figure 6.2). In the automatic baseline detector a mean baseline length of 29.6sec per channel (range: 1.5 to 55.8sec) was detected.

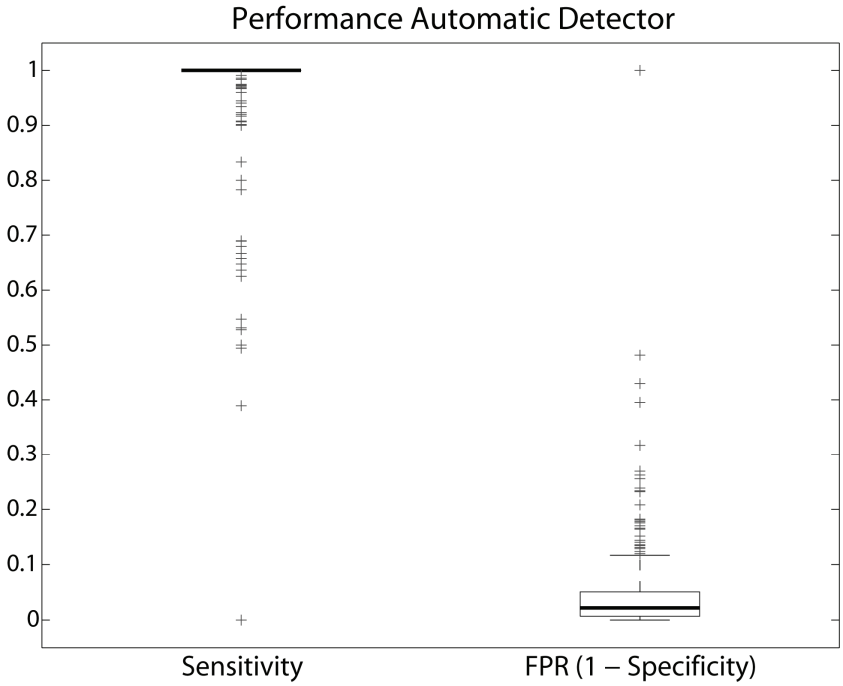

Figure 6.2. Boxplot of Sensitivity and FPR (equivalent to 1-Specificity) when automatically detecting HFOs in 278 channels. Black line: median of the distribution; boxes: 0.25 and 0.75 quantiles; crosses: outliers.

Figure 6.3 shows the average ROC curve (in black) across channels for different thresholds for the test dataset. Even though the operating point (0.95) was obtained from training data, in the test data it is situated in the right most corner. The area under the curve (AUC) was 0.99.

The average Kappa was 0.63+/-0.28, which corresponds to a moderate agreement. The mean RKD per patient was 0.42 (range: 0.01 to 0.78). In some patients the RKD score was low, indicating good agreement with the reviewers ranking (4 patients with RKD<0.2). However, for most patients the RKD score was high, indicating poor correspondence with reference rankings.

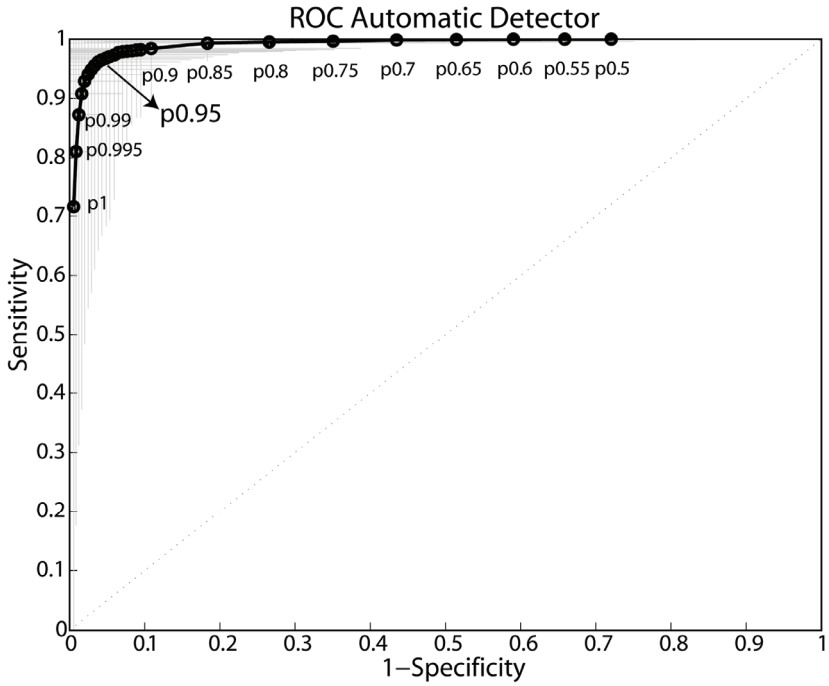

Figure 6.3. ROC showing the average performance of the detector. Black points: analyzed thresholds (only some threshold values are shown); Gray lines: 5 and 95 quantiles of ROC of individual channels.

To further ensure that the parameter selection was representative of all channels, in particular in the event detector block where less than half the channels voted for the selected parameters as their first choice, the distribution of parameters with respect to each channel's vote (which parameter/s maximized the channel's sensitivity) was analyzed. Figure 6.4 shows that the location of the 7 parameters with more votes in parameter space is very similar for 6. For 90% of the channels these 6 parameters provided the best kappa. Thus, for almost all channels their best parameter was located within a dense cloud, suggesting that the detector could be tuned to a range of parameters, which is a desirable property.

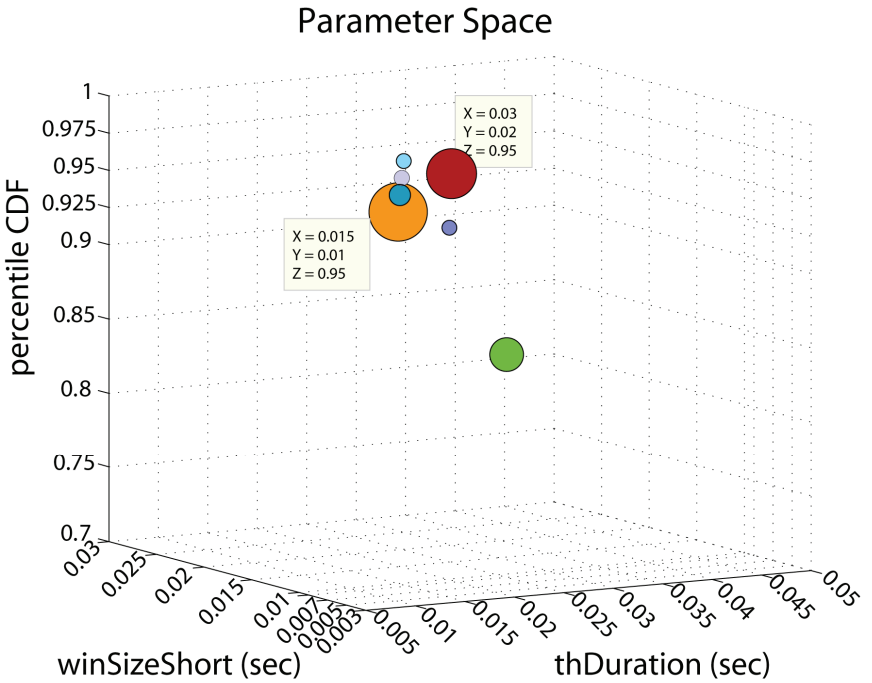

Figure 6.4. Scatter plot of set of most voted parameters in parameter space. Size of the bubble corresponds to the number of channels that voted for this parameter. Most parameters are within a clustered cloud. Boxes show the corresponding set of parameters for the two parameters with most votes. One dimension of parameter space (baseline length) is not shown since all parameters had a value of 2sec.

As a corollary to the above, when slightly changing the parameters (duration of HFO event=20ms; and short RMS window = 15ms), the performance remained almost the same (Sensitivity: 97.28 +/- 11.53%; FPR: 5.41 +/- 8.95%). Finally, when changing the energy function to the envelope computed with the Hilbert transform, the results are also very similar, achieving a sensitivity: 96.79 +/- 12.25% (median: 100%) and FPR: 5.12 +/- 9.05% (median: 2.15%). Thus, the MNI detector is robust to variability in the parameters and even in the way the energy of the signal is computed.

6.6 *Discussion and future work*

In this study, a new approach for HFO detection was proposed. The MNI detector first detects baseline segments, where no oscillatory activity is present, and then compares the energy of the EEG signal with that of the detected baselines. In this way, the local characteristics of the background are taken into consideration. The addition of baseline information is particularly important in

those channels in which the background is not flat everywhere, such as channels where a large number of spikes are present.

The detector is suitable for all brain locations, since it detected HFOs in all patients, in temporal and neocortical areas, and regardless of whether the channel was in the SOZ. Moreover, changes in parameters and energy function did not modify the performance. This is suggestive that it could generalize appropriately (with the corresponding training) to different situations, such as change in sleep stage, different contact sizes or distance to seizures. However, this remains to be tested. In agreement with other detectors, the MNI detector aims to detect as many events as possible. A second step should ensure the elimination of FP, particularly those corresponding to artefacts and non epileptogenic events. A GUI for human validation, a classification scheme or a combination of both could be incorporated to the detector.

Furthermore, HFOs were detected independently of their characteristics. A formal classification step in which HFOs could be divided into different categories and separated from sharp spikes is desirable. An ultimate goal would be the identification of pathological HFOs distinctly from physiological HFOs. However, given that a formal definition of what is pathologic does not exist (Engel *et al.,* 2009), this is a particularly challenging task.

Only events that corresponded to visually detected HFOs or baselines were considered in this study. This strict definition of the true negative events can explain the extremely low FPR. Therefore, even though automatic detections occurred, a good proportion of the EEG data was only analyzed in relation to the RKD score, but not in relation to possible FP. Furthermore, there was a great variability in RKD across subjects probably due to FP detections in these segments of EEG. Analysis of events in these EEG segments could identify events not visible to the human reviewer or on the contrary indicate FP due to artefacts. Further investigation in this regard is required.

Given that visually marking of HFOs is highly time consuming, in order for this new biomarker of epilepsy to be clinically useful, HFOs need to be detected automatically. This study focused on the evaluation of the performance of the MNI detector with respect to clear reference events, but in order for the detector to be used as a clinical tool a (semi- or automatic) post-processing step is required to identify and remove FP detections. We hypothesize that most events detected in areas not marked by the experts would be rejected in this second step, but this remains to be tested.

Channels containing continuous high frequency activity were excluded from this study because it was not possible to identify baseline segments. However, most of these channels contain high rates of HFOs and are related to epileptogenic regions. Thus, an analysis of different types of background is necessary to establish clearer definitions for automatic HFO detection in those channels.

Finally, a systematic comparison of the performance of the MNI detector with other detectors (Crepon *et al.,* 2010, Gardner *et al.,* 2007, Staba *et al.,* 2002) should be performed. Each detector was developed for a different purpose (such as detection of HFOs above 200Hz (Crepon *et al.,* 2010)), location (only temporal (Staba *et al.,* 2002)) or electrode size (micro-electrodes in (Staba *et al.,* 2002), micro- and macroelectrodes in (Worrell *et al.,* 2008)). Therefore, a systematic study comparing the detectors on the same dataset is required.

6.7 *Conclusion*

In conclusion, a new approach to HFO detection was presented in which HFO events were detected when their energy was larger than a threshold computed from automatically detected baselines. The high sensitivity of the detector and robustness to variability makes it a promising tool for the study of HFOs in humans.

Manuscript #3: A Comparison between detectors of High Frequency Oscillations

6.8 *Abstract*

Objective. High Frequency Oscillations (HFOs) are a biomarker of epileptogenicity. Visual marking of HFOs is highly time-consuming and inevitably subjective, making automatic detection necessary. We compare four existing detectors on the same dataset. **Methods**. HFOs and baselines were identified by experienced reviewers in intracerebral EEGs from 20 patients. A new feature of our detector to deal with channels where baseline cannot be found is presented. The original and an optimal configuration are implemented. Receiver operator curves, false discovery rate, and channel ranking are used to evaluate performance. **Results**. All detectors improve performance with the optimal configuration. Our detector had higher sensitivity, lower false positives than the others, and similar false detections. The main difference in performance was in very active channels. **Conclusions**. Each detector was developed for different recordings and with different aims. Our detector performed better in this dataset, but was developed on data similar to the test data. Moreover, optimizing on a particular data type improves performance in any detector. **Significance**. Automatic HFO detection is crucial to propel their clinical use as biomarkers of epileptogenic tissue. Comparing detectors on a single dataset is important to analyze their performance and to emphasize the issues involved in validation.

6.9 *Introduction*

High Frequency Oscillations (HFOs) are emerging as biomarkers of epileptogenic tissue that could help in the identification of epileptic or potentially epileptic regions during intracranial investigations. This could help the delineation of the surgical extent and in the prediction of surgical outcome (Jacobs *et al.,* 2010b).

HFOs are spontaneous EEG patterns in the range 80-500Hz, consisting of at least four oscillations that can be "clearly" distinguished from background. HFOs were first recorded with microelectrodes (20-40μm in diameter) implanted in temporal regions (Bragin *et al.,* 1999b), and recently with clinical macro-electrodes in temporal and neocortical regions (Jirsch *et al.,* 2006, Urrestarazu *et al.,* 2007, Worrell *et al.,* 2008). When recorded with macro-electrodes, HFOs are characterized by a typical duration of 30-100ms, an inter-event interval of at least 25ms, and an amplitude of 10-100μV. These EEG patterns occurring in the absence of specific stimuli, have been recorded during interictal (Staba *et al.,* 2002, Urrestarazu *et al.,* 2007), pre-ictal (Jacobs *et al.,* 2009b) and ictal (Jirsch *et al.,* 2006) periods. Interictally, they can be identified more frequently during slow wave sleep than during wakefulness (Bagshaw *et al.,* 2009, Staba *et al.,* 2004).

During interictal periods, higher rates of HFOs were observed in the seizure onset zone (SOZ) than in other areas (Bragin *et al.,* 1999c, Urrestarazu *et al.,* 2007). Even though a large proportion of HFOs co-occur with spikes, HFOs can occur also in non-spiking channels or independently from spikes (Jacobs *et al.,* 2008a). The ranking of channels according to rate (Zelmann *et al.,* 2009b) indicated that HFOs remained confined to the same region during interictal and ictal periods, while spikes presented a wider spread during seizures than interictally (Zijlmans *et al.,* 2011). Moreover, a postsurgical study showed a correlation between surgical outcome and removal of channels with high HFO rates (Jacobs *et al.,* 2010b). In summary, interictal HFOs seem to be a reliable biomarker of tissue capable of producing seizures.

Visual marking of HFOs provided a good understanding of the relation of HFOs with epilepsy (Jacobs *et al.,* 2010b, Urrestarazu *et al.,* 2007, Zijlmans *et al.,* 2009b). However, visual marking is highly time consuming (it takes about 10 hours to visually mark HFOs in a 10-channel 10-min recording) and subjectivity is inevitable. Thus, the development of automatic HFOs detectors is crucial for the systematic study of HFOs and for their eventual clinical application. The lack of a formal definition makes the detection of HFOs difficult and subjective.

Only a handful of automatic detectors based on different energy functions exist (Crepon *et al.,* 2010, Gardner *et al.,* 2007, Staba *et al.,* 2002, Zelmann *et al.,* 2010). In the first three the energy threshold is computed based on the segment of EEG under consideration, under the assumption that HFOs are rare events. On the contrary, the detector developed at the Montreal Neurological Institute (MNI) first detects baseline segments and then uses this information to compute the local energy threshold (Zelmann *et al.,* 2010). Each detector was developed for a different frequency band (above 200Hz, (Crepon *et al.,* 2010), gamma band (Gardner *et al.,* 2007)); a particular location (only temporal (Staba *et al.,* 2002)); or electrode size (microelectrodes in (Staba *et al.,* 2002), micro- and clinical macro-electrodes in (Worrell *et al.,* 2008)), small clinical macro-electrodes (Zelmann *et al.,* 2010). It is therefore important to test all the detectors on the same dataset.

In this study, we present the complete version of the MNI detector and provide a comparison between these four detectors on the same data. The new MNI detector includes a feature to deal separately with channels with very frequent or constant HF rhythmic activity. We hypothesize that all the detectors will behave similarly in those channels where HFOs are rare events, but that the MNI detector will outperform the others in channels with very frequent HFOs.

6.10 *Methods*

6.10.1 *Patient information*

Between September 2004 and April 2008, 45 patients with medically intractable epilepsy underwent depth macro-electrode (surface area 0.8mm^2) implantation at the Montreal Neurological Hospital. The depth EEG (SEEG), recorded with the Harmonie system (Stellate, Montreal, Canada), was low-pass filtered at 500Hz and sampled at 2000Hz, allowing for the identification of HFOs. Twenty patients were randomly selected, but one had to be excluded due to

continuous artefacts. All patients gave informed consent in agreement with the Research Ethics Board of the Montreal Neurological Institute and Hospital (MNI).

6.10.2 *Channel and event selection*

HFO events were identified independently by two experienced reviewers in all functioning channels during one min of slow wave sleep. Sleep stages were assessed using EOG and EMG signals, in addition to the intracranial EEG. Slow wave sleep was defined by high delta activity on the EEG, low EMG and no EOG activity (Bagshaw *et al.,* 2009). The visual marking of HFOs was performed by splitting the screen vertically and using an 80Hz high-pass filter on the left and a 250Hz high-pass filter on the right. The time resolution was increased to 0.6 sec across the monitor and only up to 10 channels were visualized simultaneously. A ripple (80-250Hz) was marked if there was a clear oscillation on the left that was not visible or had a different morphology on the right. A fast ripple (FR; 250-500Hz) was marked if it appears in the right screen (Jacobs *et al.,* 2008a). Three quarters of the FRs occurred during a ripple (74%) and the distribution of the peak of energy spectra of FRs comprises a broad frequency band (the whole 80-450Hz; Figure 6.5). Indeed, for FRs without a visually-apparent co-occurring ripple, the distribution of peak frequencies is not limited to the 250-450Hz band, but includes the 80-250Hz band as well. Both ripples and FRs seem to be similarly associated with epileptogenic tissue (e.g. Jacobs *et al.,* 2008a, Jacobs *et al.,* 2010b, Urrestarazu *et al.,* 2007, Worrell *et al.,* 2008). Therefore, we decided to group ripples and FR and refer to them as HFO events.

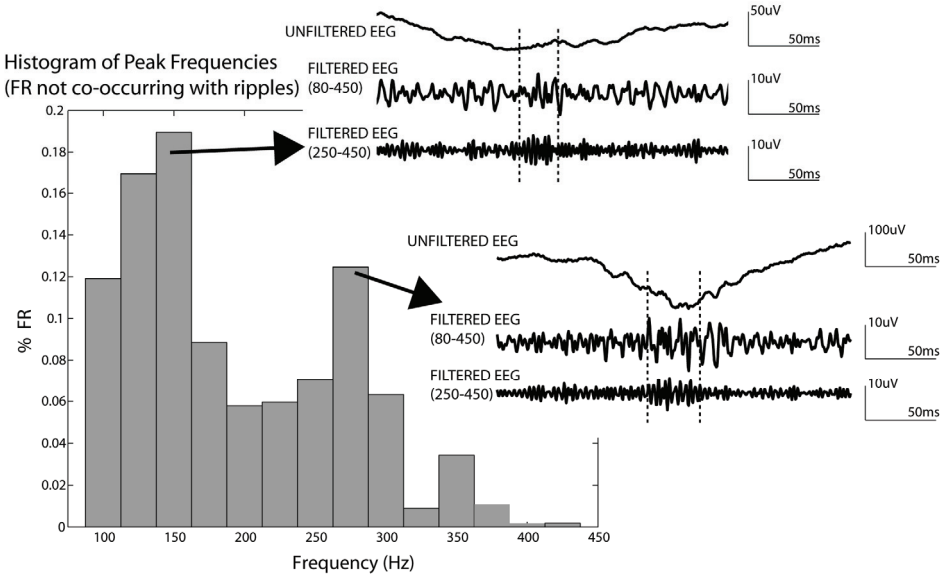

Figure 6.5. Histogram of peak frequencies of FRs not occurring with ripples. Out of the 7994 *PosAnd* HFOs, 554 corresponded to FR that did not co-occur with a visually marked ripple. The peak frequencies of these events included not only the 250-500Hz band but also the 80-250Hz band. All these events were visually marked as FR using a high-pass filter at 250Hz. Two examples are presented. Top: FR with a peak frequency at 150Hz; Bottom: FR with a peak at 265Hz. The unfiltered EEG, the filtered EEG above 80Hz and the filtered EEG above 250Hz are shown. The oscillations become visible only when filtering above 250Hz.

To evaluate the performance of the detectors, we conducted a strict validation and a more open validation. In the strict validation only events of which we were absolutely sure that they were true positives and true negatives were considered. Thus, the positive gold standard HFO events were the HFOs marked by the two reviewers (***PosAnd*** HFO events, Figure 6.6.A). Baseline segments (segments without oscillatory activity, unambiguously free of HFOs, Figure 6.6.A) were visually marked and considered as the negative gold standard (***NegBase***). This is a definition of baseline in the context of HFOs. It is useful as a comparison with HFO (which are oscillatory events), but does not intend to be a general definition of baseline activity. *NegBase* segments longer than 400ms were split to obtain a mean length of 200ms. In the more open validation we considered events and non-events more inclusively. All the events visually marked by any reviewer were considered as the positive gold standard (***PosAny*** HFO events, Figure 6.6.B). Thus, *PosAny* HFOs included the events jointly marked or marked by only one reviewer. We considered HFOs marked by one reviewer for the more open validation, under the assumption that there is a possibility that these segments are

HFOs, but with a lower probability than for segments jointly marked. In this case, the negative gold standard was any segment of EEG of 100ms long at least 25ms away from a visually marked HFO event. For the sensitivity and false positive rate (FPR = 1-specificity), we used the strict validation. To assess the false detection rate (FDR), the more open validation was used.

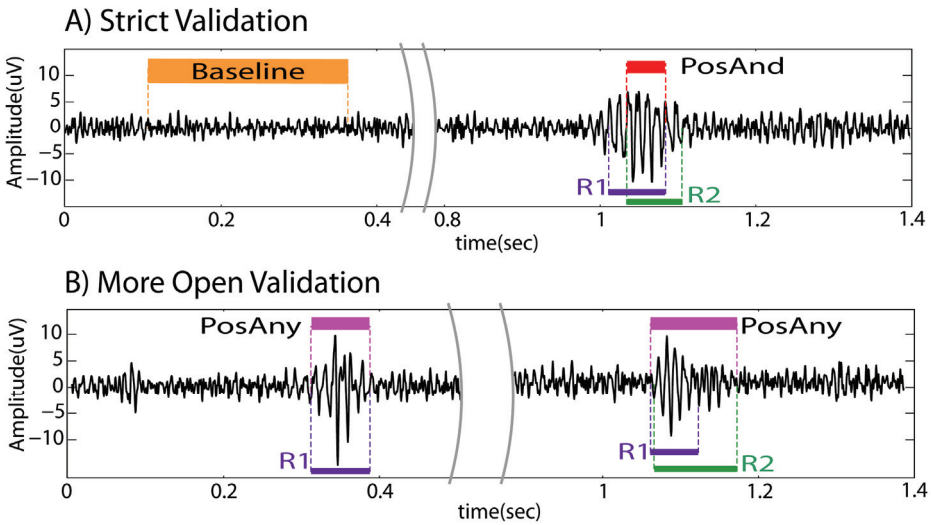

Figure 6.6. Example of Reference events. A) Strict validation. The *PosAnd* HFO is the intersection of the markings. Orange: marked baseline (*NegBase*); red: *PosAnd* HFO (intersection of markings). B) More open validation. The 1st example presents an HFO only marked by reviewer 1.The 2nd example was marked by both reviewers. The *PosAny* HFO is the union of both markings. Magenta: *PosAny* HFO (event marked by at least one reviewer).purple: HFOs marked by reviewer 1; green: HFOs marked by reviewer 2.

Channels outside the brain, with clear continuous artifacts, or with less than one *PosAnd* HFO or less than one baseline were excluded from this study. Given that the variability within channels of a patient is as large as the variability across patients, all channels were considered independently. The database therefore consisted of 19 one-min sections, each with 10-39 channels, for a total of 373 channels. Out of the 373 channels, 20% (76) were randomly selected and used for training the MNI detector, resulting in 297 channels for comparing detector performance. Of these channels, 113 were mesio-temporal and 184 were neocortical; 89 were in the SOZ of the patient.

These channels included 7994 *PosAnd* HFO events, 13552 *PosAny* HFO events and 51061 *NegBase* baselines. These events were used as the gold standard events.

6.10.3 *Automatic detectors of HFOs*

Automatic HFO detectors are largely based on the comparison of the signal energy with the EEG epoch that includes the events. The main difference among these detectors is the type of energy function computed on the filtered signal and the post-processing used to prune false detections. Since the post-processing step involves human expert in some cases, it cannot be considered when comparing the performance of the detectors and will not be evaluated in this study. The detectors are presented in order of the year of original publication.

Staba et al. (2002) developed a detector based on the energy defined as the moving average of the root mean square amplitude of a filtered signal. Each channel was filtered (100-500Hz) and segments with energy above five times the standard deviation (SD) of the mean energy of the whole EEG during more than 6ms were considered HFOs. Events less than 10ms apart were considered as a single event. Events required at least six oscillations above three SD. Because this last condition could be considered as a post-processing step, and to improve the sensitivity of this detector, it was not implemented. This detector was developed for microelectrode recordings in humans and rats in temporal regions (Staba *et al.,* 2007, Staba *et al.,* 2004). A sensitivity of 84% was reported (Staba *et al.,* 2002). We will refer to this detector as the *RMS detector*.

The detector of Gardner et al. (2007) is based on the short-time line length (Esteller *et al.,* 2001). Each channel was passed through a spectral equalizer (first order differential filter), then band-pass filtered (30-100Hz in (Gardner *et al.,* 2007), and 80-1kHz in (Worrell *et al.,* 2008)) and the energy threshold was computed as the 95 percentile of the empirical cumulative distribution function for the epoch (Worrell *et al.,* 2008). Epochs lasted 3 minutes and included the possible events. For the post-processing, an interface for human verification was implemented. The sensitivity was 89.5% in a gamma band (30-100Hz) study (Gardner *et al.,* 2007). The specificity was not reported, but it was stated that ~85% of the candidate events were rejected as false positives (Worrell *et al.,* 2008). It was applied to microelectrodes and macroelectrodes, but with the latter

no FR were detected (Worrell *et al.,* 2008). Parameters as reported in (Worrell *et al.,* 2008) will be considered. We will refer to this detector as the *LineLength detector*.

Finally, in the detector of Crepon et al. (2010) the envelope of the signal was computed with a Hilbert transform. Each channel was band-pass filtered (180-400Hz) and events were detected with a threshold five times the SD of the envelope over the whole EEG. Post validation by a reviewer with a visual interface was also implemented. The sensitivity was 100% with a specificity of 90.5%. However, only very clear events were detected and only in SOZ areas, emphasizing the lack of a common definition of HFOs across centers. Thus, care must be taken when comparing performances since not all detectors aim to identify the same "HFO event". We will refer to this detector as the *Hilbert detector*.

6.10.4 *The MNI detector*

The *MNI detector* consists of a baseline detector; a detector of HFOs in channels with baseline (that incorporates the baseline information); and a detector of HFOs in channels with continuous High Frequency (HF) activity, for channels without sufficient baseline (Figure 6.7). As the other detectors, the MNI detector aims to detect as many events as possible, even if a large number of false detections take place. The first 2 blocks of the detector are described in detail in (Zelmann *et al.,* 2010).

Band-pass filter. The EEG was first band-pass filtered (80-450Hz) using a FIR equirriple filter (fStop1=70Hz; fPass1=80Hz; fPass2=450Hz; fStop2=460Hz; stopband attenuation = -60dB). The signal was filtered forward and backwards to obtain zero-phase. To minimize the effect of filtering in the detection, the impulse response of the filter was checked to oscillate less than the minimum number of oscillations (Bénar *et al.,* 2010). In addition, we randomly selected HFOs identified using this filter from the training dataset and verified that they were

visible in the unfiltered EEG. Each detector was tested using this filter as well as their default filter.

Baseline detection (Figure 6.7.A). We define as baselines, segments of EEG where there is no oscillatory activity of any kind. The baseline detector (Chander 2007) is based on the wavelet entropy (WE) which measures the degree of randomness (vs. oscillatory behaviour) in the signal (Rosso *et al.,* 2001). To enhance the oscillatory characteristics of the signal, the WE was applied to the autocorrelation of the filtered signal (Chander 2007). The EEG was divided into segments of 125ms with 50% overlap. The normalized wavelet power of the autocorrelation was computed for each segment. A complex Morlet wavelet was used. The maximum theoretical wavelet entropy (WE_{max}) is obtained for white noise, when contributions at all scales are similar. Thus, a segment was considered as baseline (i.e. no oscillation present) when the minimum WE was larger than the threshold obtained from training (0.67 WE_{max}). Consecutive or overlapping segments were joined.

HFO detection in channels with baseline (Figure 6.7.B). The EEG with detected baselines is evaluated to assess whether "a sufficient amount" of baseline (i.e. at least 5s/min) was detected. For channels with sufficient baseline, the next block detects possible HFOs based on the energy defined as the moving average of the root mean square amplitude of the filtered signal. Segments with energy above threshold during more than 10ms were considered HFOs. Events less than 10ms apart were considered as a single event. The energy threshold was obtained by computing the empirical cumulative distribution function of each 10s baseline segment (or the entire baseline if shorter than 10s), modeling the distribution with a gamma function, and returning the value at the 99.9999 percentile as the threshold. This block of the detector is similar to (Staba *et al.,* 2002) in the energy function and to (Gardner *et al.,* 2007) in the threshold computation, but unlike the other detectors, the MNI detector considers the threshold with respect to the detected baselines.

HFO detection in continuous HF channels (Figure 6.7.C). If less than 5s/min of available baseline was found, the channel was considered as *continuous HF channel* (i.e. with continuous high frequency oscillatory activity). In these channels, the separation of HFOs from the oscillatory background cannot rely on the same methods as channels with random background. Thus, an iterative approach was implemented. At each iteration, the threshold was computed from the complete 1min band-passed EEG as the 95 percentile of the cumulative distribution function (modeled with a gamma function). Segments with energy above threshold during more than 10ms were considered HFOs. In this way, the events with the highest energy (mostly sharp spikes and HFOs riding on spikes) are first detected and removed for the following iterations. In subsequent iterations, these large events did not influence the calculation of the new threshold, allowing for the detection of HFOs that are larger than a threshold computed from the remaining background. This iterative process continues until no more HFOs are detected. In this way, a threshold is found for each 1-min recording for each channel. To avoid the effect of the successive removal of EEG segments in the length of detected HFOs, the detector was run again for that threshold. Thus, the detector is similar to the RMS detector if considering only the first iteration, but adapts the threshold to detect more events in successive iterations.

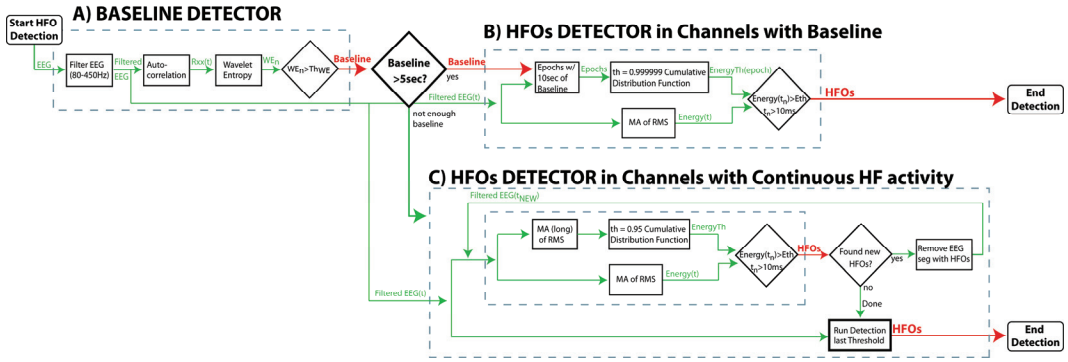

Figure 6.7. Diagram of the MNI Detector. A) Baseline Detector. B) HFOs Detection in Channels with Baseline. C) HFOs Detection in Channels with Continuous high frequency activity. If more than 5sec/min of baselines are found, HFOs are detected with respect to the baseline segments (B). If less than 5sec/min of baseline were detected, HFOs are detected with respect to the entire EEG segment in an iterative way (C).WE: wavelet entropy; Rxx: autocorrelation; th: Threshold.

Parameter optimization. The parameters of the baseline block were optimized to maximize the duration of detected baseline that overlaps with the reference. Each channel "voted" their parameters to obtain the largest baseline overlap, and the set of parameters with most votes was selected (Zelmann *et al.,* 2010). The HFO detection blocks were optimized to maximize sensitivity with respect to *PosAnd* events, while strongly limiting the detection of events within visually marked baselines and loosely limiting detections outside *PosAny* events.

Table 6.1 presents the parameters for each detector as reported in the original publications (Crepon *et al.,* 2010, Gardner *et al.,* 2007, Staba *et al.,* 2002). All parameter values of the MNI detector were obtained from optimization.

Parameters of the detectors as indicated in the original publications

	RMS Detector (Staba *et al.,* 2002)	**LineLength Detector (Worrell *et al.,* 2008)**	**Hilbert Detector (Crepon *et al.,* 2010)**	**MNI Detector**
PreProcessing				
Spectral Equalization	--	1st order difference	--	--
BP filter band	100-500Hz	80-1kHz	180-400Hz	80-450Hz
BP filter type	FIR	4th order Butterworth	FIR (win)	FIR (equirriple)
Baseline Detection				WE(Rxx)
Threshold	--	--	--	0.67
Duration	--	--	--	125ms
Min Duration Baseline	--	--	--	5sec
HFOs Detection				
Energy measure	RMS amplitude	Line Length	Hilbert Envelope	RMS amplitude
Window Size	3ms	85ms	--	10ms / 5ms
Window Size Long	--	--	--	-- / 10ms
Threshold Energy	5 STD	95 percentile	5 STD	99.9999 / 95 percentile
Thres. measured from	all EEG	Epoch (3min)	all EEG	10sec Baseline /1min EEG
Threshold Duration	6ms	80ms	--	10ms / 10ms
Min Inter Event Interval	10ms	--	--	10ms

Table 6.1. Parameters of the detectors as indicated in the original publications. Only the MNI detector incorporates the detection of baseline. For the MNI detector, the parameters of the two HFO detection blocks are given separated by / (HFOs detector in channels with baseline / HFOs detector in channels with continuous HF activity). FIR: finite impulse response filter; RMS: root mean square; WE: wavelet entropy; Rxx: autocorrelation; SD: standard deviation; --: not applicable / not specified.

6.10.5 *Performance metrics*

Receiver operating characteristic (ROC) curves measure the performance of a detector when varying the energy threshold and were used for the comparison of detectors. *PosAnd* events were considered as the true positives and *NegBase* events as the true negatives. Segments of EEG where nothing was visually marked by both reviewers were not taken into account, under the assumption that there might be HFOs in those segments, which were not visible to the human reviewer and to account for variability across reviewers. Thus, a true positive (TP) was a visually marked HFO by the 2 reviewers that was identified by the automatic detector; a false positive (FP) was an automatically detected event that corresponded to a visually marked baseline; a false negative (FN) was an HFO visually marked by the 2 reviewers that was missed by the automatic detector; and a true negative (TN) was a visually marked baseline where no HFOs were identified. The ROC curve for each channel was computed and the average across channels obtained for each threshold value (Fawcett 2006). The area under the curve (AUC) ranges from 0 to 1, with 1 representing the perfect decision maker. Since the diagonal in the ROC plane represent a random decision, no detector can have an AUC smaller than 0.5.

Cohen's Kappa coefficient (Cohen 1960) was also computed to compare each detector with the gold standard (*PosAnd* and *NegBase*) in each channel. This coefficient measures the degree of agreement between two reviewers (in this case one human and one automatic), taking into account the agreements made by chance. Kappa ≤ 0 reflects an agreement due purely to chance and Kappa = 1 indicates perfect agreement.

Given the strict definition of the *PosAnd* and *NegBase* gold standards used to compute the ROC curves, the FPR does not represent the number of automatic detections that lie outside a true detection, but rather the number of automatic detections that are within clear baselines. Thus, to also analyze the total number of detections that do not correspond to any visually marked event, we define the FDR as the number of automatically detected events that are outside any visually

marked event (*PosAny*) divided by the total number of detected events. In this way, both the total number of false detections and those corresponding to baseline segments were studied.

The ultimate goal of an automatic detector is to provide the same conclusions as when visually marking the recording. The Ranking Distance (RKD; Zelmann *et al.,* 2009b) measures the cost of obtaining a different order of channels (ordered from more to fewer events) when detecting events automatically compared to the order obtained from visually identified *PosAnd* events. For instance, if channel A has 3 visually detected events, channel B 25 and channel C 5, we expect the automatic detector to detect more events in channel B than in the other two. RKD score ranges from 0 to 1, with 0 representing exactly the same ranking, and 1 corresponding to a ranking completely upside down. Thus, even though we accept a large number of false positives under the assumption that there might be events not seen by the reviewer, the relative number of false positives to true positives should be equivalent in all the channels of each patient. For this measure, all detected events were considered (i.e. not only the true positives).

Statistical comparisons of the performance metrics were performed using balanced one-way ANOVA; post hoc comparisons were done using Tukey's honestly significant differences (HSD) test. The level of significance was set at $p<0.05$. All processing was implemented based on MATLAB.

6.11 *Results*

6.11.1 *Original configurations*

We compared our detector with the others considering the parameters, filter and thresholds in the original publications (see Table 6.1). Figure 6.8 shows the ROC curves across channels. The MNI detector considers differently channels with more than 5 s/min of detected baselines (170 channels) and channels with less than 5 s/min of baseline (127 channels). Results are presented separately for the two groups. With the original configuration, the AUC for "*Channels with*

baseline" was: 0.994 for the RMS detector; 0.84 for the LineLength detector; 0.8 for the Hilbert detector; and 0.996 for the MNI detector. For *"Channels with continuous HF activity"* the AUCs were, respectively 0.98, 0.81, 0.77 and 0.991.

When considering the energy threshold as reported in each publication (indicated as an X in Figure 6.8), the FPR was below 1% for all detectors, but the sensitivity was low for all but the MNI detector, which was significantly higher than the others (Table 6.2). The difference is not surprising since the MNI detector was optimized for a similar dataset, while the others were developed for a different definition of HFO. For instance, the Hilbert detector only considers frequencies above 180Hz and therefore cannot detect HFOs in lower frequencies. The FPR for the RMS and Hilbert detectors were significantly lower than for the LineLength or MNI detectors. The difference between these last two was not significant. The FDR was similar for all the detectors but the RMS detector, significantly lower than the others.

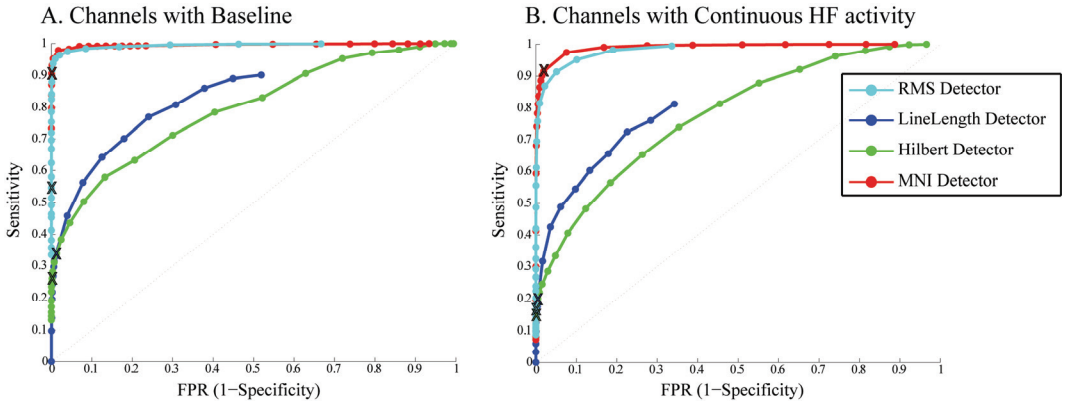

Figure 6.8. Average ROC curves for original configuration. Comparison of average ROC curves across channels considering the original parameters and filter (see Table 6.1). Channels where baseline can or cannot be found are separately shown. X: original thresholds.

The percentage of channels (out of 297) where all the *PosAnd* events were detected was: 17% (50) for the RMS detector; 6% (19) for the LineLength detector; 6% (18) for the Hilbert detector; and 68% (202) for the MNI detector.

The Kappa coefficient for all but the MNI detector was low since the sensitivity was low (Table 6.2). The Kappa for the MNI detector was significantly higher than the others. As a comparison the Kappa for reviewer 1 compared to

PosAnd & *NegBase* was 0.99 ± 0.03 (median: 1) and for reviewer 2 was 0.97 ± 0.15 (median: 1). The Kappa between the 2 reviewers (considering *NegBase* events as the true negatives) was 0.83 ± 0.22 (median: 0.93).

	Default Filter & Threshold							
	Sensitivity(%)		FPR(%)		FDR (%)		Kappa	
	Mean ±Std	Median	Mean ±Std	Median	Mean±Std	Median	Mean ±Std	Median
RMS	38.1 ± 37[a]	28.6	0.0 ± 0	0.0	16.7 ± 25[a]	0.0	0.43 ± 0.39[a]	0.39
LineLength	27.6 ± 30[a]	18.8	0.8 ± 1	0.6	59.6 ± 33	64.3	0.26 ± 0.26	0.21
Hilbert	21.1 ± 29[a]	6.3	0.1 ± 0	0.0	50.2 ± 41	50.0	0.24 ± 0.30	0.05
MNI	91.0 ± 20[a]	100.0	0.9 ± 3	0.0	55.0 ± 28	55.6	0.85 ± 0.25[a]	0.97

Table 6.2. Statistics across channels for default configuration. Sensitivity, FPR and Kappa computed using PosAnd and NegBase as reference; FDR computed with respect to PosAny events. [a] indicates significant difference with all the others ($p<0.05$). Significance difference among only some of the detectors is not indicated in this table, but explained in the text. SD: standard deviation; per: percentile.

6.11.2 *Optimum configurations*

To better compare the four detectors and to improve their performance in this dataset, the same filter was implemented for all detectors. In addition, the spectral equalizer filter of the LineLength detector was removed, which further improved performance in this detector. By using a similar filter than the one used for the reference events, the performance improves (Figure 6.9). The AUCs for "*Channels with Baseline"* were: 0.994 for the RMS detector; 0.98 for the LineLength detector; 0.989 for the Hilbert detector; and 0.996 for the MNI detector. For *"Channels with continuous HF activity"* the AUCs were, respectively 0.981, 0.943, 0.972, and 0.991.

In order to provide a comparable measure of performance across detectors, the "optimum" point in the ROC curves was selected. We define as the "optimum" energy threshold, the threshold closest to the left top corner in the ROC curves obtained with the same band-pass filter. For the MNI detector optimum thresholds were obtained separately for channels with or without baseline. For the other detectors, the optimum threshold was obtained from the ROC across all the 297 channels. The optimum thresholds are shown in the first column of Table 6.3 and are indicated as O in Figure 6.9.

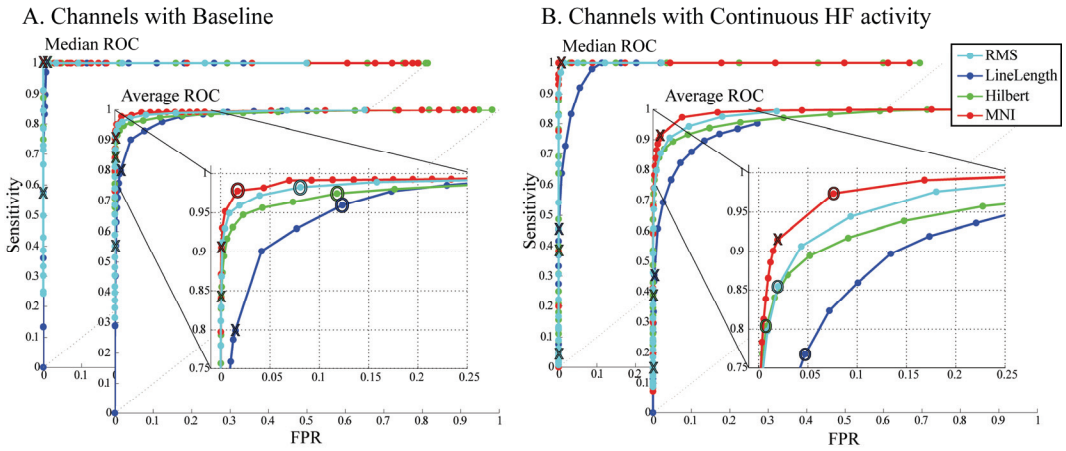

Figure 6.9. Median and average ROC across channels for the same 80-450Hz FIR filter. Channels where baseline can or cannot be found are separately shown. Insight: zoom of the average ROC. X: original thresholds; O: optimum threshold (closest to left top corner). The performance of the detectors that originally used a different filter improves considerably.

As shown in Table 6.3, the sensitivity of all detectors is good when choosing the optimum threshold and using a similar band-pass filter to the one used to mark the reference. The FPR is worse for all detectors than it was for the default threshold, but the Kappa coefficient is higher. The MNI detector had the highest sensitivity, the lowest FPR, and the highest Kappa coefficient. The sensitivity of the MNI detector was significantly higher than the others. The FPR was significantly lower than the FPR of the LineLength and Hilbert detectors but not different from the RMS detector. Kappa was significantly higher for the MNI detector and significantly lower for the LineLength detector compared to the others. The number of false detection was high. The median FDR was above 75% for all detectors, indicating that at least three quarters of the detections were false detections in most channels. The FDR of the Hilbert detector was significantly lower than that of the MNI or RMS detectors but not than that of the LineLength detector, and still high. These false detections must be removed in later steps for a detector to be used clinically.

	Same filter 80–450 Hz and optimum threshold (average ROC)								
		Sensitivity (%)		FPR (%)		FDR (%)		Kappa	
	Threshold	Mean ±Std	Median	Mean ± Std	Median	Mean ± Std	Median	Mean ± Std	Median
RMS	1STD	92.7 ± 16	100.0	5.4 ± 9	1.6	72.4 ± 32	89.6	0.58 ± 0.34	0.66
LineLength	80per	87.6 ± 21	100.0	9.0 ± 7	6.6	70.9 ± 26	79.6	0.40 ± 0.28 [a]	0.34
Hilbert	2.75STD	90.0 ± 20	100.0	7.0 ± 14	0.4	61.2 ± 36	75.8	0.60 ± 0.38	0.73
MNI	99.9/90per	97.6 ± 10[a]	100.0	4.3 ± 8	1.2	75.7 ± 24	82.9	0.75 ± 0.26 [a]	0.84

Table 6.3. Statistics across channels for optimum configuration. Threshold column indicates the optimum energy threshold (closest to left top corner in average ROC curves). Sensitivity, FPR and Kappa computed using PosAnd and NegBase as reference; FDR computed with respect to PosAny events. [a] indicates significant difference with all the others ($p<0.05$). Significance difference among only some of the detectors is not indicated in this table, but explained in the text. SD: standard deviation; per: percentile.

With this optimum configuration, the percentage of channels (out of 297) where all *PosAnd* events were detected was: 72% (214) for the RMS detector; 59% (176) for the LineLength detector; 70% (209) for the Hilbert detector; and 85% (251) for the MNI detector. Furthermore, 166 channels (56%) had perfect detection by all the detectors, comparing to only 11 channels (4%) with original configurations.

6.11.3 *Pooling all events together*

The previous ROC curves were averaged across channels. By pooling all the events, the total number of detected HFOs can be studied. The difference among detectors becomes more evident (Figure 6.10) than when averaging across channels, since only the MNI detector can detect most of the events in very active channels (where the rate of HFOs is also high). For all the events pooled together and using the same filter for all the detectors, the AUCs for "*Channels with Baseline"* were: 0.945 for the RMS detector; 0.924 for the LineLength detector; 0.921 for the Hilbert detector; and 0.951 for the MNI detector. For *"Channels with continuous HF activity"* the AUCs were, respectively 0.939, 0.855, 0.904, and 0.964.

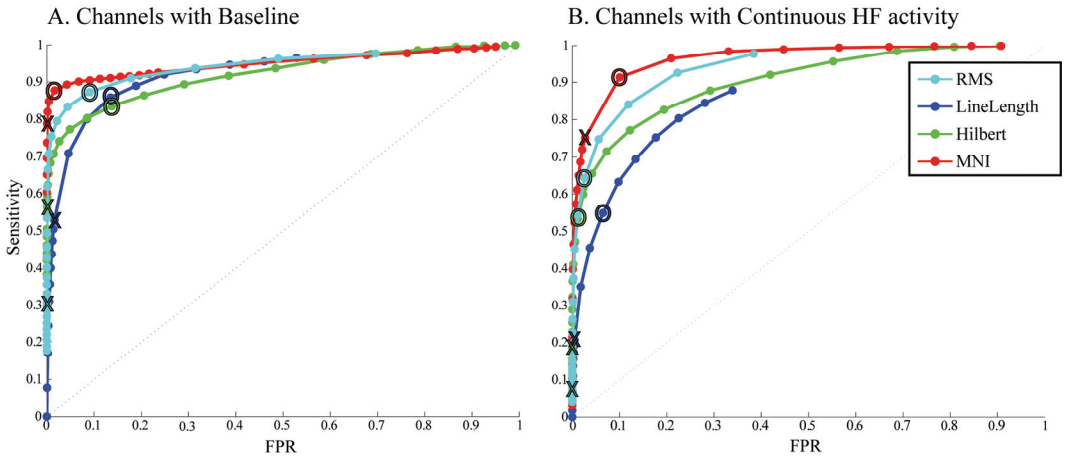

Figure 6.10. ROC curves pooling events together for the same 80-450Hz FIR filter. When pooling all the events together the difference in performance among detectors become more striking than when averaging across channels. Channels where baseline can or cannot be found are separately shown. X: original thresholds; O: optimum threshold (closest to left top corner in ROC average across channels). Thresholds are the same as in Figure 6.9.

Table 6.4 presents the sensitivity, FPR and FDR for the default and optimum configurations when pooling all events. All detectors increased the number of detected events when using the optimum threshold, but at the expense of a higher FPR and FDR. Only the MNI detector detected 90% of the events, with the lowest FPR.

	All Events Pooled Together					
	Default Filter & Threshold			80-450Hz filter & optimum threshold		
	Sensitivity (%)	FPR (%)	FDR (%)	Sensitivity (%)	FPR (%)	FDR (%)
RMS	14.0	0.0	15.5	70.3	7.1	77.3
LineLength	19.2	1.0	45.4	62.9	11.3	66.3
Hilbert	17.2	0.1	20.7	61.1	9.9	71.4
MNI	76.1	0.9	56.9	90.5	4.3	71.8

Table 6.4. Performance for all events pooled together. Left part of the table: filter and threshold as published in original publication (see Table 6.1). Right part of the table: Same 80-450Hz filter was used in all detectors and the optimum threshold obtained as in Figure 6.9. Sensitivity and FPR computed using PosAnd and NegBase as reference; FDR computed with respect to PosAny events.

Given that the very active channels contain a large rate of HFOs, by detecting more on those channels, the MNI detector detects a larger amount of total events compared to the other detectors. This type of analysis gives a better idea of the

overall performance of the detector regardless of the type of channel (Gotman and Wang 1992).

6.11.4 *Ranking distance*

The *ranking distance* (RKD) measures that the ranking of channels for each patient was similar to the one obtained from *PosAnd* reference. The mean, standard deviation and median across patients is reported (Table 6.5). The RKD of the LineLength detector improved for the optimum threshold, while the RKD for the RMS and Hilbert detectors was worse. The RKD of the MNI detector was similar in both cases. There were no significant differences among detectors for the default configuration; for the optimum configuration the RKD for the LineLength and MNI detectors was significantly lower than the RKD for the RMS and Hilbert detectors.

	RKD (across patients)			
	Default Filter & Threshold		80-450Hz filter & optimum threshold	
	Mean ± Std	Median	Mean ± Std	Median
RMS	0.54 ± 0.25	0.55	0.78 ± 0.14	0.79
LineLength	0.43 ± 0.18	0.44	0.34 ± 0.17	0.39
Hilbert	0.40 ± 0.25	0.40	0.91 ± 0.08	0.92
MNI	0.38 ± 0.18	0.39	0.38 ± 0.17	0.39

Table 6.5. RKD across patients. Left part of the table: Filter and Threshold as published in original publication (see Table 6.1). Right part of the table: Same 80-450Hz filter was used in all detectors and the optimum threshold obtained as in Figure 6.9.

As a comparison the RKD for reviewer 1 compared to the *PosAnd* events was 0.03 ± 0.05 (median: 0) and for reviewer 2 was 0.05 ± 0.18 (median: 0). When comparing reviewer 2 markings with reviewer 1 markings, the RKD was 0.07 ± 0.17 (median: 0.025). The large difference between the RKD for human reviewers and for any detector indicates that post-processing is fundamental to prune false detections and to obtain conclusions similar to the visual markings.

6.11.5 *Analysis of the detected events*

Half of the HFOs (50.5%) were detected by all the detectors when using the optimal configuration. This was particularly the case in channels were HFOs were rare, since this is an implicit assumption in all detectors except the MNI detector. In active channels however, low amplitude HFOs are only detected by the MNI detector. Figure 6.11 presents examples of events found by all detectors and some identified only by some detectors in the same channels.

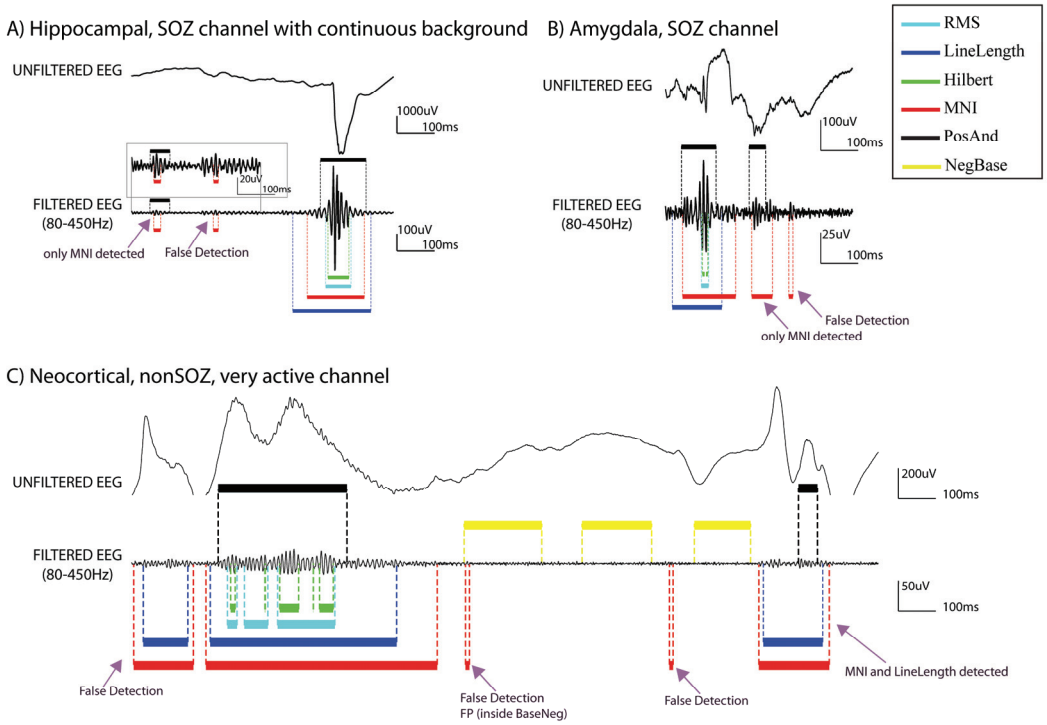

Figure 6.11. Examples of HFO detections. A) SOZ channel in the hippocampus, with continuous background activity and many spikes as the one depicted in the raw EEG. All the detectors found the 2nd event, but only the MNI detector found also the 1st one. Baselines were not found, and therefore the detector for continuous channels block was used. In addition, a false detection is shown. B) SOZ channel in the Amygdale. The 1st event was found by all detectors, the 2nd event only by the MNI detector. In this channel 10.6sec of baseline were found and HFOs were detected by the MNI detector based on that baseline. In addition, a false detection is shown. C) NonSOZ, neocortical very active channel. The epileptiform activity that is observed is repeated periodically in the recording. In this channel 16.4sec of baseline were found. Therefore HFOs were detected by the MNI detector based on that baseline. Black: *PosAnd* reference HFOs; yellow: *NegBase* reference baseline; cyan: RMS detections; blue: LineLength detections; green Hilbert detections; and red: MNI detections.

A desirable property of any detector is to detect equivalently in all types of channels. Thus, by considering all events regardless of channel, we evaluated

whether there was a difference in detection in different anatomical locations (Figure 6.12).

Detections in all areas increased when moving to the optimum configuration, but were worse in hippocampus and parahipocampus than in other regions for all detectors but the MNI detector. With the MNI detector more than 80% of the HFOs were detected regardless of region.

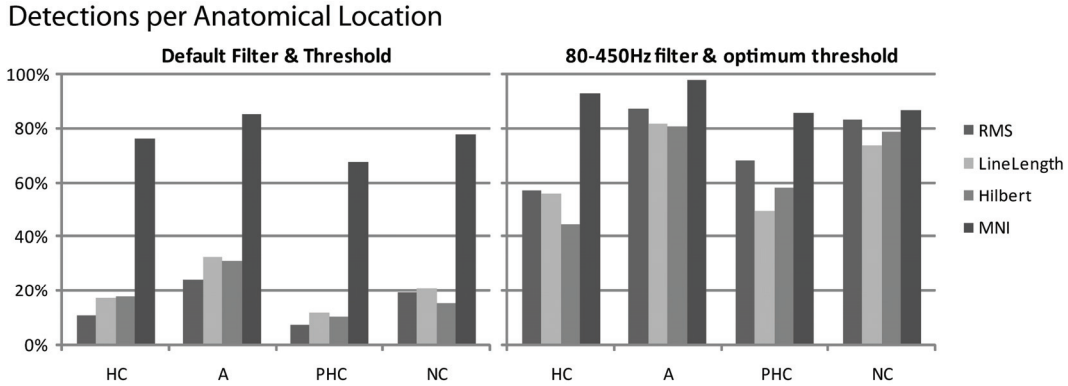

Figure 6.12. Detections per Anatomical Location. All detectors improve the sensitivity for all anatomical regions. HC: hippocampus, A: amygdale, PHC; parahippocampus, NC: neocortex.

6.12 *Discussion*

Visual markings of HFOs provided a good understanding of the relation of HFOs with epilepsy (Jacobs *et al.,* 2008a, Jacobs *et al.,* 2010b, Urrestarazu *et al.,* 2007, Zijlmans *et al.,* 2009b). But this manual procedure is highly time consuming and subjective. For the systematic study of HFOs and for a future clinical application, robust automatic detection of HFOs is necessary. In this study, we presented a comparison of performance of HFO detectors based on energy on the same dataset.

In channels with rare HFOs, considering the entire EEG segment or only the detected baselines for calculating the energy threshold does not make an important difference. In these channels, all detectors (using the appropriate filter and the optimum threshold) behaved similarly. The main difference appears in very active channels. For instance, channels with baseline segments, but very active (Figure 6.11.C) benefit from the detection with respect to clear baseline

segments (instead of the whole EEG) to detect not only the large amplitude events but also the ones with lower energy. Furthermore, some of these channels have continuous HF background activity without clear baseline sections (example in Figure 6.11.A). In these channels, only the clear, large amplitude HFOs are detected by all detectors since the threshold is computed based on the whole recording, including these large events. With an iterative approach, smaller HFOs can be detected. Since many hippocampal channels have continuous high frequency activity, it is not surprising that the difference in performance was clearest in hippocampal channels.

It is important to optimize a detector for a particular type of data instead of using directly a standard configuration. By modifying filters and thresholds the sensitivity of all the detectors was improved. Each detector was designed with an implicit definition of what an HFO is, since there is no consensus. For instance, the RMS detector was developed for hippocampal microelectrode recordings (Staba *et al.,* 2002) and considered as HFOs events with at least six oscillations above certain energy level; the LineLength detector developed for gamma activity, and later used for high frequency band (80-1000Hz) activity in microelectrodes and subdural electrodes; the Hilbert detector only considered events in the 180-400Hz band and was developed for a wake dataset (Crepon *et al.,* 2010); the MNI detector was developed for a similar dataset than the one used here for testing. The improvement in performance of the detectors designed for a different type of signal is not surprising, but it should raise awareness of the danger of using a detector without validation.

The optimum threshold was selected based on the distance to the best possible point in an ROC curve. This was a useful criterion to compare the detectors. However, when implementing a detector for research or clinical applications, this threshold selection may not be best. One may consider using a threshold optimized for a small training dataset, imposing a constrain in the number of false detections. The optimization function used for the definition of

parameters of the MNI detector is an example; imposing a maximum FPR in the ROC curves (as in Crepon *et al.,* 2010) is another.

Only events that corresponded to visually detected HFOs or baselines were considered for the calculation of sensitivity and FPR. This strict definition of the true negative events can explain the extremely low FPR, which must be interpreted with caution: a low FPR does not necessarily imply a low number of false detections, but rather a low number of detections within visually marked baselines. Furthermore, given the large number of visually marked baselines (~50,000) a 1% FPR represents 500 false detections. However, given that some segments of EEG cannot unequivocally be considered as baseline or as HFOs, we believe that considering the FPR with respect to the NegBase is appropriate. Thus, even though detections occurred, a good proportion of the EEG data was not considered for the ROC curves and for the comparison of FPR across detectors. Analysis of events in these EEG segments could identify events not visible to the human reviewer or on the contrary indicate FP due to artefacts.

Although making false detections on 66-76% of the detections seems an enormous number, it is small compared to the reported values. For instance, Crepon and colleagues reported that only about 1% of automatically detected events were kept after post-processing (Crepon *et al.,* 2010), while Worrell and colleagues kept 15% of detected events (Worrell *et al.,* 2008).

Automatic detectors consider each channel independently from each other. Therefore, the ideal gold standard should have been to review the channels in isolation. However, visual marking of HFOs is already highly time intensive. Reviewing channels in isolation would have taken too long to be feasible (since 10 consecutive channels were marked simultaneously, the time would increase considerably). In addition, since we only considered depth electrodes for this study, and since HFOs are usually visible only in a few channels simultaneously (Crepon *et al.,* 2010), we believe that visually marking HFOs in isolation would have provided similar gold standard HFOs. In any case, since the same gold

standard was used to measure the performance of all detectors, it does not affect their comparison.

The goal of an automatic detector is to provide the same conclusions that could be obtained with visual marking. Thus, even if we accept a large number of false positives, the relative number of false positives to true positives must be equivalent in all channels. This was measured with the RKD. The great variability in RKD across subjects was probably due to false positive detections, but this remains to be validated. If this is the case, the RKD would improve after post-processing. On the other hand, the variability across human reviewers was extremely low, as indicated by a high Kappa and low RKD, which was expected since visual markings were evaluated and corrected for consistency following the procedure of (Zelmann *et al.,* 2009b).

Most channels with continuous oscillatory HF activity, where baselines could not be identified, contained high rates of HFOs and were related to epileptogenic regions. Thus, an analysis of different types of background activity is under study to establish clearer definitions for automatic HFO detection in those channels (Mari *et al.,* 2012). They were common in mesial temporal regions of patients with mesial temporal lobe epilepsy. When visually marking HFOs in these channels, only oscillatory events with one clear frequency component, at least four oscillations, and energy larger than the surrounding continuous oscillatory background are considered. The iterative approach in the MNI detector detected most HFOs in these channels.

The distinction between pathological and physiological HFOs remains uncertain (Engel *et al.,* 2009). In microelectrode recordings, it is associated with a difference in frequency, with ripples regarded as normal and FR pathological (Bragin *et al.,* 1999b, Staba *et al.,* 2002). However, studies with macroelectrodes suggested that this distinction might be arbitrary. The rates of ripples and FR were higher in SOZ than outside (Jacobs *et al.,* 2008a, Urrestarazu *et al.,* 2007, Worrell *et al.,* 2008), ripples behaved similarly to FR with respect to surgical outcome

(Jacobs *et al.,* 2010b) and medication withdrawal (Zijlmans *et al.,* 2009b). Thus, ripples and FR seem to be associated with tissue that generates seizures. Moreover, physiological HFO emerging from the visual cortex had similar spectral characteristics to the HFOs emerging from epileptogenic tissue (Nagasawa *et al.,* 2012). These results indicate that frequency alone is not sufficient to discriminate between pathological and physiological HFOs. A recent study showed that events clustered into ripples and FR, but also with a third class of mixed components (Blanco *et al.,* 2010). Even though two frequency peaks (Staba *et al.,* 2002) or separate classes (Blanco *et al.,* 2010) were found, detections were made on a broad frequency band similar to the one we chose. If a distinction between ripples and FR is demonstrated, detectors should be tailored to each.

For an automatic detector to be used clinically, false detections must be discarded. Different approaches can be considered for post-processing. A semi-automatic detector in which visual validation is performed by experienced reviewers can be implemented (as in Crepon *et al.,* 2010, Worrell *et al.,* 2008). This approach allows for the removal of artefacts, the possible modification of the duration of the detected HFO, and could be used for all types of recordings. Even though expert intervention is required, the time needed is greatly reduced. Another possibility is the automatic classification of detections in events or artefact (Blanco *et al.,* 2010). After post-processing, it is important to assess whether the detections provide meaningful information for localization of the epileptogenic area. A comparison of the conclusions drawn from (semi-) automatically detected HFOs with those obtained from visual markings provides the ultimate validation for a robust detector.

In conclusion, the automatic detection of HFOs is crucial to propel the clinical use of HFOs as biomarkers of epileptogenic tissue. Automatic detectors were developed for different EEG recordings and with different aims. Given the lack of a formal definition of HFOs, comparing them in a single dataset is important to analyze their performance and to emphasize the issues involved in

validation. The MNI detector performed better than the others in this dataset (higher sensitivity, lower FPR and similar FDR), but was developed on channels similar to those used for testing. The choice of energy function does not seem to be the most relevant difference, but the approach by which the energy threshold is computed may matter. Optimizing on a particular type of data improves performance in any detector.

6.13 *Acknowledgements*

This work was supported by Grants MOP-10189 and MOP-102710 from the Canadian Institutes of Health Research. RZ was supported by National Science and Engineering Research Council (NSERC) Postgraduate Scholarship (PGSD).

6.14 *Significance*

The robust automatic detection of HFOs is crucial for the systematic study of HFOs and to propel the clinical use of HFOs as biomarkers of epileptogenic tissue. The presented automatic detector provides an original approach in first detecting baseline segments and then incorporating this local information for the detection of HFOs. This approach improves performance in very active channels, by considering the local characteristics of the baseline around the point of interest. This detector is the first to consider channels with continuous HF activity background. The presented detector performs better than other detectors, in particular in active channels and in channels with continuous HF activity background. These channels are clinically relevant, given their location or relation to epileptogenicity. This approach therefore provides key features for the clinical utilization of an automatic detector of HFOs. A comparison of existing detectors on the same dataset was important not only to analyze their performance, but also to show that optimizing on a particular type of data improves performance in any detector, and to emphasize the issues involved in validation.

Chapter 7. *Manuscript #4: The scalp EEG can see very small cortical generators of epileptic activity*

7.1 *Context*

As HFOs are produced by small brain regions, and since the EEG is greatly attenuated before reaching the scalp, HFOs are mostly recorded with intracranial electrodes. In line with this, the two previous chapters dealt with intracranial HFOs. Surprisingly, HFOs have been recently also recorded on the scalp. Scalp HFOs could become valuable to evaluate non-invasively large patient populations, to predict surgical outcome, and to plan electrode implantation.

Finding HFOs on the scalp was unexpected since a large cortical region, of several centimeters, has been considered necessary to observe brain electrical activity on the scalp. How is it possible that these small events can be observed on the scalp? There are two possible hypotheses. The predominant hypothesis is that a large cortical region is most probably involved during the HFO events visible on the scalp. However, this hypothesis contradicts findings from intracranial recordings that showed that HFOs are generated by small brain regions. Taking this second perspective, could it be that small-spatial extent HFO events are visible on the scalp?

The following manuscript studies which one of these two hypotheses is more likely to explain the presence of scalp HFOs. Since HFOs on the scalp are very rare, long segments of interictal EEG must be analyzed. Thus, the automatic detector presented in the previous chapter is a necessary tool for the detection of possible HFOs on the scalp. In order to study the cortical activity at the time of scalp HFOs, simultaneous scalp and intracranial recordings are required. This was possible in the context of collaboration with the University of Freiburg, where

such recordings are performed. This manuscript has been submitted for publication.

7.2 *Abstract*

High frequency oscillations are emerging as biomarkers of epileptogenicity. They have been shown to originate from small brain regions. Given the high resistivity of the skull and the assumption that a large cortical extent is needed to observe an event on the scalp, they have been mostly recorded with intracranial electrodes. Surprisingly, spontaneous high frequency oscillations can be recorded from the scalp. Their detection on the scalp could be useful to evaluate the development of epilepsy in large patient populations, for predicting surgical outcome, and for planning electrode implantation.

To understand how is it possible to observe these small events non-invasively, a paramount step is the analysis of the cortical correlates of scalp high frequency oscillations. Using simultaneous scalp and intracranial recordings of 11 patients, we studied the spatial distribution of scalp events on the cortical surface. For interictal epileptiform discharges the subdural contacts were, as expected, spatially extended. On the contrary, for scalp high frequency oscillations the subdural maps were focal, consisting of one or a few dipolar configurations. These topographies suggest that small cortical areas generated the high frequency oscillations seen on the scalp.

For interictal epileptiform discharges, similar scalp distributions corresponded to similar subdural distributions and averaging similar scalp topographies enhanced subdural activity. On the contrary, for high frequency oscillations, similar scalp distributions corresponded to distinct distributions on a standard 1cm subdural grid and averaging cancelled subdural activity. The assumption that a subdural grid "sees" everything that is seen by nearby scalp contacts is more valid for interictal epileptiform discharges than for high frequency oscillations.

These results suggest that the hypothesis that a large cortical region needs to be active for an event to be seen on the scalp is not valid for high frequency oscillations. Even though their generators are small, they can be observed on the scalp, with low amplitude and in a very focal region. These small extent events are undersampled on the scalp and on the grid. In agreement with this, when simulating 280 cortical sources of approximately 1cm^2, we found that we are spatially undersampling such focal events on the scalp when using 30 to 60 electrodes.

High-density scalp electrodes seem necessary to fully sample high frequency oscillations on the scalp. A better understanding of the influence of spatial sampling on the observation of high frequency brain activity on the scalp is important for their clinical use as biomarkers of epilepsy.

7.3 *Introduction*

The question of how much of the electrical signals generated in the brain can be seen on the scalp has often been raised. Simultaneous recordings of intracranial and surface electroencephalography (EEG) originally suggested that a cortical area of at least 6cm^2 is necessary for an epileptic spike to be seen on scalp (Cooper *et al.,* 1965). This value was recently increased to 10cm^2 (Tao *et al.,* 2007). In line with this, 8-15cm^2 of lateral cortex has to be active during a seizure to be visible on the scalp (Hashiguchi *et al.,* 2007). Computational models of EEG generation also support these findings (Cosandier-Rimele *et al.,* 2008). Moreover, more than 4cm^2 of lateral cortex need to be active for a spike to be observed on magnetoencephalography (Oishi *et al.,* 2002). As a result of the above studies several square centimetres have become the commonly accepted spatial extent of an event to be observed on the scalp EEG.

The traditional EEG frequency bands considered clinically relevant (up to 70Hz) have been recently challenged by the discovery of High Frequency Oscillations (HFOs; 80-500Hz). Given the high resistivity of the skull and the assumption that a large extent of cortex is needed to observe an event on the

scalp, HFOs have been mostly recorded with intracranial depth electrodes and with grids/strips on the surface of the cortex. Intracranially, pathological HFOs are short spontaneous oscillatory patterns that are emerging as a reliable biomarker of epileptogenic tissue (reviewed in: Jacobs *et al.,* 2012, Zijlmans *et al.,* 2012). HFOs identify the seizure onset zone (Jacobs *et al.,* 2008b, Urrestarazu *et al.,* 2007, Worrell *et al.,* 2008) and have good correlation with surgical outcome (Jacobs *et al.,* 2010b, Wu *et al.,* 2010). They can be recorded in mesial temporal (Bragin *et al.,* 1999b, Staba *et al.,* 2002) and neocortical structures (Jacobs *et al.,* 2009a).

Small brain regions produce HFOs. Animal studies indicate that the generators of HFOs are on the order of the cubic millimetre. Pathological fast ripples (200-600Hz) in the epileptic rat hippocampus were generated by a region of about $1mm^3$ (Bragin *et al.,* 2002), while physiological ripples (100-400Hz) in the rat's hippocampus extended 4-5mm (Chrobak and Buzsaki 1996). In the cat neocortex, physiological ripples (80-200Hz) were correlated only within the same gyrus, extending at most 9mm (Grenier *et al.,* 2001). According to the above discussion regarding the scalp recording of cortical events, it should not be possible to see HFOs on the scalp EEG.

Surprisingly, recent studies showed that spontaneous HFOs can be also recorded from the scalp. Ictal gamma activity (50-100Hz) was observed during infantile spasms (Kobayashi *et al.,* 2004) and paroxysmal gamma activity (above 30Hz), although infrequent, co-localized with the seizure onset zone (SOZ; Wu *et al.,* 2008). Interictal HFOs were first observed on scalp during continuous spike-waves during slow-wave sleep (Kobayashi *et al.,* 2010b). Careful observation of scalp EEG also allowed the identification of interictal HFOs in patients with focal epilepsy (Andrade-Valença *et al.,* 2011). The rate of scalp HFOs, however, was much smaller than the usual rate of intracranial HFOs.

HFOs recorded with intracranial EEG proved to be specific markers of epileptogenicity in patients with refractory epilepsy. The detection of HFOs non-

invasively, on scalp EEG, could broaden the use of HFOs as biomarkers. Scalp HFOs could be assessed in large patient populations with different types of epilepsies, including non-refractory and generalized forms, and over long periods. Scalp HFOs might be useful to follow the effect of medication and to predict the development of epilepsy after a first insult. They could help to plan electrode implantation and in the prediction of postsurgical outcome, as the scalp EEG can overcome the spatial limitations of intracranial EEG. Understanding the cortical correlates of scalp HFOs is a paramount step towards their clinical utilization.

There are two possible hypotheses to explain why these small extent events are visible on the scalp. Following the idea that at least $10cm^2$ of activated cortex are necessary to observe a spike on the scalp, the predominant hypothesis is that a large cortical region is most probably involved during the HFO events visible on the scalp. However, this hypothesis seems to contradict the idea that HFOs are generated by small brain regions, as observed with intracranial recordings. Taking this second viewpoint, could it be that small-spatial extent events are visible on the scalp?

In this study, we evaluate which of these two hypotheses is more likely to explain the presence of HFOs on the scalp. We assess these two hypotheses from different perspectives. Using simultaneous scalp and intracranial recordings, we analyze the cortical involvement when HFOs were visible on the scalp. We compare this spatial distribution to that of scalp spikes. We study whether similar scalp events correspond to similar subdural recordings by analyzing the averaged activity and pairwise similarity on the subdural contacts for similar scalp patterns. By applying a linear model under the assumption that the subdural contacts capture everything that is observed in overlying scalp contacts, we relate the observations on the subdural contacts to those on the scalp and study whether the subdural voltage distribution can estimate the scalp recordings. To analyze the possibility that the low rate of HFOs on the scalp is due to spatial undersampling, we simulate sources of small extent and measure their spatial distribution on the scalp.

7.4 *Methods*

7.4.1 *Patient selection and electrode placement*

Fifty-eight patients were recorded at the epilepsy center of University Medical Centre Freiburg between September 2004 and August 2009. Patients with focal cortical dysplasia and simultaneous scalp and subdural EEG recordings of good quality were selected. Eleven patients fulfilled these criteria. Patients remained in the hospital during 8 to 15 days. The clinical information of these patients is presented in Table 7.1. During some days of the investigation, the EEG was recorded at 32.768kHz, then filtered at 344Hz and down-sampled at 1.024kHz (IT med-EEG-System, Natus Europe GmbH, Munich, Germany). One hour of EEG was selected, at least one hour away from a seizure, during the first available night with simultaneous scalp and subdural recordings. Focal cortical dysplasia patients were selected on the basis that their epileptogenic area is usually focal and located in the neocortex. Night recordings were analyzed to minimize the amount of muscular (EMG) and ocular (EOG) contamination and to increase the rate of HFOs (Bagshaw *et al.,* 2009, Staba *et al.,* 2004).

Electrodes were placed exclusively for clinical reasons and included subdural grid, subdural strip, and/or depth macro-electrodes (AD-TECH Medical Instrument Corporation, Racine, WI, USA). Seven patients had subdural grids and ten had subdural strips. Eight patients had additional depth electrodes. Only subdural functioning contacts on the lateral neocortex that were parallel to the scalp were analyzed (i.e. basal strips or depth electrodes were not considered). Subdural contacts had a diameter of 4mm, an exposed surface diameter of 2.3mm, and an inter-electrode distance of 1cm. Scalp EEG electrodes were placed following the international 10-20 electrode placement system with additional low temporal electrodes. All functioning scalp contacts were analyzed. The local Ethics Committee approved this study and all patients gave informed consent.

Patient	FCD type	Age/ gender	Type of seizure	MRI	Medication	Surgery	Outcome
1	1a	47/M	SPS, GTCS	FCD R O	OXC, LEV	R O lesionectomy	1a
2	2a	17/M	SPS, CPS, GTCS	FCD R T	OXC, LEV	R T resection	1a
3	2a	33/M	SPS	FCD R T	LEV, OXC	R T pole, A resection	1a
4	2b	38/Fe	SPS, GTCS	Transmantle dysplasia L PCS	None	L P lesionectomy	1b
5	2a	17/M	SPS, CPS, GTCS	Atrophy L H	OXC	L-sAHC, ant. T resection	1a
6	1b	52/M	CPS, GTCS	HS R	OXC, LTG	R T, A resection	1a
7	2a	21/M	SPS, CPS	FCD R MTG	CBZ, LEV, TPM	R T resection	1b
8	2a	40/M	SPS, GTCS	HS L; FCD L	LEV	L T resection	1a
9	2b	18/M	SPS, CPS, GTCS	FCD L T	OXC, LEV	L T lesionectomy	1a
10	2a	42/M	SPS, CPS, GTCS	FCD R T; lenticulo-striatalal infarction L	None	R T lesionectomy	1a
11	1a	21/M	SPS, CPS	Normal	LTG, PGB	T lesionectomy	1a

Table 7.1: Clinical information of the patients. The postsurgical outcome is classified according to Engel (1993). A = amygdala; ant. = anterior; CBZ = Carbamazepine; CPS = complex partial seizure; FCD = focal cortical dysplasia; F = female; GTCS = generalized tonic-clonic seizure; H = hippocampus; HS = hippocampal sclerosis; L = left; LEV = Levetiracetam; LTG = Lamotrigine; M = masculin; MTG = middle temporal gyrus; OXC = Oxcarbazepine; P = parietal; PCS = postcentral sulcus; PGB = Pregabalin; R = right; sAHC = selective amygdalo-hippocampectomy; SPS = simple partial seizure; T = temporal; TPM = Topiramate; O = occipital.

7.4.2 *Event identification*

7.4.2.1 *Identification of scalp HFOs*

To study the correlates of scalp HFOs on the brain surface, it was important to ensure that the selected events were clear HFOs of cerebral origin. HFOs were defined as events with at least 4-oscillations of sinusoidal like morphology in the filtered EEG that stand out from the surrounding background (Worrell *et al.,* 2012). In order to obtain clear, even if few scalp HFOs, an automatic detector was first run on the scalp EEG, followed by two visual confirmations.

In the first step, a detector originally developed for intracranial EEG (Zelmann *et al.,* 2012) was implemented for the detection of possible scalp HFOs. The detector was optimized on 1-min intracranial EEG of 5 patients with focal cortical dysplasia, which were not included in this study as they had no

simultaneous scalp recordings. Intracranial recordings were used for this optimization, since we assumed that HFOs on scalp have similar characteristics as intracranial HFOs. The EEG was filtered between 80-300Hz (see description of filter below). Possible scalp HFOs were automatically detected on bipolar montage during one hour of scalp EEG. This first step led to the identification of possible events, many of which were artefacts that were later discarded. The main goal of this first step was to reduce the burden of marking 1h of EEG by allowing the reviewer to focus on possible events.

The second step involved the visual confirmation of scalp HFOs by an experienced reviewer using the Harmonie system (Stellate, Natus Medical Inc., CA, USA). For this purpose the screen was vertically divided in two. The left side showed high-passed filtered (above 80Hz) EEG at an expanded scale (270.9mm/sec). The right side showed the unfiltered EEG with a more compressed scale (30mm/sec). Only events with at least four rhythmic oscillations with regular amplitude that stand out from background were visually confirmed (Andrade-Valença *et al.,* 2011). To differentiate HFOs from EMG, the guidelines proposed by Andrade–Valença and colleagues (2011) were followed. Events co-occurring with muscle or electrode artefacts in the unfiltered EEG were rejected. Events with large frequency variability, irregular morphology, or large amplitude variations were discarded. We designed our filter with impulse response shorter than the events of interest and checked that the impulse response did not resemble the events of interest (Figure 7.2). Thus, the filtering effect ("Gibbs" phenomena) of glitches and sharp spikes were identified since they had fewer than 4 oscillations with similar amplitude and were therefore discarded.

The last step involved the confirmation of events by an independent reviewer and further discarding artefacts related to EOG activity. EOG type of activity occurred mainly simultaneously in both Fp channels, consisting of ~6 oscillations. These artefacts showed a small "burst" in the unfiltered EEG and were associated with EOG changes. EOG activity, in particular saccades, has been shown to

correspond to activity in the gamma (30-100Hz) band (Yuval-Greenberg *et al.,* 2008). Any event that was thought to correspond to EOG activity was discarded.

HFOs were marked with high specificity rather rejecting than keeping an HFO that may derive from any kind of artefact. As suggested by Bénar et al. we chose a filter with short impulse response (Figure 7.2), required HFOs to have at least 4 regular oscillations and validated the visibility of randomly selected HFOs on the unfiltered EEG (Figure 7.3), to ensure that they did not correspond to filtering sharp events (Bénar *et al.,* 2010). Examples of scalp HFOs in contrast to glitch, EMG, and EOG artefacts are illustrated in Figure 7.1.

By using this strict procedure, we are confident that the remaining events are HFOs of cortical origin. We are aware that some true events might not have been retained since we chose to have high specificity at the cost of low sensitivity. Detections occurring simultaneously in different scalp channels were considered together (referred as time-events).

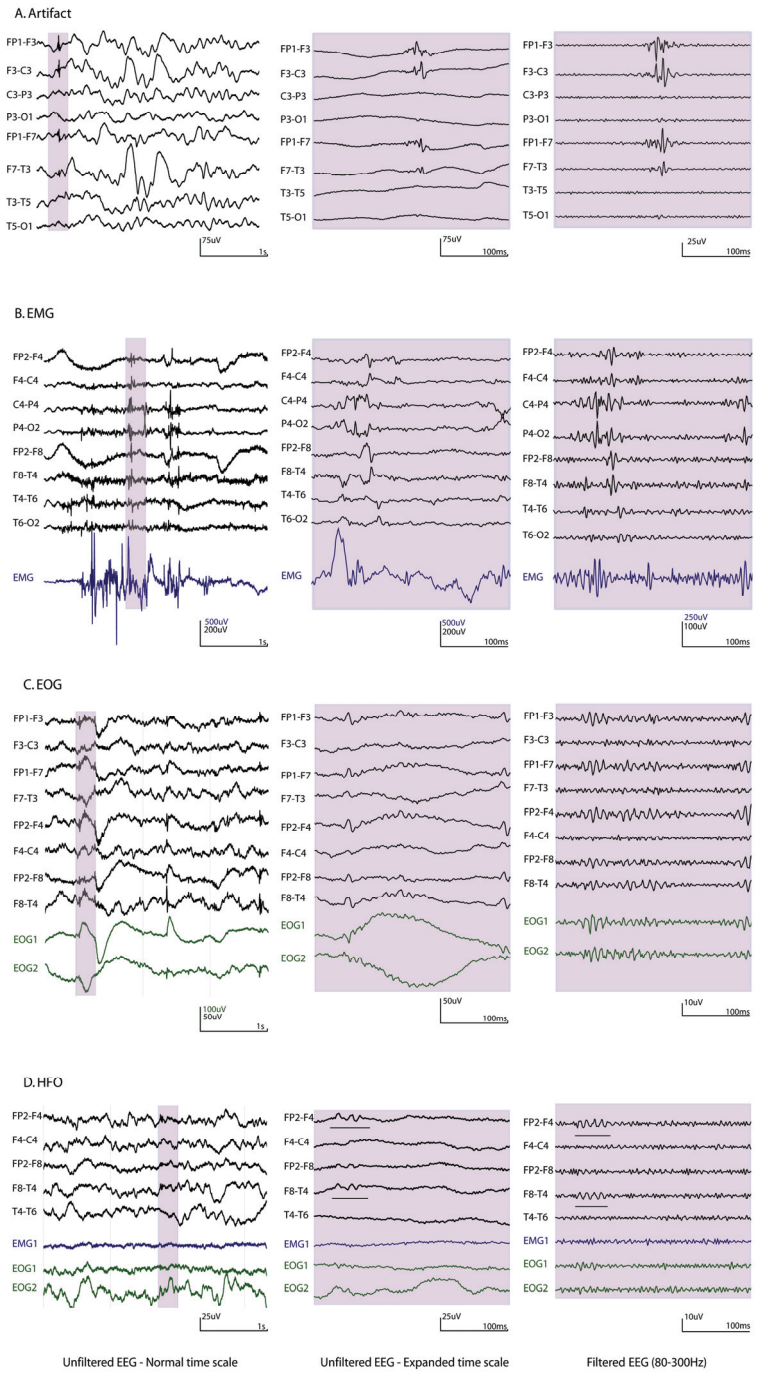

Figure 7.1. Example of scalp HFO as opposed to artefacts in patient 5. A) External artefact. The filtered EEG shows a short duration irregular oscillation, corresponding to the filtering effect of a sharp signal; it corresponds to a glitch in the unfiltered EEG. B) EMG artefact. In the filtered EEG a large amplitude irregular event is observed; it corresponds to high amplitude activity observed in the unfiltered EMG contact. C) EOG artefact. In the filtered EEG many regular oscillations are observed, particularly in Fp channels; they correspond to EOG fluctuations. D) Scalp HFO. The HFO can be observed in F8-T4 and with smaller amplitude in FP2-F4; it can also be observed in the unfiltered expanded EEG. No concomitant EMG or EOG is observed. Left column displays the unfiltered EEG with normal time scale; central column displays the unfiltered EEG with expanded time scale; right column displays the filtered (80-300Hz) EEG.

7.4.2.2 *Identification of scalp interictal epileptiform discharges*

In focal cortical dysplasia patients, interictal epileptiform discharges (IEDs) include isolated spikes or sharp waves, repetitive spikes, and paroxysmal fast patterns (Boonyapisit *et al.,* 2003). Because discharges are usually patient specific but vary across patients (Gambardella *et al.,* 1996), typical IEDs for each patient were first identified and then marked on the scalp EEG. Twenty-five IEDs per patient were marked using standard display configuration (0.5-70Hz band-pass filter; 10sec/page visualization; bipolar montage). In one patient for whom IEDs could not be found, we selected instead sharp transients that were characteristic of this patient and that might correspond to normal patterns (Patient 1 in Figure 7.4). Since these events are observed in the unfiltered EEG, a large cortical extent is expected to be necessary to observe them on the scalp, similarly to IEDs. For simplicity we will refer to all unfiltered activity as IEDs.

7.4.3 *Analysis of simultaneous scalp and subdural recordings*

For the analysis of HFOs, the EEG was filtered between 80-300Hz using a finite impulse response equirriple filter (fStop1= 70Hz; fPass1= 80Hz; fPass2= 300Hz; fStop2= 310Hz; stop-band attenuation= -60dB; pass-band ripple= 0.1dB). The impulse response of this filter is shown in Figure 7.2. For the analysis of IEDs, the EEG was filtered between 0.5-70Hz using an IIR Butterworth filter (fStop1= 0.1Hz; fPass1= 0.5Hz; fPass2= 70Hz; fStop2= 80Hz; stop-band attenuation = -60dB; pass-band ripple= 1dB). The scalp EEG and the intracranial EEG were referenced to Fz. Analysis was based on MATLAB.

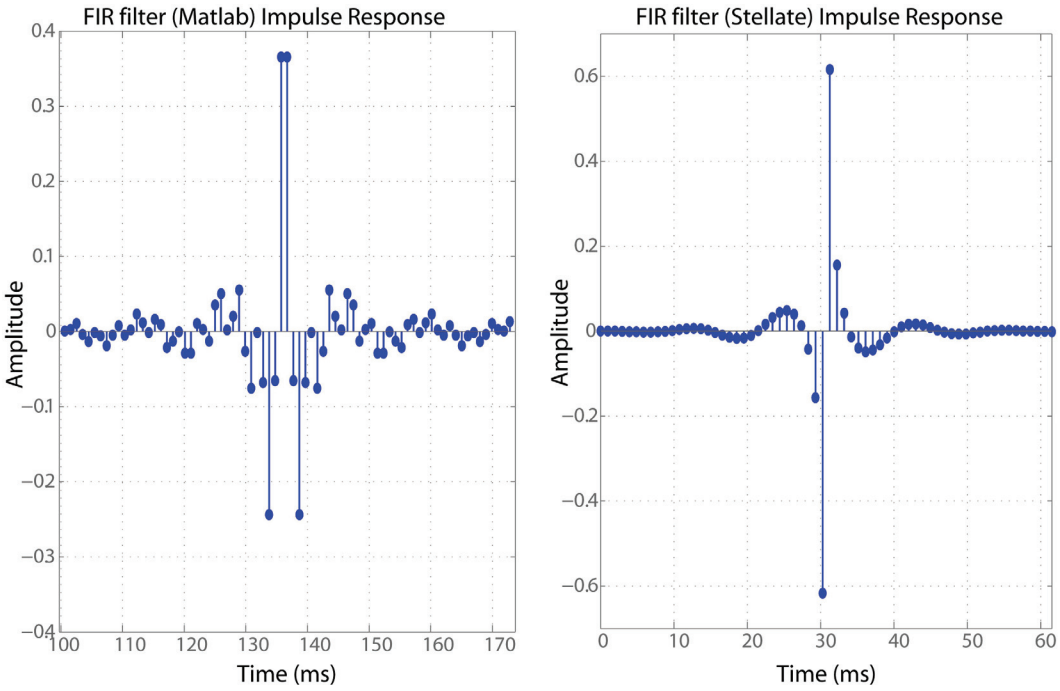

Figure 7.2. Impulse response of the FIR filters. *Left*: band pass FIR filter (80-300Hz) designed in Matlab and used for the automatic detection and analysis. *Right*: high pass FIR filter (>80Hz) used in Stellate to visualize events and discard artefacts. The impulse response of both filters is different than the four regular oscillations characteristic of HFOs and is shorter than the events of interest. Thus, when filtering sharp transients (Gibbs effect), the response of these filters was easily recognized and the artefacts rejected.

Voltage maps on the scalp and on the brain surface were created for each subject and for each time-event, corresponding to the largest peak of the electrodes involved in a time-event. For instance, an event of patient 1 occurred in channels P4-O2 and T6-O2. The largest peak in the EEG was in O2 for this time-event. The time of this peak was used for the scalp and subdural voltage maps (Figure 7.4.B).

We used the cross-correlation coefficient between voltage maps of pairs of events to study similarity between voltage maps. Similar pairs of maps were those with a correlation coefficient significantly different from zero. The percentage of statistically similar map pairs was computed by pooling all pairwise correlations. This was implemented to assess whether similar scalp voltage maps corresponded to similar subdural voltage maps; to average voltage maps of events with similar scalp topography to each other, creating scalp and subdural averaged voltage maps; and to evaluate whether a linear model could predict scalp patterns based

on subdural patterns of activation (see section below). Significance level was set to $p<0.01$.

To assess the focality vs. smoothness of the voltage maps we computed the power in the lower half of the spatial spectra. The 2D fast Fourier transform of the voltage maps was computed. The total power on the lowest half of the spatial spectra was obtained. A smooth voltage map corresponds to a smooth peak of low spatial frequency, which corresponds to high power in the lower part of the spatial spectra. On the contrary, a focal map with multiple dipolar patterns has high power at high spatial frequencies. Mann–Whitney–Wilcoxon test was used to test for differences in power between IED and HFO maps.

7.4.4 *Phase synchronization*

The relative phase was computed from the phase of the scalp EEG and the corresponding subdural EEG (Lachaux *et al.,* 1999). The phase was obtained from the Hilbert transform of the signals, and the phase lock value (PLV) was computed as

$$PLV = \frac{1}{N}\sum_{t=1}^{N} \frac{hilb_{scalp(t)}{}^{*}}{\|hilb_{scalp(t)}{}^{*}\|} \cdot \frac{\overline{hilb_{seeg(t)}{}^{*}}}{\|hilb_{seeg(t)}{}^{*}\|} \qquad \textbf{Equation 7.1}$$

where N=64ms (the median duration across events) and N/2 corresponded to the largest peak of each HFO. * denotes complex signals, and $\bar{x}$ is the conjugate of x.

For each patient a threshold was obtained as the 99 percentile of a null distribution of PLVs, consisting of at least 5000 PLVs. To obtain this null distribution with a structure similar to that of the data, each of these PLVs was computed between the scalp EEG from one event and the subdural EEG from another. Random jitter of up to 50ms was added. In patients with less than 5 events (3 patients) a global threshold was computed as the 99 percentile of a null distribution pooling all the PLVs together. In the two patients with bilateral

implantation, only the side of most HFOs (all in 1 patient, all but 1 HFO in the 2nd patient) was studied.

The channel of interest for each event was selected as the scalp channel with the largest peak. Control channels were selected as far away from the channel of interest as possible. For patients with electrodes in temporal or occipital regions, the control channel was frontal on the contralateral side. For the patient with a central grid, the control channel was parietal on the contralateral side. To compare the pooled PLVs of the channel of interest with the corresponding PLVs for the control channel and to compare the maximum PLV per event we used a paired t-test. To compare the number of events with any PLV larger than threshold across patients a Wilcoxon test was used. As before, statistical level was set at $p<0.01$.

7.4.5 *Modeling*

7.4.5.1 *Linear Model*

Assuming that an event on the scalp can be explained by the event seen in subdural contacts, we developed a forward model relating subdural events to scalp events. Details of the model are in appendix A. The basic principle of the model is that, given a set of similar scalp events and their subdural counterparts, the model should be able to predict a scalp event from its subdural counterpart.

We implemented a leave one out procedure for each patient with more than 5 scalp events (6 patients for HFOs, all 9 patients for IEDs). The forward model was therefore built from all events but one and tested in this remaining event. The scalp event was estimated from this model and a subdural event. The resulting voltage map was compared with the voltage map of the real event. As explained before, we used the cross-correlation between real and estimated voltage maps as similarity measure. The percentage of similar voltage map pairs out of all pairs is reported.

7.4.5.2 *Simulation of source extent*

In order to estimate the spatial distribution on the scalp of a focal subdural source, we simulated distributed sources using Brainstorm (Tadel *et al.,* 2011). The scalp distribution was computed with the symmetric boundary element forward model using OpenMEEG (Gramfort *et al.,* 2010, Kybic *et al.,* 2005). The standard *MNI Colin27* brain (Holmes *et al.,* 1998) was segmented into brain, inner-skull, outer-skull, and scalp. To represent a dense spatial sampling on the scalp, all vertices of the tessellated scalp and face (1082 vertices) were considered as scalp electrodes. The averaged distance between vertices on the scalp was 1.3 +/- 0.2cm, which corresponds approximately to 512 scalp electrodes (Ryynanen *et al.,* 2004). In addition, the 10-20 system, the 10-10 system, and 256 electrodes were considered. The percentage of events that could be recorded with a particular electrode placement system was compared against the number of visible events when recording on all scalp vertices. The conductivity ratios for the brain, skull, and scalp were set to 1:1/25:1 (Goncalves *et al.,* 2003, Lai *et al.,* 2005). The distribution on the subdural contacts was obtained by computing the forward model, using only 1 layer, at the inner-skull (642 vertices), with 1.23 +/- 0.16cm inter-electrode distance.

To generate the distributed focal sources, the cortex was parceled into non-overlapping patches of ~10 vertices located over gyri. This division resulted in 280 patches each corresponding to a distributed source (i.e. a continuous area of cortex simultaneously active), of 1.21 +/- 0.25cm^2. The intensity of the sources was set to 5nA.m (Alarcon *et al.,* 1994, Kobayashi *et al.,* 2005). Since the mean filtered scalp EEG background was 1.53 +/- 1.03µV, we considered 2µV as noise level for the scalp recordings. The number of sources that could be recorded, with RMS amplitude above a 4µV threshold (double the noise level), was obtained for different scalp electrode systems. Similarly, the number of observable distributed sources, with RMS amplitude above a 30µV threshold (Jirsch *et al.,* 2006), on the subdural contacts was computed.

7.5 *Results*

Scalp HFOs were found in 9 of 11 patients (82%). A total of 115 time-event HFOs were visually confirmed (total number of HFOs: 209). The mean rate was 0.21 time-events HFOs/min (range 0.02-0.78). Figure 7.3 shows an example of a scalp HFO. Even though there are IEDs in several channels, HFOs are only present in two scalp channels. They were marginally visible on the unfiltered time-expanded EEG (Figure 7.3.B). The scalp (Figure 7.3.D) and subdural (Figure 7.3.E) voltage maps correspond to the time point of the largest peak in the filtered scalp EEG (indicated by an orange arrow).

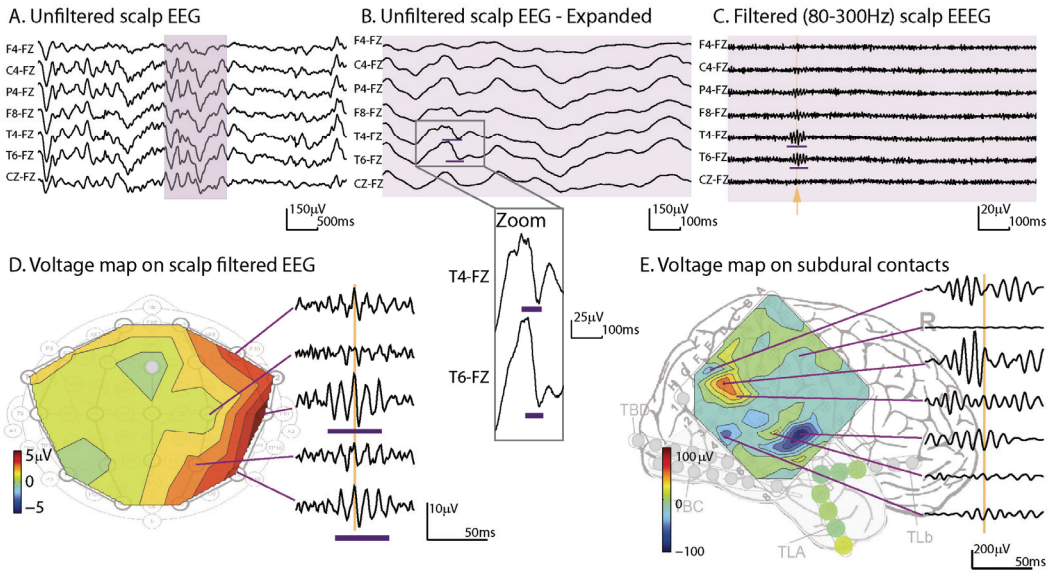

Figure 7.3. Example of scalp HFO. A) Unfiltered Scalp EEG, normal settings (patient 7). B) Section of unfiltered scalp EEG expanded in time. C) Same section band-passed filtered 80-300Hz, HFOs are visible in channels T4 and T6 (purple horizontal line). D) Voltage maps on the scalp at the time of a largest peak of a scalp HFO (indicated by arrow in C). E) Voltage map on the subdural contacts at the same time. The scalp HFOs are visible on the unfiltered EEG (Zoom insight; also indicated by purple horizontal line in B), particularly on T4 (B). Some scalp IEDs occurring at the same time do not have an associated HFO. This illustrates that the HFOs are not the effect of filtering a spike. The subdural map at a time of a scalp HFO is focal, with a few dipolar configurations. Thus, the underlying cortical generator has small spatial extent. Voltage maps represent the amplitude on scalp and subdural contacts at the time of maximum peak on the scalp (orange line). Amplitudes in scalp and grid are linearly interpolated. Strip contacts are depicted as circles with their amplitudes at this same time point.

7.5.1 *Focal or large cortical extents at the time of a scalp event?*

In order to test which hypothesis is likely to explain the presence of HFOs on the scalp, we analyzed the spatial distribution of the voltage on the subdural contacts. As expected, a large cortical region with smooth boundaries was active at the time of scalp IEDs (Figure 7.4.A). This re-affirms the concept of a large brain area being active to see unfiltered EEG activity on the scalp. In contrast, the subdural voltage maps at the time of scalp HFOs were focal, consisting of one or a few activations with a dipolar pattern (Figure 7.3.E & Figure 7.4.B).

To quantify this difference in topography, the power at the lowest half of the spatial spectra was computed. This measured how focal (vs. smooth) was the spatial distribution of the voltage maps on grids. The six patients with grids were included in this analysis and had a total of 100 HFOs and 152 IEDs. There was a significant difference between maps that corresponded to IEDs and those corresponding to HFOs (Figure 7.4.C). Maps corresponding to IEDs were smoother than those corresponding to HFOs, as measured by the percentage of power in the lowest half of the spatial spectra (IEDs median= 69.4%; HFOs median=35.3%; $p<<0.001$).

Moreover, a careful observation of the voltage maps suggests that there could be several asynchronous independent HFOs on the subdural grid at the time of a scalp HFO (see for instance Figure 7.4.B, patient 2).

The observed focal subdural configuration suggests that even though HFOs are generated by and synchronized over small regions, they can be observed on the scalp. This observation is in agreement with our second hypothesis.

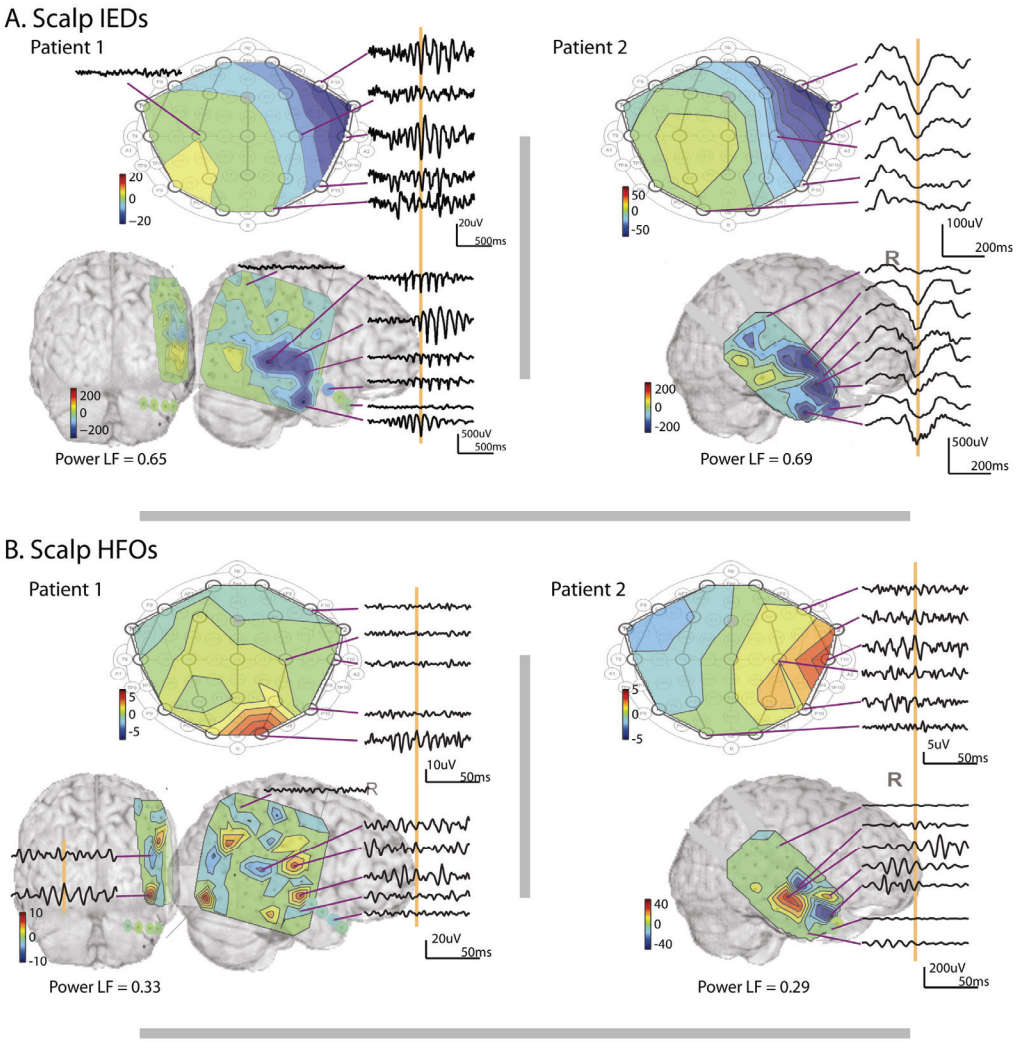

Figure 7.4. Examples of voltage maps on the scalp and on the subdural contacts at the time of the largest peak of a scalp IED (A) and a scalp HFO (B) in patients 1 and 2. The subdural map at the time of IEDs (filtered between 0.5-70Hz) extends over a large cortical region, with a smooth configuration. The subdural map at the time of HFOs (filtered between 80-300Hz) is focal, with a few dipolar configurations. Scalp and grid contacts are linearly interpolated. Strip contacts are depicted as circles with their amplitudes. C) Focality in the voltage maps was measured by the percentage of power on the lowest half of the spatial power. Voltage maps of HFOs were significantly more focal than IEDs (median power LF_HFOs= 35.3%; median power LF_IEDs = 69.4%; p<<0.001). Values for individual maps are indicated in the examples of A and B. Patient 1 typical unfiltered EEG activity consisted on sharp transients, which might represent non epileptic normal variants; Patient 2 typical IEDs consisted on spike and wave. Power LF=percentage of power in lower half of spatial frequency.

7.5.2 *Do similar scalp patterns correspond to similar cortical patterns?*

One would expect that for comparably looking scalp distributions, the underlying subdural patterns would also be similar. A pair of voltage maps was considered similar if their cross-correlation coefficient was significantly different than zero.

Figure 7.5 illustrates examples of two IEDs and two HFOs with similar scalp voltage maps for patient 7. For the IEDs (Figure 7.5.A), the pair of scalp voltage maps was similar (rxyScalp=0.96, $p<<0.01$) as well as the underlying pair of subdural voltage maps (rxySubdural=0.88, $p<<0.01$). In the case of the HFOs (Figure 7.5.B), the pair of scalp voltage maps was similar (rxyScalp=0.86, $p<<0.01$), even though the corresponding subdural voltage maps were different (rxySubdural=-0.19, p=0.11). Thus, different subdural voltage maps can result in similar scalp maps for scalp HFOs.

The percentage of similar voltage maps was computed by pooling all the pairwise comparisons together (cross-correlation between voltage maps statistically larger than zero, $p<0.01$, across all pairs of maps). It was equivalent for HFOs (58%) and for IEDs (56%). This means that for more than half of the pairs of events the scalp voltage maps were similar, regardless of whether they were IEDs or HFOs. However, the underlying subdural activity behaved differently for IEDs and HFOs. When computing this same similarity measure in the six patients with grids, 50.05% of the pairs of IEDs with similar scalp voltage maps had also similar subdural patterns (range across patients: 21.1-93.3%). On the contrary, only 14.6% of pairs of HFOs with similar scalp patterns had similar subdural patterns (range across patients: 0-25.8%). In other words, a particular scalp pattern may result from different cortical regions being active for scalp HFOs.

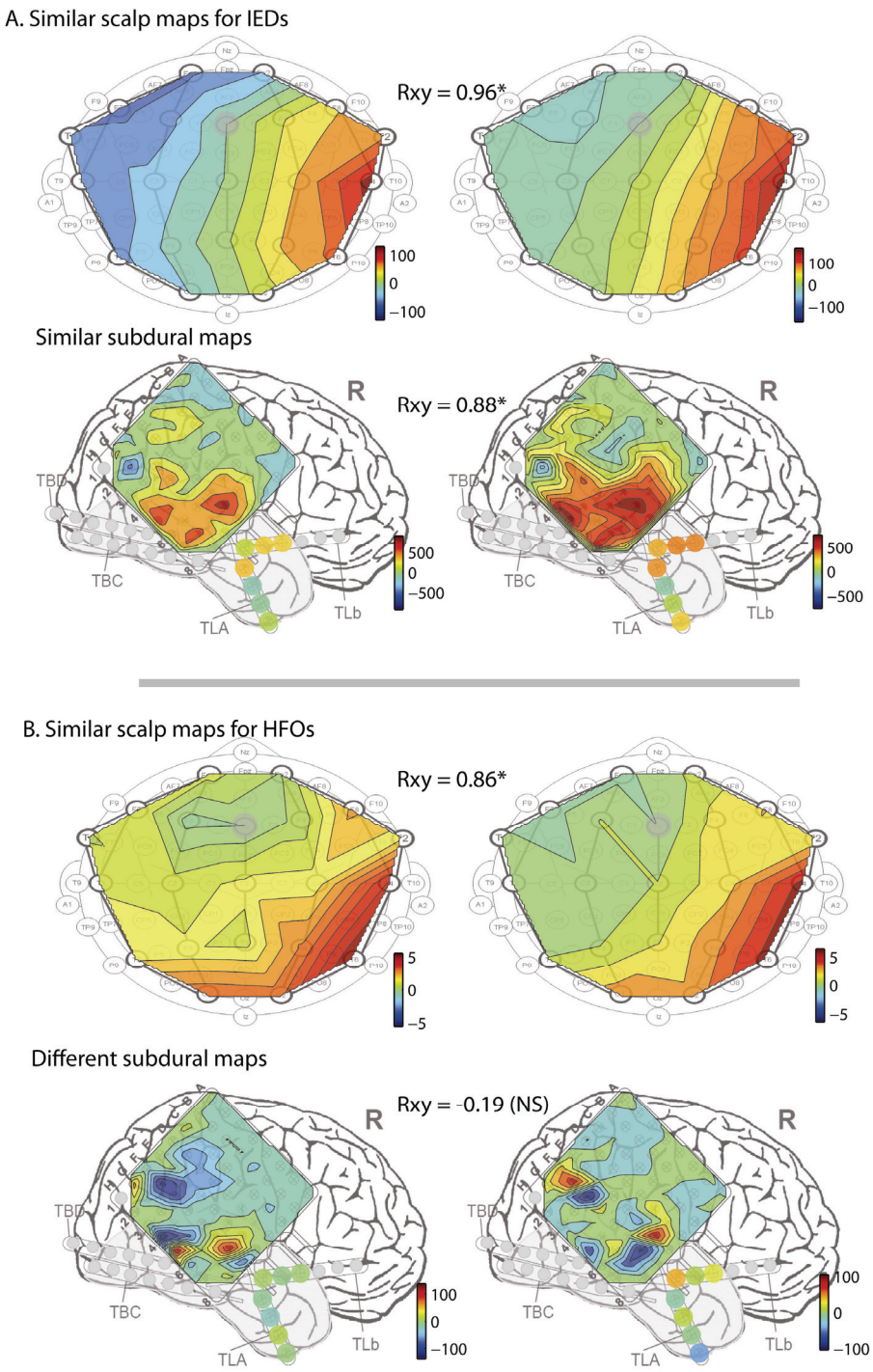

Figure 7.5. Similar pairs of HFO scalp patterns may correspond to distinct subdural patterns. The scalp distribution is similar for all events. On the subdural EEG, an extended region is activated for IEDs (A), while a focal region is activated for each HFO (B). Note that the spatial distribution is similar for individual IEDs, but differs for individual HFOs. Similarity between pairs of voltage maps is measured by the cross-correlation. rxy = cross-correlation; * indicates rxy significantly different than zero (pVal<0.01); NS=not significant.

In summary, even though a comparable percentage of similar pairwise scalp patterns are found for IEDs and HFOs; half of all the pairs of scalp IED patterns that were similar corresponded to similar subdural IED patterns; while only 1 in 7 of all the pairs of scalp HFO patterns that were similar corresponded to similar subdural patterns. These results are consistent with the idea that within a large epileptogenic area that could generate HFOs, these spontaneous events are actually generated by independent small regions.

7.5.3 *Averaged voltage maps*

Following the results of the previous sections, the validity of the first hypothesis that states that a large smooth cortical region must be active to observe events on the scalp is questionable. To further evaluate this, averaged maps of events with similar scalp topographies were studied. Under the first hypothesis, scalp voltage maps could be fully explained by subdural distributions and as a result, it would be expected that the underlying subdural maps would be enhanced when averaging voltage maps for events with similar scalp distributions.

This was the case for IEDs, for which a large spatial extent and large amplitude averaged subdural voltage map was obtained (Figure 7.6.A). Conversely, when averaging similar scalp maps of HFOs, the subdural maps cancelled each other, producing small amplitude averaged subdural maps (Figure 7.6.B). This is in line with the idea presented in the previous section that diverse underlying cortical focal activations could correspond to similar scalp HFOs.

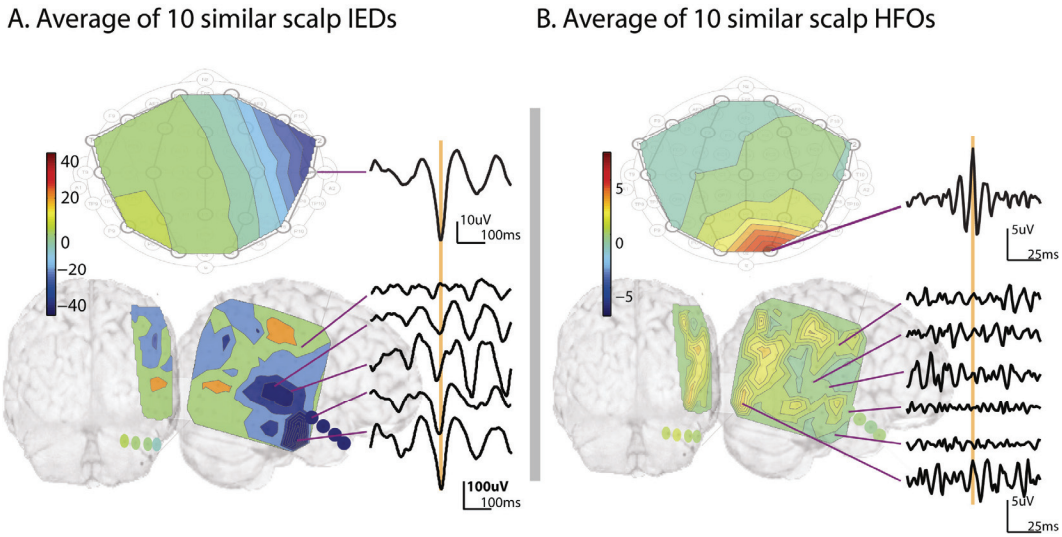

Figure 7.6. Averaged voltage maps in patient 1. A) When averaging 10 similar scalp IEDs, the simultaneous averaged subdural map shows a large active region with large amplitude. Since activity comes from similar extended regions, the average enhanced the common activity. B) When averaging 10 HFOs with similar scalp maps, the underlying subdural maps fails to show activity above noise level. Since activity comes from independent small-extent sources, averaging "*destroys*" the subdural maps, even though they are recorded as similar on the scalp. Same scale is used for averaged scalp and subdural maps.

7.5.4 *Phase Synchronization*

The PLV was significantly higher for the channels of interest than for the control channels (0.25+/-0.14; 0.17+/-0.09; p<<0.001; paired t-test). The low mean value for the channels of interest is likely due to many subdural channels not contributing to each scalp HFO. This is in line with the idea that for each event only a few subdural contacts are active. Indeed, when only considering the maximum PLV per event the mean across events was: 0.53+/-0.13 for channels of interest and 0.36+/-0.09 for control channels (Figure 7.7.A; p<<0.001; paired t-test). This maximum value represents the phase relation between the scalp channel and "the most related" subdural channel.

In this regard, an informative measure can be defined as the number of events for which the PLV was larger than the threshold of each patient. The global threshold was 0.48 (range across patients: 0.38-0.54). There was at least one PLV larger than the threshold in 69% of all events pooled together for the channels of interest; for the control channels this was the case in only 15% of the events. A

Wilcoxon test across patients showed that this difference was significant (Figure 7.7.B; $p<0.01$).

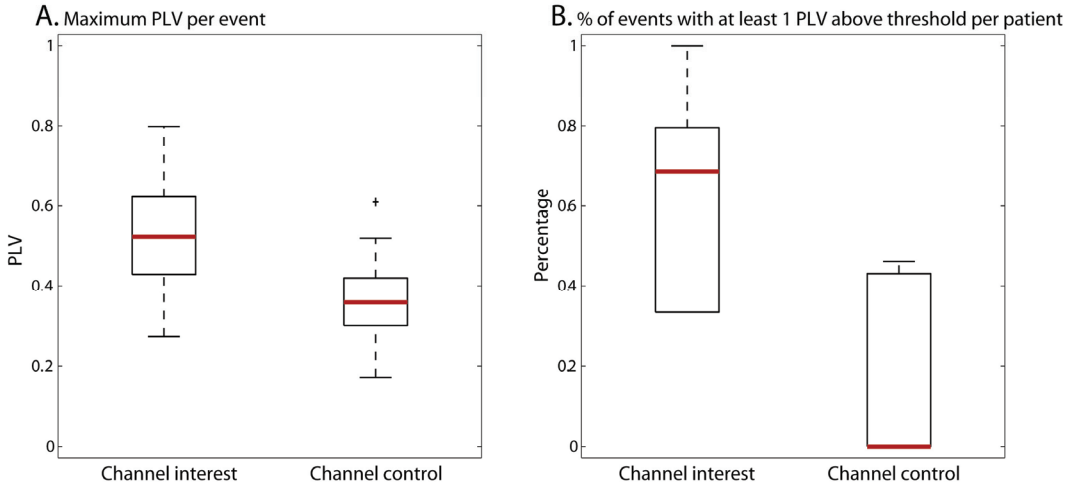

Figure 7.7. Phase synchronization. Boxplots of the maximum PLV per event (A) and percentage of events with at least one PLV larger than threshold per patient (B). The mean +/- std across maximum PLV per event for channels of interest was 0.53+/-0.13, while for control channels was 0.36+/-0.09 ($p<<0.001$; paired t-test). Median percentage of at least one PLV above threshold across patients for channels of interest was 69%, while for control channels was 0% ($p<0.01$; Wilcoxon test).

7.5.5 *Relation between subdural and scalp contacts using a linear model*

When simultaneously recording scalp and intracranial EEG, an implicit assumption is that the subdural contacts can see all the activity seen by the scalp. This implies that it is possible to predict the scalp voltage distribution based on the subdural recordings. From the previous sections we concluded that the generators of scalp HFOs are small. If these sources are smaller than the grid's inter-electrode distance, the previous assumption will not hold.

The linear model described in the Methods section could explain most of the IED events (82.7%, using a leave one out procedure) as measured by the cross correlation between the real voltage map on the scalp and the one estimated from the model (Table 7.2, Figure 7.8). This is in line with a large synchronously activated region, given that the main assumption of the model is that the subdural voltage distribution can fully explain the scalp distribution. On the other hand, the

model can only explain less than half (38%) of the scalp HFOs from subdural distributions (Table 7.2).

				%Correlated Voltage Maps	
Patient	Type Contacts	#HFOs	#IEDs	Leave1Out HFOs	Leave1Out IEDs
P1	8x8 Grid+strips	16	25	44%	96%
P2	4x8 Grid	1	25	---[a]	56%
P3	Strips	3	25	---[a]	36%
P4	8x8 Grid	13	25	8%	84%
P5	4x8 Grid(L) + strips(R)	16	25	75%	88%
P6	Strips	9	25	11%	96%
P7	8x8 Grid + strips	47	25	43%	100%
P9	4x8 Grid(L)+ strips(R)	7	25	0%	92%
P11	Strips	3	25	---[a]	96%
Average across patients		12.8	25	30% +/- SEM=29%	83% +/- SEM=22%
Percentage Correlated voltage maps				**38%**	**83%**
Rxy voltage maps				0.88 +/- 0.07	0.91 +/- 0.08

Table 7.2. Percentage of correlated voltage maps on the scalp explained by a linear model. [a]Only patients with more than 5 scalp HFOs were studied with the leave one out schema. Table is based on 25 scalp IEDs and all selected scalp HFOs per patient. Rxy=cross-correlation coefficient; L=Left; R=Right; SEM= standard error on the mean. $p<0.01$.

In the examples of the real and estimated voltage maps on the scalp the resemblance between voltage maps is remarkable for the IED (rxy=0.98, $p<<0.001$; Figure 7.8.A) and for one of the HFOs (rxy=0.94, $p<<0.001$; Figure 7.8.B). On the contrary for the second HFO, the model cannot estimate the real scalp HFO (rxy=-0.26, p=0.41; Figure 7.8.C).

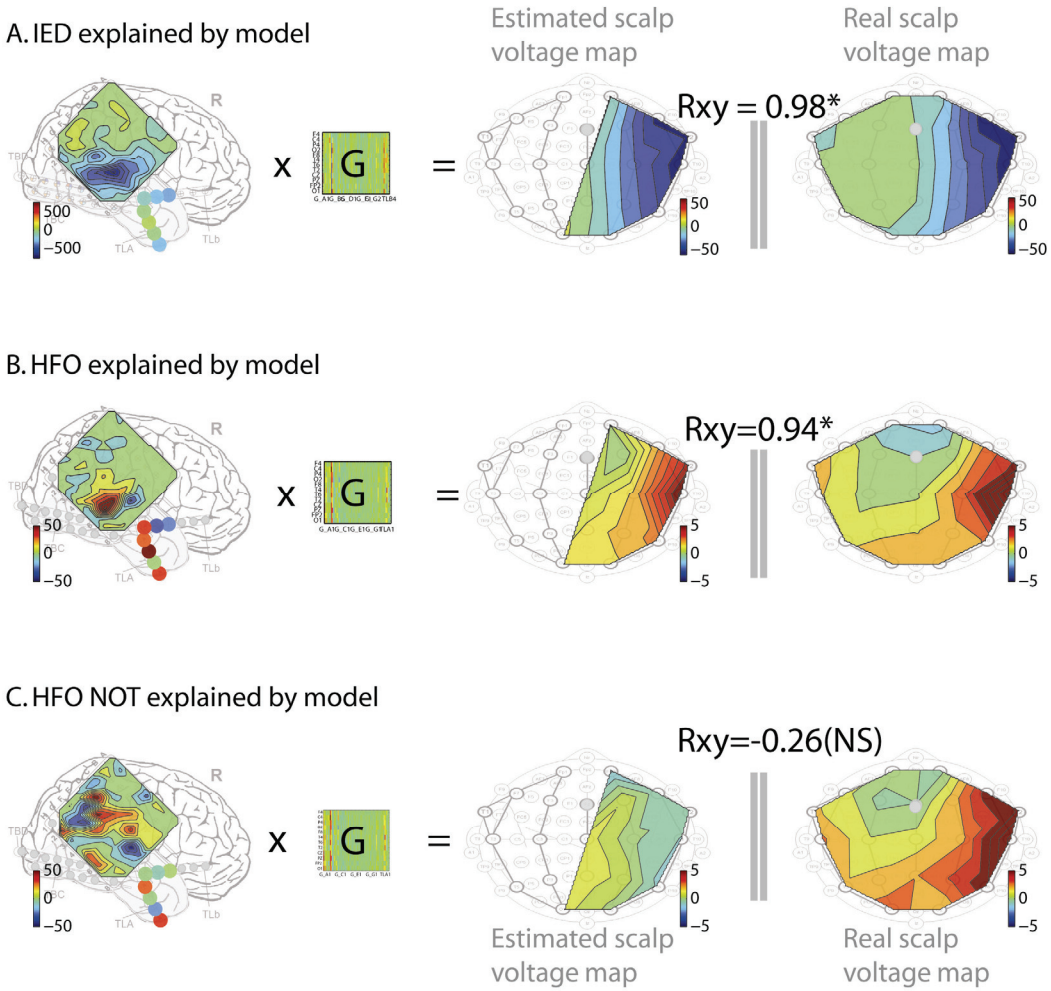

Figure 7.8. Linear Model. Example of one predicted scalp IED (A), one properly predicted scalp HFO (B) and one scalp HFO that could not be predicted from the underlying subdural activity (C). Matrix G is the model obtained with a leave one out procedure. Similarity between estimated and real scalp voltage maps is measured by the cross-correlation. rxy = cross-correlation; * indicates rxy significantly different than zero (pVal<0.01); NS=not significant.

Thus, the assumption that a subdural grid "sees" everything that is seen by the nearby scalp contacts is more valid for IEDs than for HFOs. The only explanation for the grid not seeing the same as the overlaying scalp contacts is that in some HFOs that are observed on the scalp, the underlying sources are too small and are not sampled correctly by subdural contacts separated by 1cm. In other words, we are spatially undersampling with the used subdural contacts.

7.5.6 *Simulation of scalp extent*

If activity from small cortical areas corresponds to scalp events, the spatial extent on the scalp may be small. In addition, HFO rates on scalp were much lower than rates for subdural HFOs. Thus, we are possibly spatially undersampling on the scalp (~5cm separation using the 10-20 system). On the other hand, the model could predict less than half of the scalp HFOs and the subdural maps show sometimes activity in only one electrode and not the adjacent ones. We are therefore likely undersampling on the grid as well (1cm separation). To illustrate the spatial extent on the scalp of focal sources, we simulated distributed sources of about $1cm^2$ on the cortical gyri.

Out of the 280 distributed sources of 1.21 +/- $0.19cm^2$ with intensity 5nA.m, 85% were visible on the grid with RMS amplitude larger than 30μV. Of these, 61% reached the scalp with RMS amplitude of at least 4μV, and could therefore be detected. However, given the small spatial extent of these events on the scalp, only 15% of the 145 sources visible on the scalp would be recorded with the 10-20 system, 27% with the 10-10 system, and 50% with 256 electrodes. The mean RMS amplitude was 5.25μV for all the sources observed on the scalp, 4.8μV for those recorded with 256 electrodes, 4.7μV for those recorded with the 10-10 system, and 5.1μV for those recorded with the 10-20 system.

Figure 7.9 shows examples of 2 sources of 5nA.m. One source, of 1.12 cm^2, is recorded with the 10-20 system, even though the spatial extent on the scalp is focal, since electrode O1 overlays this source. The second source of similar extent (1.55 cm^2) and identical intensity is not recorded because there is no electrode where the scalp voltage is above noise level. A denser scalp array would be necessary to record this source. The results of this simulation are not limited to HFOs, but represent any type of focal neuronal activity.

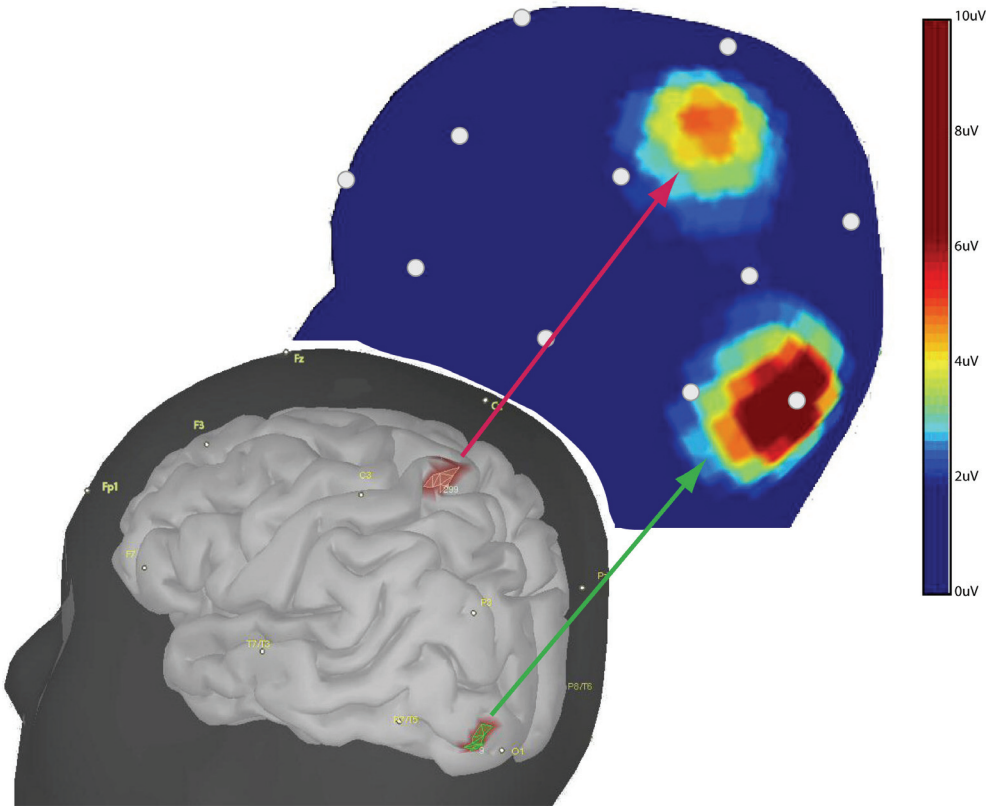

Figure 7.9. Example of 2 simulated focal sources and corresponding scalp spatial distribution. Green arrow indicates a source that is visible when placing electrodes based on the 10-20 system. Magenta arrow indicates a source that corresponds to a scalp activation of similar extent, but that will not be visible when using the 10-20 system for placement of scalp electrodes. Sources intensity=5nA.m. Noise level was considered as 2uV.

7.6 *Discussion*

In this study, we evaluated whether the traditional hypothesis that implies that a large cortical area being synchronously active is necessary to observe an HFO on the scalp or whether a focal event over a locally synchronized region is sufficient to observe an HFO on the scalp. We assessed these two hypotheses from different perspectives, using simultaneous scalp and intracranial recordings. We analyzed the spatial extent of the cortical sources by observing the spatial distribution of voltage maps on the surface of the brain at the time of scalp events (HFOs and IEDs). We studied whether similar scalp events corresponded to similar subdural patterns of activity. We related the observations on the subdural contacts to those on the scalp and studied whether the subdural voltage

distribution can estimate the scalp recordings. We simulated sources of small extent and measured their spatial distribution on the scalp.

If the first hypothesis holds, a large cortical activation with smooth boundaries would be expected. Similar cortical activity would correspond to similar scalp distributions, thus the average would be stronger than individual events, since noise would cancel out and activity (from similar large synchronous regions) would be enhanced. In addition, a linear model that relates subdural and scalp recordings would predict activity on the scalp based on subdural voltage. All this was the case for IEDs, in agreement with previous studies where this first hypothesis was proposed (Tao *et al.,* 2007).

For HFOs none of these conditions was observed. On the contrary, the spatial distribution on the cortical surface at the time of scalp HFOs was focal, consisting of one or a few dipolar configurations. Different subdural patterns were observed for similar scalp HFO patterns. Indeed, when averaging subdural maps of similar scalp patterns at the time of scalp HFOs, the subdural patterns cancelled each other. The assumption that a subdural grid "sees" everything that is being seen by the nearby scalp contacts holds for spikes but does not appear to hold for HFOs, for which the linear model cannot predict scalp activity based on the subdural voltage. Moreover, the phase synchronization between scalp HFOs and the underlying cortical activity was significantly larger than for the control channels located at a distance from the channels recording HFOs. These results point towards the validity of the second hypothesis: even though the generators of HFOs are small they can be observed on the scalp.

If activity from small cortical areas correlates with scalp events, the spatial extent on the scalp may also be smaller than expected. This and the much smaller rate of scalp HFOs compared to intracranial EEG, argues in favour of a possible spatial undersampling of scalp EEG. The fact that a linear model between the subdural contacts and the scalp could not explain the observations on the scalp together with the focality of the subdural maps for HFOs, seem to indicate that we

may be undersampling not only on the scalp, but also on the grid. The spatial undersampling was studied by simulating sources of small extent and by measuring their spatial distribution on the scalp. We found that with the 10-20 and 10-10 systems, we are likely undersampling such focal events.

7.6.1 *Small cortical extent and solid angle*

We showed, using different approaches, that a small active cortical region is sufficient to produce an HFO that is visible on the scalp. Furthermore, given the small size of the generator of HFOs, the scalp EEG could record similar looking potentials for events for which the closely located subdural contacts would see different activity.

This can be explained by the solid angle concept. As stated by Gloor: "The potential generated by a dipole layer in a volume conductor measured at any point within (or at the surface) of this conductor is proportional to the solid angle subtended by the dipole layer at the point of measurement" (Gloor 1985). Based on this concept, the difference in the percentage of similar pairs of voltage maps for subdural grids and the scalp for HFOs becomes clear; small cortical regions synchronously active can produce very different solid angles on the closely located grid but similar solid angles on the scalp.

The schematic in Figure 7.10 illustrates this concept. The amplitude recorded by each electrode depends on the amplitude of the source (which in the figure is the same for all sources) times the solid angle seen by the electrode (Figure 7.10.C & F). In the upper part of the figure, all grid electrodes see similarly the large source, while the small source is mainly recorded by the central grid electrode. This is depicted by the smooth spatial distribution for the large source and the focal spatial distribution for the small source in Figure 7.10.A as well as by the similar amplitude in all grid electrodes for the large source and the different amplitude at each electrode for the small source (Figure 7.10.C). On the scalp, the small source has a more focal spatial distribution than the large source (Figure 7.10.B), although this difference is not as large as for the grid. The lower

part of the figure illustrates the spatial distribution corresponding to two small sources. Since the size of the small sources is similar to the grid interelectrode spacing (~1cm), their location (given equivalent orientation and amplitude) defines which electrode (if any) has a large enough solid angle with the source (Figure 7.10.D & E). Source 1 (in red) forms a large angle from electrode 1, while source 2 (in orange) has a large angle from electrode 3 (Figure 7.10.D & F). The solid angle seen from each electrode is different for each source, because the grid is close to the sources. Both sources have similar angles from the scalp electrode (Figure 7.10.E & F). Thus, small-extent events may look different on the grid, but similar on the scalp. Moreover, given that the size of the source and the spacing between grid contacts is similar, an event could be recorded by a scalp electrode, but not by the underlying grid contact. In conclusion, the spatial sampling is adequate for large sources on the grid and on the scalp, but small events are undersampled on the scalp and on the grid.

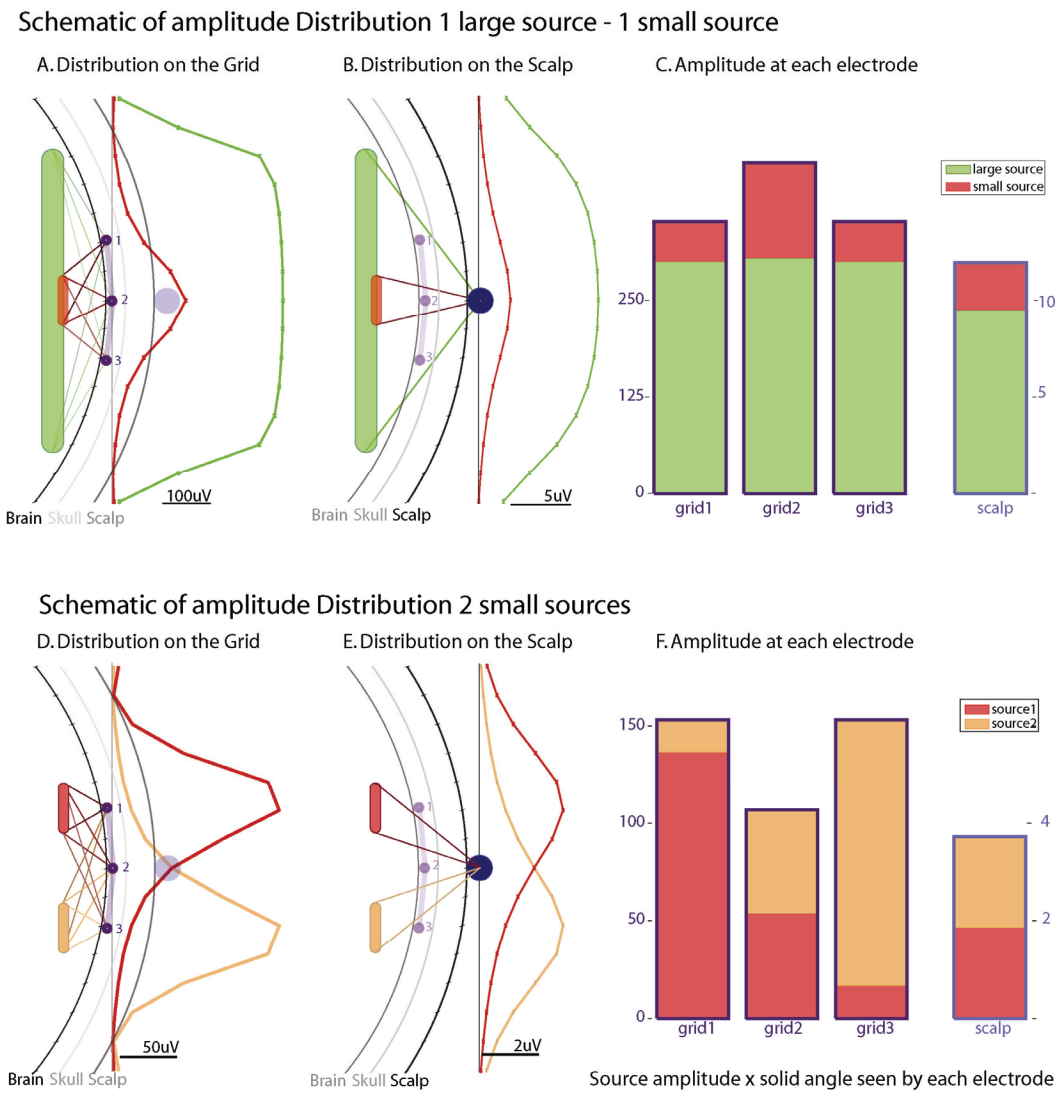

Figure 7.10. Schematic of similar scalp pattern but different subdural patterns explained by the solid angle. *Top*: A large active region that could correspond to an IED (green) is recorded by all subdural electrodes (purple; A) and by the scalp electrode (blue; B). All subdural contacts see a similar solid angle, resulting in similar amplitudes (C). The small source (red), that could represent an HFO, is recorded mainly by one subdural electrode (A) and by the scalp electrode (B). *Bottom*: Two small sources representing HFOs are similarly seen by the scalp electrode (E), but observed mainly by one subdural electrode each (D). Thus, these two sources would have comparably looking scalp topographies, but different subdural topographies. This figure was created in Matlab. The spatial distribution on the grid and on the scalp was computed by multiplying the source amplitude by the solid angles at locations separated by 5 degrees (indicated by lines at the surfaces). Sources amplitude= 100uV; skull to brain conductivity ratio 1/25; smearing effect was not considered; large source extent = 6cm; small sources extent = 1cm. Electrodes are depicted as half their real diameter to emphasize the point like assumption in the calculation of the solid angles.

7.6.2 *Noise Characteristics*

The conclusion that a large cortical extent is necessary to observe an event on the scalp was attained from unfiltered recordings (Hashiguchi *et al.,* 2007, Tao *et al.,* 2007), but there is no estimate for the spatial extent needed for high frequency (HF) bands. The noise characteristics at HF may be different from the noise characteristics of the unfiltered EEG.

It is important to properly define "*noise"* for each particular event of interest. For instance, when detecting spikes the noise is the EEG activity surrounding the spike, which could be composed of artefacts from outside of the head and physiological activity of brain origin. Thus, the signal to noise ratio would be the ratio between the amplitude of the spike (the signal) and the surrounding noise (i.e. activity that is not the one of interest). Considering this definition, a reason why it is possible to record small extent events at HF but not at low frequencies is that the noise level at HF is small. Since the EEG background is considered to decrease as one over the frequency (Buzsáki and Draguhn 2004), and because most spontaneous physiological activity occurs mainly at low frequencies, the noise level could be close to the amplifier noise floor at HF. In line with this, when measured in the arm during rest, the noise level reaches the amplifier level at about 30Hz (range across subjects: 10-100Hz; Huigen *et al.,* 2002). Our data was in agreement with low noise level at HF. In 1h filtered scalp EEG (80-300Hz), the RMS amplitude outside artefacts was 1.53 +/- 1.03μV. Given the low rate of HFOs this represents background noise. Comparably, the amplifier's noise floor was less than 1μV (as indicated by the manufacturer; IT med-EEG-System).

It is important to emphasize, that despite what it is sometimes explained in textbooks the conductivity of the skull is the same from 1Hz to 10kHz (Oostendorp *et al.,* 2000, Tang *et al.,* 2008). Therefore, IEDs and HFOs are equally attenuated before reaching the scalp.

Thus, since the noise level at HF is smaller than at low frequencies and since activity is equally attenuated at all frequencies of interest, the signal to noise ratio

at HF is large enough for small events to be detectable on the scalp. Indeed, a smaller noise level was found at HF resulting in comparable signal to noise ratio for IEDs, gamma, and ripple events at their respective frequency bands (von Ellenrieder *et al.,* 2012). Therefore, events generated by small regions, which have low amplitude on the scalp, may be below noise level in the EEG at low frequencies, but are visible when looking at HF.

7.6.3 *Undersampling on the scalp*

When assessing the number of electrodes needed to obtain accurate source localization of IEDs in the unfiltered EEG, there is increased accuracy up to 64 electrodes, but little is gained in using more (Lantz *et al.,* 2003), in particular at realistic (unfiltered) noise levels (Ryynanen *et al.,* 2004). However, in low noise environments, of about 1μV, a large number of electrodes would allow the accurate reconstruction of more sources (Ryynanen *et al.,* 2004). Our results are in agreement with this statement. Our simulations showed that focal sources of the estimated size of HFO generators (approximately $1cm^2$) corresponded to focal scalp patterns and that the number of sources recovered increased with an increased number of electrodes at 2μV noise level. Thus, the low rate of scalp HFOs observed in visual studies (Andrade-Valença *et al.,* 2011) is likely due, at least in part, to spatial undersampling of these focal events.

Interelectrode distance is about 6cm for the 10-20 system (21 electrodes), 3.3cm for the 10-10 system (64 electrodes), 1.6cm for 256 electrodes, and about 1.1cm for 512 electrodes (Ryynanen *et al.,* 2004). When recording simulated activity with 1.3 +/- 0.2cm interelectrode distance, 61% of the sources recorded by the grid were recorded at the scalp with amplitude at least double the noise level.

In cognitive neuroscience, thousands of trials can be averaged to observe HF activity non-invasively (Curio 2000). Even after averaging HF activity was not observed in all patients (e.g.: Ball *et al.,* 2008), while in a similar task HF activity was observed in all patients when recorded with intracranial electrodes (Miller *et*

al., 2007b). This inter-subject variability could be due to poor spatial sampling on the scalp, which improved with averaging in some but not all subjects. Since pathological HFOs are spontaneous events, they cannot be averaged and have to be identified individually. Given the small extent of the HFO sources and the need to detect individual HFOs, a large number of scalp contacts may therefore be necessary to systematically observe HFOs on the scalp. The need for high-density scalp electrodes might not be limited to the study of HFOs. A study on the usefulness of EEG source imaging for focus localization during pre surgical planning showed that it had a sensitivity of 84% with a specificity of 88% if a large number of electrodes (128-256) was used for the reconstruction (Brodbeck *et al.,* 2011).

7.6.4 *Undersampling on the subdural contacts*

We are likely undersampling not only on the scalp but also on the grid. For HFOs the subdural maps showed some activations that occurred only at 1 contact and the model could not predict scalp activity based on subdural activity. Thus, the grid might be sampling poorly events that are in the order of the 1cm of separation between contacts. These results are in agreement with the size of about $1mm^3$ observed for the generators of HFOs (Bragin *et al.,* 2002). Moreover, the optimal inter-electrode spacing to avoid undersampling and aliasing has been suggested to be 1.25mm (Freeman *et al.,* 2000).

Intracranial HFOs were sometimes recorded simultaneously at several electrodes, covering several square centimetres. It has been suggested that they correspond to simultaneously activated regions (Crepon *et al.,* 2010). In our data, oscillatory activity was observed on subdural contacts at the time of scalp HFOs. The different morphology of these subdural EEG activities (e.g. Figure 2.E; patient 2 in Figure 3.B) is likely explained by independent small regions generating independent HFOs within the same window of time. However, we did not study this systematically.

7.6.5 *Methodological considerations*

Skull holes alter the electrical signal recorded on the scalp (Heasman *et al.,* 2002). Burr holes produced during surgery produce a large localization error, particularly for radial dipoles below the hole and tangential dipoles in the edges of the hole (Bénar and Gotman 2002, Heasman *et al.,* 2002). When filling the burr holes with methacrylate, which is commonly done after depth electrode implantation, the localization error is reduced (Bénar and Gotman 2002). We believe that the influence of burr hole in our signal was minimal. In particular since in some subjects, scalp HFOs and IEDs were observed in more than a single scalp electrode and different events had different scalp distributions. Furthermore, scalp electrodes were placed following the 10-20 system as closely as possible, but avoiding being near holes or sutures. The electric field on top of the holes is the one mostly distorted, and this distortion rapidly falls with distance (Heasman *et al.,* 2002). Even if there was an effect of the holes, the effect should be similar for IEDs and HFOs and therefore all the comparisons made throughout this paper hold.

The subdural contacts were placed exclusively for clinical reasons. This implies that we can only infer from the area covered by the grid and strips, but there might be contribution from other not covered areas. Even though the coverage was limited, the comparison between IEDs and HFOs remains valid.

The analysed hour of EEG was selected during night to minimize the effect of artefacts and maximize the number of HFOs. Part of this hour was slow wave sleep, but the sleep stage was not consistent during the whole hour. This could have reduced the number of identified events (Bagshaw *et al.,* 2009). The strict procedure to discard possible artefacts probably additionally restricted the number of identified HFOs on the scalp. Indeed, the mean rate of scalp HFOs in this study was 0.21/min, which is smaller than a previous study (0.49/min in Andrade-Valença *et al.,* 2011).

In some of the examples, oscillatory activity could be observed in the subdural contacts extending beyond the seizure onset zone (e.g. Patient 1 in Figure 7.4.B). Even though HFO rates are higher in the seizure onset zone, HFOs are observed also in other regions (Jacobs *et al.,* 2009a, Urrestarazu *et al.,* 2007).

The attenuation effect of the silastic membrane holding the electrodes when using subdural grids does not seem to avoid the propagation of spikes (Tao *et al.,* 2007) and is probably small compared to skull impedance. Although the frequency characteristics of the silastic membrane are not known, if attenuation takes place it should have a similar effect on the background, thus maintaining the signal to noise ratio.

7.6.6 *Clinical implications*

The present study not only confirms that HFOs are visible on the scalp EEG but also provides insight into the characteristics of intracranial patterns that correspond to an HFO visible on the scalp. Our analyses point towards the need of higher spatial sampling in intracranial and scalp recordings to obtain consistent information on HFO distributions. This observation has been the subject of debate, but it is important for epileptologists, who would like to use HFOs as biomarkers. Recent technical developments allow the use of high-density arrays of electrodes on the scalp (Lantz *et al.,* 2003). Newly developed intracranial electrodes consist of an increasing number of recording sites, hybrid electrodes, and microarrays for single cell recording (Worrell *et al.,* 2012). A future challenge of clinical research would be to evaluate which combination of intracranial and scalp electrode density will be ideal to analyse HFOs in the clinical context.

Our results showed an application of combined scalp and intracranial EEG recordings. Scalp HFOs may be seen in this simultaneous approach and may help to overcome the spatial restriction of intracranial EEG. It was suggested that HFOs occurring outside the intracranially recording area might be the reason why some patients continued to have seizures after the majority of HFO generating brain areas were removed (Jacobs *et al.,* 2010b, Wu *et al.,* 2010). Thus, with the

methods described in this paper, it would be interesting to evaluate if scalp HFOs in regions other than the ones covered by intracranial electrodes may serve as a negative predictor for postsurgical seizure freedom.

Understanding that the possibility of recording HFOs non-invasively is mainly an issue of spatial sampling is important because it provides a direct link between HFOs recorded with intracranial electrodes and on the scalp. This opens the opportunity to use scalp HFOs as biomarkers for the localization of epileptic tissue as well as for measuring disease activity. Scalp HFOs could become a valuable tool in large patient populations. They might be useful to follow the direct and long-term effects of medication, to predict the development of epilepsy after an insult, and to help targeting intracranial implantation.

7.7 *Conclusion*

We found that the traditional hypothesis regarding the extent of cortex necessary for events to be visible on the scalp does not hold for HFOs. The spatial distribution on the cortical surface at the time of scalp HFOs was focal, consisting of one or a few activations with a dipolar pattern. Scalp HFOs with similar pairwise scalp distribution may correspond to distinct patterns of activation on a standard 1cm subdural grid. Finally, a linear model could predict less than half of the scalp HFOs from the subdural grid pattern. We conclude that these results are caused by undersampling these focal events on the scalp and on the grid. This study is the first step towards a better understanding of the spatial characteristics of the cortical HF signals and their repercussion on the necessary spatial sampling of subdural and scalp signals. We suggest that a dense array of scalp electrodes may be necessary to study scalp HFOs systematically. HFOs could become powerful biomarker of epileptogenicity even on the scalp EEG.

7.8 *Acknowledgements*

We thank Dr. Federico Melani for his help in the identification of interictal epileptiform discharges. We thank Francois Tadel and Dr. Sylvain Baillet for their

suggestions on how to implement brainstorm for our simulations. We are grateful to Dr. Matthias Dümpelmann for his help in obtaining the data. This project was founded in part by DAAD short-term scholarship, the Savoy Foundation, and grant MOP-102710 from the Canadian Institutes of Health Research.

7.9 *Appendix A*

7.9.1 *Linear model*

There is a linear relation between subdural contacts and scalp, since tissue in between (skull, scalp, dura) is purely resistive at the frequencies of interest. Thus, it is possible to create a linear model of the form

$$mScalp_{MxN} = G_{MxK}\ x\ mIEEG_{KxN}\ (+error) \qquad \textbf{Equation 7.2}$$

or in matrix form (ignoring the error term)

$$\begin{bmatrix} sScalp_{Ch1}^{HFO1} & \dots & sScalp_{Ch1}^{HFON} \\ \dots & \ddots & \vdots \\ sScalp_{ChM}^{HFO1} & \dots & sScalp_{ChM}^{HFON} \end{bmatrix} = G_{MxK} \begin{bmatrix} sIEEG_{Ch1}^{HFO1} & \dots & sIEEG_{Ch1}^{HFON} \\ \dots & \ddots & \vdots \\ sIEEG_{ChK}^{HFO1} & \dots & sIEEG_{ChK}^{HFON} \end{bmatrix}$$

where mScalp is an MxN matrix containing the concatenated scalp EEG signal ($sScalp_{Chi}^{HFOi}$); mIEEG is a KxN matrix containing the concatenated intracranial EEG signal at the time of the scalp events ($sIEEG_{ChM}^{HFO1}$); and G_{MxK} is the forward model to estimate. M is the number of scalp channels; K is the number of subdural channels; and N is the number of scalp events.

Assuming that the noise is Gaussian the matrix G_{MxK} can be obtained from the training set by

$$G_{MxK} = (mIEEG_{train}^{'}\ x\ mIEEG_{train})^{+}\ x\ mIEEG_{train}^{'}\ x\ mScalp_{train} \qquad \textbf{Equation 7.3}$$

where *train* are the training events; ' is the transpose operator; $^{+}$ is the inverse of the matrix (pseudo inverse since these are non-square matrices). G_{MxK} is estimated for all but one event at each run. We estimated the matrix G_{MxK} using

the backslash operator in Matlab which provides the least square solution. At each run the estimated $mScalp_{test}$ event was obtained as

$$\boldsymbol{mScalp_{test} = G_{MxK}\, x\, mIEEG_{test}} \qquad \textbf{Equation 7.4}$$

This procedure was repeated for all events in the leave one out schema.

7.10 *Significance*

This manuscript showed that even though the generators of HFOs cover a small cortical surface, they can be observed on the scalp, with low amplitude and in a very focal region. This is a first step towards a better understanding of the spatial characteristics of these cortical high frequency signals and the repercussion of these characteristics on the spatial sampling of subdural and scalp signals necessary to record HFOs. A dense distribution of scalp electrodes may be necessary to study scalp HFOs systematically and for the future clinical use of scalp HFOs as biomarkers of epilepsy.

Chapter 8. *Conclusions and future directions*

8.1 *Summary of findings*

The objective of this thesis was the detection and analysis of HFOs to improve their systematic study and to advance towards their clinical application as a biomarker of epileptogenic tissue. In this regards, an essential methodological challenge was the automatic detection of these sporadic events. It was also important to ensure stable detections and to assess the minimum duration of interictal EEG needed to obtain reliable information. In the case of non-invasively recorded HFOs, a fundamental question was to understand how is it possible to see these small events on the scalp. These challenges had to be addressed to make progress towards the clinical application of HFOs and they were the focus of this thesis.

Visual marking provided a good understanding of the relation of HFOs with epilepsy (reviewed in Jacobs *et al.,* 2012, Zijlmans *et al.,* 2012) and is considered the gold standard. But it is highly time consuming and subjectivity is inevitable. A procedure to systematize the detection of HFOs was developed and presented in Chapter 5 (Zelmann *et al.,* 2009b). This procedure is routinely being used when identifying interictal HFOs, to ensure consistency among reviewers and to evaluate stability in the detections. This study was the first to evaluate the minimum duration needed to obtain consistent information when marking the EEG. We showed that analyzing 5min of interictal EEG provided the same information as longer intervals.

For the systematic study of HFOs and to promote their clinical application, automatic detection is necessary. An automatic detector of intracranial HFOs was presented in Chapter 6 (Zelmann *et al.,* 2010, Zelmann *et al.,* 2012). This detector consists of a baseline detector (i.e. segments without oscillatory components); a

detector of HFOs in channels where there are baseline sections free of oscillatory activity; and a detector of HFOs in channels where the baseline is not clear (e.g. very active channels). The MNI detector provides an original approach in detecting HFOs using a statistical threshold obtained from the detected baseline, thus incorporating local information. It is the first detector to explicitly consider channels with continuous HF oscillatory activity, first described in Mari et al. (2012). These features improved performance for the intracranial detection of HFOs.

Existing detectors have been developed with different implicit definitions of what to detect as an HFO. They were developed for different frequency bands (above 200Hz, (Crepon *et al.,* 2010),gamma band (Gardner *et al.,* 2007)), different brain regions (e.g. only mesial temporal (Staba *et al.,* 2002)), and diverse electrode sizes (microelectrodes in (Staba *et al.,* 2002), micro and clinical macro-electrodes in (Worrell *et al.,* 2008)), small clinical macroelectrodes (Zelmann *et al.,* 2010, Zelmann *et al.,* 2012). When optimized for a particular type of data (EEG recorded with small clinical macroelectrodes, band passed filtered between 80-450Hz) all detectors performed similarly for channels in which HFOs are rare events. In very active channels or in channels with continuous HF oscillatory activity, the MNI detector outperformed the others. Comparing the detectors in a single dataset was important not only to analyze their performance, but also to raise awareness of the danger of using a detector "out of the box" and to stress the issues involved in validation (Zelmann *et al.,* 2012). In Chapter 7 (Zelmann et al., submitted), the MNI detector was used to detect possible scalp HFOs that were then validated by an expert reviewer. We used a semi-automatic approach to obtain good accuracy with reduced human intervention.

The discovery of HFOs on the scalp was unexpected. Studies on spikes and seizures showed that a large cortical area is needed to observe them on the scalp (Hashiguchi *et al.,* 2007, Tao *et al.,* 2007). Based on this observation, given the small size of the generators of HFOs as assessed intracranially, and considering the high resistivity of the skull, most research on HFOs has been done with

invasive recordings. In order to move towards the systematic study of HFOs on the scalp a fundamental step was the study of the underlying cortical activity at the time of scalp HFOs. In other words, it was important to understand how is it possible that these small events are visible on the scalp. Analyzing simultaneous recordings of scalp and intracranial EEG at the time of scalp HFOs, we showed that the underlying activity was focal, sometimes less than one square centimetre (Chapter 7; Zelmann et al., submitted). Within a large region that could produce HFOs, a small region seems to generate each event. Even though the generators are small they can be observed on the scalp, with low amplitude and in a very focal region. We showed that the traditional 10-20 or 10-10 electrode systems cannot consistently spatially sample HFOs on the scalp. Grids, which usually have an inter-electrode distance of about 1cm, also do not seem appropriate to sample HFOs on the surface of the brain. The much lower rate of HFOs on the scalp (Andrade-Valença *et al.,* 2011) than intracranially can be explained in part by spatial undersampling. A dense distribution of scalp electrodes with at least 256 electrodes seems therefore necessary to fully spatially sample HFOs on the scalp.

8.2 *Limitations*

8.2.1 *General limitations when studying HFOs*

Some limitations apply to all studies on HFOs, such as the limited spatial sampling. Since intracranial recordings are limited to the location where the electrodes are, it is only possible to infer the importance of a region (e.g. in terms of epileptogenicity) if it is in the area covered by grids and strips or around depth contacts. In other words, it is impossible to know if there is relevant activity originating from other not covered areas.

Another general limitation involves the large amount of recorded data. Acquiring a large number of channels at high temporal sampling rates during several days results in large datasets. The technology to allow large data transfer and storage is available and should not be a limiting a factor any longer.

Analyzing, summarizing, and properly displaying large amount of information are challenging aspects and should be addressed. Methods to visualize and summarize results are being developed. For instance, visualizing HF power in subdural grids during seizures (Akiyama *et al.,* 2011a) and cognitive paradigms (Lachaux *et al.,* 2007) have been proposed. For depth electrodes, a method to map the SOZ to anatomical images has been described (David *et al.,* 2011).

Analysis of large datasets requires automatic detectors as the one presented in Chapter 6. HFOs are spontaneous small amplitude events that in most channels occur only rarely. Thus, HFOs must be individually detected. The EEG is non-stationary, fluctuating with brain state (e.g. sleep stage), and only during short intervals it can be considered quasi-stationary. Low signal to noise ratio and variability in background activity make the detection of HFOs challenging during long intervals. Incorporating local baseline information (as presented in Chapter 6) improves performance in very active channels and may be a good strategy to use over long periods. Evaluating stability in long intervals, with the procedure presented in Chapter 5, could also be important. This remains to be studied.

HFOs were first recorded with microelectrodes in mesial temporal regions (Bragin *et al.,* 1999a, Bragin *et al.,* 1999b). The possibility of a clinical use became real when HFOs were also recorded with clinical macroelectrodes in mesial temporal and neocortical regions (Jirsch *et al.,* 2006). Although HFOs recorded with micro and macroelectrode seem related to epileptogenic tissue, the same events are not necessarily being recorded. Diverse mechanisms could generate HFOs (Jefferys *et al.,* 2012), and the underlying mechanisms of HFOs recorded with such different sizes could be different. When simultaneously recording HFOs with micro and macroelectrodes, the frequency distribution was different (Worrell *et al.,* 2008). Within similar sizes no difference in rate or peak frequency was observed (Châtillon *et al.,* 2011). Further studies on the characteristics of HFOs recorded simultaneously with different electrode dimensions might provide insight into whether the same or different events are

recorded by different types of electrodes and which contact size is the best to record pathological HFOs.

As highlighted in Chapter 6, there is no consensus across groups on what to detect as an HFO. As a result, published detectors were optimized using diverse filter settings, HFO duration, and statistical relation to background. Details regarding each detector as well as a comparison in the same dataset were provided in Chapter 6 (Zelmann *et al.,* 2012). When comparing results from different centers, it is important to take into account not only the difference in the optimization of the detectors, but also the electrode size, the number and distribution of the contacts, the sampling rate and filters, and the quality of the data. This situation is not unique to HFOs but applies to any study based on EEG. Until a unique general definition is established for HFOs, it is important not to use a detector "out of the box" because what is valid in one center would probably not be valid for another place. The detector of choice should be trained and validated for a dataset with characteristics similar to the dataset of interest in order to obtain good performance (Chapter 6, Zelmann *et al.,* 2012).

8.2.2 *Specific limitations of the presented studies*

As a running definition for the detection of HFOs the following has been proposed: at least four oscillations of sinusoidal like morphology in the filtered EEG (above 80 Hz) with energy larger than the 95 percentile of the surrounding background (Worrell *et al.,* 2012). This is a first step towards standardization, but this definition is only marginally helpful, since it is fuzzy and therefore subject to broad interpretation on what should be detected as an HFO. The studies presented in this thesis were limited by this definition. The visual labeling studied in Chapter 5, the MNI detector presented in Chapter 6, and the scalp HFOs identified in Chapter 7 were based on it. This definition is likely to evolve as better characterization of HFOs and differentiation between physiological and pathological HFOs is achieved. As the definition of HFO is refined, detectors should be adapted accordingly. Standardization is fundamental for the

development of robust automatic detectors and comparison of studies across centers, and should be pursued.

HFO rates are higher when recorded in mesial temporal than in neocortical structures. In line with this, the hippocampus is particularly prone to develop seizures. Physiological HFOs might be inherently different in different regions. Channels with continuous HF activity are more common in mesial temporal and occipital regions than in other regions (Melani *et al.,* in press). However, the detector presented in Chapter 6, detects HFOs in all brain regions using the same threshold. Although training uses channels uniformly distributed from all locations, a unique threshold is obtained. Further research might show whether different regions should be considered separately.

Given the lack of a formal definition of HFO, the validation of automatic detectors is not trivial. In order to validate the detections a "gold standard" is needed. As in the validation of other electrophysiological signals, human expert's detections can be considered as the gold standard. But variability among reviewers has to be considered. In this regard, a possibility is to consider more than 1 reviewer (as in (Gardner *et al.,* 2007); (Chapter 6, Zelmann *et al.,* 2010)), although agreement between reviewers can be poor (Gardner *et al.,* 2007). To obtain a reliable gold standard, it is important to control for inter-reviewer reliability and for consistency in the markings (as presented in Chapter 5; Zelmann *et al.,* 2009b). Ensuring small inter-reviewer variability has the advantage of obtaining uniform labeling of events. For instance, before implementing this procedure an event could be identified as a single long HFO by one reviewer while labeled as two short events by others. However, the flip side of the coin is that it might be fruitful to explore different definitions before a firm definition is accepted.

In any case, the ultimate validation will be given by the usefulness of the detections in terms of relation to the epileptogenic regions or cognitive function location. To date, the goal (as presented in Chapter 6) is to obtain the same

conclusions by the automatic methods as by the human experts. This selection of gold standard is logical and it is commonly utilized in studies based on EEG. However, this choice limits what is considered as "good" HFOs to those events that can be observed by the human reviewer, restricting the usefulness of automatic detectors to what is already known. Automatic detectors might identify events not clear to the human eye (e.g. buried in noise) and could therefore provide interesting results independently of human interpretation.

All presented studies were limited by the selection of recordings performed during slow wave sleep. Given that the rate of HFOs is the highest during this sleep stage (Bagshaw *et al.,* 2009, Staba *et al.,* 2004) we chose this stage for the visual and automatic identification of events. However, the performance of the automatic detector was not evaluated at other stages nor was the assessment of a minimum duration of EEG that must interpreted to obtain reliable results. Thus, the obtained results cannot be directly generalized. The parameters of the automatic detector are likely to be different at different stages and longer intervals might be needed to provide stable information during wakefulness. The automatic detector presented in Chapter 6 was also limited to recordings with small clinical macroelectrodes. Its performance might be different if optimized and implemented in recordings with microelectrodes.

The study presented in Chapter 7 was limited by signal quality. When recording simultaneous scalp and intracranial EEG, scalp electrodes are placed and glued at the end of the surgical intervention. Since they are not re-glued afterwards, the EEG signal recorded on the scalp degrades over time. To minimize this limitation, we selected the first available night with scalp electrodes (Zelmann *et al.,* submitted). But even with this criterion, this scalp EEG was more noisy than normal scalp EEG recordings. Subdermal electrodes remain stable during the days of the recordings (Jacobs *et al.,* 2010a). Simultaneous intracranial and subdermal recordings have not been studied, but they are likely to provide interesting conclusions.

8.3 *Future directions*

The projects presented in this thesis advanced several methodological aspects for the systematic study of HFOs, opening also new venues for research. In this section new directions of research are proposed.

8.3.1 *Improving the identification of HFOs*

We showed that analyzing HFO rates during 5min provided the same information as longer intervals, and provided a procedure to evaluate it (Chapter 5; Zelmann *et al.,* 2009b). Given the relation of interictal HFOs with epileptic tissue, this suggests that shorter implantation periods might be sufficient to delineate the epileptogenic zone.

Intraoperative EEG recordings are sometimes performed (Wu *et al.,* 2010), but time is always a limitation in the operating room. Since short intervals seem sufficient to obtain relevant information, HFOs might provide the necessary specificity to increase accuracy in the delineation of the area to resect during surgery. Adapting the procedure presented in Chapter 5 could ensure stability in the intraoperative identification of HFOs.

The rate of HFOs in a channel seems a reliable marker of underlying epileptogenic tissue and it has been the most commonly used measure. Apart from considering the raw rate of HFOs, extensions to this measure or other measures might result the most appropriate to characterize HFOs. For instance, in Chapter 5 we presented an extension to the raw measure of rates, the ranking of the channels with respect to the rates. This measure was used also in the comparison of automatic detections with the gold standard, since the relative number of detected HFOs in each channel of a patient is more important than the total number of detections. This measure was also adapted to compare the ranking of channels during interictal, pre-ictal, and ictal periods. It was shown that HFOs remain more confined than spikes when comparing interictal and ictal periods (Zijlmans *et al.,* 2011). This measure could also be adapted, for instance, to compare the ranking of channels when recording simultaneously with micro and macroelectrode. As

examples of other measures, a combination of entropy and power in HF band could differentiate between pre-ictal and interictal periods (Gadhoumi *et al.,* 2012). Their variability at different times (e.g. interictal vs. pre-ictal vs. ictal) could be related to the intrinsic epileptogenicity of the tissue. The ranking of channels was developed for rates (Zelmann *et al.,* 2009b), but any feature could be used in the cost matrix.

HFOs can occur at the same time or independently of spikes (Urrestarazu *et al.,* 2007). Separating between sharp spikes, HFOs riding on spikes, and HFOs alone could be important. Interesting features to differentiate among them might be related to patterns in the time-frequency plane. For instance, a pattern consisting of lines of spectra would correspond to spikes, while islands would correspond to HFOs. Apart from the morphology of the patterns, features, such as the power in an island around the main peak, the time-frequency location of a peak, and the power at that peak could be extracted. In particular, creating these maps with discrete wavelets could help in the quantification of the differences and the development of classifiers.

Physiological and pathological HFOs cannot be distinguished at this point. Since HFOs seem a good marker of epileptogenic tissue, a reasonable assumption is that epileptic tissue produces such high rates of HFOs that even if some physiological HFOs occur they are minimal comparing with the number of pathological HFOs. In line with this, a study relating memory performance with HFOs showed that the majority of HFOs recorded with macroelectrodes seemed pathological and not linked to memory function (Jacobs *et al.,* 2011a). Nevertheless, the systematic differentiation between physiological and pathological HFOs is important from research and clinical application perspectives. Frequency is not sufficient to distinguish between them (Engel *et al.,* 2009). Other measures, such as power, entropy, temporal distribution, and cross-frequency coupling could become useful features to discriminate between physiological and pathological HFOs. For instance, physiological HFOs in the occipital lobe and pathological HFOs in epileptogenic regions of the same patient

had similar morphology, but differ in the coupling with delta oscillations (Nagasawa *et al.,* 2012). This could be a factor to differentiate between physiological and pathological HFOs or it might reflect an intrinsic characteristic of certain brain location. Further studies are needed to determine which measure is the most informative of the relation of HFOs with the epileptogenic region.

8.3.2 *Automatic detection of HFOs*

Automatic detectors of HFOs are usually designed to detect as many events as possible at the cost of a large number of false detections. For an automatic detector to be used clinically, these false positives must be discarded. To differentiate HFOs from artefacts, a possible post-processing step is to automatically classify the detections (Blanco *et al.,* 2010, von Ellenrieder *et al.,* 2012). Another common approach, employed in Chapter 7 and by others (e.g. Crepon *et al.,* 2010), is to implement a semi-automatic detector in which experienced reviewers performed visual validation. Even though expert intervention is required, their time is greatly reduced compared to a full visual analysis. Fully automatic detectors are ideal and could achieve labeling of massive datasets, but high sensitivity and high specificity is required. Moving in this direction, an interesting approach would be an adaptive system. A supervised approach could be used to first optimize the parameters on a particular type of data. Then, the detector could be run for a particular dataset. After detecting possible events with a high sensitivity low specificity detector, clustering could be implemented to remove artefacts, and the remaining events validated by an expert reviewer. An adaptive approach could allow learning from preceding detections, to gradually reduce the need of expert validation. In this way, excellent performance while significantly reducing human intervention can be achieved.

Another approach within a supervised framework is a pattern-matching detector. In this schema, a few HFOs and baselines per channel are used for training (e.g. the first minute or the first N events) and the automatic detector is run thereafter. This could result in a more specific detector, but probably with lower sensitivity to small or less common events.

Most automatic detectors have been developed for intracranial electrodes. The principles are similar for the non-invasive detection of HFOs, and existing detectors could be used (as in Chapter 7). However, to obtain robust detections, automatic detectors must be tailored to the identification of events on the scalp. Only one detector has been developed specifically for scalp HFOs (von Ellenrieder *et al.,* 2012). Incorporating local baseline information improved performance in intracranial data (Zelmann *et al.,* 2012) and could be helpful on the scalp.

HFOs could help delineating the area to resect during a surgical procedure (Wu *et al.,* 2010). For an automatic detector to be useful in the operating room data should be processed in almost real-time and new ways of visualizing the data and summarizing the analysis should be developed. For instance, methods developed for 3D visualization of intracranial contacts overlaying on MRI images (e.g. LaViolette *et al.,* 2011) could be adapted to display HFO rates.

Automatic detectors have been developed at different centers with different recording equipment, electrode size, noise characteristics, and implicit definitions. Evaluating diverse detectors in the same dataset highlighted the danger of using standard configurations without validation (Zelmann *et al.,* 2012). For the clinical acceptance of automatic detectors of HFOs, multicentre studies in which data from various centers is used to evaluate a detector are necessary. In addition, integrating automatic detection and appropriately summarizing the analysis (e.g. indicating the ranking of channels with respect to rates) into clinical software could be valuable.

8.3.3 *Non-invasive HFOs*

HFOs can be recorded non-invasively with a traditional electrode placement but with low rates (Andrade-Valença *et al.,* 2011). We explained how, even though HFOs are events of small spatial extent, they could be recorded non-invasively, and that to consistently record HFOs dense electrode arrays seem necessary. This opens the possibility to systematically study HFOs on the scalp.

We studied the cortical correlates at the time of the peak of scalp HFOs. An interesting next step is the analysis of scalp activity at the time of intracranial HFOs. A source localization method for oscillations has recently been developed (Lina *et al.,* 2012). Its application to scalp HFOs could provide interesting information.

Understanding that the possibility of recording HFOs non-invasively is in part an issue of spatial sampling is important because it provides a direct link between HFOs recorded intracranially and on the scalp. In other words, there is no special characteristic of the HFOs observed on the scalp; they are not exceptionally spatially extended. Amplitude, location, and orientation determine whether an HFO is visible on the scalp or not. Understanding this spatial sampling limitation may allow a different perspective in cognitive and clinical studies. This opens the possibility to further study the clinical relevance of HFOs on the scalp.

Scalp HFOs could be a valuable tool in large patient population. Scalp HFOs were more specific to the SOZ than spikes (Andrade-Valença *et al.,* 2011). Since intracranial HFOs vary with medication similarly to seizures (Zijlmans *et al.,* 2009b), scalp HFOs might be useful to follow the effect of medication. In animal models, HFOs appeared in rats that later developed epilepsy (Bragin *et al.,* 2004). If the same happens in humans, scalp HFOs could predict the development of epilepsy after a first insult. Not removing regions that generate high rate of intracranial HFOs was associated with poor surgical outcome (Jacobs *et al.,* 2010b); therefore recording of widespread scalp HFOs could be related to bad surgical prognosis. HFOs were evoked by single pulse stimulations (van 't Klooster *et al.,* 2011); reactivity of scalp HFOs to photic stimulation, hyperventilation, or transcranial magnetic stimulation could be investigated. Intracranial HFOs have been observed in lesional (Jacobs *et al.,* 2009a, Staba *et al.,* 2007) and non-lesional (Andrade-Valença *et al.,* 2012) patients and have been recorded in temporal (Bragin *et al.,* 1999b) and neocortical regions (Urrestarazu *et al.,* 2007). Since scalp HFOs could be analyzed as part of a routine EEG investigation a large variety of focal and generalized epileptic syndromes could be

studied. Scalp HFOs could also help targeting intracranial implantation. Subsequent to the understanding that even though the generators of HFOs are small they can be recorded on the scalp (Chapter 7; Zelmann *et al.,* submitted), these directions are likely going to be thoroughly investigated in the near future.

8.4 *Conclusions*

The work presented in this thesis addressed challenges that needed to be solved for the systematic study of HFOs and to propel the clinical utilization of HFOs as biomarkers of tissue capable of producing seizures. A procedure to assess stability in the detections allows to systematize the study of HFOs. The developed automatic detector would likely help advancing towards the clinical application of HFOs. The analysis of scalp HFOs showed that with better spatial sampling HFOs could be thoroughly studied non-invasively. These scientific and methodological advances are important steps towards the incorporation of HFOs as a clinical biomarker of epileptogenic tissue. Hopefully, in the near future, it will become regular clinical practice to evaluate the presence of HFOs during the pre-surgical intracranial evaluation and during routine scalp EEG investigation.

References

Acar ZA, Makeig S. (2010) Neuroelectromagnetic forward head modeling toolbox. *J Neurosci Methods* 190:258-270.

Adrian ED, Matthews BH. (1934) The interpretation of potential waves in the cortex. *J Physiol* 81:440-471.

Aghakhani Y, Kinay D, Gotman J, Soualmi L, Andermann F, Olivier A, Dubeau F. (2005) The role of periventricular nodular heterotopia in epileptogenesis. *Brain* 128:641-651.

Akhtari M, Bryant HC, Mamelak AN, Flynn ER, Heller L, Shih JJ, Mandelkern M, Matlachov A, Ranken DM, Best ED, DiMauro MA, Lee RR, Sutherling WW. (2002) Conductivities of three-layer live human skull. *Brain Topogr* 14:151-167.

Akiyama T, Chan DW, Go CY, Ochi A, Elliott IM, Donner EJ, Weiss SK, Snead OC, 3rd, Rutka JT, Drake JM, Otsubo H. (2011a) Topographic movie of intracranial ictal high-frequency oscillations with seizure semiology: epileptic network in Jacksonian seizures. *Epilepsia* 52:75-83.

Akiyama T, McCoy B, Go CY, Ochi A, Elliott IM, Akiyama M, Donner EJ, Weiss SK, Snead OC, 3rd, Rutka JT, Drake JM, Otsubo H. (2011b) Focal resection of fast ripples on extraoperative intracranial EEG improves seizure outcome in pediatric epilepsy. *Epilepsia* 52:1802-1811.

Akiyama T, Otsubo H, Ochi A, Ishiguro T, Kadokura G, Ramachandrannair R, Weiss SK, Rutka JT, Carter Snead O, 3rd. (2005) Focal cortical high-frequency oscillations trigger epileptic spasms: confirmation by digital video subdural EEG. *Clin Neurophysiol* 116:2819-2825.

Alarcon G, Guy CN, Binnie CD, Walker SR, Elwes RD, Polkey CE. (1994) Intracerebral propagation of interictal activity in partial epilepsy: implications for source localisation. *J Neurol Neurosurg Psychiatry* 57:435-449.

Allen PJ, Fish DR, Smith SJ. (1992) Very high-frequency rhythmic activity during SEEG suppression in frontal lobe epilepsy. *Electroencephalogr Clin Neurophysiol* 82:155-159.

Andrade-Valença L, Mari F, Jacobs J, Zijlmans M, Olivier A, Gotman J, Dubeau F. (2012) Interictal high frequency oscillations (HFOs) in patients with focal epilepsy and normal MRI. *Clin Neurophysiol* 123:100-105.

Andrade-Valença LP, Dubeau F, Mari F, Zelmann R, Gotman J. (2011) Interictal scalp fast oscillations as a marker of the seizure onset zone. *Neurology* 77:524-531.

Attarian HP, Undevia NS. (2012) *Atlas of electroencephalography in sleep medicine*. Springer Verlag.

Avoli M, D'Antuono M, Louvel J, Kohling R, Biagini G, Pumain R, D'Arcangelo G, Tancredi V. (2002) Network and pharmacological mechanisms leading to epileptiform synchronization in the limbic system in vitro. *Prog Neurobiol* 68:167-207.

Axmacher N, Elger CE, Fell J. (2008) Ripples in the medial temporal lobe are relevant for human memory consolidation. *Brain* 131:1806-1817.

Bagshaw AP, Jacobs J, LeVan P, Dubeau F, Gotman J. (2009) Effect of sleep stage on interictal high-frequency oscillations recorded from depth macroelectrodes in patients with focal epilepsy. *Epilepsia* 50:617-628.

Baillet S, Garnero L. (1997) A Bayesian approach to introducing anatomo-functional priors in the EEG/MEG inverse problem. *IEEE Trans Biomed Eng* 44:374-385.

Baillet S, Mosher JC, Leahy RM. (2001) Electromagnetic brain mapping. *Signal Processing Magazine, IEEE* 18:14-30.

Ball T, Demandt E, Mutschler I, Neitzel E, Mehring C, Vogt K, Aertsen A, Schulze-Bonhage A. (2008) Movement related activity in the high gamma range of the human EEG. *Neuroimage* 41:302-310.

Ball T, Kern M, Mutschler I, Aertsen A, Schulze-Bonhage A. (2009) Signal quality of simultaneously recorded invasive and non-invasive EEG. *Neuroimage* 46:708-716.

Batra S, Lin D, Recinos PF, Zhang J, Rigamonti D. (2009) Cavernous malformations: natural history, diagnosis and treatment. *Nat Rev Neurol* 5:659-670.

Bear MF, Connors BW, Paradiso MA. (2007) *Neuroscience : exploring the brain*. Lippincott Williams & Wilkins, Philadelphia, PA.

Bénar CG, Chauviere L, Bartolomei F, Wendling F. (2010) Pitfalls of high-pass filtering for detecting epileptic oscillations: a technical note on "false" ripples. *Clin Neurophysiol* 121:301-310.

Bénar CG, Gotman J. (2002) Modeling of post-surgical brain and skull defects in the EEG inverse problem with the boundary element method. *Clin Neurophysiol* 113:48-56.

Berger H. (1929) Über das Elektrenkephalogramm des Menschen. *European Archives of Psychiatry and Clinical Neuroscience* 87:527-570.

Blanco JA, Stead M, Krieger A, Stacey W, Maus D, Marsh E, Viventi J, Lee KH, Marsh R, Litt B, Worrell GA. (2011) Data mining neocortical high-frequency oscillations in epilepsy and controls. *Brain* 134:2948-2959.

Blanco JA, Stead M, Krieger A, Viventi J, Marsh WR, Lee KH, Worrell GA, Litt B. (2010) Unsupervised classification of high-frequency oscillations in human neocortical epilepsy and control patients. *J Neurophysiol* 104:2900-2912.

Blume KG. (2008) Drug-resistant Epilepsy. In Engel J, Pedley TA, (eds) *Epilepsy: a comprehensive textbook*. Lippincott Williams & Wilkins, Philadelpia, pp. 1365-1370.

Boonyapisit K, Najm I, Klem G, Ying Z, Burrier C, LaPresto E, Nair D, Bingaman W, Prayson R, Luders H. (2003) Epileptogenicity of focal malformations due to abnormal cortical development: direct electrocorticographic-histopathologic correlations. *Epilepsia* 44:69-76.

Bragin A, Azizyan A, Almajano J, Wilson CL, Engel J, Jr. (2005) Analysis of chronic seizure onsets after intrahippocampal kainic acid injection in freely moving rats. *Epilepsia* 46:1592-1598.

Bragin A, Engel J, Jr., Wilson CL, Fried I, Buzsaki G. (1999a) High-frequency oscillations in human brain. *Hippocampus* 9:137-142.

Bragin A, Engel J, Jr., Wilson CL, Fried I, Mathern GW. (1999b) Hippocampal and entorhinal cortex high-frequency oscillations (100--500 Hz) in human epileptic brain and in kainic acid--treated rats with chronic seizures. *Epilepsia* 40:127-137.

Bragin A, Engel J, Jr., Wilson CL, Vizentin E, Mathern GW. (1999c) Electrophysiologic analysis of a chronic seizure model after unilateral hippocampal KA injection. *Epilepsia* 40:1210-1221.

Bragin A, Mody I, Wilson CL, Engel J, Jr. (2002) Local generation of fast ripples in epileptic brain. *J Neurosci* 22:2012-2021.

Bragin A, Wilson CL, Almajano J, Mody I, Engel J, Jr. (2004) High-frequency oscillations after status epilepticus: epileptogenesis and seizure genesis. *Epilepsia* 45:1017-1023.

Bragin A, Wilson CL, Engel J. (2003) Spatial stability over time of brain areas generating fast ripples in the epileptic rat. *Epilepsia* 44:1233-1237.

Brodbeck V, Spinelli L, Lascano AM, Wissmeier M, Vargas MI, Vulliemoz S, Pollo C, Schaller K, Michel CM, Seeck M. (2011) Electroencephalographic source imaging: a prospective study of 152 operated epileptic patients. *Brain* 134:2887-2897.

Burgess RC. (2003) Volume Conduction. In Editors-in-Chief: Michael JA, Robert BD, (eds) *Encyclopedia of the Neurological Sciences*. Academic Press, New York, pp. 724-729.

Buzsáki G. (2002) Theta oscillations in the hippocampus. *Neuron* 33:325-340.

Buzsáki G, Draguhn A. (2004) Neuronal oscillations in cortical networks. *Science* 304:1926-1929.

Buzsáki G, Lopes da Silva FH. (2012) High frequency oscillations in the intact brain. *Prog Neurobiol*.

Buzsáki RD, Traub, Pedley TA. (2003) The cellular basis of EEG activity. In Ebersole JS, Pedley TA, (eds) *Current practice of clinical electroencephalography*. Lippincott Williams & Wilkins, Philadelphia.

Canolty RT, Edwards E, Dalal SS, Soltani M, Nagarajan SS, Kirsch HE, Berger MS, Barbaro NM, Knight RT. (2006) High gamma power is phase-locked to theta oscillations in human neocortex. *Science* 313:1626-1628.

Chabardes S, Prabhu S, Tanriverdi T. (2011) Surgery for temporal lobe epilepsy: pros, cons and comparison between different procedures. In Rosenow F, Ryvlin P, Luders H, (eds) *Themesialtemporallobeepilepsies* John Libbey Eurotext, Montrouge, pp. 245-262.

Chadwick DW, Porter RJ, Emilio P, Pellock JM. (2008) Overview: General Approaches to Treatment. In Engel JJ, Pedley TA, (eds) *Epilepsy: a comprehensive textbook*. Lippincott Williams & Wilkins, Philadelpia, pp. 1117-1119.

Chander R. (2007) Algorithms to detect high frequency oscillations in human intracerebral EEG. *Biomedical Engineering*. McGill University Montreal, pp. vii, 123 p.

Chang BS, Schomer DL, Niedermeyer E. (2011) Normal EEG and sleep: adults and elderly. In Schomer DL, Lopes da Silva FH, (eds) *Niedermeyer's Electroencephalography: Basic Principles, Clinical Applications, and Related Fields*. Lippincott Williams & Wilkins, Philadelphia pp. 183-214.

Châtillon CE, Zelmann R, Bortel A, Avoli M, Gotman J. (2011) Contact size does not affect high frequency oscillation detection in intracerebral EEG recordings in a rat epilepsy model. *Clin Neurophysiol* 122:1701-1705.

Chern JJ, Patel AJ, Jea A, Curry DJ, Comair YG. (2010) Surgical outcome for focal cortical dysplasia: an analysis of recent surgical series. *J Neurosurg Pediatr* 6:452-458.

Chrobak JJ, Buzsaki G. (1996) High-frequency oscillations in the output networks of the hippocampal-entorhinal axis of the freely behaving rat. *J Neurosci* 16:3056-3066.

Cohen J. (1960) A coefficient of agreement for nominal scales. *Educational and Psychological Measurement* 20:37-46.

Colgin LL, Moser EI. (2009) Hippocampal theta rhythms follow the beat of their own drum. *Nat Neurosci* 12:1483-1484.

Cooper R, Winter AL, Crow HJ, Walter WG. (1965) Comparison of Subcortical, Cortical and Scalp Activity Using Chronically Indwelling Electrodes in Man. *Electroencephalogr Clin Neurophysiol* 18:217-228.

Cosandier-Rimele D, Merlet I, Badier JM, Chauvel P, Wendling F. (2008) The neuronal sources of EEG: modeling of simultaneous scalp and intracerebral recordings in epilepsy. *Neuroimage* 42:135-146.

Cover TM, Thomas JA. (1991) *Elements of information theory*. Wiley, New York.

Crepon B, Navarro V, Hasboun D, Clemenceau S, Martinerie J, Baulac M, Adam C, Le Van Quyen M. (2010) Mapping interictal oscillations greater than 200 Hz recorded with intracranial macroelectrodes in human epilepsy. *Brain* 133:33-45.

Crone NE, Boatman D, Gordon B, Hao L. (2001a) Induced electrocorticographic gamma activity during auditory perception. Brazier Award-winning article, 2001. *Clin Neurophysiol* 112:565-582.

Crone NE, Hao L, Hart J, Jr., Boatman D, Lesser RP, Irizarry R, Gordon B. (2001b) Electrocorticographic gamma activity during word production in spoken and sign language. *Neurology* 57:2045-2053.

Crone NE, Korzeniewska A, Franaszczuk PJ. (2011) Cortical gamma responses: searching high and low. *Int J Psychophysiol* 79:9-15.

Crone NE, Sinai A, Korzeniewska A. (2006) High-frequency gamma oscillations and human brain mapping with electrocorticography. *Prog Brain Res* 159:275-295.

Curia G, Longo D, Biagini G, Jones RS, Avoli M. (2008) The pilocarpine model of temporal lobe epilepsy. *J Neurosci Methods* 172:143-157.

Curio G. (2000) Linking 600-Hz "spikelike" EEG/MEG wavelets ("sigma-bursts") to cellular substrates: concepts and caveats. *J Clin Neurophysiol* 17:377-396.

Dale AM, Sereno MI. (1993) Improved localizadon of cortical activity by combining eeg and meg with mri cortical surface reconstruction: A linear approach. *Journal of Cognitive Neuroscience* 5:162-176.

Daunizeau J, Mattout J, Clonda D, Goulard B, Benali H, Lina JM. (2006) Bayesian spatio-temporal approach for EEG source reconstruction: conciliating ECD and distributed models. *IEEE Trans Biomed Eng* 53:503-516.

David O, Blauwblomme T, Job AS, Chabardes S, Hoffmann D, Minotti L, Kahane P. (2011) Imaging the seizure onset zone with stereo-electroencephalography. *Brain* 134:2898-2911.

de Peralta Menendez RG, Gonzalez Andino SL. (1994) Single dipole localization: Some numerical aspects and a practical rejection criterion for the fitted parameters. *Brain Topogr* 6:277-282.

Draguhn A, Traub RD, Bibbig A, Schmitz D. (2000) Ripple (approximately 200-Hz) oscillations in temporal structures. *J Clin Neurophysiol* 17:361-376.

Dworetzky B, Herman S, Tatum WOI. (2011) Artifacts of Recording. In Schomer DL, Lopes da Silva FH, (eds) *Niedermeyer's Electroencephalography: Basic Principles, Clinical Applications, and Related Fields*. Lippincott Williams & Wilkins, Philadelphia pp. 239-266.

Ebersole JS. (2009) Chapter 5 - Dipole Source Modeling in Epilepsy: Contribution to Clinical Management. In Simon S, Timothy AP, (eds) *Blue Books of Neurology*. Butterworth-Heinemann, pp. 53-64.

Ebersole JS, Pedley TA. (2003) *Current practice of clinical electroencephalography*. Lippincott Williams & Wilkins, Philadelphia.

Endres DM, Schindelin JE. (2003) A new metric for probability distributions. *Information Theory, IEEE Transactions on* 49:1858-1860.

Engel J, Jr., Bragin A, Staba R, Mody I. (2009) High-frequency oscillations: what is normal and what is not? *Epilepsia* 50:598-604.

Engel JJ, Shewmon D. (1993) Overview: who should be considered a surgical candidate. *Surgical treatment of the epilepsies* 2.

Engel JJ, Van Ness P, Rasmussen T, Ojemann L. (1993) Outcome with respect to epileptic seizures. In Engel JJ, (ed) *Surgical treatment of the epilepsies*. Raven Press, New York, pp. 609-621.

Esteller R, Echauz J, Tcheng T, Litt B, Pless B. (2001) Line length: an efficient feature for seizure onset detection. *Engineering in Medicine and Biology Society, 2001. Proceedings of the 23rd Annual International Conference of the IEEE*, pp. 1707-1710 vol.1702.

Fawcett T. (2006) An introduction to ROC analysis. *Pattern Recognition Letters* 27.

Feindel W. (1993) Toward a surgical cure for epilepsy: the work of Wilder Penfield and his school at the Montreal Neurological Institute. In Engel JJ, (ed) *Surgical treatment of the epilepsies*. Raven Press, New York, pp. 1-9.

Fisher RS. (1989) Animal models of the epilepsies. *Brain Res Brain Res Rev* 14:245-278.

Fisher RS, Webber WR, Lesser RP, Arroyo S, Uematsu S. (1992) High-frequency EEG activity at the start of seizures. *J Clin Neurophysiol* 9:441-448.

Foffani G, Uzcategui YG, Gal B, Menendez de la Prida L. (2007) Reduced spike-timing reliability correlates with the emergence of fast ripples in the rat epileptic hippocampus. *Neuron* 55:930-941.

Freeman WJ, Rogers LJ, Holmes MD, Silbergeld DL. (2000) Spatial spectral analysis of human electrocorticograms including the alpha and gamma bands. *J Neurosci Methods* 95:111-121.

Frost JD, Jr., Lee CL, Hrachovy RA, Swann JW. (2011) High frequency EEG activity associated with ictal events in an animal model of infantile spasms. *Epilepsia* 52:53-62.

Gabriel C, Peyman A, Grant EH. (2009) Electrical conductivity of tissue at frequencies below 1 MHz. *Phys Med Biol* 54:4863-4878.

Gadhoumi K, Lina JM, Gotman J. (2012) Discriminating preictal and interictal states in patients with temporal lobe epilepsy using wavelet analysis of intracerebral EEG. *Clin Neurophysiol*.

Galvani L. (1791) *Aloysii Galvani De viribus electricitatis in motu musculari commentarius*. Ex Typographia Instituti Scientiarum, Bononiae.

Gambardella A, Palmini A, Andermann F, Dubeau F, Da Costa JC, Quesney LF, Andermann E, Olivier A. (1996) Usefulness of focal rhythmic discharges on scalp EEG of patients with focal cortical dysplasia and intractable epilepsy. *Electroencephalogr Clin Neurophysiol* 98:243-249.

Gardner AB, Worrell GA, Marsh E, Dlugos D, Litt B. (2007) Human and automated detection of high-frequency oscillations in clinical intracranial EEG recordings. *Clin Neurophysiol* 118:1134-1143.

Gloor P. (1969) The work of Hans Berger. *Electroencephalogr Clin Neurophysiol* 27:649.

Gloor P. (1985) Neuronal generators and the problem of localization in electroencephalography: application of volume conductor theory to electroencephalography. *J Clin Neurophysiol* 2:327-354.

Goncalves SI, de Munck JC, Verbunt JP, Bijma F, Heethaar RM, Lopes da Silva FH. (2003) In vivo measurement of the brain and skull resistivities using an EIT-based method and realistic models for the head. *IEEE Trans Biomed Eng* 50:754-767.

Gotman J, Crone NE. (2011) High-Frequency EEG Activity. In Schomer DL, Lopes da Silva FH, (eds) *Niedermeyer's Electroencephalography: Basic Principles, Clinical Applications, and Related Fields*. Lippincott Williams & Wilkins, Philadelphia, pp. 1203-1225.

Gotman J, Wang LY. (1992) State dependent spike detection: validation. *Electroencephalogr Clin Neurophysiol* 83:12-18.

Gramfort A, Papadopoulo T, Olivi E, Clerc M. (2010) OpenMEEG: opensource software for quasistatic bioelectromagnetics. *Biomed Eng Online* 9:45.

Grenier F, Timofeev I, Steriade M. (2001) Focal synchronization of ripples (80-200 Hz) in neocortex and their neuronal correlates. *J Neurophysiol* 86:1884-1898.

Grova C, Daunizeau J, Lina JM, Benar CG, Benali H, Gotman J. (2006) Evaluation of EEG localization methods using realistic simulations of interictal spikes. *Neuroimage* 29:734-753.

Guerrini R, Barba C. (2010) Malformations of cortical development and aberrant cortical networks: epileptogenesis and functional organization. *J Clin Neurophysiol* 27:372-379.

Hämäläinen M, Hari R, Ilmoniemi RJ, Knuutila J, Lounasmaa OV. (1993) Magnetoencephalography—theory, instrumentation, and applications to noninvasive studies of the working human brain. *Reviews of Modern Physics* 65:413-497.

Hämäläinen MS, Ilmoniemi RJ. (1994) Interpreting magnetic fields of the brain: minimum norm estimates. *Med Biol Eng Comput* 32:35-42.

Hashiguchi K, Morioka T, Yoshida F, Miyagi Y, Nagata S, Sakata A, Sasaki T. (2007) Correlation between scalp-recorded electroencephalographic and electrocorticographic activities during ictal period. *Seizure* 16:238-247.

Hasselmo ME. (2005) What is the function of hippocampal theta rhythm?--Linking behavioral data to phasic properties of field potential and unit recording data. *Hippocampus* 15:936-949.

Heasman BC, Valentin A, Alarcon G, Garcia Seoane JJ, Binnie CD, Guy CN. (2002) A hole in the skull distorts substantially the distribution of extracranial electrical fields in an in vitro model. *J Clin Neurophysiol* 19:163-171.

Helmholtz H. (1853) Ueber einige Gesetze der Vertheilung elektrischer Ströme in körperlichen Leitern, mit Anwendung auf die thierisch-elektrischen Versuche (Schluss.). *Annalen der Physik* 165:353-377.

Henson RN, Mattout J, Phillips C, Friston KJ. (2009) Selecting forward models for MEG source-reconstruction using model-evidence. *Neuroimage* 46:168-176.

Hoekema R, Wieneke GH, Leijten FS, van Veelen CW, van Rijen PC, Huiskamp GJ, Ansems J, van Huffelen AC. (2003) Measurement of the conductivity of skull, temporarily removed during epilepsy surgery. *Brain Topogr* 16:29-38.

Holmes CJ, Hoge R, Collins L, Woods R, Toga AW, Evans AC. (1998) Enhancement of MR images using registration for signal averaging. *J Comput Assist Tomogr* 22:324-333.

Huigen E, Peper A, Grimbergen CA. (2002) Investigation into the origin of the noise of surface electrodes. *Med Biol Eng Comput* 40:332-338.

Ibarz JM, Foffani G, Cid E, Inostroza M, Menendez de la Prida L. (2010) Emergent dynamics of fast ripples in the epileptic hippocampus. *J Neurosci* 30:16249-16261.

Isnard J, Guenot M, Sindou M, Mauguiere F. (2004) Clinical manifestations of insular lobe seizures: a stereo-electroencephalographic study. *Epilepsia* 45:1079-1090.

Ives JR. (2005) New chronic EEG electrode for critical/intensive care unit monitoring. *J Clin Neurophysiol* 22:119-123.

Jacobs J, Banks S, Zelmann R, Zijlmans M, Jones-Gotman M, Gotman J. (2011a) Ripples in the hippocampus correlate with epileptogenicity and not with memory function. *AES2011*. American Epilepsy Society, Baltimore,MD.

Jacobs J, Kerber K, Levan P, Dümpelmann M, Korinthenberg R, Schulze-Bonhage A. (2010a) Occurrence of high frequency oscillations depends on pathology in patients with Focal cortical dysplasia. *AES2010*. American Epilepsy Society, San Antonio, TX.

Jacobs J, Kobayashi K, Gotman J. (2011b) High-frequency changes during interictal spikes detected by time-frequency analysis. *Clin Neurophysiol* 122:32-42.

Jacobs J, LeVan P, Chander R, Hall J, Dubeau F, Gotman J. (2008a) Interictal high-frequency oscillations (80-500 Hz) are an indicator of seizure onset areas independent of spikes in the human epileptic brain. *Epilepsia* 49:1893-1907.

Jacobs J, Levan P, Chander R, Hall J, Dubeau F, Gotman J. (2008b) Interictal high-frequency oscillations (80-500 Hz) are an indicator of seizure onset areas independent of spikes in the human epileptic brain. *Epilepsia*.

Jacobs J, Levan P, Chatillon CE, Olivier A, Dubeau F, Gotman J. (2009a) High frequency oscillations in intracranial EEGs mark epileptogenicity rather than lesion type. *Brain* 132:1022-1037.

Jacobs J, Staba R, Asano E, Otsubo H, Wu JY, Zijlmans M, Mohamed I, Kahane P, Dubeau F, Navarro V, Gotman J. (2012) High-frequency oscillations (HFOs) in clinical epilepsy. *Prog Neurobiol*.

Jacobs J, Zelmann R, Jirsch J, Chander R, Dubeau CE, Gotman J. (2009b) High frequency oscillations (80-500 Hz) in the preictal period in patients with focal seizures. *Epilepsia*.

Jacobs J, Zijlmans M, Zelmann R, Chatillon CE, Hall J, Olivier A, Dubeau F, Gotman J. (2010b) High-frequency electroencephalographic oscillations correlate with outcome of epilepsy surgery. *Ann Neurol* 67:209-220.

Jacobs J, Zijlmans M, Zelmann R, Olivier A, Hall J, Gotman J, Dubeau F. (2010c) Value of electrical stimulation and high frequency oscillations (80-500 Hz) in identifying epileptogenic areas during intracranial EEG recordings. *Epilepsia* 51:573-582.

Jasper HH. (1958) The ten twenty electrode system of the international federation. *Electroencephalogr Clin Neurophysiol Suppl* 10:371-375.

Jasper HH, Andrews HL. (1938) Electro-encephalography: III. Normal differentiation of occipital and precentral regions in man. *Archives of Neurology & Psychiatry* 39:96.

Jasper HH, Penfield W. (1949) Electrocorticograms in man: effect of voluntary movement upon the electrical activity of the precentral gyrus. *Arch. Psychiatr. Z. Neurol.*:163–174.

Jefferys JG, Menendez de la Prida L, Wendling F, Bragin A, Avoli M, Timofeev I, Lopes da Silva FH. (2012) Mechanisms of physiological and epileptic HFO generation. *Prog Neurobiol*.

Jerbi K, Freyermuth S, Dalal S, Kahane P, Bertrand O, Berthoz A, Lachaux JP. (2009) Saccade related gamma-band activity in intracerebral EEG: dissociating neural from ocular muscle activity. *Brain Topogr* 22:18-23.

Jirsch JD, Urrestarazu E, LeVan P, Olivier A, Dubeau F, Gotman J. (2006) High-frequency oscillations during human focal seizures. *Brain* 129:1593-1608.

Jiruska P, Finnerty GT, Powell AD, Lofti N, Cmejla R, Jefferys JG. (2010) Epileptic high-frequency network activity in a model of non-lesional temporal lobe epilepsy. *Brain* 133:1380-1390.

Jones-Gotman M, Sziklas V, Djordjevic J, Dubeau F, Gotman J, Angle M, Tampieri D, Olivier A, Andermann F. (2005) Etomidate speech and memory test (eSAM): a new drug and improved intracarotid procedure. *Neurology* 65:1723-1729.

Kahane P, Dubeau F. (in press) Intracerebral Depth Electrodes Electroencephalography (stereo-encephalography). In Ebersole JS, Pedley TA, (eds) *Current practice of clinical electroencephalography*.

Kauppinen P, Hyttinen J, Laarne P, Malmivuo J. (1999) A software implementation for detailed volume conductor modelling in electrophysiology using finite difference method. *Comput Methods Programs Biomed* 58:191-203.

Khalilov I, Le Van Quyen M, Gozlan H, Ben-Ari Y. (2005) Epileptogenic actions of GABA and fast oscillations in the developing hippocampus. *Neuron* 48:787-796.

Khosravani H, Pinnegar CR, Mitchell JR, Bardakjian BL, Federico P, Carlen PL. (2005) Increased high-frequency oscillations precede in vitro low-Mg seizures. *Epilepsia* 46:1188-1197.

Kim W, Stramotas S, Choy W, Dye J, Nagasawa D, Yang I. (2011) Prognostic factors for post-operative seizure outcomes after cavernous malformation treatment. *J Clin Neurosci* 18:877-880.

Kobayashi K, Agari T, Oka M, Yoshinaga H, Date I, Ohtsuka Y, Gotman J. (2010a) Detection of seizure-associated high-frequency oscillations above 500Hz. *Epilepsy Res* 88:139-144.

Kobayashi K, Inoue T, Watanabe Y, Oka M, Endoh F, Yoshinaga H, Ohtsuka Y. (2009) Spectral analysis of EEG gamma rhythms associated with tonic seizures in Lennox-Gastaut syndrome. *Epilepsy Res* 86:15-22.

Kobayashi K, Oka M, Akiyama T, Inoue T, Abiru K, Ogino T, Yoshinaga H, Ohtsuka Y, Oka E. (2004) Very fast rhythmic activity on scalp EEG associated with epileptic spasms. *Epilepsia* 45:488-496.

Kobayashi K, Watanabe Y, Inoue T, Oka M, Yoshinaga H, Ohtsuka Y. (2010b) Scalp-recorded high-frequency oscillations in childhood sleep-induced electrical status epilepticus. *Epilepsia* 51:2190-2194.

Kobayashi K, Yoshinaga H, Ohtsuka Y, Gotman J. (2005) Dipole modeling of epileptic spikes can be accurate or misleading. *Epilepsia* 46:397-408.

Koessler L, Maillard L, Benhadid A, Vignal JP, Felblinger J, Vespignani H, Braun M. (2009) Automated cortical projection of EEG sensors: anatomical correlation via the international 10-10 system. *Neuroimage* 46:64-72.

Kovach CK, Tsuchiya N, Kawasaki H, Oya H, Howard MA, 3rd, Adolphs R. (2011) Manifestation of ocular-muscle EMG contamination in human intracranial recordings. *Neuroimage* 54:213-233.

Kwan P, Brodie MJ. (2000) Early identification of refractory epilepsy. *N Engl J Med* 342:314-319.

Kybic J, Clerc M, Abboud T, Faugeras O, Keriven R, Papadopoulo T. (2005) A common formalism for the integral formulations of the forward EEG problem. *IEEE Trans Med Imaging* 24:12-28.

Lachaux JP, Axmacher N, Mormann F, Halgren E, Crone NE. (2012) High-frequency neural activity and human cognition: Past, present and possible future of intracranial EEG research. *Prog Neurobiol*.

Lachaux JP, George N, Tallon-Baudry C, Martinerie J, Hugueville L, Minotti L, Kahane P, Renault B. (2005) The many faces of the gamma band response to complex visual stimuli. *Neuroimage* 25:491-501.

Lachaux JP, Jerbi K, Bertrand O, Minotti L, Hoffmann D, Schoendorff B, Kahane P. (2007) A blueprint for real-time functional mapping via human intracranial recordings. *PLoS One* 2:e1094.

Lachaux JP, Rodriguez E, Martinerie J, Varela FJ. (1999) Measuring phase synchrony in brain signals. *Hum Brain Mapp* 8:194-208.

Lai Y, van Drongelen W, Ding L, Hecox KE, Towle VL, Frim DM, He B. (2005) Estimation of in vivo human brain-to-skull conductivity ratio from simultaneous extra- and intra-cranial electrical potential recordings. *Clin Neurophysiol* 116:456-465.

Landis JR, Koch GG. (1977) An application of hierarchical kappa-type statistics in the assessment of majority agreement among multiple observers. *Biometrics* 33:363-374.

Lantz G, Grave de Peralta R, Spinelli L, Seeck M, Michel CM. (2003) Epileptic source localization with high density EEG: how many electrodes are needed? *Clin Neurophysiol* 114:63-69.

Latikka J, Kuurne T, Eskola H. (2001) Conductivity of living intracranial tissues. *Phys Med Biol* 46:1611-1616.

LaViolette PS, Rand SD, Raghavan M, Ellingson BM, Schmainda KM, Mueller W. (2011) Three-dimensional visualization of subdural electrodes for presurgical planning. *Neurosurgery* 68:152-160; discussion 160-151.

Law SK. (1993) Thickness and resistivity variations over the upper surface of the human skull. *Brain Topogr* 6:99-109.

Le Van Quyen M, Bragin A, Staba R, Crepon B, Wilson CL, Engel J, Jr. (2008) Cell type-specific firing during ripple oscillations in the hippocampal formation of humans. *J Neurosci* 28:6104-6110.

Leuthardt EC, Schalk G, Wolpaw JR, Ojemann JG, Moran DW. (2004) A brain-computer interface using electrocorticographic signals in humans. *J Neural Eng* 1:63-71.

Levesque M, Bortel A, Gotman J, Avoli M. (2011) High-frequency (80-500 Hz) oscillations and epileptogenesis in temporal lobe epilepsy. *Neurobiol Dis* 42:231-241.

Lew S, Wolters CH, Anwander A, Makeig S, MacLeod RS. (2009) Improved EEG source analysis using low-resolution conductivity estimation in a four-compartment finite element head model. *Hum Brain Mapp* 30:2862-2878.

Li J, Wang K, Zhu S, He B. (2007) Effects of holes on EEG forward solutions using a realistic geometry head model. *J Neural Eng* 4:197-204.

Lin J. (1991) Divergence measures based on the Shannon entropy. *Information Theory, IEEE Transactions on* 37:145-151.

Lina J, Chowdhury R, Lemay E, Kobayashi E, Grova C. (2012) Wavelet-based localization of oscillatory sources from magnetoencephalography data. *IEEE Trans Biomed Eng*.

Liu AK, Belliveau JW, Dale AM. (1998) Spatiotemporal imaging of human brain activity using functional MRI constrained magnetoencephalography data: Monte Carlo simulations. *Proc Natl Acad Sci U S A* 95:8945-8950.

Loscher W. (2011) Critical review of current animal models of seizures and epilepsy used in the discovery and development of new antiepileptic drugs. *Seizure* 20:359-368.

Luders HO, Najm I, Nair D, Widdess-Walsh P, Bingman W. (2006) The epileptogenic zone: general principles. *Epileptic Disord* 8 Suppl 2:S1-9.

Macdonald RL, Rogawski MA. (2008) Cellular effects of antiepileptic drugs. In Engel J, Pedley TA, (eds) *Epilepsy: a comprehensive textbook*. Lippincott Williams & Wilkins, Philadelpia, pp. 1433-1445.

Manning JR, Jacobs J, Fried I, Kahana MJ. (2009) Broadband shifts in local field potential power spectra are correlated with single-neuron spiking in humans. *J Neurosci* 29:13613-13620.

Marescaux C, Vergnes M, Depaulis A. (1992) Genetic absence epilepsy in rats from Strasbourg--a review. *J Neural Transm Suppl* 35:37-69.

Mari F, Zelmann R, Andrade-Valenca L, Dubeau F, Gotman J. (2012) Continuous high-frequency activity in mesial temporal lobe structures. *Epilepsia* 53:797-806.

McNamara JO. (1984) Kindling: an animal model of complex partial epilepsy. *Ann Neurol* 16 Suppl:S72-76.

Melani F, Zelmann R, Mari F, Gotman J. (in press) Continuous High Frequency Activity: a peculiar SEEG pattern related to specific brain regions. *Clin Neurophysiol*.

Merlet I, Gotman J. (2001) Dipole modeling of scalp electroencephalogram epileptic discharges: correlation with intracerebral fields. *Clin Neurophysiol* 112:414-430.

Michel CM, Murray MM, Lantz G, Gonzalez S, Spinelli L, Grave de Peralta R. (2004) EEG source imaging. *Clin Neurophysiol* 115:2195-2222.

Miller KJ, denNijs M, Shenoy P, Miller JW, Rao RP, Ojemann JG. (2007a) Real-time functional brain mapping using electrocorticography. *Neuroimage* 37:504-507.

Miller KJ, Leuthardt EC, Schalk G, Rao RP, Anderson NR, Moran DW, Miller JW, Ojemann JG. (2007b) Spectral changes in cortical surface potentials during motor movement. *J Neurosci* 27:2424-2432.

Mosher JC, Leahy RM, Lewis PS. (1999) EEG and MEG: forward solutions for inverse methods. *IEEE Trans Biomed Eng* 46:245-259.

Mosher JC, Lewis PS, Leahy RM. (1992) Multiple dipole modeling and localization from spatio-temporal MEG data. *IEEE Trans Biomed Eng* 39:541-557.

Nagasawa T, Juhasz C, Rothermel R, Hoechstetter K, Sood S, Asano E. (2012) Spontaneous and visually driven high-frequency oscillations in the occipital cortex: intracranial recording in epileptic patients. *Hum Brain Mapp* 33:569-583.

Nariai H, Nagasawa T, Juhasz C, Sood S, Chugani HT, Asano E. (2011) Statistical mapping of ictal high-frequency oscillations in epileptic spasms. *Epilepsia* 52:63-74.

Nicholson PW. (1965) Specific impedance of cerebral white matter. *Exp Neurol* 13:386-401.

Niedermeyer E. (2005a) Abnormal EEG patterns: epileptic and paroxysmal. In E N, FH LdS, (eds) *Electroencephalography: basic principles, clinical applications and related fields*. Lippincott, Williams & Wilkins, Philadelphia, pp. 235–260.

Niedermeyer E. (2005b) Depth electroencephalography. In E N, FH LdS, (eds) *Electroencephalography: basic principles, clinical applications and related fields*. Lippincott, Williams & Wilkins, Philadelphia, pp. 709–724.

Niedermeyer E. (2005c) Epileptic seizure disorders. In E N, FH LdS, (eds) *Electroencephalography: basic principles, clinical applications and related fields*. Lippincott, Williams & Wilkins, Philadelphia, pp. 505-620.

Nunez PL, Srinivasan R. (2006) *Electric fields of the brain : the neurophysics of EEG*. Oxford University Press, New York.

Ochi A, Otsubo H, Donner EJ, Elliott I, Iwata R, Funaki T, Akizuki Y, Akiyama T, Imai K, Rutka JT, Snead OC, 3rd. (2007) Dynamic changes of ictal high-frequency oscillations in neocortical epilepsy: using multiple band frequency analysis. *Epilepsia* 48:286-296.

Ogren JA, Wilson CL, Bragin A, Lin JJ, Salamon N, Dutton RA, Luders E, Fields TA, Fried I, Toga AW, Thompson PM, Engel J, Jr., Staba RJ. (2009) Three-dimensional surface maps link local atrophy and fast ripples in human epileptic hippocampus. *Ann Neurol* 66:783-791.

Oishi M, Otsubo H, Kameyama S, Morota N, Masuda H, Kitayama M, Tanaka R. (2002) Epileptic spikes: magnetoencephalography versus simultaneous electrocorticography. *Epilepsia* 43:1390-1395.

Okamoto M, Dan H, Sakamoto K, Takeo K, Shimizu K, Kohno S, Oda I, Isobe S, Suzuki T, Kohyama K, Dan I. (2004) Three-dimensional probabilistic anatomical cranio-cerebral correlation via the international 10-20 system oriented for transcranial functional brain mapping. *Neuroimage* 21:99-111.

Oostendorp TF, Delbeke J, Stegeman DF. (2000) The conductivity of the human skull: results of in vivo and in vitro measurements. *IEEE Trans Biomed Eng* 47:1487-1492.

Otsubo H, Ochi A, Imai K, Akiyama T, Fujimoto A, Go C, Dirks P, Donner EJ. (2008) High-frequency oscillations of ictal muscle activity and epileptogenic discharges on intracranial EEG in a temporal lobe epilepsy patient. *Clin Neurophysiol* 119:862-868.

Pascual-Marqui RD, Michel CM, Lehmann D. (1994) Low resolution electromagnetic tomography: a new method for localizing electrical activity in the brain. *Int J Psychophysiol* 18:49-65.

Pellock JM, Nordli DRJ, Dulac O. (2008) Drug treatment in children. In Engel J, Pedley TA, (eds) *Epilepsy: a comprehensive textbook*. Lippincott Williams & Wilkins, Philadelpia, pp. 1249-1258.

Peyman A, Holden SJ, Watts S, Perrott R, Gabriel C. (2007) Dielectric properties of porcine cerebrospinal tissues at microwave frequencies: in vivo, in vitro and systematic variation with age. *Phys Med Biol* 52:2229-2245.

Pfurtscheller G, Neuper C, Kalcher J. (1993) 40-Hz oscillations during motor behavior in man. *Neurosci Lett* 164:179-182.

Plonsey R, Heppner DB. (1967) Considerations of quasi-stationarity in electrophysiological systems. *Bull Math Biophys* 29:657-664.

Poolman P, Frank RM, Luu P, Pederson SM, Tucker DM. (2008) A single-trial analytic framework for EEG analysis and its application to target detection and classification. *Neuroimage* 42:787-798.

Ray S, Niebur E, Hsiao SS, Sinai A, Crone NE. (2008) High-frequency gamma activity (80-150Hz) is increased in human cortex during selective attention. *Clin Neurophysiol* 119:116-133.

Rosenow F, Luders H. (2001) Presurgical evaluation of epilepsy. *Brain* 124:1683-1700.

Rosso OA, Blanco S, Yordanova J, Kolev V, Figliola A, Schurmann M, Basar E. (2001) Wavelet entropy: a new tool for analysis of short duration brain electrical signals. *J Neurosci Methods* 105:65-75.

Rush S, Driscoll DA. (1968) Current distribution in the brain from surface electrodes. *Anesth Analg* 47:717-723.

Ryynanen OR, Hyttinen JA, Laarne PH, Malmivuo JA. (2004) Effect of electrode density and measurement noise on the spatial resolution of cortical potential distribution. *IEEE Trans Biomed Eng* 51:1547-1554.

Scherg M, Bast T, Berg P. (1999) Multiple source analysis of interictal spikes: goals, requirements, and clinical value. *J Clin Neurophysiol* 16:214-224.

Siapas AG, Wilson MA. (1998) Coordinated interactions between hippocampal ripples and cortical spindles during slow-wave sleep. *Neuron* 21:1123-1128.

Sinai A, Bowers CW, Crainiceanu CM, Boatman D, Gordon B, Lesser RP, Lenz FA, Crone NE. (2005) Electrocorticographic high gamma activity versus electrical cortical stimulation mapping of naming. *Brain* 128:1556-1570.

Speckmann E-J, Elger CE. (2005) Introduction to the neurophysiological basis of EEG and DC potentials. In Niedermeyer E, Lopes da Silva F, (eds) *Electroencephalography: basic principles, clinical applications and related fields*. Lippincott, Williams & Wilkins, Philadelphia, pp. 17–29.

Staba RJ, Bragin A. (2011) High-frequency oscillations and other electrophysiological biomarkers of epilepsy: underlying mechanisms. *Biomark Med* 5:545-556.

Staba RJ, Frighetto L, Behnke EJ, Mathern GW, Fields T, Bragin A, Ogren J, Fried I, Wilson CL, Engel J, Jr. (2007) Increased fast ripple to ripple ratios correlate with reduced hippocampal volumes and neuron loss in temporal lobe epilepsy patients. *Epilepsia* 48:2130-2138.

Staba RJ, Wilson CL, Bragin A, Fried I, Engel J, Jr. (2002) Quantitative analysis of high-frequency oscillations (80-500 Hz) recorded in human epileptic hippocampus and entorhinal cortex. *J Neurophysiol* 88:1743-1752.

Staba RJ, Wilson CL, Bragin A, Jhung D, Fried I, Engel J, Jr. (2004) High-frequency oscillations recorded in human medial temporal lobe during sleep. *Ann Neurol* 56:108-115.

Steriade M. (2003) The corticothalamic system in sleep. *Front Biosci* 8:d878-899.

Steriade M. (2006) Grouping of brain rhythms in corticothalamic systems. *Neuroscience* 137:1087-1106.

Stern JM, Engel J. (2004) *Atlas of EEG patterns*. Lippincott Williams & Wilkins.

Tadel F, Baillet S, Mosher JC, Pantazis D, Leahy RM. (2011) Brainstorm: a user-friendly application for MEG/EEG analysis. *Comput Intell Neurosci* 2011:879716.

Tallon-Baudry C, Bertrand O, Delpuech C, Pernier J. (1996) Stimulus specificity of phase-locked and non-phase-locked 40 Hz visual responses in human. *J Neurosci* 16:4240-4249.

Tang C, You F, Cheng G, Gao D, Fu F, Yang G, Dong X. (2008) Correlation between structure and resistivity variations of the live human skull. *IEEE Trans Biomed Eng* 55:2286-2292.

Tao JX, Baldwin M, Hawes-Ebersole S, Ebersole JS. (2007) Cortical substrates of scalp EEG epileptiform discharges. *J Clin Neurophysiol* 24:96-100.

Tellez-Zenteno JF, Pondal-Sordo M, Matijevic S, Wiebe S. (2004) National and regional prevalence of self-reported epilepsy in Canada. *Epilepsia* 45:1623-1629.

Theodore WH, Spencer SS, Wiebe S, Langfitt JT, Ali A, Shafer PO, Berg AT, Vickrey BG. (2006) Epilepsy in North America: a report prepared under the auspices of the global campaign against epilepsy, the International Bureau for Epilepsy, the International League Against Epilepsy, and the World Health Organization. *Epilepsia* 47:1700-1722.

Towle VL, Bolanos J, Suarez D, Tan K, Grzeszczuk R, Levin DN, Cakmur R, Frank SA, Spire JP. (1993) The spatial location of EEG electrodes: locating the best-fitting sphere relative to cortical anatomy. *Electroencephalogr Clin Neurophysiol* 86:1-6.

Urrestarazu E, Chander R, Dubeau F, Gotman J. (2007) Interictal high-frequency oscillations (100-500 Hz) in the intracerebral EEG of epileptic patients. *Brain* 130:2354-2366.

van 't Klooster MA, Zijlmans M, Leijten FS, Ferrier CH, van Putten MJ, Huiskamp GJ. (2011) Time-frequency analysis of single pulse electrical stimulation to assist delineation of epileptogenic cortex. *Brain* 134:2855-2866.

Van Gompel JJ, Stead SM, Giannini C, Meyer FB, Marsh WR, Fountain T, So E, Cohen-Gadol A, Lee KH, Worrell GA. (2008) Phase I trial: safety and feasibility of intracranial electroencephalography using hybrid subdural electrodes containing macro- and microelectrode arrays. *Neurosurg Focus* 25:E23.

Van Veen BD, van Drongelen W, Yuchtman M, Suzuki A. (1997) Localization of brain electrical activity via linearly constrained minimum variance spatial filtering. *IEEE Trans Biomed Eng* 44:867-880.

von Ellenrieder N, Andrade-Valenca LP, Dubeau F, Gotman J. (2012) Automatic detection of fast oscillations (40-200 Hz) in scalp EEG recordings. *Clin Neurophysiol* 123:670-680.

Wang G, Yang L, Worrell G, He B. (2009) The relationship between conductivity uncertainties and EEG source localization accuracy. *Conf Proc IEEE Eng Med Biol Soc* 2009:4799-4802.

Wennberg R, Valiante T, Cheyne D. (2011) EEG and MEG in mesial temporal lobe epilepsy: where do the spikes really come from? *Clin Neurophysiol* 122:1295-1313.

Widmaier EP, Raff H, Strang KT. (2006) *Vander's human physiology : the mechanisms of body function*. McGraw-Hill Higher Education, Boston.

Wolters CH, Anwander A, Tricoche X, Weinstein D, Koch MA, MacLeod RS. (2006) Influence of tissue conductivity anisotropy on EEG/MEG field and return current computation in a realistic head model: a simulation and visualization study using high-resolution finite element modeling. *Neuroimage* 30:813-826.

Worrell GA, Gardner AB, Stead SM, Hu S, Goerss S, Cascino GJ, Meyer FB, Marsh R, Litt B. (2008) High-frequency oscillations in human temporal lobe: simultaneous microwire and clinical macroelectrode recordings. *Brain* 131:928-937.

Worrell GA, Jerbi K, Kobayashi K, Lina JM, Zelmann R, Le Van Quyen M. (2012) Recording and analysis techniques for high-frequency oscillations. *Prog Neurobiol*.

Wu JY, Koh S, Sankar R, Mathern GW. (2008) Paroxysmal fast activity: an interictal scalp EEG marker of epileptogenesis in children. *Epilepsy Res* 82:99-106.

Wu JY, Sankar R, Lerner JT, Matsumoto JH, Vinters HV, Mathern GW. (2010) Removing interictal fast ripples on electrocorticography linked with seizure freedom in children. *Neurology* 75:1686-1694.

Ylinen A, Bragin A, Nadasdy Z, Jando G, Szabo I, Sik A, Buzsaki G. (1995) Sharp wave-associated high-frequency oscillation (200 Hz) in the intact hippocampus: network and intracellular mechanisms. *J Neurosci* 15:30-46.

Young GB, Ives JR, Chapman MG, Mirsattari SM. (2006) A comparison of subdermal wire electrodes with collodion-applied disk electrodes in long-term EEG recordings in ICU. *Clin Neurophysiol* 117:1376-1379.

Yuval-Greenberg S, Tomer O, Keren AS, Nelken I, Deouell LY. (2008) Transient induced gamma-band response in EEG as a manifestation of miniature saccades. *Neuron* 58:429-441.

Zelmann R. (2007) Classifying responses to imagined movements in scalp and intracranial EEG for a Brain Computer Interface. *Biomedical Engineering*. McGill University Montreal, pp. viii, 135 p.

Zelmann R, Jacobs J, Zijlmans M, Châtillon C, Dubeau F, Gotman J. (2009a) Is There A Natural Division Between Ripples And Fast Ripples In Humans? *AES2009*. American Epilepsy Society, Boston, MA, p. .

Zelmann R, Lina J, Schulze-Bonhage A, Gotman J, Jacobs J. (submitted) The scalp EEG can see very small cortical generators of epileptic activity.

Zelmann R, Mari F, Jacobs J, Zijlmans M, Chander R, Gotman J. (2010) Automatic detector of high frequency oscillations for human recordings with macroelectrodes. *Conf Proc IEEE Eng Med Biol Soc* 2010:2329-2333.

Zelmann R, Mari F, Jacobs J, Zijlmans M, Dubeau F, Gotman J. (2012) A comparison between detectors of high frequency oscillations. *Clin Neurophysiol* 123:106-116.

Zelmann R, Zijlmans M, Jacobs J, Chatillon CE, Gotman J. (2009b) Improving the identification of High Frequency Oscillations. *Clin Neurophysiol* 120:1457-1464.

Zijlmans M, Jacobs J, Kahn YU, Zelmann R, Dubeau F, Gotman J. (2011) Ictal and interictal high frequency oscillations in patients with focal epilepsy. *Clin Neurophysiol* 122:664-671.

Zijlmans M, Jacobs J, Zelmann R, Dubeau F, Gotman J. (2009a) High frequency oscillations and seizure frequency in patients with focal epilepsy. *Epilepsy Res* 85:287-292.

Zijlmans M, Jacobs J, Zelmann R, Dubeau F, Gotman J. (2009b) High-frequency oscillations mirror disease activity in patients with epilepsy. *Neurology* 72:979-986.

Zijlmans M, Jiruska P, Zelmann R, Leijten FS, Jefferys JG, Gotman J. (2012) High-frequency oscillations as a new biomarker in epilepsy. *Ann Neurol* 71:169-178.